ENERGY EFFICIENT SOLIDS FEED SYSTEM FOR HIGH PRESSURE PROCESSES

James Michael Craven, MEng, AMIChemE, GradEI

Department of Chemical and Biological Engineering

The University of Sheffield

Project Supervisors

Professor V N Sharifi

Professor J Swithenbank

A thesis submitted to the University of Sheffield for the degree of

Doctor of Philosophy

July 2014

Summary

Solids feeding and handling systems have been cited as one of the most common contributors to process downtime where combustion and gasification systems are concerned. They are often wasteful, inefficient and require offline maintenance at regular intervals, especially when used in conjunction with pressurised processes. Lock hoppers and slurry feeders are the two most commonly deployed type of feed system where feeding solids to high pressures is necessitated; however, both systems are inherently inefficient and present a burden on the overall efficiency of the process they are feeding to.

A new system for efficiently feeding solid fuels to high pressure processes has been developed over the course of this study. The system, named the Hydraulic Lock Hopper (HLH), takes the form of a new lock hopper that utilises water as an incompressible fluid during the compression stage. It disposes of the need for inert gas or gas compressors as is required by conventional lock hopper systems, and vastly increases their operational efficiency. The HLH has demonstrated the feeding of a range of fuels including wood pellets, torrefied spruce pellets and ground anthracite grains to pressures as high as 25 barg. Two modes of operation have been developed, one whereby the energy requirement to feed is minimised (Mode 1), and another whereby the volume of high pressure gas vented to the atmosphere is reduced to near nil (Mode 2). In addition to this, the HLH has been developed to operate without the forward leakage of air in order to minimise explosive atmospheres.

Energy savings of around 82% and 75% compared to a conventional single lock hopper were consistently demonstrated when operating the HLH in Mode 1 and Mode 2 respectively. Energy savings were found to be lower in all cases when compared to a dual lock hopper, with a dual lock hopper being found to require approximately half the energy required by a conventional single lock hopper. Mode 1 was found to require less energy than Mode 2 at all operating pressures; however, Mode 2 was found to be the most efficient mode of operation where lock gas contamination with syngas (15 MJ/Nm^3) in excess of 12 vol% takes place (25 barg).

The mass flow rate of the HLH was found to stay broadly constant irrespective of operating pressure due to the power drawn by the pump being variable and in turn, the compression time being maintained broadly constant. Mass flow rates were found to vary between 25 g/s and 29 g/s for both Mode 1 and Mode 2, and Mode 1 was found to have a slightly larger mass flow rate than Mode 2 in all cases. The HLH was also found to have a negligible impact on fuel moisture content. Increases in fuel moisture content were consistently found to be less than 1 wt% in both modes of operation.

A detailed economic assessment revealed the HLH to be cost competitive with a conventional lock hopper regardless of plant capacity for an operating pressure of 25 barg. It was also found that where pressures in excess of 33.7 barg are present, the HLH is more economically favourable than a conventional lock hopper (assuming a plant with a capacity of 100 MW). Such a breakeven pressure was found to decrease for plants with higher capacities, and therefore it can be said that the HLH is most economically favourable for large capacity plants with high operating pressures.

Acknowledgements

Firstly, I would like to thank my supervisors, Professor Vida Nasserzadeh Sharifi and Professor Jim Swithenbank for their help, guidance and support throughout the course of my studies. Their presence has not only driven and motivated me throughout, but has enriched my research as a whole.

I would also like to thank all of the technical staff in the Department of Chemical and Biological Engineering for their technical assistance and ingenuity. Special thanks go to Mike O'Meara, David Palmer, Dean Haylock, Ian Watts, Horace McFarlane, Adrian Lumby, Keith Penny and Mark Jones, without whom much of the work presented in this thesis would not be possible.

I would like to thank the Biomass and Fossil Fuel Research Alliance and the Engineering and Physical Science Research Council for their financial support throughout this research programme, and Greg Kelsall, Peter Sage, John Gardner and Dr David Peralta-Solorio for their continued interest in my studies.

And last, but by no means least, I would like to thank Alice Craven (née Labsvirs), for all of her love, support and fundamental lack of understanding of what I have been studying for the past three years. While she has not contributed to this work whatsoever in terms of technical content, she has made my life more enjoyable over its duration.

Table of Contents

List of Figures

List of Tables

Nomenclature

Upper Case Symbols		*SI Unit*
A	Area of a hoppers cylinder section	m^2
A	Surface area (Equation 4-25)	m
A_{fc}	Cross-sectional area of filter cake	m^2
B	Minimum hopper outlet diameter	m
C	Concentration	mol/m^3
C	Design constant (Equation 3-19)	-
C_0	Base cost	£
C_A	Capital cost of a piece of equipment of size or capacity S_A	£
C_B	Capital cost of a piece of equipment of size or capacity S_B	£
C_c	Current cost	£
C_p	Specific heat capacity (constant pressure)	J/kg K
C_v	Specific heat capacity (constant volume)	J/kg K
D	Diameter of a hoppers cylinder section	m
D_c	Inside diameter of a cylinder at a junction with a cone	m
D_e	Nominal plate diameter	m
D_i	Inside diameter of a cylinder/cone at the point	m
D_t	Tank diameter	m
F_b	Screw bearing factor	-
F_d	Screw diameter factor	-
F_f	Screw flight factor	-
F_m	Material factor	-
F_o	Screw overload factor	-
F_p	Screw paddle factor	-
F_U	Effective pull of a conveyor	N
H	Height of a hoppers cylindrical section	m
H	Henry's constant (Equation 3-10)	$Pa\ m^3/mol$
H_L	Liquid depth	m
HP	Total screw power requirement	W
HP_f	Screw power requirement to run an empty conveyor	W
HP_m	Screw power requirement to solely convey material	W
I	Current cost index	-
I_0	Base cost index	-
J	Mass fraction	-

Upper Case Symbols (Cont.)		*SI Unit*
J	Joint factor (Equations 7-1, 7-2 and 7-5)	-
K	Mathematical parameter determined from the yield locus gradient (m)	-
K	Stress ratio (Equation 4-5)	-
K_0	Compression ratio	-
K_{st}	Maximum rate of pressure increase	Pa m/s
L	Length	m
L_{fc}	Filter cloth resistance	m
M	Molar mass	kg/mol
M_p	Mass of a particle	kg
N	Rotational rate	rpm
P	Pressure	Pa
P_0	Known initial pressure	Pa
P_a	Initial pressure	Pa
P_{atm}	Atmospheric pressure at sea level	Pa
P_A	Mechanical power for the drive drum	W
P_f	Pressure equivalent due to friction	Pa
P_i	Internal pressure	Pa
P_M	Mechanical motor power for the drive drum	W
P_{max}	Maximum explosion pressure	Pa
P_{max0}	Known maximum explosion pressure	Pa
P_p	Pumping power	W
Q	Heat	J
R	Ideal gas constant	J/mol K
R	Radius (Section 3.6)	m
R_m	Tensile strength	Pa
S	Entropy	J/K
S	Specific surface area (Equation 2-2)	m^2/m^3
S_A	Size or capacity of a piece of equipment	-
S_B	Size or capacity of a piece of equipment	-
T	Temperature	K
U	Circumference of a hoppers cylindrical section	m
U	Internal energy (Equation 3-2)	J
V	Volume	m^3
V_f	Volume of filtrate	m^3
V_p	Volume of a particle	m^3

Upper Case Symbols (Cont.)		*SI Unit*
V_{Voids}	Volume of voids	m^3
W	Work	J

Lower Case Symbols

d	Diameter of an opening into a vessel	m
d_i	Internal pipe diameter	m
d_p	Particle diameter	m
e	Minimum wall thickness for a conical shell	m
e_1	Minimum thickness of a cylindrical shell at a junction	m
e_2	Minimum thickness of a conical shell at a junction	m
e_c	Minimum wall thickness required for a cylindrical shell	m
e_{fc}	Filter cake voidage	-
e_h	Minimum head thickness for a flat unstayed head	m
e_j	Thickness of a knuckle where a cylindrical and conical section meet	m
e_p	Minimum head thickness	m
e_s	Thank thickness	m
f	Nominal design stress	Pa
ff	Hopper flow factor	-
ff_c	Flowability	-
f_f	Friction factor	-
f_t	Tank material design stress	Pa
g	Gravitational acceleration	m/s^2
h	Height	m
k	Beverloo shape coefficient	-
l	Length	m
l_1	Length of a knuckle along a cylindrical section	m
l_2	Length of a knuckle along a conical section	m
l_{fc}	Filter cake thickness	m
m	Mass flow rate	kg/s
m	Yield locus gradient (Equation 4-10)	-
m_B	Mass of belt	kg
m_b	Total mass of material on a belt	kg
m_R	Mass of all rotating drums excluding the mass of the drive drum	kg
n	Moles	mol

Lower Case Symbols (Cont.)		*SI Unit*
n	Exponent (Equation 7-7)	-
n_p	Number of particle contacts	-
p	Design pressure	Pa
q	Screw volumetric flow rate	m^3/s
r	Inside radius of curvature of a knuckle	m
r_{fc}	Specific resistance of a filter cake	m^{-2}
r_m	Mean radius	m
r_o	Distance from the virtual apex of a hopper to the hopper outlet	m
r_t	Tangential radius of curvature	m
t	Time	s
t_w	Wall thickness	m
u	Fluid velocity	m/s
u_s	Velocity of solids	m/s
v	Belt velocity	m/s
z	Height of a hoppers cylindrical section	m

Greek Symbols

α	Angle	°
α	Conical half angle (Equations 3-15 and 3-16)	°
γ	Ratio of specific heat capacities (C_p/C_v)	-
δ	Effective angle of internal friction	°
ε	Voidage	-
η	Drive efficiency	-
η_g	Dynamic viscosity of gas	Pa s
θ	Semi-included angle of a hopper slope	°
κ_x	Compressibility	Pa^{-1}
μ_f	Filtrate viscosity	Pa s
μ_R	Roller friction coefficient	-
μ_T	Table support friction coefficient	-
ρ	Density	kg/m^3
ρ_b	Bulk density	kg/m^3
ρ_f	Fluid density	kg/m^3
ρ_{fi}	Filtrate density	kg/m^3
ρ_L	Liquid density	kg/m^3

Greek Symbols (Cont.)		*SI Unit*
ρ_p	Particle density	kg/m^3
σ_1	Consolidation stress	Pa
σ_c	Unconfined yield stress	Pa
σ_{crit}	Critical stress for flow	Pa
σ_D	Developed stress	Pa
σ_E	Normal stress where the yield locus meets the large Mohr circle	Pa
σ_h	Horizontal stress	Pa
σ_{hp}	Hoop stress	Pa
σ_{hc}	Conical hoop stress	Pa
σ_l	Longitudinal stress	Pa
σ_{lc}	Conical longitudinal stress	Pa
σ_r	Radial stress	Pa
σ_v	Vertical stress	Pa
σ_w	Wall normal stress	Pa
σ_α	Normal stress	Pa
τ_E	Shear stress where the yield locus meets the large Mohr circle	Pa
τ_w	Wall shear stress	Pa
τ_α	Shear stress	Pa
υ_{fc}	Volume of filter cake deposited per volume of filtrate	-
φ	Angle of internal friction	°
ϕ_w	Kinematic angle of wall friction	°

Acronyms

AC	Alternating Current
AGR	Acid Gas Removal
AMSL	Above Mean Sea Level
ASTM	American Society for Testing and Materials
ASU	Air Separation Unit
BFB	Bubbling Fluidised Bed
BS	British Standard
CCS	Carbon Capture and Storage
CCU	Carbon Capture and Utilisation
CEMA	Conveyor Equipment Manufacturers Association
CEPCI	Chemical Engineering Plant Cost Index
CFB	Circulating Fluidised Bed
CHP	Combined Heat and Power
DC	Direct Current
DECC	Department of Energy and Climate Change
DIPPR	Design Institute for Physical Properties
DOE	Department of Energy
DTG	Derivative Thermogravimetric
ECN	Energy Centre of the Netherlands
EERC	Energy and Environmental research Centre
EPRI	Electric Power Research Institute
EU	European Union
F-T	Fischer-Tropsch
FB	Fixed Bed
FEED	Front End Engineering Design
FMA	Foster Miller Associates
FSO	Full Scale Output
GE	General Electric
GHG	Greenhouse Gas
HB	Hardness Brinell
HHV	Higher Heating Value
HLH	Hydraulic Lock Hopper
IEC	International Electrotechnical Commission
IGCC	Integrated Gasification Combined Cycle
KBR	Kellogg, Brown and Root

Acronyms (Cont.)

LEL	Lower Explosive Limit
LHV	Lower Heating Value
LIT	Layer Ignition Temperature
LOC	Limiting Oxygen Concentration
LPF	Linear Pocket Feeder
MDEA	Methyl-diethanolamine
MEA	Monoethanolamine
MIE	Minimum Ignition Energy
MIT	Minimum Ignition Temperature
MST	Material Science Corporation
MSW	Municipal Solid Waste
NETL	National Energy Technology Laboratory
OFGEM	Office of Gas and Electricity Markets
Petcoke	Petroleum coke
PFT	Powder Flow Tester
PSD	Particle Size Distribution
PWR	Pratt and Whitney Rocketdyne
RMS	Root Mean Square
STP	Standard Temperature and Pressure
Syngas	Synthesis gas
TG	Thermogravimetric
UK	United Kingdom
US	United States
USA	United States of America

Chemical Species

C	Carbon
CH_4	Methane
CO	Carbon monoxide
CO_2	Carbon dioxide
COS	Carbonyl sulphide
CS_2	Carbon disulphide
H_2	Hydrogen
H_2O	Water/steam
H_2S	Hydrogen sulphide
HCl	Hydrochloric acid
HCN	Hydrogen cyanide
N_2	Nitrogen
NH_3	Ammonia
NOx	Nitrogen containing oxides
O_2	Oxygen
SOx	Sulphur containing oxides

1

INTRODUCTION

1.1 Background

Worldwide energy consumption currently stands at an estimated 12,500 Mtoe, a level which constitutes a 54% increase on figures reported in 1990 (Enerdata, 2012, BP, 2013). 87% of this figure is derived from fossil fuels, and while this poses a slight improvement on levels recorded in 1990 (88%), such a proportion is still far too high for sustainable development (BP, 2013). As of 2013, coal reserves stand at approximately 861 thousand million tonnes, natural gas reserves stand at 187 trillion cubic metres, and oil reserves stand at 236 thousand million tonnes (BP, 2013). If production rates are maintained at current levels, reserves only stand to last for another 109 years in the case of coal, 55.7 years in the case of natural gas, and 52.9 years in the case of oil (BP, 2013). With the link between carbon dioxide (CO_2) emissions and climate change being further compounded, and the contribution conventional fuels make to CO_2 emissions unsustainable, it is clear that a shift in the way modern society operates is needed.

Where the United Kingdom (UK) is concerned, total primary energy consumption currently stands at approximately 204 Mtoe, a value which represents a 3.7% decrease from the level recorded in 1990 (BP, 2013). The UK has done much to combat climate change in recent years, and has legislation in place which poses as the world's first long-term legally binding framework to tackle climate change – the Climate Change Act 2008. The Climate Change Act requires greenhouse gas (GHG) emissions to be reduced by ≥34% of 1990 levels by 2020 and by ≥80% of 1990 levels by 2050 (DECC, 2012a).

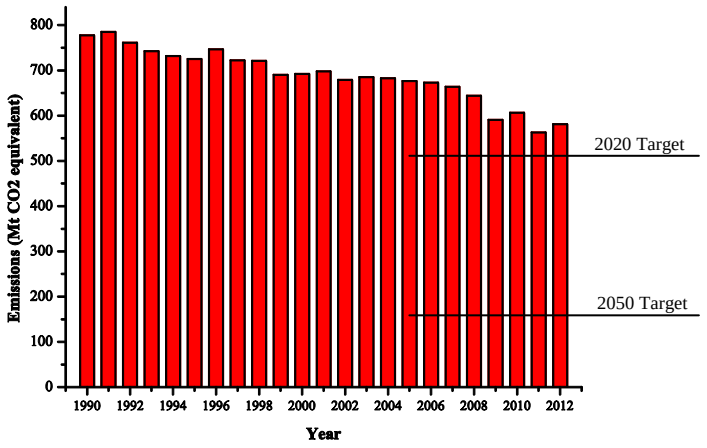

Figure 1-1: UK CO_2 emissions from 1990 to 2012 and in relation to current targets set (DECC, 2012b).

Figure 1-1 provides an overview of the current status of CO_2 emissions in the UK and in relation to the current targets set. Clearly the target set for 2050 is ambitious, not least because conventional fuels currently makeup a significant portion of the UK's energy mix. In 2012, approximately 95% of the total energy consumed was generated through non-renewable means, and around 87% was produced using coal, oil or gas.

Fuel	Consumption (Mtoe)	Percentage of Consumption (%)
Oil	68.5	33.6
Natural Gas	70.5	34.6
Coal	39.1	19.2
Nuclear	15.9	7.8
Hydro-electricity	1.2	0.6
Renewable	8.4	4.2

Table 1-1: UK 2012 energy consumption by fuel and as a percentage of total consumption (BP, 2013).

Given our large reliance on fossil fuels, it is unrealistic to propose that current technologies are disposed of in favour of new and emerging low carbon technologies overnight, not least due to such technologies presenting significant drawbacks of their own. Instead, a composite approach should be taken, which primarily focuses on improving the efficiencies of conventional energy producing processes, while new low carbon technologies are developed further so that they are more robust, reliable and flexible in their output.

1.1.1 Gasification

Gasification is one such technology that can provide both a carbon-free and more efficient conventional power supply in the form of biomass gasification when integrated as a combined cycle

(IGCC). IGCC presents potential coal conversion (coal-to-electricity) efficiencies as high as 50-55%. When compared to conventional coal combustion plants which typically operate with conversion efficiencies of 33-35%, the advantage of such a process is fully realised (Rezaiyan and Cheremisinoff, 2005).

Further to overall operational efficiencies, IGCC technologies also compare favourably to conventional processes from an environmental emission stand point. Carbon dioxide emissions per MWh of electricity produced using IGCC technologies have been shown to be reduced by approximately 19% (potentially 43-57%) compared to conventional combustion systems and emissions of nitrogen (NOx) and sulphur (SOx) oxides have been shown to be reduced by approximately 32% and 88% respectively (NETL, 2010a). Such emission reductions, in addition to decreased particulate and heavy metal emissions, present extremely favourable operating conditions when compared to conventional processes.

Feedstock	Syngas Capacity (MW_{th})	Gasifiers	Plants
Coal	36315	201	53
Petroleum	17938	138	56
Gas	15281	59	23
Petcoke	911	5	3
Biomass/Waste	373	9	9
Total	**70,818**	**412**	**144**

Table 1-2: Status of worldwide gasification industry by fuel as of 2010 (NETL, 2010b).

Fundamentally, gasification is a conversion process taking a carbon containing feedstock and converting it into a more valuable and flexible gaseous fuel. As such, gasification can process a wide variety of feedstocks: coal, petroleum, petroleum coke (petcoke), gas, biomass and waste. Table 1-2 highlights the current status of the gasification industry worldwide in terms of the various feedstocks mentioned and the associated synthesis gas (syngas) capacity they present. Further to the figures displayed in Table 1-2 are a number of gasifiers currently under construction and planned for construction between now and 2016. Incorporating such plants into the figures displayed in Table 1-2 increases syngas capacity to a potential 122,107 MW_{th} (NETL, 2010b).

1.1.2 High pressure gasification

Gasification at high pressure constitutes a major step change in the way in which gasification is carried out. Practically all modern gasifiers operate at pressures above 10 bar, with some designs presenting operating pressures as high as 100 bar (Higman and Van der Burgt, 2008). One of the principal advantages of operating at elevated pressure is decreased equipment size. However, the benefit of

operating at high pressure is fully realised where the energy cost for product gas compression in atmospheric cases is taken into account. When high pressure gasification is integrated with combined cycle power production, a continuous supply of gaseous fuel at pressure is produced for use in the gas turbine stage, and the only energy required relating to compression is that of pressurising the feedstock.

Further to power production in IGCC systems, gasification can be linked with many other processes through the use of the product syngas. Syngas, broadly defined as a gaseous mixture of carbon monoxide (CO) and hydrogen (H_2) provides the foundation on which many chemical and fuel production processes are based. Figure 1-2 highlights a number of chemical species able to be synthesised using syngas as a primary feedstock.

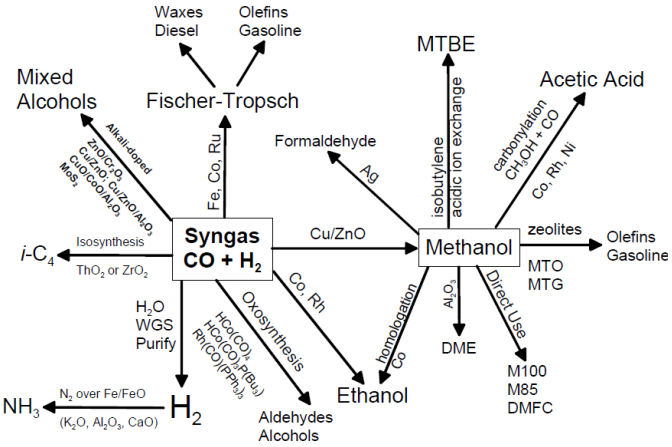

Figure 1-2: Potential syngas conversion routes (Spath and Dayton, 2003).

High pressure gasification lends itself particularly well to the production of ammonia and methanol due to the high operating pressures involved in both of their synthesis routes. Ammonia requires a pure hydrogen feedstock free of any sulphur contaminants at pressures of 130-180 bar (Higman and Van der Burgt, 2008), and similarly methanol requires a carbon monoxide and hydrogen mixture typically at a ratio of 2:1 (H_2:CO) at pressures of 50-101 bar (Eastland, 1975, Klier, 1982). Therefore, gasification at elevated pressure acts as the ideal precursor to such downstream processes as it produces a useable feedstock at, or close to the required operating pressure.

Figure 1-3 shows the current status of gasification in terms of syngas application and capacity, and highlights the proposed change in application over time. The projection of syngas capacity in terms of "planned" installations indicates that the power and energy market is becoming more prevalent, while chemical synthesis processes still maintain a presence. However, the two sectors are not necessarily mutually exclusive as a new concept called "swing and stash" can be utilised. The process essentially uses gasification in partnership with a water-gas shift reactor to produce a consistent and pure stream of hydrogen. The hydrogen stream can then be selectively swung between two (or more) downstream

processes to produce electricity and/or chemical products. In essence, the system allows the gasification unit to operate with a continuous output and facilitates the storage of hydrogen in chemical bonds (Griffiths, 2012).

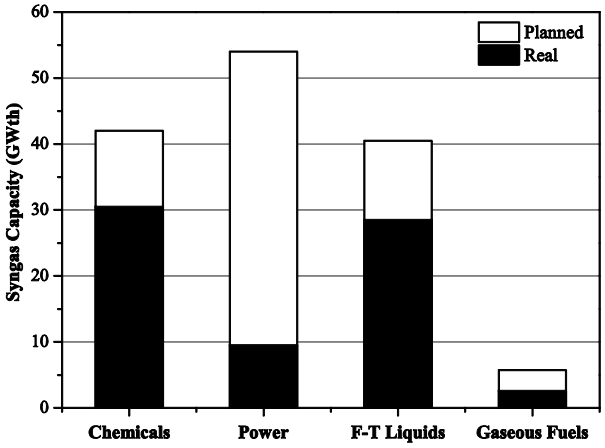

Figure 1-3: Capacity of syngas from gasification by sector (Higman and Van der Burgt, 2008).

1.1.3 High pressure solids feed systems

The advantages from carrying gasification out at elevated pressure are clear; however, the process of fuel feeding to high pressure environments becomes challenging and costly where gasification utilises solid feedstocks. Figure 1-4 displays four of the most widely used gasifiers operating in industry. The Shell gasifier accounts for approximately 41% of gasifiers currently in operation, the Sasol-Lurgi gasifier accounts for approximately 26% and the GE and E-Gas gasifiers account for approximately 23% and 0.06% respectively (NETL, 2010b). All four gasifiers operate at pressures exceeding that of the atmosphere and typically utilise a solid fuel (coal) as their feedstock. Therefore, such designs require a high pressure feed system to facilitate the feeding of a solid fuel while the operating pressure inside the gasifier is maintained.

The two most established high pressure solids feed systems currently in use in industry today are lock hoppers and slurry feeders. Lock hoppers constitute a dry solids feed system where no external element is required to be added to the fuel to facilitate feeding, whereas slurry feeders utilises a solid laden slurry typically made up with water (60-70 wt% solids) (Hawrych, 1981). Both the Shell and Sasol-Lurgi gasifiers use lock hoppers and the GE and E-Gas gasifiers use slurry feeding systems (NETL, 2014). The main advantage of lock hoppers over slurry feeders is that lock hoppers do not require any further treatment of the feedstock being fed. Treatment is required in the case of slurry feeders, typically with water, and the amount of water required is usually surplus to gasification requirements and serves to decrease cold gas efficiencies (fuel-to-gas efficiency). But the advantage of slurry feeders over lock hoppers is that they can utilise conventional positive displacement pumps

to bring about feeding, and consequently have far more modest energy requirements to feed. Where lock hoppers are concerned, large amounts of energy are required to compress the lock gas used to pressurise the fuel being fed, and on top of this, the energy used for pressurisation is almost immediately wasted during the depressurisation stage which is required in order to feed a new batch of fuel.

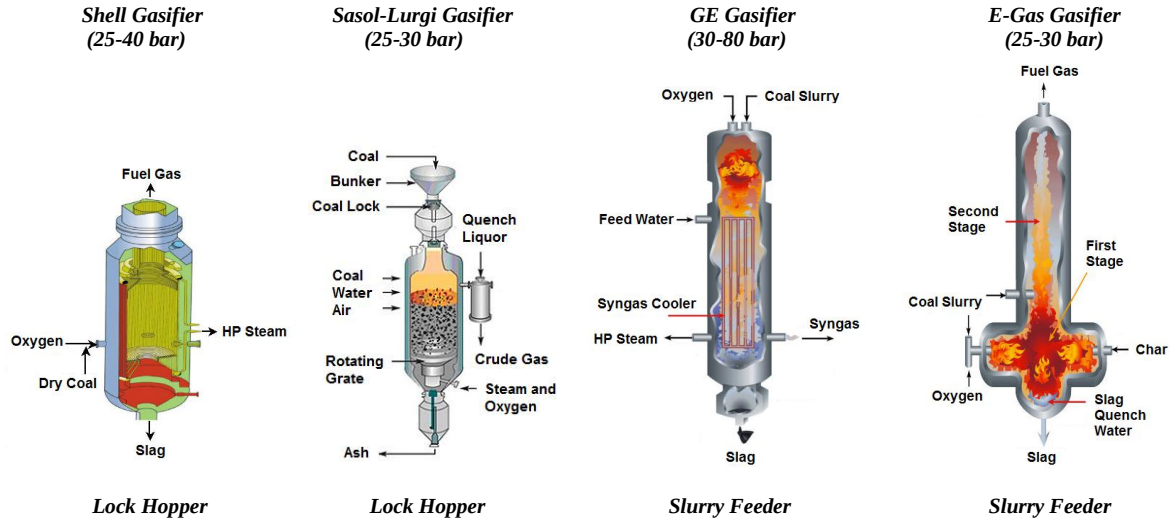

Figure 1-4: Dry and slurry fed gasifiers operating at elevated pressure (Rezaiyan and Cheremisinoff, 2005, Higman and Van der Burgt, 2008, NETL, 2014).

Operating advantages and disadvantages aside, assessing both types of feed system in terms of the overall cost of feeding it is found that lock hoppers operating at pressures below 50 atm are cheaper than slurry feeding systems, with slurry feeders outperforming lock hoppers in terms of cost at higher pressures (DOE, 1965). However, both feed systems present fundamental flaws in their operation as previously mentioned. Lock hoppers in particular are commonly the cause of process downtime, and slurry feeders present a large burden on the overall process efficiency through the enthalpy of vaporisation (Holt, 2001, Clayton et al., 2002). It is therefore crucial that in order for high pressure gasification systems to prosper, an efficient and reliable feed system is developed.

1.2 Objective of research

The principal objective of this PhD study is to design and develop a novel feed system for feeding solid materials to high pressure environments. The work carried out as part of this study will be framed in the energy industry, and more specifically, the gasification industry. However, it is anticipated that the outcome of this research will be able to be applied to any system that involves the feeding of solid materials to high pressure processes.

The main objectives of this PhD study, in addition to that principally stated, are as follows:

- To carry out a detailed search of the literature on high pressure solids feed systems to gain a greater insight into the current area of research.
- To construct, commission and extensively test a new type of feed system for feeding solids to high pressure environments to assess its reliability and operational efficiency.
- To develop a theoretical model in order to predict operational parameters relating to the new feed system.
- To characterise a broad range of materials in terms of their physical properties in order to improve the understanding of how solid materials flow.
- To carry out an economic assessment of the new feed system in order to gauge its potential use in future systems.

Overall, the objectives of this work seek to provide a better understanding of the landscape in terms of high pressure solids feed systems, and to develop a new technology for efficiently feeding solid fuels to high pressure processes.

1.3 Thesis layout

This thesis presents the work carried out for the period 1st September 2011 to 10th July 2014 and is split into eight chapters which can be summarised as follows:

Chapter one introduces the main area of research and highlights the research topic in a wider context. Gasification in general and gasification at high pressure are discussed, in addition to the role of feed systems for feeding solid fuels to pressurised processes. The key objectives of this study are detailed.

Chapter two provides an extensive study into the key elements relating to high pressure gasification and high pressure solids feed systems. Solids feed systems used in atmospheric and pressurised processes are reviewed in detail, and systems currently available/in development are compared in terms of their throughput, flexibility and operational efficiency.

Chapter three details the proposed system for feeding solid materials to high pressure environments. The operational procedure of the proposed system is discussed and the potential efficiency gain the system presents over competing systems is examined. Design calculations relating to the construction of the system are undertaken and detailed.

Chapter four provides an overview of the tests required to be undertaken in order to characterise a solid material in terms of its physical and flow properties. Results from such tests are detailed for a range of solid fuels including wood pellets, torrefied pellets, torrefied wood chips, anthracite grains, milled wood pellets and pulverised coal, and the implications they have on the design of the proposed feed system are discussed.

Chapter five provides an overview of the constructed experimental rig/feed system which takes the form of a new type of lock hopper that utilises an incompressible fluid for compression. It details the results generated from feeding a range of fuels to pressures as high as 25 barg, and examines the affect the feed system has on the fuels being fed. It compares experimental results regarding energy use to those determined theoretically, and to a conventional lock hopper via a small scale comparison.

Chapter six presents further experimental work relating to the experimental rig/feed system. It details work regarding a vacuum precursory stage that aims to increase process safety by minimising the forward leakage of air into gasification systems. It explores the benefit of introducing such a stage to the proposed feed system and details the affect it has on the existing operational cycle in terms of mass flow rate and energy requirement.

Chapter seven details the changes required to be made to the feed system developed in this study if such a system is to be scaled up for use in a commercial setting. An economic comparison between the feed system developed in this study and a conventional lock hopper system is made, and the effect of feed capacity and operating pressure on capital cost is examined.

Chapter eight lists the conclusions made from the work undertaken in this study and presented in the chapters previously mentioned. In addition to this, chapter eight details recommendations for further work to be carried out regarding the feed system developed.

2

LITERATURE REVIEW

2.1 Introduction

This chapter provides an extensive study into current and past work relating to feed systems used for feeding solid materials to high pressure processes. Feed systems both found in the literature and in practice on working sites are reviewed, as well as those currently in development. In addition to this, the applications of the feed systems reviewed are discussed as well as the materials used in conjunction with such systems.

From the literature, it is found that high pressure solids feed systems can be split into six main categories: rotary valve feeders, lock hoppers, plug-forming feeders, piston feeders, dynamic feeders and slurry feeders (Wilén and Rautalin, 1993, Lau et al., 2002, Swanson et al., 2003). Each of these categories will be discussed in the following sections, and the designs within will be detailed.

2.2 Rotary valve feeders

Rotary valve feeders present one of the most common types of feed system associated with solid materials. They are simple in their operation and are comprised of two main components: a central rotor and a valve housing. Rotors used in rotary valves contain a series of vanes that protrude from the centre in a star-like formation, and a seal is able to be made between the vanes and the valve housing.

The rotor rotates continuously around a central point and allows the constant feeding of solid material from one region to another through simultaneous charging and discharging of material (Cleveland, 1971, Kraus, 1981, Marcus et al., 1990, Woodcock and Mason, 1996). Figure 2-1 shows an example of a typical rotary valve feeder along with various rotor configurations.

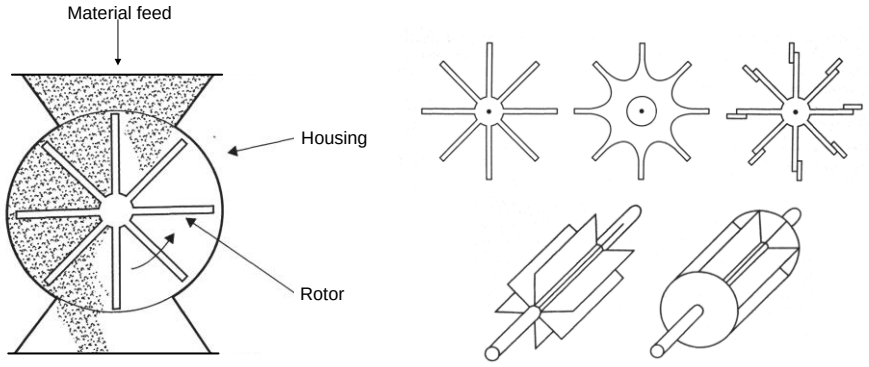

Figure 2-1: Schematic of a typical rotary valve feeder and common rotor geometries (Woodcock and Mason, 1996, Mills, 2004).

While the operating principle of a rotary valve is simple, there is one fundamental disadvantage in their use to feed solid materials to high pressure processes – pressure leakage (Guzdar and Harvey, 1982, Schell, 1988, Woodcock and Mason, 1996). Although a seal between the valve housing and the central rotor is continuously maintained during operation, for each rotation of the rotor, a portion of high pressure gas is allowed to be discharged from the high pressure region being fed to. Once the solid material is fed to the high pressure region via the rotor, a pocket of high pressure gas is stored in the vacancy left where the solid material was previously located. When the rotor is turned ready to be filled with a fresh batch of solid material, the high pressure gas is able to escape via the feeding hopper and this thus leads to a net decrease in pressure from the high pressure region (Woodcock and Mason, 1996). If both low and high pressure regions were to be sealed, the rotary valve feeder would continue discharging pressure from the high pressure region until both regions were at an equal pressure. This phenomenon is inherent in the operation of rotary valves at elevated pressures and represents their main drawback. As a consequence, rotary valves are usually reserved for use in atmospheric and low pressure processes. While there are designs available that enable feeding to pressures as high as 10-12 bar, systems are typically inefficient and encounter a large energy penalty to ensure that the pressure of the system being fed to is maintained (Levelton, 1982, Wilén and Rautalin, 1993).

2.2.1 Pressure leakage

One way to reduce the effect that pressure leakage has on the system is to connect the regions of the rotor that are filled with solid material to those that are empty and filled with high pressure gas. As

well as reducing the amount of pressure that is leaked, this balances the pressure exerted on the rotor, and enables a more secure seal to be obtained. An example of such a device is shown in Figure 2-2 (Wilén and Rautalin, 1993, Knoef and Vis, 2001).

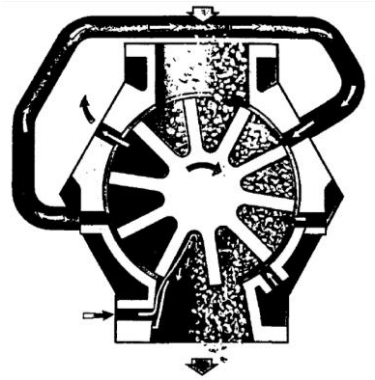

Figure 2-2: Rotary valve developed by A. Ahlstrom Corporation (Rautalin and Wilén, 1992).

Further to pressure balancing is a process called "venting" which is used to reduce the effect that pressure leakage has on pocket filling (Woodcock and Mason, 1996). Venting provides an alternative path for the high pressure gas and is typically facilitated by a series of vent holes in the body of the valve or by a pipe leading to atmosphere. Two common examples of this practice are body venting and hopper venting where the high pressure gas contained within the rotor on the up-stroke is vented via the body of the valve and the hopper respectively (Marcus et al., 1990). Figure 2-3 displays a schematic of both processes.

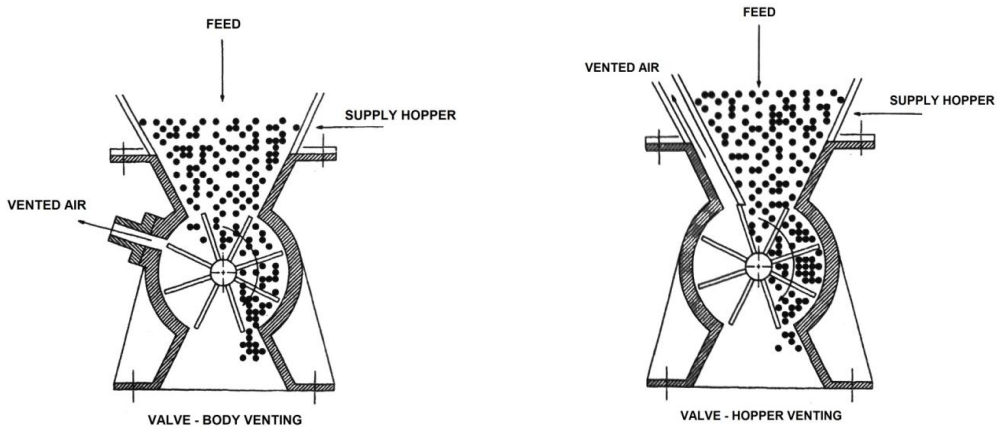

Figure 2-3: Examples of body and hopper venting in a pressurised rotary valve (Woodcock and Mason, 1996).

2.2.2 High-pressure steam usage in rotary valves

In addition to pressure balancing and valve venting, it is common for rotary valves operating at medium to high pressures to incorporate high pressure steam to ensure effective rotor discharge. As

the pocket of material being fed to high pressure approaches the high pressure environment (180 degrees through rotation), a blast of high pressure steam is administered to the pocket. The use of high pressure steam not only ensures total discharge but seeks to maintain the pressure of the vessel being fed to, as without its presence pressure would have to be maintained by alternative means (Lau et al., 2002, Rautalin and Wilén, 1992, Wilén and Rautalin, 1993). Figure 2-4 displays a design commercially available from MST Corporation, formerly developed by Bauer, and a design developed by Ingersoll-Rand (IMPCO Division) which incorporates a steam jacket further to the use of high pressure steam to encourage total rotor discharge. The incorporation of such a device (steam jacket) is to ensure even thermal expansion during operation and therefore promotes a close clearance between the rotor and valve body (Levelton, 1982).

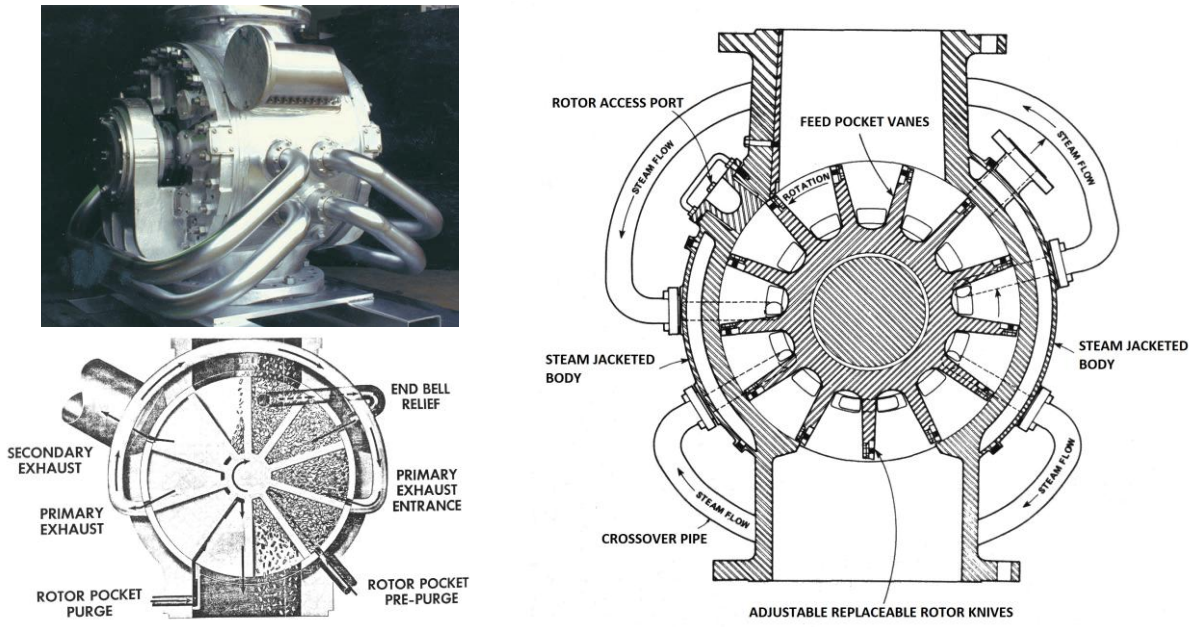

Figure 2-4: A rotary valve commercially available from MST Corporation (left) and developed by Ingersoll-Rand (IMPCO Division) (right) (Grace et al., 1989, MST, 2010).

Although rotary valve feeders are usually described as low pressure systems (Marcus et al., 1990), feeding to pressures as high as 12 bar has been reported when high pressure steam has been incorporated in their operation (Levelton, 1982, Wilén and Rautalin, 1993, Lau et al., 2002). Rotary valve feeders are used extensively in the wood pulping industry, typically feeding wood chips, wood residues and sawdust (Levelton, 1982, Swanson et al., 2003). However, rotary valves have also been used to feed a variety of biomass materials including bagasse, straw and bamboo (Lau et al., 2002). It is preferable for materials being fed to be dry and pre-treated to a size of ≤50 mm prior to feeding, as performance efficiency and throughput is greatly increased with dry and uniformly sized feedstocks (Levelton, 1982).

Advantages of rotary valve feeders are: low power consumption to operate, good feed rate control, low capital cost and compact size. However, their main disadvantage of pressure leakage when used to feed to medium and high pressure environments means pressure has to be maintained by alternative means or through the use of high pressure steam as previously discussed. This in turn increases the capital and running costs and vastly increases power consumption due to the requirement of a continuous supply of high pressure steam or inert gas. Further to this, rotary valve feeders are vulnerable to moist and sticky feeds and present the possibility of jamming due to the interaction of the solid material being fed with valve seals (Levelton, 1982, Lau et al., 2002). Commercial designs are available from: A. Ahlstrom Corporation, Ingersoll-Rand Incorporated/IMPCO Division (Beloit), Kamyr Incorporated, Zeppelin Systems, Koppers Company Incorporated, Meyer and MST Corporation (Lau et al., 2002, MST, 2010, Zeppelin, 2011, Meyer, 2012).

2.2.3 Asthma feeder

The Asthma feeder developed by Kamyr Incorporated differs from conventional rotary valve feeders in the way in which solid material is administered to high pressure environments, but incorporates many of their design cues. Figure 2-5 highlights its operation and an example of a 550 litre design.

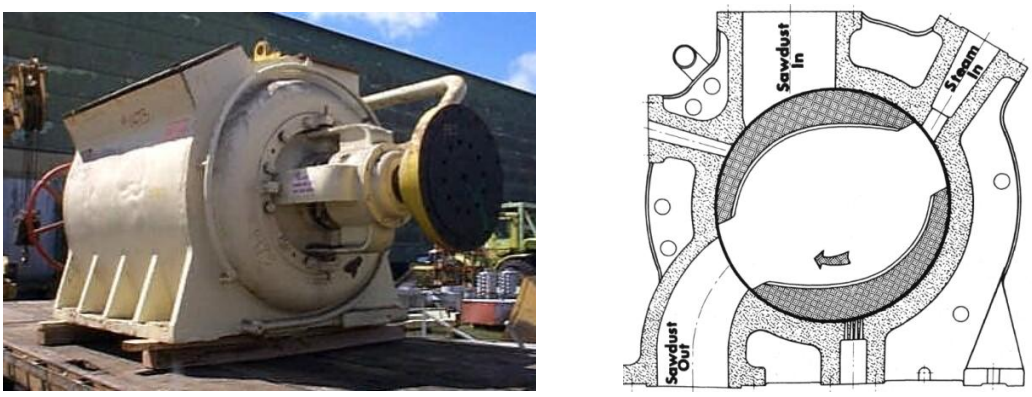

Figure 2-5: Asthma feeder developed by Kamyr Incorporated (Rautalin and Wilén, 1992, Kamyr, 2006).

The Asthma feeder contains a rotating hollow chamber which allows material to be passed from one end of the chamber to the other. The chamber is enclosed within a larger pressure chamber which separates a low pressure (atmospheric pressure) region from a high pressure region (destination vessel). The larger of the two chambers contains three key feeding lines: solid material in, solid material out and high pressure steam in. Solid material is fed to the hollow cavity of the chamber from the solid material feeding line. The chamber rotates until the hollow chamber is then lined up both with the steam in and solid material out feeding lines. High pressure steam is then blown into the hollow cavity of the chamber and displaces the solid material, effectively blowing the material into the

solid material out feeding line. The hollow chamber continues its rotation passing a depressurisation vent which acts to reduce the pressure within the hollow cavity and restores it back to low/atmospheric pressure. The cycle is then able to start anew (Rautalin and Wilén, 1992).

The Asthma feeder was originally developed for the paper and pulping industry to feed sawdust and wood residues to high pressure environments. It is able to operate continuously feeding to pressures as high as 10.34 bar with flow rates as high as 52 tonnes/h and has demonstrated the feeding of biomass materials such as straw, bamboo, jute and bagasse, as well as sawdust and wood residues (Rautalin and Wilén, 1992, Lau et al., 2002). A full scale Asthma feeder has a feeding capacity of 39 ft^3 (approx 1.1 m^3) per revolution (Kamyr, 1973).

2.2.4 Rotary valve overview

Further to the designs discussed in this section are a number of designs developed by alternative companies. Table 2-1 details feeding rates, feed materials and operating pressures associated with such designs.

Manufacturer	Feed Material	Feeding Capacity (tonnes/h)	Operating Pressure (bar)
A. Ahlstrom Corp.	Wood chips	90	12.00
C. E. Bauer (MST Corp.)	Wood chips, sawdust	113	10.34
Ingersoll-Rand Inc./IMPCO (Beloit)	Wood chips	181	10.34
Kamyr Inc.	Wood chips, sawdust	52	10.34
Koppers Company Inc.	Coal	32	10.34

Table 2-1: Overview of medium to high pressure rotary valves (Levelton, 1982).

2.3 Lock hoppers

Lock hoppers are generally considered to be the most common type of feed system where high pressure gasification is concerned (Rezaiyan and Cheremisinoff, 2005, Higman and Van der Burgt, 2008). Their operation is simple and feeding is facilitated through a central chamber or lock that undergoes cycles of pressurisation and depressurisation (Levelton, 1982, Rautalin and Wilén, 1992, Wilén and Rautalin, 1993, Mills, 2004). Although continuous operation can be brought about by operating lock hoppers in parallel, lock hoppers can be considered to be batch feed systems due to the cyclic way in which they operate. Figure 2-6 displays a design for a lock hopper developed by T. R. Miles Consulting Engineers which incorporates a metering bin and a screw feeder to enable continuous operation. Knife-gate valves are used to separate the lock vessel from the atmosphere and

the high pressure process being fed to, and compression is brought about by a stream of gas at pressure (Levelton, 1982, Guzdar and Harvey, 1982, Knoef and Vis, 2001).

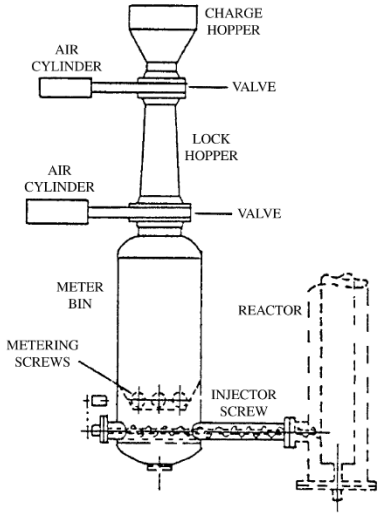

Figure 2-6: Lock hopper feed system developed by T. R. Miles Consulting Engineers (Cummer and Brown, 2002).

Making reference to Figure 2-6, the operating principle of a typical lock hopper is as follows. The top valve connecting the charge hopper to the lock hopper is opened and solid material is fed via gravity to the lock hopper. The valve is then closed and the lock hopper is pressurised using a stream of gas at pressure until the pressure inside the lock hopper equals that of the process being fed to. The bottom valve connecting the lock hopper to the high pressure process is then opened and solid material is fed via gravity to the process downstream. The bottom valve is then closed and the gas at pressure contained in the lock hopper is vented to the atmosphere. Atmospheric pressure is regained in the lock hopper and the cycle is able to start anew (Gencsoy, 1977, Jenike, 1984, Schell, 1988, Rautalin and Wilén, 1992, Wilén and Rautalin, 1993, Cummer and Brown, 2002).

Although lock hoppers represent one of the most common types of feed system for feeding solid materials to high pressure processes, they are not without their drawbacks. One fundamental to their operation is their large reliance on gas used for pressurisation, most commonly nitrogen. The largest portion of energy required by the feed system is used in this step and is ultimately wasted during the depressurisation stage (Hoffert and Stotler, 1973, Gencsoy, 1977, Rautalin and Wilén, 1992, Van der Drift et al., 2004). Both the energy and the gas used for pressurisation are wasted due to pressurisation cycling, and losses are seen to increase with increasing pressure (Funk and Reimert, 1977). Furthermore, where lock hoppers are used in close proximity with gasifiers, syngas dilution and lock gas contamination with syngas takes place due to gas mixing. Syngas dilution with nitrogen presents a significant problem where chemical synthesis processes are concerned as such processes typically

require a nitrogen free, pure syngas stream. And lock gas contamination with syngas presents a problem irrespective of the downstream process due to the loss of product gas encountered through lock gas venting. While some processes seek to minimise syngas dilution with nitrogen through utilising syngas as the pressurising gas, far higher degrees of lock gas contamination are brought about and in turn far greater energy penalties are incurred (Higman and Van der Burgt, 2008). It is for this reason that nitrogen is predominantly used as the pressurising gas in lock hopper systems.

Although they present disadvantages in their operation, lock hoppers are the most widely tested and deployed high pressure feed system where gasification is concerned (Schell, 1988, Rezaiyan and Cheremisinoff, 2005, Higman and Van der Burgt, 2008). They are capable of operating at pressures as high as 90 bar and delivering feed capacities of up to 80 tonnes/h (Lau et al., 2002). Notable designs are the: Lurgi, Macawber Controlveyor and the Miles Biomass System (Swanson et al., 2003). The Lurgi lock hopper has a reported energy requirement of approximately 24 kJ/kg at 25 bar and 100 kJ/kg at 76 bar (DOE, 1965).

Further to the designs discussed in this section are a number of designs developed by alternative companies. Table 2-2 details feeding rates, feed materials and operating pressures associated with such designs.

Manufacturer	Feed Material	Feeding Capacity (tonnes/h)	Operating Pressure (bar)
Lurgi	Coal	70	84.94
Petrocarb Inc.	Peat, coal, ore, dolomite	55	41.37
T. R. Miles Consulting	Wood chips, wood pellets	2	20.68
Macawber	Coal	12	31.03

Table 2-2: Overview of lock hoppers (Levelton, 1982).

2.3.1 Dual lock hoppers

One way to minimise waste and increase the cycle efficiency of lock hoppers is to use two lock hopper units running in parallel (Hawrych, 1981, Guzdar and Harvey, 1982, Jenike, 1984, Lau et al., 2002, Swanson et al., 2003). This allows one lock hopper's central chamber to be partially pressurised during the opposing lock hoppers depressurisation stage, and in turn reduces the energy lost due to depressurisation. Figure 2-7 highlights such a design used at a pilot plant in Dorsten, Germany.

Theoretically, dual lock hoppers can save up to half of the energy required for pressurisation compared to conventional single lock hoppers (Jenike, 1984). However, in practice only around 30-40% of the energy losses encountered can be recovered (Funk and Reimert, 1977, Hawrych, 1981). Where dual lock hoppers are used, it is common to have three lock hopper units operating in parallel. This allows

a continuous flow of solid material to the downstream process to be maintained while one unit is taken offline for maintenance (Jenike, 1984).

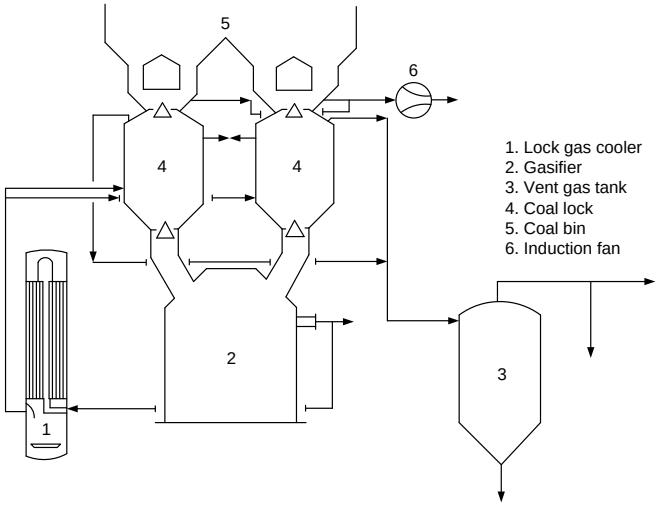

Figure 2-7: Dual lock hopper arrangement for a pilot plant in Dorsten (Funk and Reimert, 1977).

2.3.2 Liquid sealed lock hoppers

One type of lock hopper design that differs from conventional gas filled lock hoppers is the liquid sealed lock hopper. The liquid sealed lock hopper harnesses both the reliability and functionality of standard gas filled lock hoppers but looks to resolve the operational disadvantages that standard gas filled lock hoppers present. Process gas leakage is minimised, valves are able to be kept lubricated and free of discharge when feeding dusty feedstocks, and minimal amounts of compression work are required compared to gas filled lock hoppers (Casperson, 1983).

Liquid filled lock hoppers utilise an incompressible fluid, typically water, to minimise the compression work required (Casperson, 1983). Solid feed material is passed from atmospheric or low pressure through the incompressible fluid and into the high pressure environment while the pressure boundary is maintained by pumping the incompressible fluid against the process pressure. Therefore, the only compression work required is that needed to pump an incompressible fluid against pressure.

One particular design of note is displayed in Figure 2-8, whereby almost no compression work is required. A series of screw feeders and valves allow permanent troughs of water to be maintained while feeding solid material to high pressures. The pressure boundary is maintained by the closing of valves and the only work required is that for replenishing the water absorbed by the fuel, and the small amount of pressure stored in each of the compressed water pockets. Similarly, this concept can be used to remove solid material from a high pressure environment, ensuring process pressure is maintained at all times (Casperson, 1983).

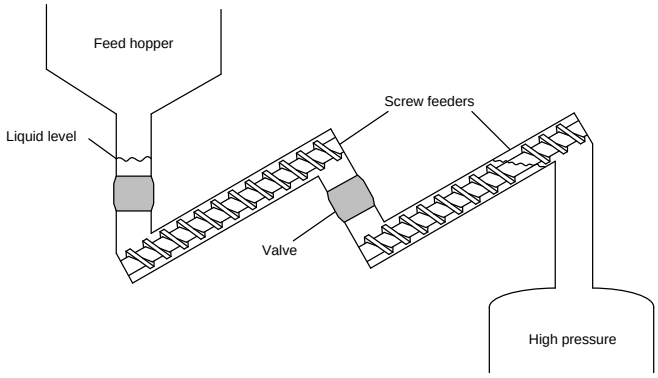

Figure 2-8: Example of a liquid filled lock hopper (Casperson, 1983).

Although liquid filled lock hoppers present advantages in terms of the compression work required, minimisation of gas leakage, and the wear encountered with process valves, the fundamental drawback of liquid filled lock hoppers is that the material being fed becomes saturated with water. In applications such as combustion and gasification where fuel moisture content directly affects process efficiency, it means that standard gas filled lock hoppers or alternative feed systems are chosen in favour. However, it is important to state that liquid filled lock hoppers present an efficient feed system for avenues that do not require dry feedstocks (Casperson, 1983).

2.4 Plug-forming feeders

Plug-forming feeders propose a fundamental difference to feed systems such as lock hoppers and rotary valve feeders through the way in which the pressure seal is created. Lock hoppers and rotary valves create a pressure seal through mechanical means, whereas plug-forming feeders act to create a dense plug of material that poses as the pressure boundary (Schell, 1988). Plug-forming feeders can be split into two key categories: screw plug-forming feeders and piston plug-forming feeders, and each of these categories will be discussed in the following sections.

2.4.1 Screw plug-forming feeders

Screw plug-forming feeders can be broadly described as systems that utilise a screw to create a dense plug of material to form a pressure boundary (Levelton, 1982). While numerous designs are available incorporating different screw geometries, screw plug-forming feeders most commonly utilise a variable cross-sectional screw which sits inside a tapered screw casing. As solid material is promoted through the screw, the constant rotational motion coupled with the decreasing available volume due to the constricted throat of the of screw case forms a plug of material which acts as the pressure boundary between the atmosphere and the high pressure environment being fed to (Smith and Pote, 1983, Mills,

2004). Figure 2-9 shows an example of both a variable and a constant cross-sectional screw plug-forming feeder.

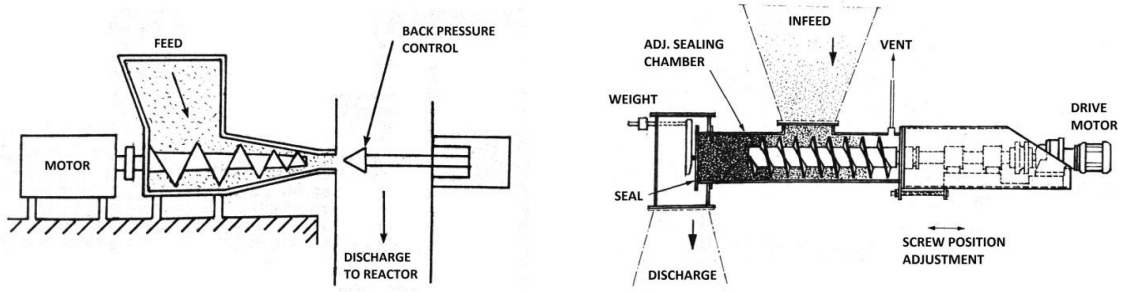

Figure 2-9: Example of a variable screw plug-forming feeder with conical blow back damper (left) and a constant cross-sectional screw feeder with weighted non-return valve (right) (Levelton, 1982).

Plug-forming feeders are commonly used in the paper and pulping industry, and wood chips are regularly handled as feedstocks. Due to the high moisture content of wood chips (up to 50 wt%), dewatering typically takes place during the densification stage and consequently perforated plates have to be fitted to allow the moisture generated to be drained (Swanson et al., 2003, Sattari-Far, 2003). As the feed material increases in density and passes through the throat section of the feeder, it enters a cylindrical plug pipe where further densification is encountered. A device called a blow back damper, choke or weighted non-return valve enables a back pressure to be exerted and the density of the plug to be increased further (Levelton, 1982, Wilén and Rautalin, 1993, Mills, 2004). At this stage, the solid feed is now dense enough to facilitate a pressure seal by itself.

One important feature of the blow back damper is that it provides a secondary pressure seal if the plug formed is not dense enough to facilitate a pressure seal alone (Johanson, 1991). The blow back damper is provided with enough force so that it creates a seal with the cylindrical plug pipe and further increases the density of the feed material until a suitable pressure seal is generated by the feed unaided. It is common for blow back dampers to be conical in shape, although flat weighted non-return valves can also be used. An important function of the blow back damper when in a conical arrangement is that it facilitates the breaking up of the plug once the material is fed to the high pressure chamber. This has a particular advantage where less dense large surface area feedstocks are required (Lau et al., 2002, Swanson et al., 2003). A variable cross-sectional screw feeder developed by Koppers Company Incorporated utilises such a device, and has demonstrated the feeding of wood chips to pressures as high as 13.79 bar at feed rates of 25.4 tonnes/h. The Koppers screw feeder also has an energy requirement of approximately 20 kJ/kg (Levelton, 1982). Similarly, the General Electric Company has developed an extrusion type plug-forming feeder for a coal fed gasifier (GEGAS-D). It has demonstrated the feeding of coal to pressures as high as 20.68 bar at feed rates of

0.91 tonnes/h. The feeder is also fitted with a "chopper" which seeks to break up the dense plug formed once it has entered the gasifier (Levelton, 1982).

Screw plug-forming feeders can utilise various screw types: variable cross-section, constant cross-section and multiple intermeshing screws (Levelton, 1982). Intermeshing or twin screw feeders are generally adopted when higher pressures are encountered and good control of feeding is required. They also have the added advantage of wiping each other and the barrel in which they sit, clean. This ensures that feed material is kept moving and avoids caking which is a common operational problem when dealing with screw plug-forming feeders (Guzdar and Harvey, 1982, Levelton, 1982). Examples of varying screw types produced by and available from MST Corporation are displayed in Figure 2-10, and an example of a twin screw feed system for feeding coal to high pressure reactors developed by Werner and Pfleider is shown in Figure 2-11.

Figure 2-10: Screw types available from MST Corporation (MST, 2010).

The design developed by Werner and Pfleider predominantly consists of two co-rotating screws situated in a heated barrel (Wiedmann and Mack, 1977, Gall and Johnson, 1983). Accurate feeding of coal to the screw feeding section is ensured by a coal conveyor, hopper and weigh belt feeder working in series prior to coal injection to the screw feeding element. The co-rotating screws fully intermesh with each other as displayed in Figure 2-11 and the self-wiping motion promotes continuous conveyance of coal without the formation of dead spots (Wiedmann and Mack, 1977, Levelton, 1982). The Werner and Pfleider screw feeder has been proven to feed both coal and sawdust to pressures as high as 1500 psi (103.42 bar), and has a maximum theoretical feeding pressure of 206.8 bar. Feeding rates as high as 0.45 tonnes/h with coal and 0.1 tonnes/h with sawdust have been reported, with energy requirements of 81 kJ/kg at pressures of 103.42 bar (Levelton, 1982).

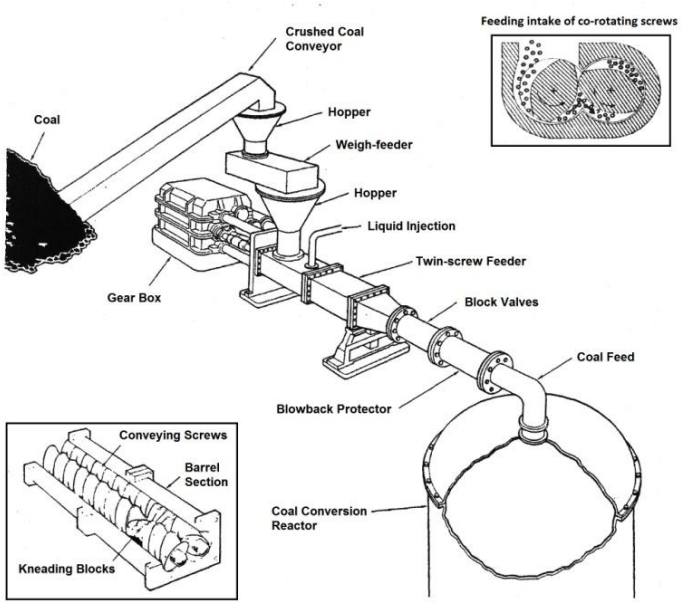

Figure 2-11: Twin screw feeder developed by Werner and Pfleider (Guzdar and Harvey, 1982).

Although screw plug-forming feeders present advantages in terms of low inert gas consumption, continuous feeding and compact design, disadvantages prove costly both in terms of maintenance and operation (Lau et al., 2002). High frictional forces garner high energy consumption and thus high operational costs, and severe erosion of mechanical parts means equipment has to be replaced on a regular basis. In addition to this, where very dry materials are required to be fed, plug formation can be problematic. Although the implementation of a weighted non-return valve or a blow back damper looks to promote plug formation, the lack of moisture present in the feed can cause problems when feeding (Sattari-Far, 2003). Commercial designs are available from: Metso Corporation (formerly Sunds Defibrator), Kamyr Incorporated, A. Ahlstrom Corporation, Koppers Company Incorporated, General Electric Company, Werner and Pfleider and MST Corporation (Wilén and Rautalin, 1993, Lau et al., 2002, Cummer and Brown, 2002, Swanson et al., 2003, MST, 2010, Metso, 2009).

2.4.2 Piston plug-forming feeders

Piston plug-forming feeders are another group of feed systems that utilise a plug of solid material to create and maintain a pressure boundary. The principal difference to competing designs incorporating screws is that a hydraulic piston is used to generate the plug. Figure 2-12 shows a design developed by TK Energi to feed biomass to high pressure environments.

The feed system is comprised of an atmospheric supply hopper, a hydraulic piston and a tapered plug-tube. Solid material is fed to the main body of the feeding device from the atmospheric supply hopper via gravity. The hydraulic piston acts on the feed material and compresses it through the tapered plug-

tube until a plug of material is formed. High radial pressures are generated in the plug and a pressure seal is maintained due to the plug once the hydraulic piston has retreated to its original position; this in turn allows further solid material to be fed. During the compression stage, a plug is transported to the high pressure environment while simultaneously adding to the dense material contained within the plug-tube (Van der Drift et al., 2004).

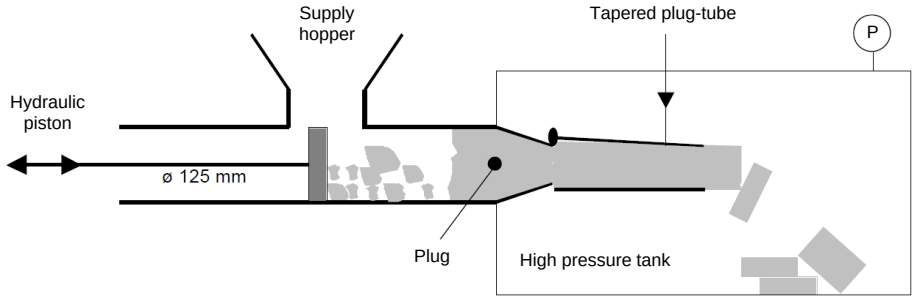

Figure 2-12: Overview of a small scale piston plug-forming feeder developed by TK Energi (Van der Drift et al., 2004).

The main drawback as with all plug-forming feeders is the high frictional force generated by forming the plug; this leads to high power consumption and mechanical wear. However, piston plug-forming feeders are more suited to feeding dry fuels than screw plug-forming feeders. The feed system developed by TK Energi displayed in Figure 2-12 is capable of feeding to pressures as high as 20 bar at feed rates of 10 tons/h (9.07 tonnes/h) and has demonstrated feeding of torrefied wood, straw and bagasse (Lau et al., 2002, Van der Drift et al., 2004). Further to both screw and piston plug-forming feeders are a number of designs developed which incorporate both feeding principals. These feed systems are discussed in the following sections.

2.4.3 Foster-Miller screw-piston plug-forming feeder

The Foster-Miller screw-piston plug-forming feeder was developed to feed pulverised coal to pressurised reactors and utilises a hydraulic ram incorporated into a constant cross-sectional screw feeder to further densify plugs of material formed (Harding, 1977, Guzdar and Harvey, 1982, Swanson et al., 2003). The feed system developed by Foster-Miller Associates is comprised of a supply hopper, a constant cross-sectional screw feeder, a feeding barrel, a hydraulic cylindrical ram and a weighted non-return valve. Solid material is fed via gravity from the supply hopper to the screw feeder. The screw feeder retracts via the hydraulic ram and simultaneously rotates delivering a portion of solid material to the feeding barrel which is void due to the retraction of the screw feeder. The hydraulic ram acts and pushes the screw feeder forward causing the formation of a dense plug of material. Once

the pressure exerted by the hydraulic ram and the plug formed exceeds the pressure of the high pressure vessel being fed to, the weighted non-return valve opens and allows the feeding of material to the high pressure vessel. In this case, the plugs of material formed do not form an absolute seal, but form a plug with low permeability. Once the check valve is returned to its closed position, the cycle is able to start anew (Harding, 1977).

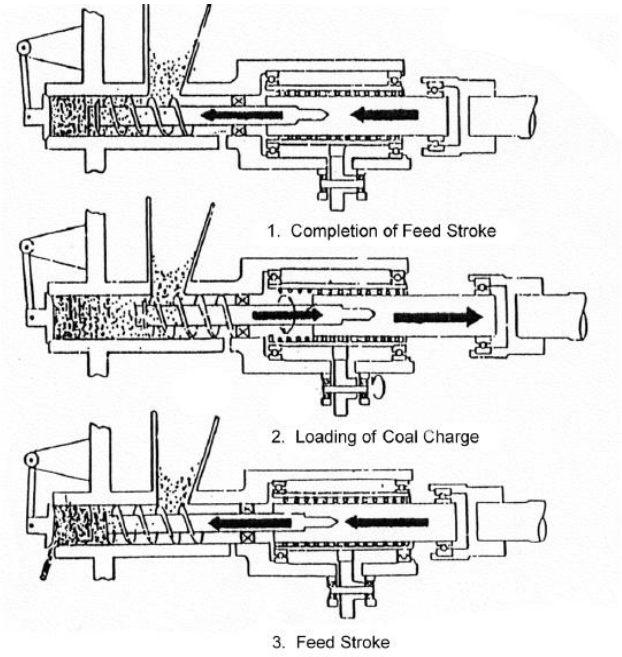

Figure 2-13: Operating principle of the Foster-Miller screw-piston plug-forming feeder (Harding, 1977).

Disadvantages of the feed system are that it operates as a batch process, has a large power requirement and encounters severe wear due to high frictional forces generated during plug formation. The screw-piston plug-forming feeder has demonstrated reliable feeding of pulverised coal to pressures as high as 1200 psi (82.74 bar) with low pressure leakage through the plugs of material formed (Harding, 1977).

2.4.4 Ingersoll-Rand heated screw plug-forming feeder

Ingersoll-Rand have developed a plug-forming feeder which utilises a heated screw to aid plug formation. A schematic of the feed system is shown in Figure 2-14. The feed system is comprised of a feeding hopper, a screw, a barrel fitted with heating elements, a nozzle and a hydraulic injection cylinder. Coal is fed via gravity from the feeding hopper to the rotating screw. The screw conveys the coal along the barrel and compacts the coal sufficiently so that a plug of material is formed. The heating elements fitted to the barrel in which the screw rotates can be employed accordingly depending on the feedstock being processed and the rigidity of the plug formed. Once the plug of material formed is able to sufficiently prevent pressure leakage it is subsequently discharged into the

high pressure environment through the nozzle by the hydraulic injection cylinder. The addition of heat seeks to promote coal to its semi-plasticised state. As the screw continues to operate, the coal is further compacted and agglomerated, and a cylindrical plug of material able to maintain a pressure boundary is formed (Mistry and Chen, 1977, Mistry and Hathaway, 1982).

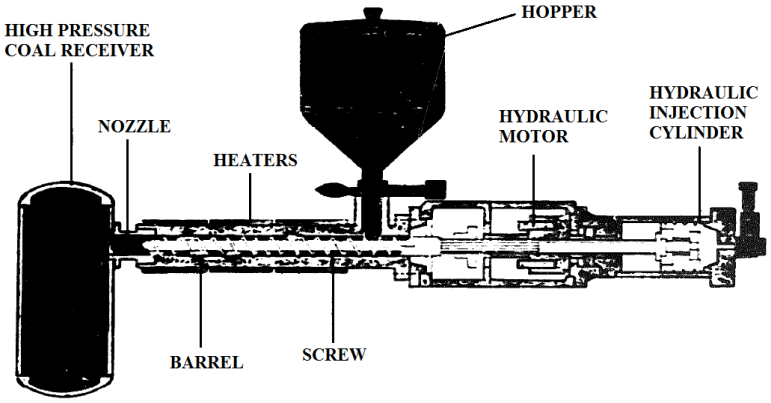

Figure 2-14: Ingersoll-Rand heated screw plug-forming feeder (Mistry and Chen, 1977).

Although the application of heating elements solves some of the operational problems encountered in conventional screw plug-forming feeders, operational problems specific to the new design are generated. Pockets of volatile vapours are created during operation due to the heating and partial pyrolysis of the feedstock. When the feedstock is compressed, the pockets of vapour formed are also compressed and this in turn causes plugs of material to be periodically discharged with force into the high pressure vessel being fed to; such a phenomenon therefore poses unpredictability in the feeding rate. In addition to this, the volatile vapours formed also tend to migrate back to the atmospheric feeding hopper due to the pressure differential in place. This causes the condensation of volatile vapours on the incoming feed material and increases the likelihood of problems such as bridging and solids holdup taking place. Problems due to the condensation of volatile vapours on incoming feedstock can be minimised through the employment of vents in the barrel near to the intake area of the feeder (Mistry and Chen, 1977).

The Ingersoll-Rand heated screw plug-forming feeder has demonstrated feeding rates of coal as high as 2 tons/h (1.81 tonnes/h) to pressures as high as 750 psi (51.71 bar) (Mistry and Hathaway, 1982). A typical energy requirement with (51.71 bar) and without (20.68 bar) the employment of the heating elements is 75 kJ/kg (Guzdar and Harvey, 1982). A similar design developed by the National Aeronautics and Space Administration is available which incorporates a heated screw feeder without the extrusion mode. Coal is heated in a screw fed barrel to temperatures where the coal assumes plastic properties, and extrusion is enabled by further screw feeding (Ryason, 1980).

2.4.5 Vattenfall screw-piston plug-forming feeder

Vattenfall Energiesystem AB have also developed a screw-piston feeding device to feed low density biomass fuels such as peat and straw (Knoef and Vis, 2001, Lau et al., 2002). A schematic of the system is shown in Figure 2-15.

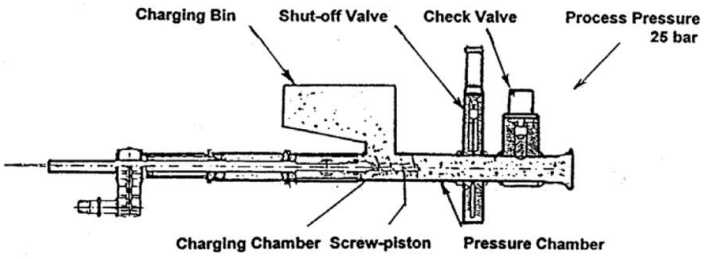

Figure 2-15: Vattenfall screw-piston plug-forming feeder for feeding biomass fuels (Knoef and Vis, 2001).

The feed system incorporates similar components to competing screw-piston plug-forming feeders and consists of a charging bin, a cylindrical chamber in which a hydraulically enabled feeding screw sits and a check valve to ensure a secure pressure seal is maintained if plug formation fails. The screw used in the system developed by Vattenfall both operates as a screw feeding device and as a piston. Solid material is fed from the charging bin to the rotating screw which is seated in the cylindrical chamber. The screw continues to feed the solid material towards the pressure chamber until the onset of plug formation. The charging of solid material from the charging bin is stopped and the piston component of the screw feeder is then enabled. The screw is then advanced in the direction of the pressure chamber which further densifies the plug of material and ensures a secure pressure seal is formed, utilising the plug of solid material as the pressure boundary. As a new plug of material is formed, a previously formed plug is promoted to the high pressure vessel being fed to; the screw-piston retreats and the cycle is able to start anew (Knoef and Vis, 2001).

The screw-piston feeder developed by Vattenfall Energiesystem AB has demonstrated the feeding of low density materials such as peat and straw to pressures as high as 25 bar and at feed rates as high as 3.6 tonnes/h (Knoef and Vis, 2001).

2.4.6 Stake Technology coaxial feeder

The Stake Technology coaxial feeder was developed for digesting cellulosic biomass and utilities a coaxial screw and a separate piston to form and recompress a plug of material before feeding to high pressure environments. A schematic of the feed system is shown in Figure 2-16.

The feed system developed by Stake Technology consists of a screw feeder lined atmospheric hopper, a main central screw which operates inside a hollow piston (sleeve) and a conical blow back damper.

Solid material is fed via the screw feeder lined atmospheric hopper to the main central screw feeder located below the hopper. Material is then fed via the central screw feeder to a plug compression channel. The central feeder operates within the hollow piston while the piston simultaneously moves backwards in the direction of the atmospheric feeding hopper. During this operation, solid material is fed to the front of the piston face into the plug compression channel; the piston is said to be in its back position at this stage. The piston then advances and compresses the material forming a plug; material is said to be most compact where the surface of the piston acts. The material adjacent to the hollow chamber of the piston is less compact and further compression of the material in this area is brought about by further feeding from the main central screw. The geometry of the plug channel (plug channel taper) can be altered depending on the feedstock being used to create a more substantial plug of material. The piston continues to advance and the plug of material formed is fed against the conical blow back damper which acts to maintain a pressure seal during plug formation, and to break up the plug of material once the plug is exerted against it. Once the piston has advanced to its farthest point, it retreats and the blow back damper resumes the pressure seal (Guzdar and Harvey, 1982, Levelton, 1982, Rautalin and Wilén, 1992).

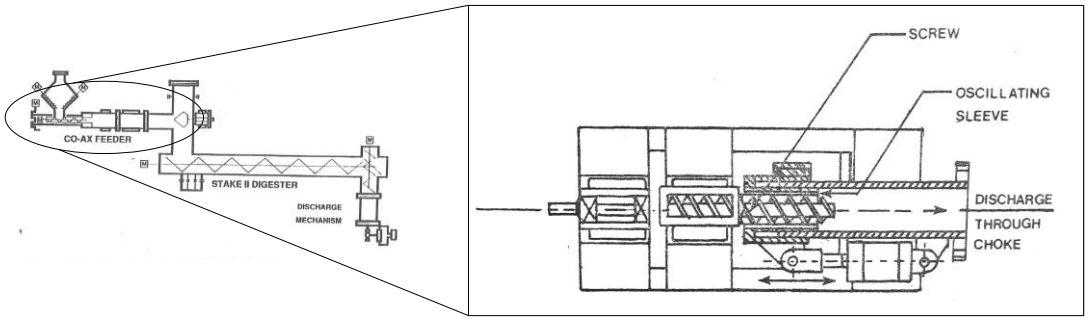

Figure 2-16: Schematic of the coaxial feeder developed by Stake Technology (Levelton, 1982, Rautalin and Wilén, 1992).

The Stake Technology coaxial feed system was developed for digesting cellulosic biomass under pressure. It has demonstrated the feeding of wood chips at a rate of 4-5 tonnes/h to a pressure of 300 psi (20.68 bar) and has an energy requirement of approximately 60 kJ/kg (Guzdar and Harvey, 1982). Feeding of wood sawdust, bark (5 cm square), bagasse and straw have also been reported to be fed to pressures as high as 55.15 bar (Levelton, 1982).

2.4.7 Plug-forming feeder overview

Table 2-3 provides an overview of the plug-forming feeders discussed in this section as well as further designs available from alternative companies. Feed systems are characterised by feed rates, feed materials and operating pressures.

Manufacturer	Feed Material	Feeding Capacity (tonnes/h)	Operating Pressure (bar)
Koppers Company Inc.	Wood chips	25.40	13.79
General Electric Co.	Coal	0.91	20.68
Werner & Pfleiderer	Coal, sawdust	0.45	103.42
TK Energi	Torrefied wood, straw, bagasse	9.07	20.00
Foster-Miller Associates	Coal	-	82.74
Ingersoll-Rand	Coal	1.81	51.71
Stake Technology	Wood chips, sawdust, bark, bagasse, straw	5.00	55.15
Vattenfall Energiesystem AB	Peat, straw	3.60	25.00

Table 2-3: Overview of plug-forming feeders. Adapted from (Levelton, 1982).

2.5 Piston feeders

Piston feeders are conceptually the same as lock hoppers, but include a displacement piston to conserve the high pressure gas typically vented to atmosphere. The use of hydraulics allows much of the compression work to be done by an incompressible fluid and thus energy required for compression is vastly reduced when compared to conventional lock hopper systems (Guzdar and Harvey, 1982). Many types of piston feeders are available in the literature and the following section aims to provide an overview of those developed for use in high pressure applications.

2.5.1 Fortum piston feeder

The Fortum piston feeder utilises three principal components: a feeding bin, a constant cross-sectional screw feeder and two hydraulically linked pistons. Feeding is able to take place semi-continuously by simultaneous charging and discharging of solid material from atmospheric pressure to high pressure environments. Figure 2-17 displays a schematic of the Fortum piston feeder.

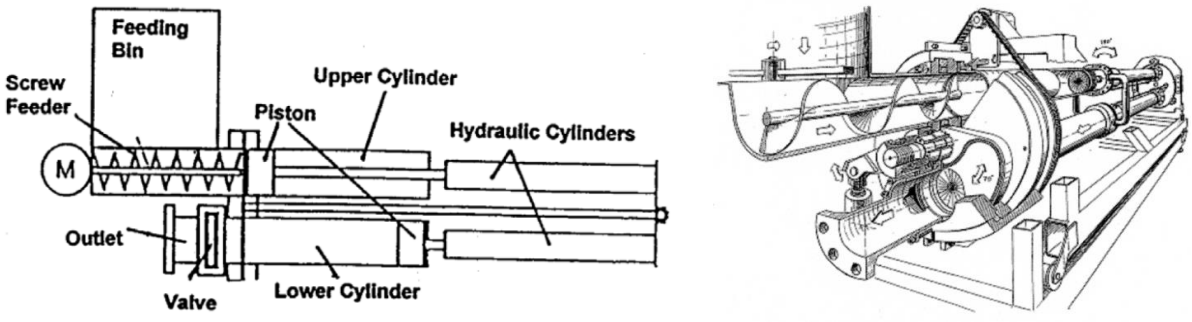

Figure 2-17: Schematic of the Fortum piston feeder (Lau et al., 2002, Swanson et al., 2003).

Solid material is fed from the feeding bin via the screw feeder to the upper cylinder (C1), and acts against the upper piston (P1). P1 is hydraulically linked to the lower piston (P2) so that as P1 is compressed and driven forward, P2 acts in the opposite direction towards the feeding bin. The piston setup is so that a force in one direction (right) causes an opposing force in the opposite direction (left), allowing a reduced footprint of the feeder. When C1 is full and P1 is fully depressed, a valve (V1) is shut sealing C1, and C1 and C2 (lower cylinder) rotate parallel to each other through 180 degrees so that the positions of C1 and C2 are exchanged. As solid material is fed to C2, P2 is retracted and a force is exerted on P1 and in turn the material contained within C1, until the pressure inside C1 is brought up to or above system pressure. V1 is then opened and the solid material is fed from the outlet of C1 to the desired pressurised environment as C2 continues to be filled with solid material. When C1 is empty and in turn C2 is full, both V1 and V2 are closed and C1 and C2 rotate parallel through 180 degrees. V1 is opened and the cycle is able to start anew allowing a new batch of solid material to be fed to C1 and a batch of material to be fed to the pressurised environment from C2 once the material in C2 has been sufficiently compressed, and V2 has been opened (Lau et al., 2002, Swanson et al., 2003).

Advantages of the Fortum design are low inert gas consumption and low energy consumption for compression (Lau et al., 2002). The Fortum piston feeder has a reported energy requirement of 18 kJ/kg and has fed to pressures as high as 23 bar. Feed rates of approximately 1 tonne/h feeding materials such as peat, saw dust and sludge have been demonstrated (Lau et al., 2002, Swanson et al., 2003).

2.5.2 Ingersoll-Rand coaxial piston feeders

The Ingersoll-Rand coaxial piston feeder utilises a similar principal to that of the Fortum piston feeder, whereby the seal is formed mechanically with the piston sealing against the material cylinder (Mistry and Chen, 1977, Mistry and Wise, 1978). The key advantage of the coaxial piston feeder is in the use of a twin transport and gas exclusion piston setup. The transport piston serves to provide a seal between the atmospheric feeding hopper and high pressure destination vessel, transport the feed material to the high pressure environment, provide a means of protecting the piston seals from abrasive interactions, and clean the transport cylinder of feed material before the start of a new cycle. The gas exclusion piston serves to enable pressure equalisation of the feed charge and to return gas at process pressure back to the process (Mistry and Wise, 1978, Mistry and Hathaway, 1982). Figure 2-18 highlights the five key stages in its operation.

Solid material is fed from a hopper via gravity to the cavity between the gas exclusion and the transport piston. The transport piston proceeds and inert gas is then fed via ports in the face of the gas exclusion piston and pressurises the pocket of feed material up to or above system pressure. Both

pistons then move simultaneously allowing the pocket of pressurised feed material to be transported towards the discharge opening where the solid material is then fed to the high pressure vessel via gravity. As the solid material drops, the gas exclusion piston moves so that its face meets the face of the transport piston. Pressurised gas that is trapped between the two pistons is able to be vented through the ports located in the gas exclusion piston. The two pistons then move towards their original positions, again leaving a cavity available for a fresh batch of solid material to be fed (Mistry and Chen, 1977, Mistry and Wise, 1978, Hawrych, 1981, Levelton, 1982, Mistry and Hathaway, 1982, Swanson et al., 2003). The Ingersoll-Rand coaxial piston feeder can be thought of as a moving lock hopper, as inert gas is required to bring the transport cavity up to system pressure.

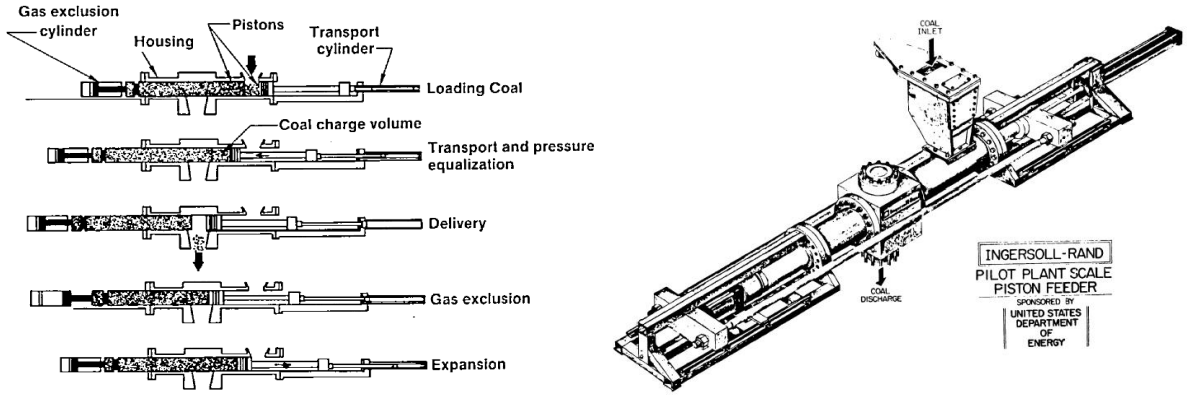

Figure 2-18: Operational stages of the Ingersoll-Rand coaxial piston feeder (Mistry and Hathaway, 1982).

Further to the single coaxial piston feeder developed by Ingersoll-Rand is the double acting piston feeder. The operating principle is similar to the single coaxial piston feeder described above and is outlined in Figure 2-19. The feed system contains two pistons located at a fixed distance from each other within a common shaft, a floating piston between the two pistons and two atmospheric feeding hoppers (Mistry and Wise, 1978, Bell Jr, 1979, Hawrych, 1981).

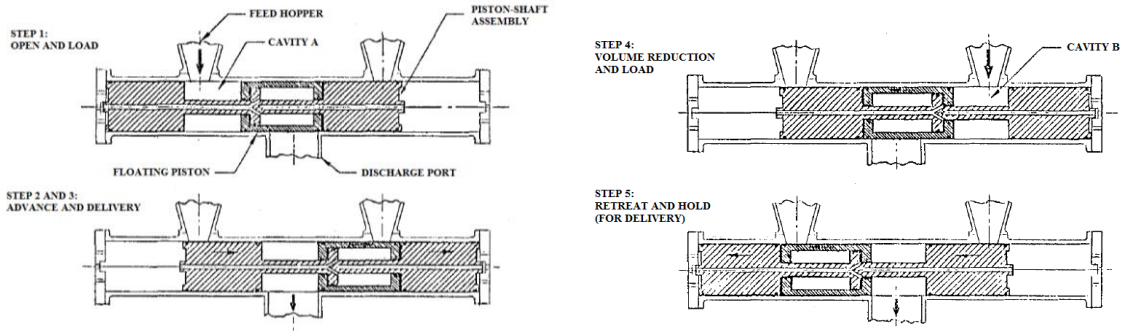

Figure 2-19: Operational stages of the Ingersoll-Rand double acting piston feeder (Mistry and Wise, 1978).

Solid material is fed from an atmospheric hopper via gravity to cavity A (left). The floating piston is currently located above the discharge port, effectively sealing the high pressure region from the atmosphere. Piston A (left) acts, pushing the batch of feed material against the floating piston which in turn acts against piston B. The floating piston and piston B are displaced to the furthest point (right) which in turn allows the batch of solid material to be fed to the high pressure environment. The floating piston then acts against piston A simultaneously returning the portion of pressurised gas back to the high pressure environment and allowing a region (cavity B) between piston B and the floating piston to be formed where a new batch a solid material can be fed from the second atmospheric feeding hopper. This cycle then takes place in reverse allowing the second batch of material to be fed to the high pressure environment. The overall cycle is then ready to start anew (Mistry and Chen, 1977, Mistry and Wise, 1978, Bell Jr, 1979, Hawrych, 1981).

The Ingersoll-Rand coaxial piston feeder has demonstrated the feeding of coal at feed rates of up to 2.5 tons/h (2.27 tonnes/h) and to back pressures of up to 100 bar. It is envisaged that operation at such back pressures is possible with the double piston arrangement with increased throughputs; however, the single coaxial piston design was chosen in favour during development due to its simpler design (Hawrych, 1981, Levelton, 1982, Swanson et al., 2003). The energy requirement of the single coaxial piston feeder operating at a pressure of 23 bar is approximately equal to 13 kJ/kg (Levelton, 1982).

2.5.3 Foster-Miller linear pocket feeder

The linear pocket feeder developed by Foster-Miller Associates comprises a system whereby a series of pistons connected in series are utilised to feed solid material to pressurised processes without the need for inert gas. The feeder is composed of a tubular conveyor containing a series of equally spaced pistons connected by a chain, an atmospheric feeding hopper, a water-gas transfer station whereby pockets of pressurised gas are recovered by displacing water, and an accompanying gas dryer (Harding, 1977, Chandrasekhar and Harding, 1978, Hawrych, 1981, Fleming et al., 1982, Guzdar and Harvey, 1982, Schell, 1988).

Solid material is fed at atmospheric pressure via gravity to one of the pockets on the continuously moving drive chain. The pockets present a series of seals from high pressure to atmospheric pressure by the presence of the pistons used to form the pockets. The solid material is discharged to the high pressure process via gravity and the pocket formed by the pistons is in turn filled with high pressure gas. The pocket of high pressure gas then enters a water-gas transfer station. The pocket of high pressure gas is displaced by water and is released allowing it to be fed back to the system via a dryer due to the water-gas station being maintained at a slightly higher pressure than the high pressure process itself. As the pistons continue to move through the water-gas station and along the chain conveyor, a pocket of water is discharged to a reservoir, treated and re-used in the process (Harding,

1977, Chandrasekhar and Harding, 1978, Hawrych, 1981, Fleming et al., 1982). Continuous feeding is presented and the feed rate is controlled by the speed of the conveyor chain.

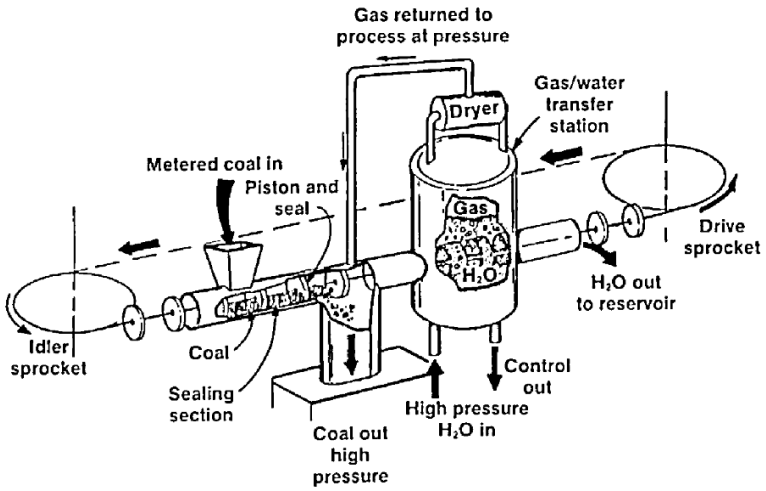

Figure 2-20: Foster-Miller linear pocket feeder process overview (Guzdar, 1985, Schell, 1988).

The water-gas station comprises the primary advantage of the Foster-Miller linear pocket feeder. It allows the compression work to be done by an incompressible fluid (water) and high pressure gas to be recycled. Pressures are also able to be balanced using the high pressure recycle and thus no extra work is required for the piston drive chain to overcome high pressures; only frictional forces are required to be overcome (Fleming et al., 1982). The Foster-Miller linear pocket feeder is capable of feeding to pressures as high as 1000 psi (68.95 bar) and has demonstrated the feeding of coal at flow rates of 5 tons/h (4.54 tonnes/h) (Hawrych, 1981, Fleming et al., 1982, Guzdar and Harvey, 1982, Swanson et al., 2003). A typical energy requirement at 34.5 bar is approximately 28 kJ/kg (Levelton, 1982).

2.5.4 Schlepper displacement piston feeder

The Schlepper piston feeder developed by Lurgi is perhaps the simplest piston feeder developed to date. It utilises a single displacement piston to promote semi-continuous feeding of solid material to high pressure environments (Funk and Reimert, 1977, Hawrych, 1981, Levelton, 1982, Guzdar and Harvey, 1982).

Solid material is fed via gravity from the supply hopper through a ball valve to the main feeding chamber. The displacement piston is deployed forming a seal between the supply hopper and the main feeding chamber. Pressure equalisation takes place by opening two valves in the pressure equalisation pipe connecting the main feeding chamber and the high pressure destination vessel. A valve is opened allowing the solid material from the main feeding chamber to be fed to the high pressure destination

vessel. The piston is then advanced, effectively reducing the amount of high pressure gas contained within the main feeding chamber to a minimum. The sealing valve is then closed and the piston is retracted to its original position allowing the cycle to start anew (Funk and Reimert, 1977, Hawrych, 1981, Levelton, 1982, Guzdar and Harvey, 1982).

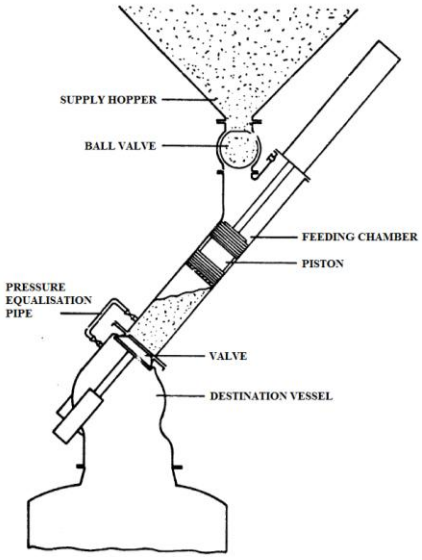

Figure 2-21: Schlepper piston feeder developed by Lurgi (Guzdar and Harvey, 1982).

The volume of high pressure gas between the face of the piston and the sealing valve is minimal. Once the piston has been retracted the gas is available at sub-atmospheric pressure and thus does not hamper the flow of solids from the next batch of feed material. To ensure smooth operation, a limited charge must be metered to the main feeding chamber per cycle to ensure an adequate seal is formed by the piston in the feeding chamber. The main advantage of the Schlepper piston feeder is that the waste of gas at pressure is minimised (Funk and Reimert, 1977, Hawrych, 1981, Guzdar and Harvey, 1982).

The Lurgi Schlepper piston feeder is capable of feeding coal to pressures as high as 30 bar and delivering flow rates of 20 tonnes/h (Funk and Reimert, 1977, Levelton, 1982). Further to the Lurgi Schlepper piston feeder, there are a number of designs for single displacement piston feeding devices available. Notably are those presented by Stevenson and Chambert which use similar setups to that displayed by the piston device developed by Lurgi (Stevenson, 1985, Chambert and Skog, 1992, Hallgren et al., 1993).

2.5.5 Putzmeister EKO high-density solids pump

Putzmeister have developed a number of systems to feed dry solids, slurries and partial slurries to high pressure environments. Such feed systems have been developed for use in a range of industries,

including biogas production, sewage treatment, waste recycling, power production, mining and paper/pulping (Putzmeister, 2009, Putzmeister, 2010c). The feed system displayed in Figure 2-22 is used primarily to feed food remains and organic waste to biogas plants (anaerobic digesters). Designs developed to feed slurries and partial slurries are discussed in Section 2.7.4.

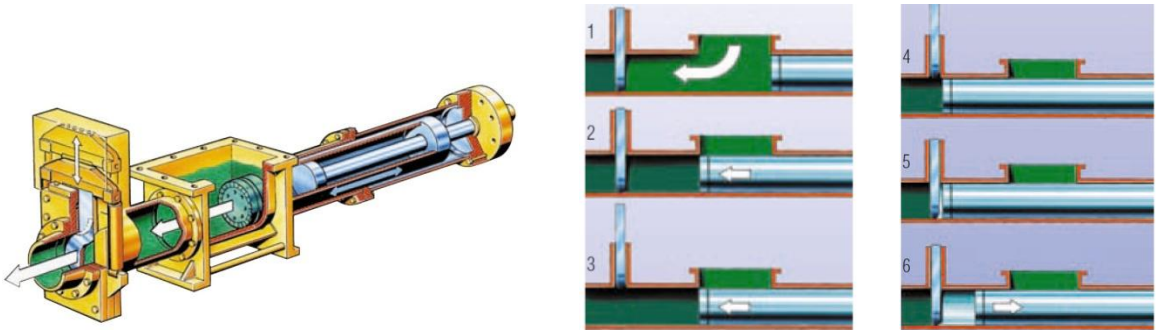

Figure 2-22: Putzmeister EKO high density solids pump (Putzmeister, 2010c).

The operating principle of the Putzmeister EKO high density solids pump is as follows. The main feeding piston is retracted and material is fed to the cavity left by the piston via an atmospheric feeding hopper (1). The piston then proceeds, compressing the material and advancing it into the supply cylinder; in doing so it creates a seal between the vessel being fed to and the atmospheric feeding hopper (2). When the feed material is sufficiently compressed, the gate valve to the high pressure vessel is opened and the feeding piston advances once again, feeding the material to the high pressure destination vessel (3 and 4). The gate valve is then closed flush with the face of the feeding piston and prevents any reverse flow of material (5). The feeding piston returns to its starting position and allows the cycle to start anew (6) (Putzmeister, 2010c).

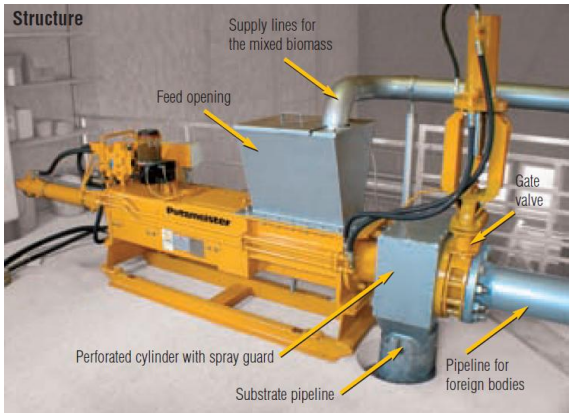

Figure 2-23: Putzmeister EKO solids pump for feeding waste mixtures to biogas plants (Putzmeister, 2010a).

When the Putzmeister EKO solids pump is used to feed food waste and other biomass streams containing mixtures of organic and inorganic components, it incorporates a perforated cylinder which

facilities the separation of organic components. During the compression stage (2-4), the gate valve is kept closed. When the piston advances, the feed material is compressed against the perforated cylinder and organic matter is allowed to be passed into the desired vessel through said perforations (substrate pipeline in Figure 2-23). The valve retains the undesired inorganic matter on the piston side and when the gate valve is opened, the inorganic matter is passed to a discharge line (pipeline for foreign bodies in Figure 2-23) and discarded (Putzmeister, 2010a).

The Putzmeister EKO solids pump is commercially available and has demonstrated feeding rates of 4.5 m^3/h to pressures as high as 35 bar. Common materials used in conjunction with the system are: food waste, highly dewatered sludges from filter presses, dried paper pulp, and screenings from sewage treatment works (Putzmeister, 2010a, Putzmeister, 2010c).

2.5.6 High pressure rotary piston feeder

The rotary piston feeder by Gencsoy and Gardner was first developed at the University of West Virginia to feed pulverised coal to gasifiers operating at elevated pressures. The feeder is comprised of a solids feeding hopper, a rotating disk, a rotating housing and a reciprocating cam-driven piston. A schematic of the systems is shown in Figure 2-24 (Gardner et al., 1977, Hawrych, 1981, Levelton, 1982).

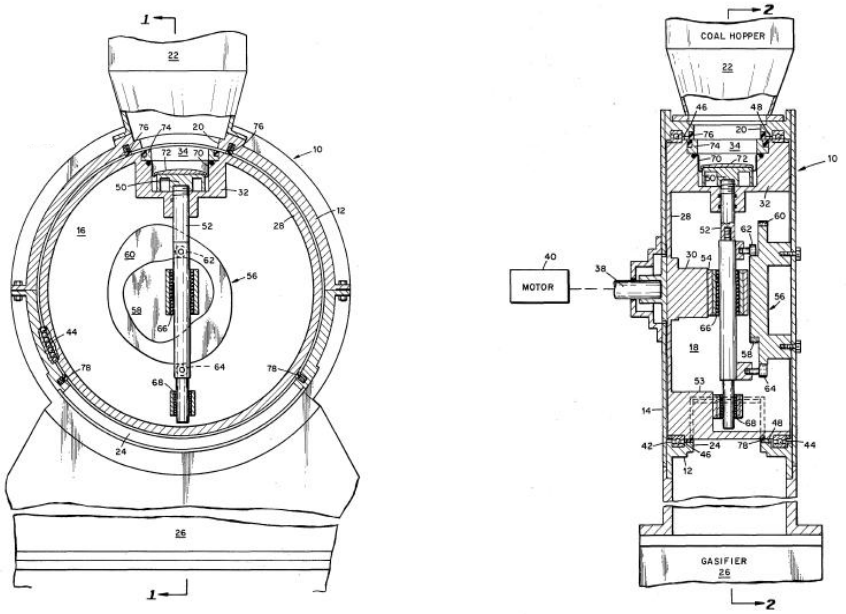

Figure 2-24: High pressure rotary piston feeder (Gencsoy, 1977).

The operating principle of the rotary piston feeder is as follows. Coal is fed from the solids feeding hopper to the void presented by the retracted piston contained within the central rotating disk. When

the void is filled with coal the disk and housing rotates and the piston head remains in a constant position through 135 degrees of rotation. During the next 75 degrees of rotation the piston head is advanced, driven by the same motor used for rotation and a series of cam and cam followers. The coal empties due to gravity and during the following 60 degrees of rotation the piston is located at its furthest point of extension. During the following 70 degrees of rotation the piston head retracts to its original loading position and remains in its loading position until the full revolution has been completed. The cycle is then ready to start anew (Gardner et al., 1977, Gencsoy, 1977).

The reciprocating piston arrangement provides the key advantage compared to lock hoppers as the piston allows the preservation of pressure while feeding solid material in batches. The high pressure rotary piston feeder has been designed to feed pulverised coal to pressures as high as 68.95 bar and can operate at feed rates of 9.6 tonnes/h (Levelton, 1982).

2.5.7 Ingersoll-Rand rotary valve piston feeder

Further to the coaxial piston feeder, Ingersoll-Rand have developed a rotary valve piston feeder which incorporates a hydraulic piston into a modified rotary valve. The feed system is comprised of a single piston situated within a rotating hollow cylinder which contains an opening on one side (Mistry and Chen, 1977). Figure 2-25 displays the operating principle of the rotary valve piston feeder.

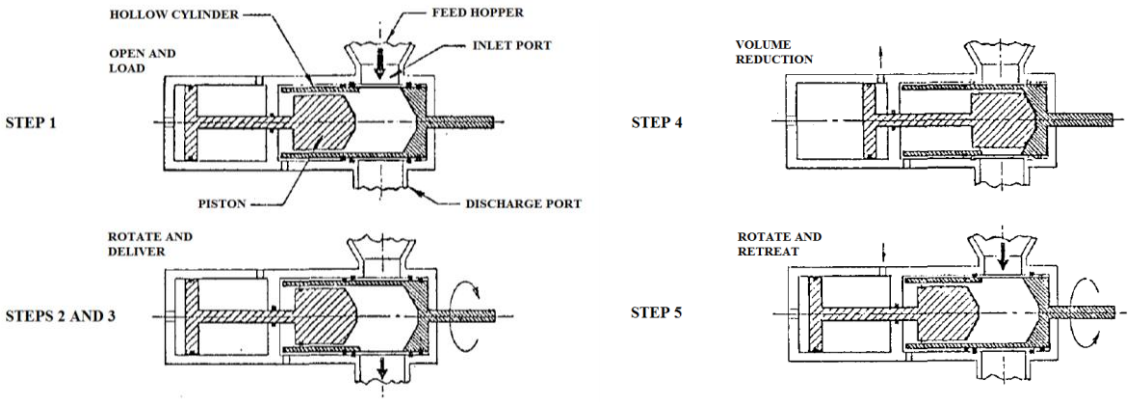

Figure 2-25: Rotary valve piston feeder developed by Ingersoll-Rand (Mistry and Wise, 1978).

In the first step the hollow cylinder is situated so that the opening of the cylinder is located at the inlet of the atmospheric feeding hopper. A portion of solid material is fed via gravity from the hopper to the hollow cylinder through the opening and closing of a valve. The cylinder rotates through 180 degrees and the batch of solid material is fed to the high pressure environment situated below. The hydraulic piston proceeds, displacing the gas at pressure occupying the hollow cylinder. Once the piston has finished the displacement stroke, the cylinder is rotated through a further 180 degrees and the piston is retracted allowing the cycle to start anew (Mistry and Chen, 1977).

The rotary valve piston feeder is one of four feed systems developed by Ingersoll-Rand. Aside from preliminary system considerations relating to seals and operational problems, the rotary valve piston feeder has not been developed any further (Mistry and Wise, 1978).

2.5.8 Conspray dynamic sleeve piston feeder

The Conspray dynamic sleeve piston feeder utilises a novel pressurised sleeve in which a hydraulic piston sits, to feed coal to high pressure reactors. The feed system consists of an atmospheric feeding hopper, a moving sleeve, a coaxial hydraulic piston and a pressurised valve housing/seal. Figure 2-26 highlights the operating principle.

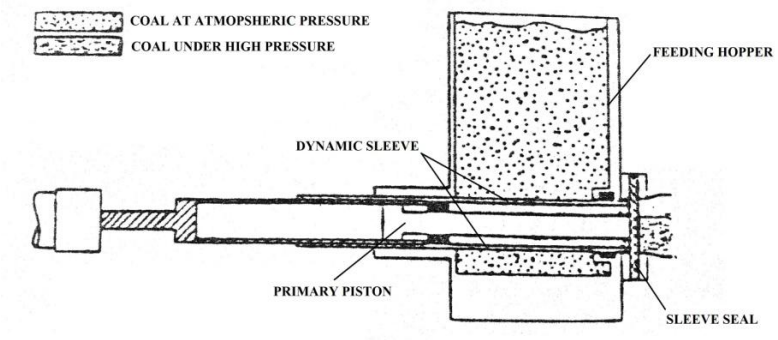

Figure 2-26: Conspray dynamic sleeve piston feeder (Levelton, 1982).

The feeding cycle begins with the sleeve and the piston being retracted, sitting flush with the outer wall of the feeding hopper. The sleeve of the device is then extended into the feeding hopper and is subsequently charged and filled with solid material due to its own motion as the sleeve is extended to the valve assembly on the opposing wall of the hopper. The sleeve enters the valve assembly through the sleeve seal which consists of a concentric seal or valve housing around the outside diameter of the sleeve. The valve housing is filled with hydraulic oil and undergoes pressurisation and depressurisation during the feeding system's operation. Once the sleeve is properly seated in the sleeve seal it is said to be fully charged with solid material and is isolated from the atmospheric feeding hopper. The hydraulic oil within the valve housing undergoes pressurisation and is brought up to a pressure exceeding that of system pressure to maintain an adequate seal between the sleeve and the valve housing. The interior of the sleeve containing the charge of solid material is at atmospheric pressure at this point and is subsequently pressurised to system pressure. Once pressure equalisation has been achieved the gate valve separating the interior of the sleeve from the pressurised environment is opened. The hydraulic piston seated at the outer wall of the feeding hopper is then advanced into the sleeve containing the pressurised solid material and the piston proceeds until it is seated with the open gate valve on the opposing side of the hopper. The gate valve is then closed and valve housing

and sleeve are depressurised to atmospheric pressure. The sleeve and piston are then retracted to their original starting position on the outer wall of the feeding hopper and the cycle is able to start anew (Levelton, 1982).

One additional feature of the Conspray dynamic sleeve feeder is that the hydraulic piston is able to operate in both a uniaxial and coaxial arrangement. The piston contains a secondary piston located within the primary piston. When the sleeve and piston are retracted at the end of the feeding cycle, the secondary piston located within the main body of the primary piston remains in place, extended towards the valve housing and gate valve. When the sleeve is advanced in the first stage of the feeding cycle, the secondary piston and the sleeve create a "collar" of solid material around the secondary piston. The collar of solid material and the valve housing are pressurised and the secondary piston is retracted, leaving a portion of feed material with a pressurised head space. Once the secondary piston is fully retracted and inside the primary pistons body, the gate valve to the high pressure environment is opened and both the primary and secondary pistons act coaxially. The solid material is fed to the high pressure environment and the cycle is able to start anew (Levelton, 1982).

The secondary piston is typically used when the material being fed tends to pack. The retraction of the secondary piston provides suitable void space for packed materials. Although the employment of the secondary piston seeks to ensure reliable operation, its use decreases the overall efficiency of the feeder due to an increased requirement of pressurising gas for the pressurisation stage. It is therefore preferential to operate the feeder without the secondary piston. The Conspray dynamic sleeve piston feeder has successfully demonstrated the feeding of coal and wood to pressures as high as 86.20 bar at feeding rates of 3 tonnes/h and 10 tonnes/h respectively (Levelton, 1982). A typical energy requirement operating at 20.68 bar is approximately 20 kJ/kg (Guzdar and Harvey, 1982).

2.5.9 Foster-Miller fluidised piston feeder

The fluidised piston feeder developed by Foster-Miller Associates consists of a pressurising valve, valves for material in and out, a pressure relief valve and a displacement piston (Harding, 1977). The fluidised piston feeder was developed to feed pulverised coal to high pressure processes and the operating principle of the system is shown in Figure 2-27.

During the intake stage, the coal inlet valve is opened and the displacement piston is retracted allowing the feeding of a coal-gas mixture to the space previously occupied by the piston. The inlet valve seat is purged of coal via a blast of pressurised gas and is subsequently reseated. The pressurising valve is then opened allowing a charge of pressurising gas at a pressure higher than that of the pressurised receiver vessel to be fed to the coal-gas mixture. When the pressure of the coal-gas mixture exceeds that of the pressurised receiving vessel, the spring-loaded coal out/discharge valve

opens and the coal-gas mixture is fed to the high pressure receiving vessel. After the coal has been fed and the valve seat is clear of coal, the coal out/discharge valve closes and the displacement piston is reseated, allowing the venting of pressurised gas via the pressure relief valve. Once the pressurised gas has been vented, the pressure relief valve is closed and the process is ready to start anew (Harding, 1977, Chandrasekhar and Harding, 1978).

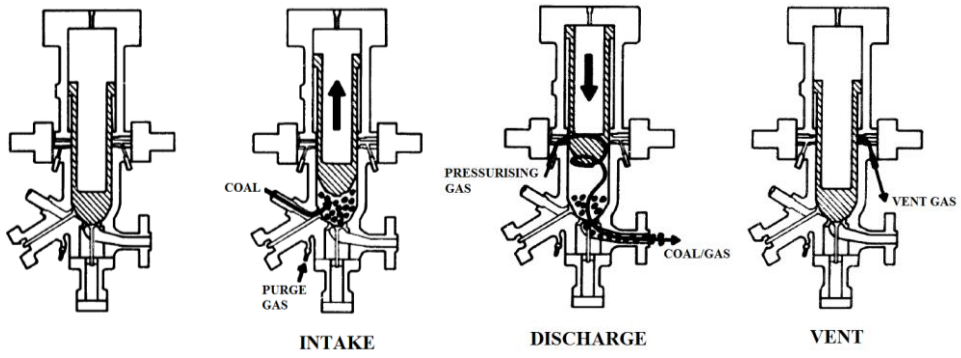

Figure 2-27: Operating principle of the Foster-Miller fluidised piston feeder (Harding, 1977).

The principal difference to common piston feeders is that the feed material is not fed via the displacement piston itself, but by the pressurised transport gas at a higher pressure than system pressure; the piston only acts to displace the pressurised gas once the material has been fed (Harding, 1977). The Foster-Miller fluidised piston feeder has demonstrated the feeding of coal at feed rates of 100-400 lb/h (0.045-0.18 tonnes/h) and has operated at pressures as high as 900 psi (62.05 bar) (Chandrasekhar and Harding, 1978).

2.5.10 Piston feeder overview

Table 2-4 provides an overview of the piston feeders discussed in this section. Feed systems are characterised by feed rates, feed materials and operating pressures.

Manufacturer	Feed Material	Feeding Capacity (tonnes/h)	Operating Pressure (bar)
Fortum	Peat, sawdust, sludge	1.00	23.00
Ingersoll-Rand (Co-axial)	Coal	2.27	100.00
F.M.Associates (LPF)	Coal	4.54	68.95
Lurgi Schlepper	Coal	20.00	30.00
Putzmeister EKO	Food waste, dewatered sludge, paper pulp	~4.50	35.00
University West Virginia	Coal	9.60	68.95
Conspray dynamic sleeve	Coal, wood	3.00	86.20
F.M.Associates (Piston)	Coal	0.18	62.05

Table 2-4: Overview of piston feeders.

2.6 Dynamic feed systems

Dynamic feed systems are classed as systems that utilise the constant movement of solids to maintain a pressure seal. They can be broadly split into two main categories: gravity driven and centrifugal driven, and each of these categories will be discussed in the following sections.

2.6.1 Gravity driven dynamic feeders

Gravity driven dynamic feeders utilise the acceleration due to gravity to maintain a pressure seal between a region of high pressure and the atmosphere (Higman and Van der Burgt, 2008). Solid material is fed to the top of a tall vessel situated above a high pressure vessel, and the solid material is allowed to flow down into the high pressure vessel (Visconty, 1956). To ensure that the pressure boundary is maintained, the height of the falling solid material must be such that the static height of the column of solid material is more or equal to the pressure of that in the high pressure vessel. This static head can be approximated using Equation 2-1.

$$\Delta P < \rho g h$$

Equation 2-1

Where ΔP is the pressure difference required to be overcome (Pa), ρ is the density of the solid material being fed (kg/m^3), g is the acceleration due to gravity (m/s^2) and h is the static head/height (m) (Higman and Van der Burgt, 2008). Further to this, the velocity at which the solid material being fed travels must be equal to or greater than the velocity of the gas migrating through the void space contained between the solid material. The velocity at which the solid material must travel in order to maintain a pressure boundary can be determined by Equation 2-2.

$$u_s \geq \frac{\Delta P . \varepsilon^2}{5 . h . \eta_g . S^2}$$

Equation 2-2

Where u_s is the solid velocity (m/s), ε is the void space between the solid material being fed, η is the dynamic viscosity of the migrating gas (Pa s), S is the specific surface area of the solid material (m^2/m^3) and 5 is an empirical constant (Higman and Van der Burgt, 2008). An example of such a feed system is shown in Figure 2-28.

Although gravity driven dynamic feeders are simple in their operation, they are limited to relatively low pressure processes due to their bulky design. To provide context, if a process operating at 20 bar was required to be fed to, a structure with a height of around 200 m would be needed. It has been suggested that gravity driven systems are to work in series as multistage devices to achieve higher

pressures. However, such arrangements present further complexities in their use as well as higher capital costs (Higman and Van der Burgt, 2008).

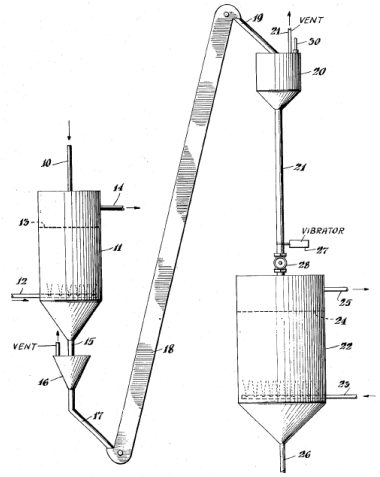

Figure 2-28: Gravity driven dynamic feeder developed by Visconty (Visconty, 1956).

2.6.1.1 Lockheed ball conveyor

The Lockheed ball conveyor presents a design similar to conventional gravity driven dynamic feeders that incorporates a series of metal balls to facilitate feeding. The ball conveyor was developed to feed pulverised coal to high pressure processes and a schematic of the system is shown in Figure 2-29.

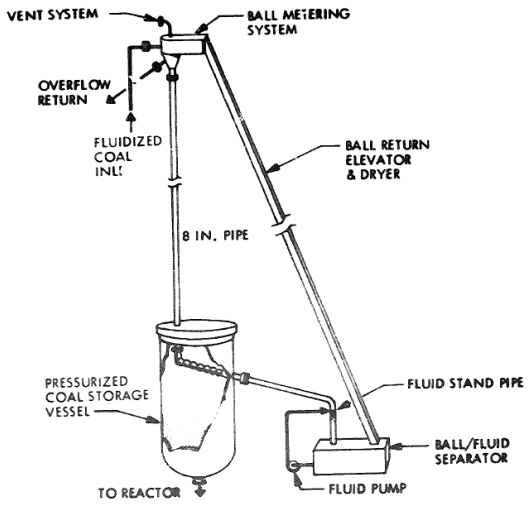

Figure 2-29: Ball conveyor developed by Lockheed Missiles Space Company (Bonin et al., 1977).

The ball conveyor is comprised of a standpipe, a series of metal balls, a ball return elevator, a ball metering bin, a coal input line and a ball/fluid separator. A series of metal balls are fed via the ball elevator to the top of the standpipe along with coal which is fluidised and fed via the coal input line.

Coal is sandwiched between the balls and the balls and coal are fed down the standpipe towards the high pressure vessel. The balls are held up prior to being returned to the top of the standpipe via the ball elevator, and coal is subsequently fed to the system. Gas leakage while returning the balls via the ball conveyor is prevented via a liquid lock/gland seal. The ball conveyor developed by Lockheed has demonstrated feeding to pressures of 1.6 psi/ft (0.36 bar/m) of standpipe using solid steel balls (Bonin et al., 1977).

2.6.2 Centrifugal driven dynamic feeders

Centrifugal driven dynamic feeders differ from gravitational devices in the sense that their operation is not limited by the acceleration due to gravity. Fundamentally they utilise the same principal as gravity driven dynamic feeders; however, centrifugal devices utilise the centrifugal acceleration developed through rotation to enhance the feeding operation (Higman and Van der Burgt, 2008).

A number of theoretical centrifugal devices have been proposed over the years, most notably those by Van der Burgt (Figure 2-30), Staudinger, Duch, Bretz, Meyer and Bonin (Staudinger, 1977, Duch, 1977, Van der Burgt, 1978, Bretz, 1980, Van der Burgt, 1982, Meyer et al., 1982, Meyer et al., 1983, Bonin et al., 1983, Meyer et al., 1984). Devices commonly incorporate a rotor which rotates around a central point and discharges solid material at speed. Although many designs are available in the literature, rotors usually take the form of one of two designs. Either rotors are comprised of two parallel plates that rotate simultaneously above and below each other, or they are comprised of a series of channels (centrifugal nozzles or sprues) down which solid material is fed. Rotor size and rotational speed are required to be increased as operating pressure increases (Staudinger, 1977), and some designs require rotational speeds as high as 5000 rpm (Van der Burgt, 1982).

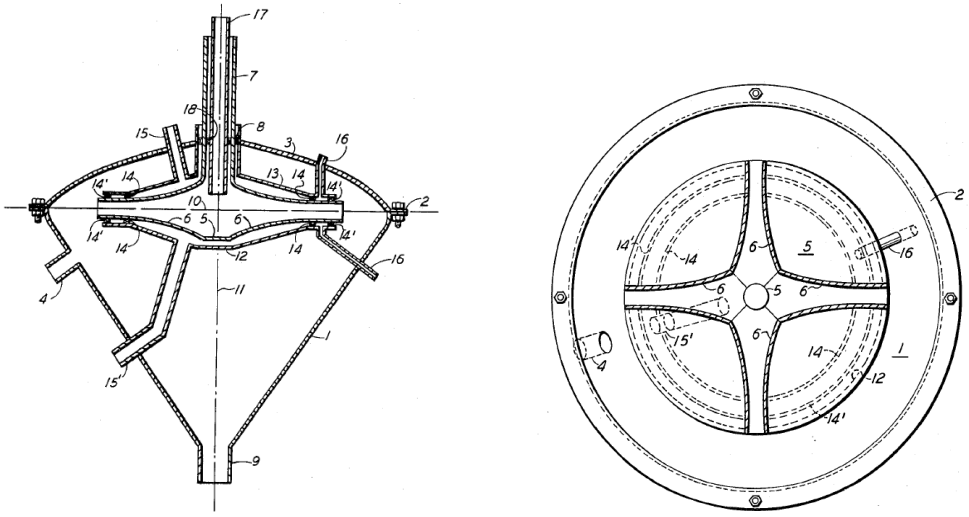

Figure 2-30: Centrifugal dynamic solids feeder developed by Van der Burgt (Van der Burgt, 1982).

2.6.2.1 Lockheed kinetic extruder

The Lockheed kinetic extruder was developed in the 1970s to feed pulverised coal to high pressure gasifiers, and poses as one of the first centrifugal driven high pressure solids feed systems to reach the industrial development stage (Bonin et al., 1977, Combustion Engineering Inc., 1994). The feed system is predominantly composed of a rotor enclosed in a high pressure housing. The rotor contains a hollow hub and a series of channels (sprues) that lead radially outward from the central hub. At the end of each of the sprues is a small chamber which is left open to the desired high pressure environment. Within these chambers are inlets for transport gas which is administered to the chamber at a pressure higher than that of the operating process pressure being fed to (Guzdar and Harvey, 1982, Meyer et al., 1984, Combustion Engineering Inc., 1994).

The operating principle for the kinetic extruder is as follows. Solid material is fluidised and transferred pneumatically from a region of atmospheric pressure to a region of low pressure (sub-atmospheric) contained within the hollow hub of the spinning rotor (Meyer et al., 1984). The solid material is transferred into the sprues (Figure 2-32) due to the centrifugal force imparted on the material, and a compacted moving plug is formed within each of the sprues. The plug creates a seal between the atmospheric/sub-atmospheric region and high pressure environment being fed to due to the motion and the low permeability of the plug of material. Transport gas, typically air or nitrogen is introduced at a pressure higher than that of the process pressure, and the solid material is fed to the high pressure environment (Guzdar and Harvey, 1982, Meyer et al., 1983, Bonin et al., 1983, Meyer et al., 1984, Combustion Engineering Inc., 1994). The process is continuous in its operation and the rate of feeding is determined by the speed of the central rotor, the centrifugal force imparted on the solid material being fed and the pressure differential encountered between the atmosphere/low pressure region and the high pressure destination (Schell, 1988).

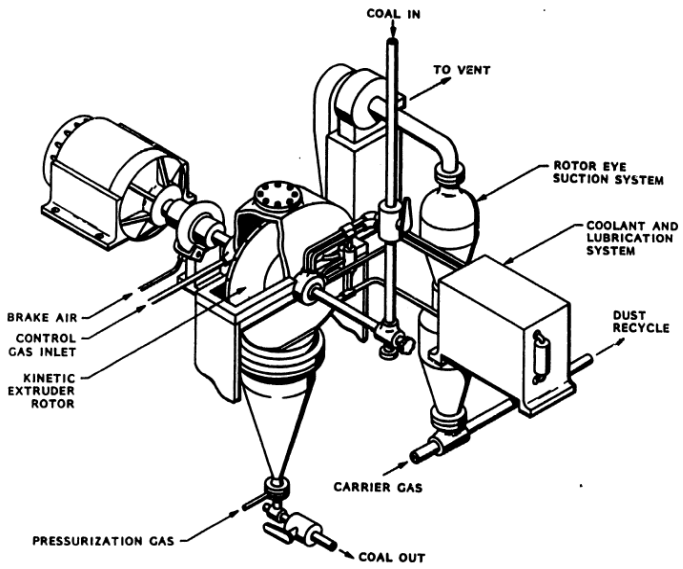

Figure 2-31: Kinetic extruder developed by Lockheed (Combustion Engineering Inc., 1994).

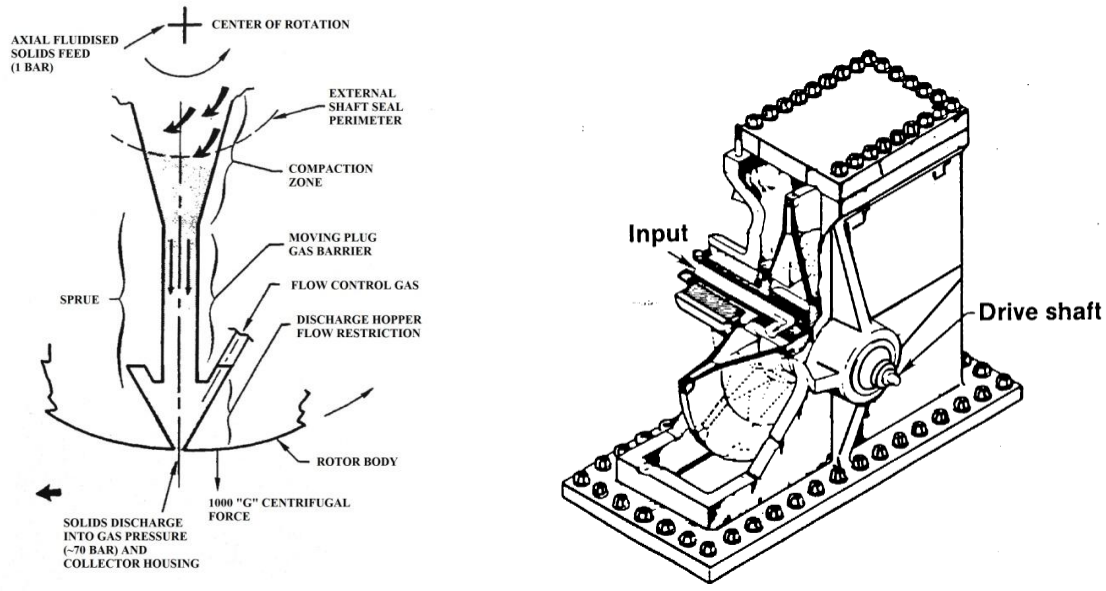

Figure 2-32: Example of a sprue within the hollow rotor of the kinetic extruder (Guzdar and Harvey, 1982).

Compared to lock hopper systems, the kinetic extruder has a smaller footprint, lower inert gas usage and lower power consumption. Capital costs for the kinetic extruder approach that of conventional lock hopper systems, and capital costs are found to be similar irrespective of size and throughput (Combustion Engineering Inc., 1994). An energy requirement of approximately 90 kJ/kg is required to feed coal to a pressure of 400 psi (27.56 bar), and a throughput of 2.25 tonnes/h has been achieved at this pressure (Combustion Engineering Inc., 1994).

2.6.2.2 Foster-Miller centrifugal plug-feeder

Further to Foster-Miller's screw-piston plug-forming feeder is their centrifugal plug-forming feeder, which like their screw-piston design utilises the solid material being fed to act as the pressure boundary. The centrifugal plug-feeder was developed to feed coal and is comprised of an atmospheric or low pressure feeding hopper, a downcomer supply pipe, and a centrifugal rotor containing a series of sprues (hollow supply cavities) (Harding, 1977, Chandrasekhar and Harding, 1978, Hawrych, 1981). Figure 2-33 displays a schematic of the feed system.

Pulverised coal is fed to the feeder via the stationary downcomer pipe. The coal is picked up by an impeller and subsequently forced into the feeding passages or sprues. The sprues, shown in Figure 2-33, converge to form a throat section and the coal fed forms a dynamic seal as it flows to the throat sections of the sprues. Plugs of coal are formed and act as temporary pressure boundaries between the high pressure vessel being fed to and the low/atmospheric feeding hopper. As more coal is compacted against the formed plugs, the centrifugal force experienced by said plugs causes plug feeding and in

turn the generation of a new plugs/pressure boundaries. The plugs of coal formed are permeable and so gas leakage during operation is experienced where insufficient coal flow rates are produced. Therefore, in order to operate with minimised gas leakage and a stable pressure boundary, the velocity of the coal must be equal to or more than the velocity of the retreating high pressure gas permeating through the coal plugs. It is common for rotational speeds to be increased over what is required to ensure coal velocities exceed that of the retreating gas (Harding, 1977).

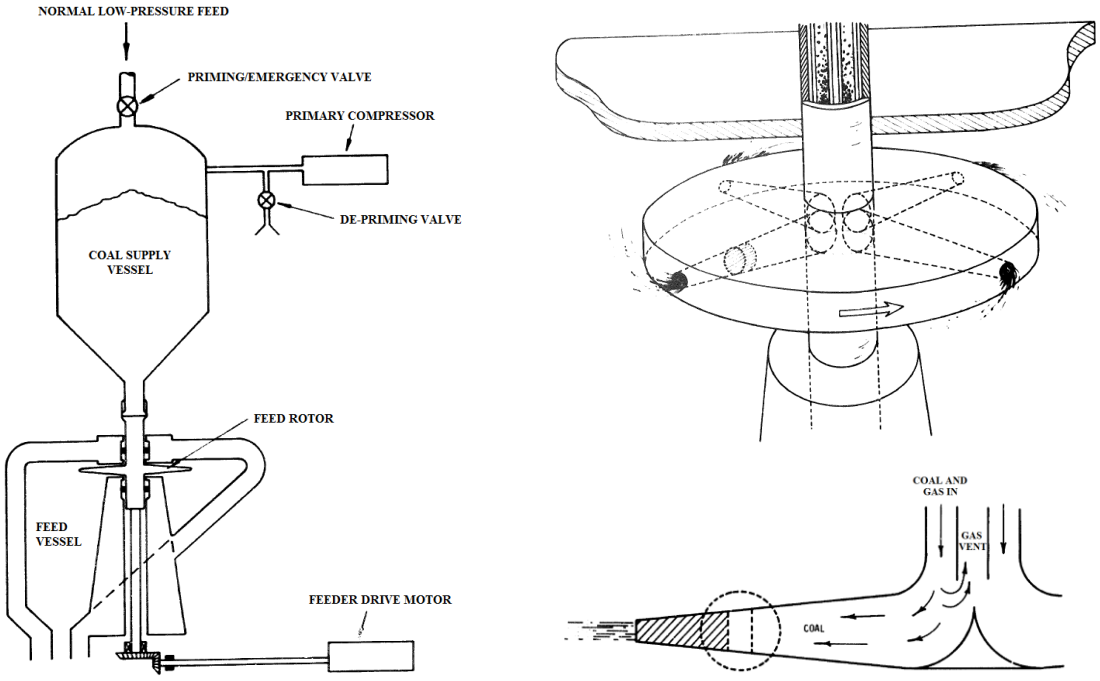

Figure 2-33: Schematic of the Foster-Miller centrifugal plug-feeder (Harding, 1977).

Advantages of the centrifugal plug-feeder are its small size, power savings compared to commercial technologies (lock hoppers) and continuous operation (Harding, 1977, Chandrasekhar and Harding, 1978). The centrifugal plug-feeder has demonstrated feeding rates as high as 1 ton/h (0.91 tonnes/h) at pressures of 40 psi (2.76 bar) and 0.25 tons/h (0.23 tonnes/h) at pressures of 185 psi (12.76 bar). Different flow rates and operating pressures were achieved by varying the outlet diameter of the sprues contained within the central rotating hub; 0.25 inch and 0.15 inch for 40 psi (1 ton/h) and 185 psi (0.25 tons/h) respectively (Harding, 1977).

2.6.3 Dynamic feed systems overview

Table 2-5 provides an overview of the dynamic feed systems discussed in this section. Feed systems are characterised by feed rates, feed materials and operating pressures.

Manufacturer	Feed Material	Feeding Capacity (tonnes/h)	Operating Pressure (bar)
Lockheed Kinetic Extruder	Coal	2.25	27.56
Foster-Miller centrifugal plug-feeder	Coal	0.91	12.76
Lockheed Ejector	Coal	0.45	3.45

Table 2-5: Overview of dynamic feed systems.

2.7 Slurry feed systems

Further to feed systems used for feeding dry solids to high pressure environments are slurry feeders, which hold characteristics similar to conventional liquid pumps. Slurry feeders, alongside lock hoppers are one of the most common subset of high pressure feed systems used in the field of high pressure gasification and can be found in a number of operating plants. Processes such as the GE Energy process, E-Gas process, Hygas process and H-Coal process all utilise coal slurries, and slurry feeders have been used to feed coal to gasifiers operating at pressures as high as 1500 psi (103.42 bar) (Ferretti, 1974, Bair and Tarman, 1977, Hawrych, 1981, Higman and Van der Burgt, 2008). Pumping solid-slurries presents a much less energy intensive route to feeding solids to high pressures than when feeding dry solids due to the use of a transport medium (typically water). Once solids are maintained in a continuously flowing mixture of solid-water, the mixture can be treated as an incompressible fluid and pumped against significant back pressures with little compression work.

Coal slurries are typically made up of 60-70 wt% coal and 30-40 wt% water (Hawrych, 1981, Higman and Van der Burgt, 2008). Such a large quantity of water poses as their biggest drawback when used in gasification processes, as gasification systems only require around half of the water contained in slurries (10-20 wt%) for steam formation and use in the water-gas shift reaction. A large amount of energy is required to vaporise the excess moisture present in slurries and cold gas efficiencies suffer as a consequence; cold gas efficiencies being of the order of 70% for slurry-fed systems and around 80% for dry-fed systems (Higman and Van der Burgt, 2008). Slurry based feed systems also compound particularly poor operational efficiencies where high moisture content, low rank coals are used. Moisture contents as high as 40-45% are common with lignites and such moisture contents don't contribute to any of the moisture used to make up the slurry (Higman and Van der Burgt, 2008).

Although water is the most commonly used transport medium in slurry feeders, it is possible to use other fluids. The Hygas process has experience using both water and an aromatic light oil (a by-product from the process) to form a slurry. The oil used has approximately 25% the heat of vaporisation of water and requires little additional heating once in the reactor. This usually constitutes

the main advantage of using competing transport mediums over water; however, consideration has to be given to the effect the medium has on the process as a whole (Bair and Tarman, 1977).

2.7.1 Typical slurry feed system

A typical coal-slurry feed system is shown in Figure 2-34. The system is comprised of an eductor-mixer, a slurry blend tank, a recirculating centrifugal pump and an injection pump (positive displacement).

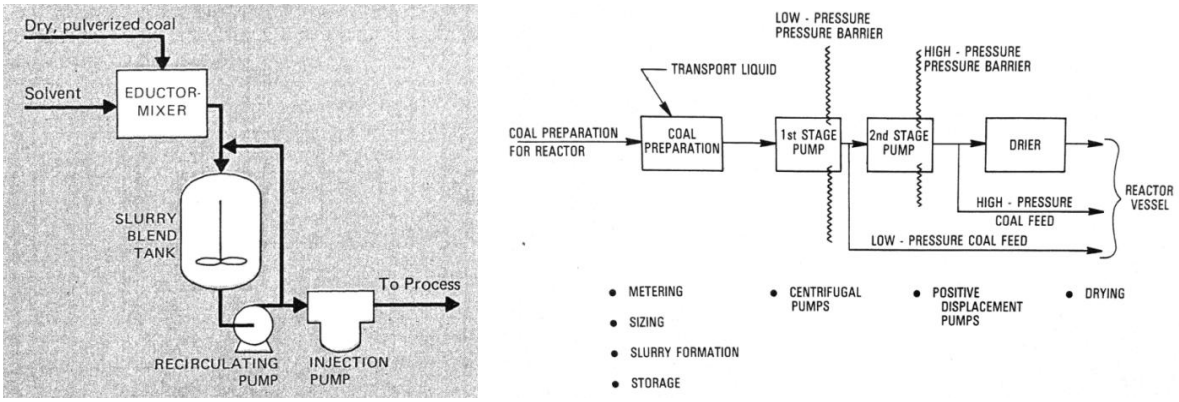

Figure 2-34: Common components required for a slurry feed system and a schematic of a typical slurry feeder (Ferretti, 1974, Gall and Johnson, 1983).

Pulverised coal is first entrained by the eductor unit from a continuous flow of water into the system. The coal-water mixture is then further mixed by a slurry blend tank to ensure slurry uniformity. The recirculating pump acts to serve the suction side of the injection pump and recycle any excess slurry back to the blend tank to ensure adequate suspension of coal particles. The injection pump in this case is a positive displacement plunger pump which serves to pump the slurry against the required back pressure (Ferretti, 1974). It is common for slurry type feed systems to employ both centrifugal pumps and positive displacement pumps running in series to facilitate the feeding of slurries to high pressure environments. Centrifugal pumps serve to feed slurried coal to pressures of the order of 6 bar, and where higher pressures are encountered, centrifugal pumps serve to feed positive displacement pumps which are capable of feeding to pressures in excess of this (Ferretti, 1974, Hawrych, 1981, Gall and Johnson, 1983, Rautalin and Wilén, 1992).

Slurry type feed systems have many advantages over dry solids feeders. The equipment and technology is developed and commercially available, instrumentation is simple, and distribution of feed to multiple streams is far easier than when dealing with dry solids. Their key drawback, aside from the burden they present on efficiency when associated with thermal systems, is the abrasiveness of the slurry being fed. Slurries cause wear of mechanical parts and consequently systems have to be

taken offline on a regular basis to allow for maintenance to be carried out. In addition to this, low volumetric flow rates are encountered when feeding to particularly high pressures (Ferretti, 1974, Gall and Johnson, 1983, Rautalin and Wilén, 1992).

2.7.2 Slurry pre-treatment and downstream processes

Aside from slurry makeup, pre-treatment of slurries usually refers to slurry preheating. The preheating of slurries compensates for the thermodynamic losses that arise from the use of water as a transport medium, and presents the following advantages over slurry systems without preheating.

The heat required for evaporation becomes lower at increased temperatures and preheating means that slurries have to be heated less in the reactor/gasifier after feeding. If slurries are preheated sufficiently, flash vaporisation can take place on entry to the reactor/gasifier which presents increased reactor space for carbon conversion, and in turn reduces oxygen consumption. Further to this, water also becomes less dense with increasing temperature, and in turn the water requirement for slurry makeup on a volume basis is reduced. An added advantage of slurries over dry solids is that preheating not only refers to the transport medium, but also to the fuel itself; thus the fuel is also able to be preheated prior to entering the reactor/gasifier (Higman and Van der Burgt, 2008).

Alternatively to slurry pre-treatment, slurries can undergo drying downstream of the feeder to minimise the effect that water has on process efficiencies. Typical drying systems are composed of spray dryers and cyclones which seek to prompt flash vaporisation and efficient solid-gas separation once the fuel has been de-slurried respectively (Air Products and Chemicals Inc, 1971, Morel, 1977, Hawrych, 1981, Gall and Johnson, 1983, Rautalin and Wilén, 1992). A typical setup is as follows. After the slurry has been fed to the high pressure reactor/gasifier the slurry is atomised and subsequently heated by a process gas stream at a temperature of approximately 800-900°C. The coal-gas mixture is then transferred to a cyclone which separates the coal ready for feeding to the main body of the gasifier, and allows the transfer of the humidified gas either for use in slurry preheating or in the water-gas shift reaction (Air Products and Chemicals Inc, 1971, Morel, 1977, Hawrych, 1981, Gall and Johnson, 1983).

Both pre-heating and slurry drying seek to increase the overall efficiency of the gasification process; however, both processes lend themselves to wholly different gasifier designs. Pre-heating suggests the use of a slurry-fed gasifier, whereas slurry drying suggests the use of a dry-fed gasifier. Overall IGCC efficiencies for entrained-flow gasifiers are approximately 38% and 50% for slurry-fed and dry-fed systems respectively (Higman and Van der Burgt, 2008). Therefore, increasing the overall efficiency from the lower level of 38% is more attractive due to the limitations and inefficiencies projected by slurry drying for use in dry-fed gasifiers. Current IGCC dry-fed gasifier's efficiencies remain at

approximately 50% with minor increases possible from the addition of a second stage (1-2%). This minor increase in efficiency is largely due to only part of the steam injected to the process being converted to a useful product; the remainder acts as a burden on the gasifier. Furthermore, slurry-fed systems incorporating extreme preheating stand to make more advances in overall efficiencies when operating at higher pressures (Higman and Van der Burgt, 2008).

2.7.3 Kamyr Hydrofeeder

The Hydrofeeder is a system developed by Kamyr Incorporated to feed wood chips to digesters operating at high pressure (350 psi/24.13 bar). Kamyr have further developed this feed system to feed coal slurries, handling lump coal sized up to 100 mm. The feeder is comprised of a pressure housing containing a tapered rotor which makes up a pressure balanced four-part rotary valve (Funk and Reimert, 1977, Funk and Sherman, 1977, Richter and Richter, 1984, Prough, 1993). Figure 2-35 highlights a schematic of the system.

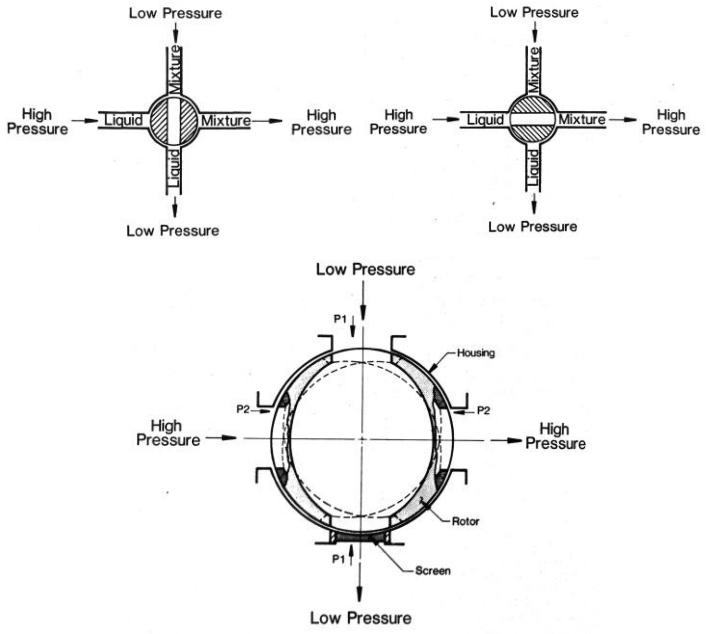

Figure 2-35: Hydrofeeder developed by Kamyr Incorporated (Funk, 1983).

The four-part rotor is the only moving part of the feed system. The basic operating principle is that two streams of liquid and solid-liquid flow independently of each other in a low and high pressure state, vertically and horizontally respectively (Funk and Reimert, 1977). The operating cycle is as follows. The central rotor starts its operation in the vertical low pressure position and is filled with a portion of solid-liquid slurry. A screen is in place at the far edge of the rotor housing in the low pressure outlet position and filters the solid-liquid slurry of large (>6 mm) particles. The remaining

slurry containing sub-6 mm particles passes through the screen and is subsequently recycled, being fed to the slurry mixing vessel for further use in the low pressure slurry stream. The central rotor then rotates through 90 degrees and allows the high pressure horizontal stream of liquid to enter the rotor. The high pressure stream flushes the rotor of solid material and forms a solid laden slurry. The slurry is subsequently fed to the desired high pressure environment and the rotor continues to move through a further 90 degrees, allowing another batch of low pressure slurry to enter the rotor. This cycle is repeated allowing semi-continuous feeding of slurry to high pressure environments (Funk and Reimert, 1977, Hawrych, 1981, Funk, 1983, Rautalin and Wilén, 1992).

Developments and adaptations of the Kamyr Hydrofeeder consist of introducing a screen to reduce the amount of liquid passing through each cycle of operation, introducing a scalloped central chamber to increase throughput, and using both wood chips and coal as feedstocks (Funk and Reimert, 1977, Funk, 1983, Rautalin and Wilén, 1992). The Hydrofeeder developed by Kamyr Incorporated has demonstrated feed rates of wood chips and coal slurries of up to 500 tons/h (453.59 tonnes/h) at back pressures of up to 1500 psi (103.42 bar) for coal and 350 psi (24.13 bar) for wood chips (Hawrych, 1981, Funk, 1983).

2.7.4 Putzmeister piston-driven slurry pumps

Further to dry solids pumps, Putzmeister have developed a number of piston-driven pumps for delivering slurries. Namely the KOV piston pump utilising ball valves and the KOS high density solids pump. Figure 2-36 displays a schematic of both types of pump.

The KOV piston pump operates in a similar manner to a typical positive displacement piston-driven device. Two ball valves are situated in series in a common pipe, separated tangentially by a piston and a piston chamber. As the piston is retracted the bottom ball valve opens due to a suction force being exerted on both the ball and the slurry, this in turn exerts a force on the top ball valve ensuring its closure and a portion of slurry being drawn in from the feeding chamber. When the piston is fully retracted and the piston chamber is at its maximum volume, the piston advances exerting a force on the slurry; this prompts the closure of the bottom ball valve and subsequently the opening of the top ball valve. The slurry is fed against a given back pressure through the top ball valve and to the desired process. The cycle starts anew once the piston has completed its feed stroke (Putzmeister, 2010b).

The KOS high density solids pump incorporates two pistons operating in parallel connected by an S-transfer tube which is able to pivot from one piston exit to another. The S-transfer tube serves to isolate a given piston from back pressure while the piston chamber is being filled. Typically a solid laden slurry is screw fed to a piston chamber from above the dual piston configuration. The S-transfer tube leaves the primary piston chamber being filled open to the atmosphere while the opposing

secondary piston is sealed; during this, the opposing secondary piston is at its furthest advancement and ready to be filled after it has retreated. Once the primary piston chamber has been filled, the S-transfer tube pivots and seals the primary piston chamber from the atmosphere and pressurises the piston chamber and slurry. The primary piston advances pushing the slurry into the high pressure environment via the S-transfer tube. Simultaneously, the secondary piston retreats and the piston chamber is filled with a batch of slurry at atmospheric pressure. The S-transfer tube then pivots sealing the secondary piston chamber from the atmosphere and the secondary piston advances feeding the batch of slurry to the high pressure environment. The cycle is continuous and ensures the continuous feeding of slurry against a back pressure (Putzmeister, 2009).

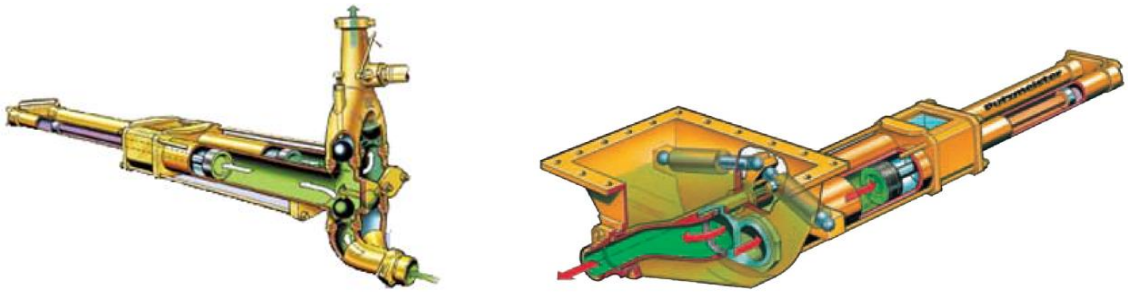

Figure 2-36: Putzmeister KOV piston pump (left) and KOS high density solids pump (right) (Putzmeister, 2009, Putzmeister, 2010b).

The KOV piston pump has fed materials containing up to 70% solids (20 mm) to back pressures of 130 bar and at flow rates of up to 60 m^3/h. Comparatively, the KOS piston pump has demonstrated the feeding of viscous sludges such as highly dewatered sewage sludges, oil sludges, bio waste and chemical and organic high density solids to back pressures of 130 bar at flow rates of up to 400 m^3/h (Putzmeister, 2009, Putzmeister, 2010b). Similar piston-driven slurry pumps to those developed by Putzmeister are available from Schwing America Incorporated and Chandra Helicon Pump Pvt. Ltd. (Finch, 1985, Helicon, 2010).

2.7.5 Slurry pump overview

Table 2-6 provides an overview of slurry feeders discussed in this section. Feed systems are characterised by feed rates (approximated on a mass basis using the density of water), feed materials and operating pressures.

Manufacturer	Feed Material	Feeding Capacity (tonnes/h)	Operating Pressure (bar)
Kamyr Inc.	Wood chips and coal	453.59	103.42
Putzmeister KOV	Sludges	~60.00	130.00
Putzmeister KOS	Sludges	~400.00	130.00
Schwing America Inc.	Concrete	~120.00	200.00
Chandra Helicon Pump Pvt. Ltd	Sludges	~100.00	23.54

Table 2-6: Overview of slurry feeding systems.

2.8 Recent research activity

Much of the information available in the literature regarding high pressure solids feed systems relates to work carried out in the 1970s and 1980s, where a surge of work was carried out in collaboration with coal fed gasifiers operating at elevated pressure (Jet Propulsion Laboratory, 1977). In the intervening years, research and development into high pressure solids feed systems has diminished, and only a small number of systems are currently under development. This section aims to provide an overview of these systems and the achievements made to date.

2.8.1 Stamet Posimetric high pressure solids feeder

The Stamet Posimetric feeder, sponsored by an agency of the United States Government, now acquired by GE Energy LLC was developed to feed dry granular coal continuously to high pressure environments. The feed system takes design cues from rotary valves and dynamic feed systems and utilises a spool formed by two disks or vanes contained within a hub which rotates inside a stationary housing (Firth, 1991, Aldred and Saunders, 2007). Figure 2-37 provides a process overview of the system.

Solid feed material is fed to the spool from a storage hopper via gravity. The solid material enters the pump and is locked between the two textured disks/vanes which rotate within the smooth stationary casing. The feed material is transferred from the inlet of the spool to the disengagement zone at the outlet duct via rotation, and is guided out by an abutment (protrusion into the outlet duct); this disengages the material from lockup between the textured walls of the disks/vanes. The solid particles are now in motion at this stage and produce a moving solids seal which is continuously created due to the continuous rotational motion of the spool and simultaneous solids lockup. The solid material is then released into the outlet vessel and collected via gravity while a new portion of solid material forms the seal at the outlet (Aldred, 2000, Aldred and Saunders, 2007).

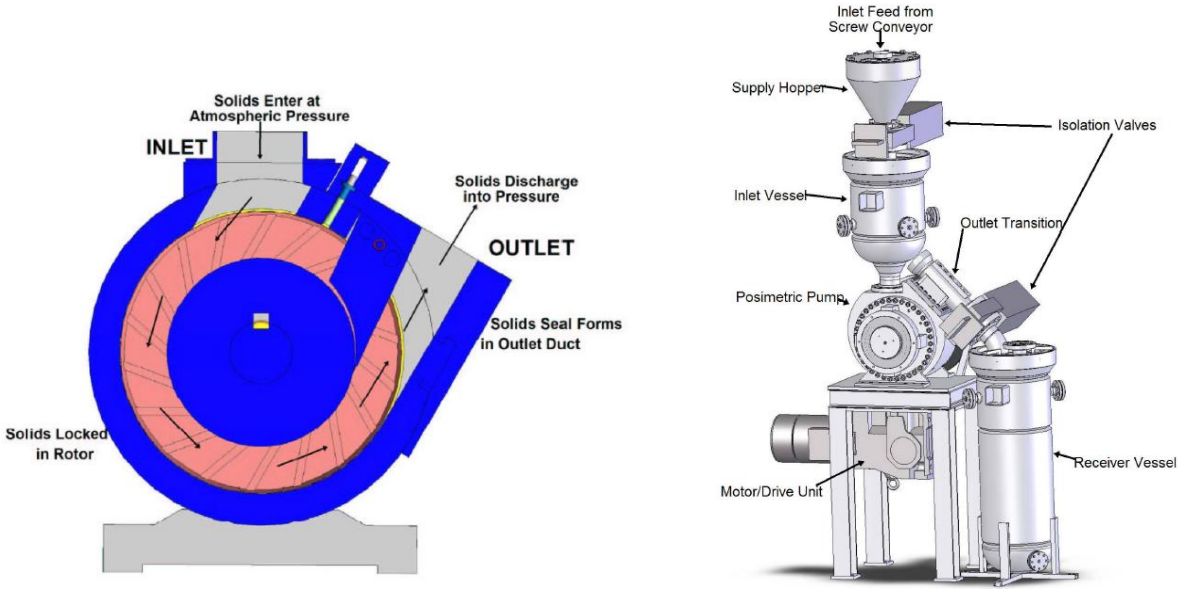

Figure 2-37: Stamet Posimetric feeder and the test rig arrangement (Aldred and Saunders, 2007).

The requirements for inert gas have been shown to be very small compared to conventional lock hopper systems, and future development of a commercial-scale feeder capable of feed rates as high as 30 tonnes/h has been proposed (Aldred and Saunders, 2007). Feed rates of approximately 0.55 tonnes/h have been achieved and granular pulverised coal has been fed to pressures in excess of 1000 psi (68.95 bar) (Aldred and Saunders, 2007).

2.8.2 TK Energi 3-piston feeder

The TK Energi 3-piston feeder embodies a piston-driven feed system that utilises three separate pistons to maintain a seal while feeding. Figure 2-38 shows an overview of the operating procedure of the 3-piston feeder.

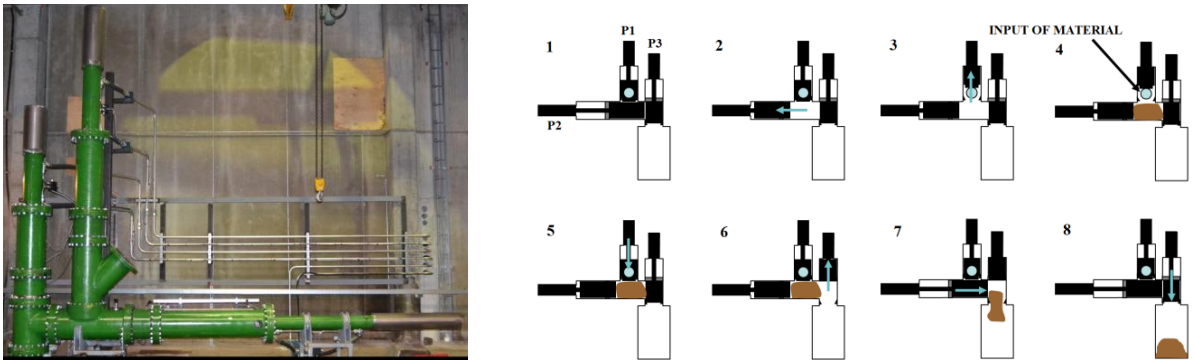

Figure 2-38: TK Energi 3-piston feeder and operating procedure (Koch, 2011a, Koch, 2011b).

The process takes place as follows. Piston 2 (P2) and piston 1 (P1) retract allowing an opening for the feed material and the exposition of the feed entry point respectively. Solid material is fed into the opening supplied by P2, and P1 is moved down creating a seal that prevents further feeding of solid material. Piston 3 (P3) is then moved up allowing the solid material to be exposed to the high pressure chamber for the first time, and P2 then exerts a force on the feed material and deposits it into the high pressure chamber via gravity. P3 is then reseated in its respective seal and the process starts anew (Swanson et al., 2003, Koch, 2011a).

One of the main advantages of the TK Energi system is the minimisation of inert gas needed for operation. Due to the 3-piston design, one piston always presents a seal and the escape of process pressure/gas is prevented at all times. Therefore, pressurised gas is able to be recycled minimising the need for subsequent inert gas. TK Energi have developed a pilot scale feed system based on the 3-piston setup and have demonstrated feeding of various biomass materials, coal and waste to pressures as high as 30 bar and at flow rates of up to 0.25 tonnes/h (10 m^3/h). The 3-piston feeder has an energy requirement of approximately 59 kJ/kg feeding against a pressure of 30 bar (Koch, 2011a, Koch, 2011b). Further to their pilot scale feeder, TK Energi have designs available for a full scale 3-piston feeder which has a proposed feed rate of 62.5 tonnes/h (100 m^3/h) and is capable of feeding to pressures as high as 35 bar (Koch, 2011a).

2.8.3 PWR tractor-mill linear dry solids extrusion pump

The tractor-mill linear dry solids extrusion pump developed by Pratt and Whitney Rocketdyne Incorporated (PWR) utilises a phenomenon observed in a pressurised tube/pipe to feed solid materials to high pressure processes. When a given length of tube is filled with solid material and pressurised at one end, the solid material forms a plug and plugs the tube for a period of time. When the high pressure stream permeates through the solid material, pressure equalisation takes place and the solid material is ejected from the atmospheric or lower pressure end of the tube. The PWR linear extrusion pump utilises this phenomenon by incorporating a moving walled plugged pipe (Sprouse and Matthews, 2006, Sprouse and Matthews, 2008). Figure 2-39 shows an overview of the design.

The length of the pipe and the speed at which the walls are moving determines the level at which the formed plug is maintained. Sufficient wall friction is required to ensure a plug seal and to prevent the plug from being released prematurely (Sprouse and Matthews, 2008). Two designs were initially developed by PWR, one that utilised a rolling mill whereby the moving pipe walls were made up of a series of rollers, and another that utilised a set of twin rotating belts (straight moving tracks). The design incorporating the twin rotating belts shown in Figure 2-39 was chosen to be developed further in preference to the rolling mill design due the presence of high inter-particle friction zones being found during operation with the rolling mill (Sprouse and Matthews, 2008, Bell and Towler, 2010).

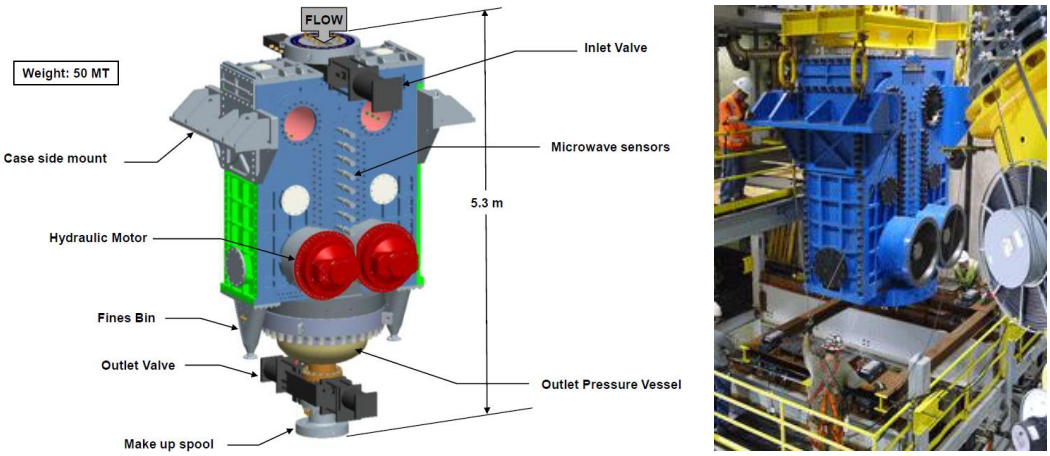

Figure 2-39: PWR tractor-mill linear dry solids extrusion pump design (EERC, 2012, Saunders, 2012).

The system operates as follows. Solid material is fed via a supply hopper to the inlet section of the pump. Material enters the dynamic zone of the feeder and forms a series of stable arches between two/twin moving belts. When the solid material has formed a stable arch, the material is said to be in lockup and no slip or movement is encountered when the solid material is in the lockup stage (Fusselman et al., 2010). The twin rotating belts advance the formed arches from the inlet to the outlet of the pump and ultimately to the high pressure process. Further to the natural stability of the formed arches of material, an increasing load is transferred to the twin rotating belts which promotes increased stability of the arches. Solid material in lockup is able to be released by separating the twin belts at the outlet of the pump. This allows the locked material to be broken up prior to being fed to the desired process at pressure (Fusselman et al., 2010, Saunders, 2012). It can be observed that the successful operation of the PWR solids pump relies heavily on the ability of the bulk solid being fed to form multiple stable arches between the twin rotating belts. Limits are therefore imposed on particle size and in turn the relative voidage present in the bulk material. Figure 2-40 displays the operating principle of the PWR solids feeder.

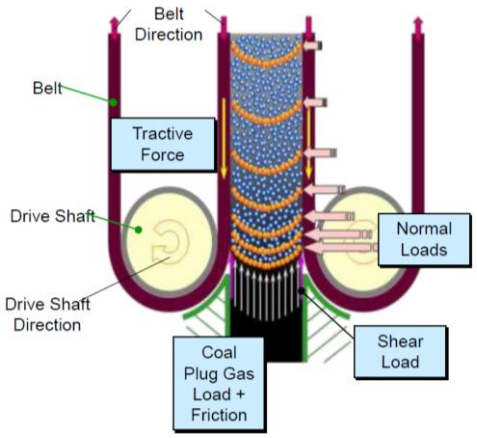

Figure 2-40: Operating principle of the PWR tractor-mill linear dry solids extrusion pump (Saunders, 2012).

The PWR tractor-mill linear solids feeder is currently being developed to feed coal, petcoke and biomass-coal mixtures at flow rates as high as 25 tons/h (22.68 tonnes/h) and to pressures of approximately 1000-1200 psia (68.95-82.74 bara) (NETL, 2009, Saunders, 2012). A 16.67 tons/h (15.12 tonnes/h) design has already been developed and demonstrated (Sprouse and Matthews, 2008).

2.9 Overview of high pressure solids feed systems

An overview of the feed systems developed for feeding solid materials to high pressure processes is shown in Table 2-7. Feed systems are split into the six key categories available for undertaking such an operation and are presented alongside their maximum demonstrated feeding capacity and operating pressure.

Feed System Category	Manufacturer	Feed Material	Feeding Capacity (tonnes/h)	Operating Pressure (bar)
Rotary Valves	A. Ahlstrom Corp.	Wood chips	90.00	12.00
	C. E. Bauer (MST Corp.)	Wood chips, sawdust	113.00	10.34
	Ingersoll-Rand Inc./IMPCO (Beloit)	Wood chips	181.00	10.34
	Kamyr Inc.	Wood chips, sawdust	52.00	10.34
	Koppers Company Inc.	Coal	32.00	10.34
Lock Hoppers	Lurgi	Coal	70.00	84.94
	Petrocarb Inc.	Peat, coal, ore, dolomite	55.00	41.37
	T. R. Miles Consulting	Wood chips, wood pellets	2.00	20.68
	Macawber	Coal	12.00	31.03
Plug-forming Feeders	Koppers Company Inc.	Wood chips	25.40	13.79
	General Electric Co.	Coal	0.91	20.68
	Werner & Pfleiderer	Coal, sawdust	0.45	103.42
	TK Energi	Torrefied wood, straw, bagasse	9.07	20.00
	Foster-Miller Associates	Coal	-	82.74
	Ingersoll-Rand	Coal	1.81	51.71
	Stake Technology	Woodchips, sawdust, bark, bagasse, straw	5.00	55.15

	Vattenfall Energiesystem AB	Peat, straw	3.6	25.00
Piston-driven Feeders	Fortum	Peat, sawdust, sludge	1.00	23.00
	Ingersoll-Rand (coaxial piston)	Coal	2.27	100.00
	Foster-Miller Associates (L.P.F)	Coal	4.54	68.95
	Lurgi Schlepper	Coal	20.00	30.00
	Putzmeister EKO	Food waste, dewatered sludge, dried paper pulp	~4.50	35.00
	University West Virginia	Coal	9.60	68.95
	Conspray dynamic sleeve	Coal, wood	3.00	86.20
	Foster-Miller Associates (Piston)	Coal	0.18	62.05
	TK Energi	Biomass, coal, waste	0.25	30.00
Dynamic Feeders	Lockheed Kinetic Extruder	Coal	2.25	27.56
	Foster-Miller centrifugal plug-feeder	Coal	0.91	12.76
	Lockheed Ejector	Coal	0.45	3.45
	Stamet Posimetric	Coal	0.55	68.95
	PWR Linear Tractor-mill	Coal, petcoke, biomass	16.67	68.95
Slurry Feeders	Kamyr Inc.	Wood chips, coal	453.59	103.42
	Putzmeister KOV	Sludges	~60.00	130.00
	Putzmeister KOS	Sludges	~400.00	130.00
	Schwing America Inc.	Concrete	~120.00	200.00
	Chandra Helicon Pump Pvt. Ltd	Sludges	~100.00	23.54

Table 2-7: Overview of feed systems developed for feeding solid materials to high pressure processes (multiple sources previously stated in each associated section).

2.10 Defining an opening for further research

A comprehensive and thorough review of the literature relating to high pressure solids feed systems has been carried out, and from the information gleaned a definitive area requiring further research has been identified.

The practice of feeding solid materials to high pressure environments has been problematic since its conception, and in the context of high pressure gasification it is considered to be one of the major problems impeding continuous operation (Davey et al., 1998, Higman and Van der Burgt, 2008, Lackner et al., 2010). Lock hoppers currently represent the market leader when it comes to feeding fuel to pressurised gasifiers, and although there have been a number of designs proposed to replace them, initial interest dating as far back as 1977 (Gencsoy, 1977), lock hoppers remain the feed system of choice (Rautalin and Wilén, 1992, Lau et al., 2002, Van der Drift et al., 2004, Cummer and Brown, 2002, Holt, 2001, Bio-EnergySystems, 1984, Rezaiyan and Cheremisinoff, 2005, Higman and Van der Burgt, 2008).

However, lock hoppers are not without their drawbacks, and are often the cause of process downtime due to maintenance. Valves are found to fail due to degradation, solids are found to holdup and impede flow, inefficiencies are brought about through pressurisation cycling, and large quantities of gas for pressurisation are required (Schell, 1988, Lau et al., 2002, Van der Drift et al., 2004, Higman and Van der Burgt, 2008, Rezaiyan and Cheremisinoff, 2005). Succinct fuel feeding is a prerequisite for the success of high pressure gasification and can perhaps be considered the primary step in the gasification process. Fuel feeding poses as the main barrier to the commercial success of gasification, and it is therefore imperative that alternatives to commercial lock hoppers are developed, or at the very least, operational problems are resolved (Clayton et al., 2002).

With a renewed interest in gasification and practically all modern gasification processes being carried out at elevated pressure (10-100 bar) (Higman and Van der Burgt, 2008), the development of a reliable and efficient high pressure solids feed system is of paramount importance. This statement therefore provides the context and the drive for the research detailed in this study, and presents the principal objective of developing an efficient and reliable way in which to feed solid fuels to high pressure gasifiers.

3

THEORY AND DESIGN CALCULATIONS

3.1 Introduction

As outlined in Chapter 1, pressure plays an integral role in improving the overall efficiency of a gasification process. But in order to enable such efficiency gains, the problem of feeding a solid fuel against a back pressure has to first be overcome. It was found in Chapter 2 that lock hoppers are one of the most widely deployed type of feed system for carrying out this role, but it was also found that they are one of the most significant contributors to process downtime due to maintenance (Holt, 2001, Clayton et al., 2002, Rezaiyan and Cheremisinoff, 2005). Common drawbacks of conventional lock hoppers are sealing valve failure, solids holdup and inefficiency due to pressurisation cycling. In addition to this, they have a large reliance on pressurisation/transport gas, operate non-continuously and dilute product syngas streams when using inert gases for pressurisation (Schell, 1988, Lau et al., 2002, Van der Drift et al., 2004, Higman and Van der Burgt, 2008, Rezaiyan and Cheremisinoff, 2005).

It is for these reasons that a new lock hopper feed system is proposed in the first phase of this research that looks to counter the drawbacks encountered with conventional lock hoppers and capitalise on the advantages that they present.

3.2 Case for pressurised gasification

Before the proposed feed system is detailed, it is appropriate at this point to analyse the energy savings brought about through operating the gasification process at pressure in order to provide context for the need to develop pressurised systems. Although it was found from the literature that the process of feeding a solid material to a high pressure environment is inherently difficult, the results shown in Figure 3-1 highlight the key advantage of operating the gasification process at pressure and the need for high pressure solids feed systems.

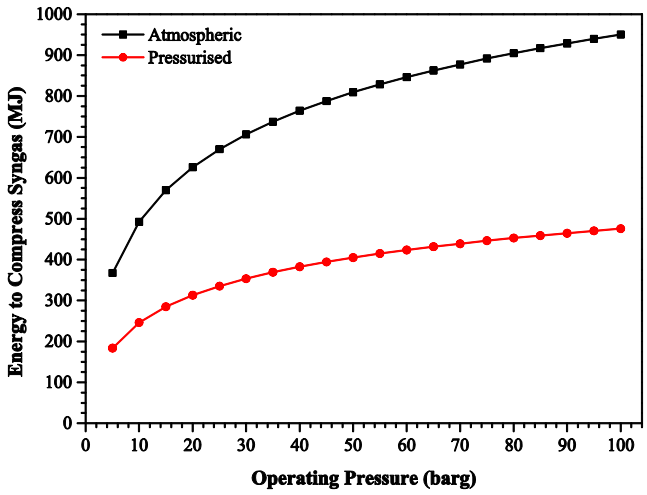

Figure 3-1: Compression energy comparison between an atmospheric and pressurised gasification process.

Figure 3-1 highlights the compression energy requirement for a crude gasification process generating a product gas at a range of pressures. The process assumes 1 tonne of pure carbon is combusted incompletely with pure oxygen to produce a gaseous stream of pure carbon monoxide ($C + ½O_2 \rightarrow CO$). While gasification entails a whole host of reactions and also incorporates steam as a feedstock, cold gas efficiencies are not wildly different to the assumed process.

$$\text{Cold gas efficiency (\%)} = \frac{\text{Heating value in product gas (MW)}}{\text{Heating value in feedstock (MW)}} \times 100$$

Equation 3-1

Cold gas efficiencies in modern gasification plants typically range between 70% and 80% and product gas streams are primarily made up of carbon monoxide and hydrogen which have broadly similar molar heating values (Maurstad, 2005, Higman and Van der Burgt, 2008). Assuming carbon is incompletely combusted with pure oxygen brings about a cold gas efficiency of 71.8% and therefore the process described poses as a suitable assumption for compression calculations.

Gas compression is assumed to take place isothermally in both cases, and the carbon feedstock is assumed to have a bulk density of 600 kg/m^3 and a voidage of 60%. The results shown in Figure 3-1 indicate that operating the process at pressure to produce a product gas at pressure saves around half of the compression energy. In this case, this is largely due to the large oxygen requirement (equivalence ratio of 0.5) and the energy required to compress the oxygen. In reality, gasification processes operate with an equivalence ratio between 0.2 and 0.4, and the product gas contains contaminant species such as carbon dioxide, nitrogen and methane (Higman and Van der Burgt, 2008, Crocker and Neathery, 2010). Each of these conditions acts to favour the pressurised process as contaminant species means a larger volume of product gas needs to be compressed in the atmospheric case, and smaller equivalence ratios means a smaller volume of oxidant has to be compressed in the pressurised case. Therefore, compression savings are more likely to be of the order of 60% to 80%. Although the savings shown in Figure 3-1 are more modest, they still highlight the fundamental advantage of operating the gasification process at an elevated pressure.

3.3 Proposed high pressure solids feed system

While conventional lock hoppers require a fraction of the energy required for oxygen compression, one of their biggest drawbacks remains their inefficiency as well as their large reliance on a transport gas for pressurisation. The design proposed in this research study takes the form of a new lock hopper that utilises water as an incompressible fluid to carry out the compression work. The use of water both reduces the work required for compression and negates the need for transport gas. In brief, water is used as a moveable piston. The water level acts as the piston face and allows the bulk of the compression work to be carried out by the water and in turn the pump used to introduce the water into the high pressure environment. Figure 3-2 highlights a schematic diagram of the proposed feed system, named the Hydraulic Lock Hopper (HLH).

The HLH consists of a feeding hopper operating at atmospheric pressure (H1), a lock hopper (H2) which undergoes pressurisation and depressurisation cycles, and a high pressure collection vessel (H3). H1 and H2 are separated by a valve (V1) and similarly H2 and H3 are separated by a valve (V2). Further to this, H2 and H3 are connected by a separate pipe outside of the main body of the feed system which contains an isolation valve (V3). This connecting pipe is used for pressure equalisation and recompression. Another connecting pipe is attached to H2 which contains a valve (V4) used to isolate the water being fed from a high pressure pump (P1). P1 is able to pump water against pressure and is thus used to recompress the depressurised gas in the pressurisation step, pumping water from a storage container (S1). Similarly to this, a third pipe used to drain the water once recompression has taken place is connected to H2 which contains a valve (V5) which is opened and closed accordingly to drain and seal H2.

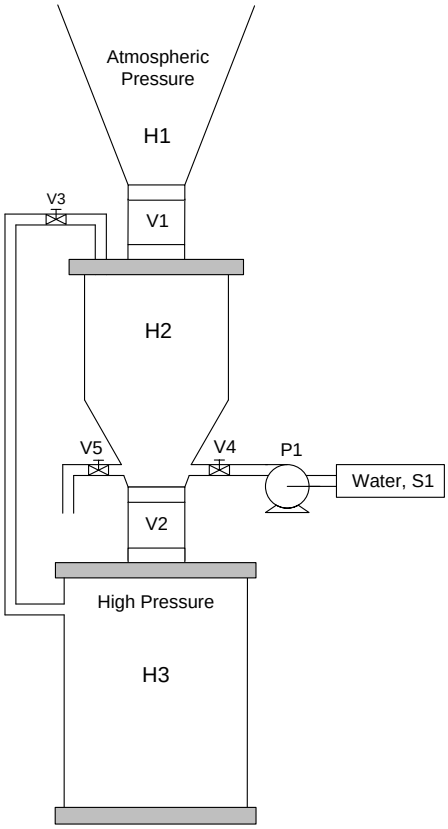

Figure 3-2: Schematic diagram of the Hydraulic Lock Hopper.

3.3.1 Modes of operation: Operating principles and procedures

The HLH presents two modes of operation which are discussed in Section 3.3.1.1 and 3.3.1.2 below. Mode 1 is the least energy intensive of the two modes and requires a volume of water to be pumped to H2 that is approximately equal to the void space contained between the material being fed. The main disadvantage of Mode 1 is that a volume of high pressure gas is still vented and ultimately wasted as found in conventional lock hoppers. Mode 2 counters this drawback by filling H2 completely with water so that the volume of high pressure gas vented is minimised. Although Mode 2 minimises the volume of gas vented, more energy is required to operate the HLH in Mode 2 as a larger volume of water has to be pumped in the compression stage. It is anticipated that Mode 2 will generate higher energy savings compared to conventional lock hoppers where the gas being vented is contaminated with product syngas. The following two sections provide an overview of the operating principals of both modes of operation.

3.3.1.1 Mode 1 operation

V1 is opened and fuel is fed via gravity from H1 to H2. V1 is then closed and V3 is opened allowing pressure equalisation between H2 and H3. V2 is then opened and the fuel is fed via gravity to its

desired destination, H3. V2 is then closed and V4 is opened allowing water from S1 to be pumped using P1 against pressure into H2. The water level acts as a piston pushing the gas from H2 back into H3, thus recompressing the system. When the desired pressure in H3 is reached (i.e. the original operating pressure), P1 is stopped and V4 is closed. V3 is then closed and the water contained within H2 is drained through the drainage pipe by opening V5. Once the water has been drained from H2, V5 is closed and the cycle is ready to start anew.

3.3.1.2 Mode 2 operation

Similarly to Mode 1, V1 is opened and fuel is fed via gravity from H1 to H2. V1 is then closed and V3 is opened allowing pressure equalisation between H2 and H3. V2 is then opened and the fuel is fed via gravity to its desired destination, H3. V2 is then closed and V4 is opened allowing water from S1 to be pumped using P1 against pressure into H2. The water level acts as a piston pushing the gas from H2 back into H3, thus recompressing the system. When H2 has been filled to capacity with water, P1 is stopped and V4 is closed; H2 is now full of water and H3 is at a pressure exceeding that of the original process pressure. V3 is then closed and the water contained within H2 is drained through the drainage pipe by opening V5. Once the water has been drained from H2, V5 is closed and the cycle is ready to start anew.

3.3.2 Advantages of the Hydraulic Lock Hopper

The new design presented above counters many of the stated disadvantages of conventional lock hoppers, but perhaps chiefly is that of inefficiency. One of the biggest drawbacks of current lock hopper systems is that a large proportion of the energy used for compression is wasted during the depressurisation stage. In the proposed system, the compression work is carried out by an incompressible fluid and the process gas is recycled through recompression. The consumption of transport gas is greatly reduced through the use of an incompressible fluid, and in turn syngas dilution with inert gas is avoided.

Problems encountered with valve sealing failure due to dusty environments are also potentially avoided through the substitution of gate valves with ball valves. The use of water for recompression means that the dusty environments encountered are reduced due to hopper cleaning during the recompression stage, and any remaining material contained in H2 is washed away during depressurisation/water drainage. Problems encountered with solids holdup can also be potentially avoided if the way in which pressure equalisation of H2 and H3 is altered to that previously stated. If V2 is opened prior to V3, thus equalising the pressure in H2 and H3 as would have happened if V3 was opened as normal, the disturbance in the feed material due to a large increase in pressure in H2

will prompt the free flowing of feed material from H2 to H3. As the pressure is then equalised V2 can then be closed and the process carried out as normal.

But perhaps the greatest advantage that the HLH presents, especially when compared to competing high pressure solids feed system designs, is its ability to be retrofitted to existing lock hopper units. All that is required is a supply of water, high pressure pipe work and fittings, and a high pressure water pump. Conventional gas compressors can be disposed of, and supplies of inert gas are no longer required. Therefore, retrofitting can be brought about at a relatively small cost, especially when compared to the construction and integration of wholly new technologies.

3.4 Theoretical efficiency gain of the Hydraulic Lock Hopper

One of the main advantages of the HLH is that it is able to operate with a relatively low energy requirement due to the use of an incompressible fluid. This section details the equations used, assumptions made and the results from the calculations assessing the theoretical increase in operating efficiency generated by the HLH over a conventional lock hopper.

3.4.1 Equations related to compression work

3.4.1.1 The first law of thermodynamics

One of the fundamental principles related to this work is the first law of thermodynamics which states that:

$$\Delta U = Q - W$$

Equation 3-2

Where ΔU is equal to the change in internal energy (J), Q is equal to the heat added to the system (J) and W is equal to the work done by the system (J) (Wark Jr., 1989). Similarly, the first law can be written as "ΔU = Q + W" where W is equal to the work done *on* the system rather than *by* the system (Shavit and Gutfinger, 1995, Atkins and De Paula, 2006). The first law provides a thermodynamic expression for the conservation of energy, which can be dissected further to provide a useful expression for the work required for compression or generated by expansion as shown in Equation 3-3.

$$W = \int_{V_1}^{V_2} P \, dV$$

Equation 3-3

Where W is equal to the compression or expansion work carried out on or by a system (J), P is the changing pressure (Pa), and V_1 and V_2 are the initial and final volumes of the system respectively

(m^3). The sign convention in this case agrees with Equation 3-2, as if an expansion takes place, the volume increases and the work output is seen to be positive. If this is then used in Equation 3-2, the work value becomes negative which corresponds to work being done *by* a system. Similarly, if compression takes place, the volume decreases and the work output is seen to be negative. If this is then used in Equation 3-2, the work value becomes positive which corresponds to work being done *on* a system.

3.4.1.2 Ideal gas and Boyle's law

One important relationship and of significant importance in this case is that of the ideal gas law and more specifically, Boyle's law which constitutes a special case of the ideal gas law.

$$PV = nRT$$

Equation 3-4

$$P_1V_1 = P_2V_2 = Constant$$

Equation 3-4a

Where P_1 and P_2 are equal to the initial and final pressure (Pa), V_1 and V_2 are equal to the initial and final volume (m^3), n is equal to the number of moles (mol), R is the ideal gas constant (8.314 J/mol K) and T represents a constant temperature (K). Boyle's law only holds at a constant temperature and essentially constitutes a form of conservation of energy (Atkins and De Paula, 2006).

3.4.1.3 Compression work

A quasistatic process where "PV^{γ} = constant" is called a polytropic process. A number of these processes are detailed below; however, only those relationships relating to an isothermal and an adiabatic process are of interest in this case (Atkins and De Paula, 2006).

Process	Constant	Relationship
Isochoric	Volume	$\gamma = \infty$
Isobaric	Pressure	$\gamma = 0$
Isothermal	Temperature	$\gamma = 1$
Adiabatic	No heat loss	$\gamma = C_p/C_v$

Table 3-1: Overview of polytropic processes and corresponding values for γ (Shavit and Gutfinger, 1995).

Substituting Equation 3-4a into Equation 3-3 and integrating with respect to volume with the constraint of γ=1 produces a relationship for the work required or generated by an isothermal compression or expansion respectively (O'Neill, 1993, Atkins and De Paula, 2006).

$$W = nRT \ln\left[\frac{V_2}{V_1}\right]$$

Equation 3-5

Similarly, substituting Equation 3-4 into Equation 3-3 and integrating with respect to volume with the constraint of $\gamma = C_p/C_v$ where C_p and C_v are a substances specific heat capacities (kJ/kg K) at constant pressure and constant volume respectively, produces a relationship for the work required or generated by an adiabatic compression or expansion respectively (O'Neill, 1993, Atkins and De Paula, 2006).

$$W = \frac{PV^{\gamma}\left(V_2^{1-\gamma} - V_1^{1-\gamma}\right)}{1-\gamma}$$

Equation 3-6

Although Equation 3-5 and Equation 3-6 allow the work required to compress a gas to be calculated, they do not provide a means to calculate the power requirement of a real compressor. This is because in a real compressor, the gas being compressed first has to be drawn into the compressor at a given suction pressure and discharged from the compressor after it has been compressed. Equation 3-5 and Equation 3-6 only provide a means to calculate the work required in the compression stage.

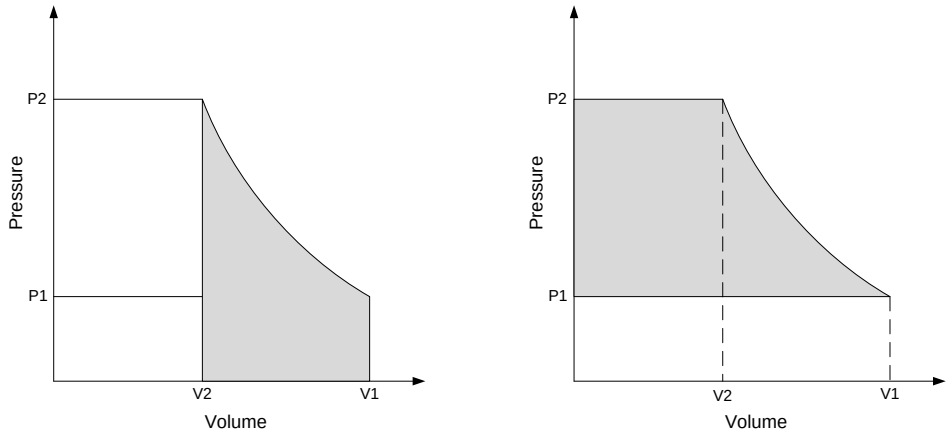

Figure 3-3: PV diagram of a real (right) and ideal (left) compression cycle (O'Neill, 1993).

The work involved in the compression stage alone is shown on the left hand side of Figure 3-3, and the work required by a real compressor is shown on the right hand side of Figure 3-3. Interestingly, integrating to find the work associated with a compressor operating isothermally produces the same relationship as shown in Equation 3-5. However, integrating to find the work associated with a compressor operating adiabatically produces Equation 3-7 (O'Neill, 1993).

$$W = nRT \frac{\gamma}{\gamma - 1}\left(\left(\frac{P_2}{P_1}\right)^{\frac{\gamma-1}{\gamma}} - 1\right)$$

Equation 3-7

The minimum amount of work required by a compressor occurs when the compression takes place isothermally, and therefore Equation 3-5 provides a means to assess the lower energy limit for compression. Conversely, the maximum amount of work required by a compressor occurs when the compression takes place adiabatically, and in turn Equation 3-7 can be used to determine the upper energy limit for compression.

3.4.1.4 Compressibility

Further to the relationships between pressure and volume and the work required for compression is the relationship between volume and pressure and the compressibility of an individual substance. The general equation for compressibility states that:

$$\kappa_x = -\frac{1}{V}\left(\frac{\partial V}{\partial P}\right)_x$$

Equation 3-8

Where κ_x is the compressibility (Pa^{-1}), V is the volume (m^3), P is the pressure (Pa) and the subscript x is either stated as T or S for temperature or entropy respectively, and in turn for an isothermal or adiabatic compressibility respectively (Wark Jr., 1989, Atkins and De Paula, 2006). In an isothermal case the differential is taken at constant temperature and in an adiabatic case the differential is taken at no heat loss (dQ=0) for an irreversible process and at constant entropy (dQ=TdS=0) for a reversible process (Wark Jr., 1989). Where no change in entropy occurs, the process can also be said to be isentropic. The relationship between the isothermal compressibility and the adiabatic/isentropic compressibility is stated as Equation 3-9.

$$\frac{\kappa_T}{\kappa_S} = \frac{C_p}{C_V} = \gamma$$

Equation 3-9

Where γ is the ratio of the specific heat capacities (kJ/kg K) of a substance C_p/C_v at constant pressure and volume respectively (Atkins and De Paula, 2006). Compressibility and pressure with respect to liquids is largely governed by the finite volume that the liquid molecules occupy, whereas ideal gas theory applies for gas species. Gas molecules act as point sources of mass, and pressure is due to the momentum exchange when such masses collide with a wall as per the kinetic theory of gases. Table 3-2 displays the compressibility's of common substances at specific temperatures and pressures and their respective percentage decrease in volume.

Generally, compressibility decreases significantly with initial increases in pressure and less significantly with larger pressures, and compressibility decreases significantly with increases in

temperature at low pressures and less significantly at high pressures (1000-2000 bar) (Perry et al., 1997). Table 3-2 highlights the main advantage of using water in the recompression stage in the HLH.

Substance	Compressibility κ_T (Pa^{-1})	Temperature (°C)	Pressure (bar)	Volume Decrease (%)
Benzene	7.7×10^{-10}	20	200	1.53
Mercury	3.95×10^{-11}	20	300	0.118
Methanol	9.5×10^{-10}	20	200	1.88
Water	4.9×10^{-10}	20	13	0.0637
Water	4.3×10^{-10}	20	200	0.856

Table 3-2: Compressibility's of common substances (Perry et al., 1997).

3.4.2 Compression work calculation and comparison

The three key variables concerned with the proposed feed system are operating pressure, process volume to lock hopper volume fraction (H3/H2) and feed material voidage; that is the void space required to be pressurised in H2 when filled with fuel. The following graphs and tables are the product of Equation 3-3 to Equation 3-7 and highlight the compression work required in each scenario where the above stated factors are varied.

3.4.2.1 Effect of process to lock hopper volume fraction (H3/H2)

The volume fraction of H3 to H2, where H3 represents the high pressure collection vessel and H2 is the lock hopper where pressurisation and depressurisation takes place, plays an integral part in the overall efficiency of compression. Figure 3-4 highlights the energy saving generated by the HLH operating in both Mode 1 and Mode 2 compared to a conventional lock hopper with varying fractions of H3/H2, and the energy required for compression by the HLH per unit volume of H2. Calculations assume an operating pressure of 25 barg and a fuel voidage of 50%. Compression is assumed to take place isothermally in all cases, and the figures shown act to provide a preliminary assessment of the energy required for compression by each process. In reality it is likely that the compression phase will take place somewhere between being isothermal and adiabatic. To provide context for the values shown in Figure 3-4 regarding the energy requirement of the HLH, a conventional single lock hopper was determined to require a constant of approximately 4.2 MJ/m^3 at an operating pressure of 25 barg. Such a value was determined assuming an isothermal compression.

One key phenomenon that Figure 3-4 highlights is that when operating in Mode 1, as the volume fraction of the high pressure collection vessel (H3) to the lock hopper (H2) increases, the amount of energy saved by the HLH decreases, and eventually reaches an approximate plateau past a given volume fraction. Therefore, in order to maximise the energy savings generated by the HLH in Mode 1 compared to a conventional lock hopper, a small H3 compared to H2 is required. However, the

limiting factor in this case is the volume required for feeding fuel and so the minimum volume H3 can be is equal to H2 in order to maximise throughput – thus the fraction of H3/H2 becomes 1. It is therefore realised that a separate intermediate hopper between H2 and H3 of equal volume to H2 is required in order to maximise the efficiency of the HLH running in Mode 1. It is proposed that the connecting pipe containing the valve V3 will be changed so that H2 is now linked to the new intermediate hopper which will be referred to as H4 from now on. A schematic of the new design of the HLH is shown in Figure 3-5.

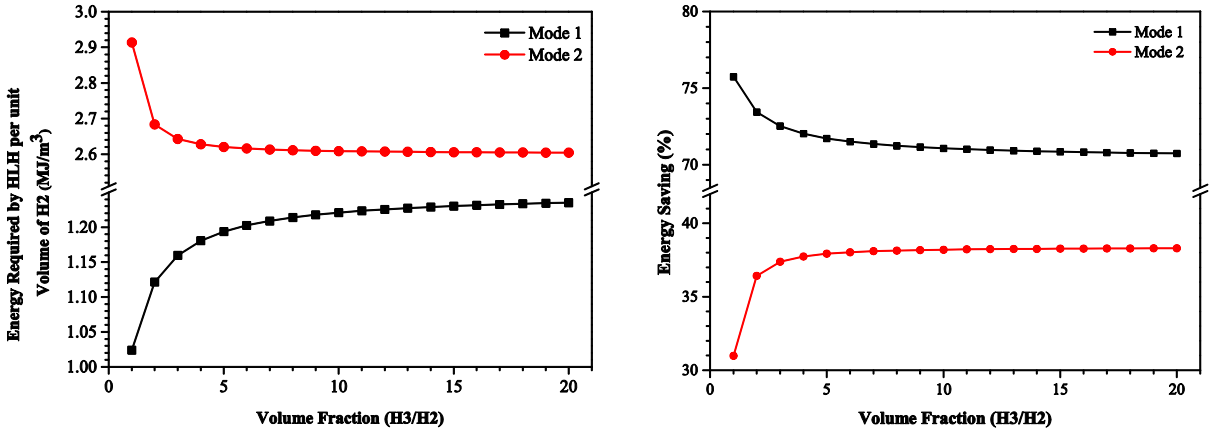

Figure 3-4: Compression energy required by the HLH per unit volume of H2 (left) and energy savings generated by the HLH over a conventional lock hopper (right), both at varying volume fractions of H3 to H2.

Examining the same variable (volume fraction of H3/H2) for Mode 2 suggests different changes to be made to the HLH. As the volume fraction of H3/H2 decreases in Mode 2, the energy saving compared to a conventional lock hopper is also shown to decrease – significantly at volume fractions ≤ 1. Mode 2 is therefore seen to perform at its best compared to a conventional lock hopper where the volume of H2 is small in relation to H3 – the opposite of what favours Mode 1. Although the design of the HLH has been changed to accommodate further energy savings generated by Mode 1 (Figure 3-5), the HLH can also be run as before by leaving V6 open and thus using H4 to further increase the volume of the high pressure collection vessel.

It is important to state that in reality the feed system presents itself as the primary boundary between the atmosphere and a high pressure process, and the feed system is directly connected to an overall working process at pressure. Therefore, H3 represents the volume of the working process and is in turn inherently much larger than that of H2 which favours the use of Mode 2. Changing the design of the HLH to that displayed in Figure 3-5 allows both modes of operation to be analysed by having the pressure boundary situated at V6 or V2 for Mode 1 or Mode 2 respectively.

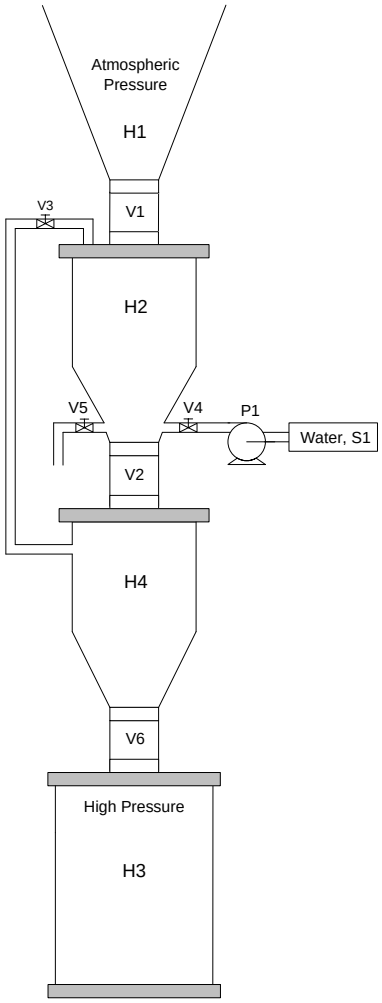

Figure 3-5: Updated schematic diagram of the HLH.

Further to this, the theoretical work presented regarding the energy savings of Mode 1 operating with an equal volume chamber to H2 located below (H4) suggests another mode of operation (Mode 3) can be assessed further to Mode 1 and Mode 2. Mode 3 presents the possibility to reduce the energy required for compression by Mode 2 further but still minimise/negate the volume of process gas at pressure vented to the atmosphere. Mode 3 carries out the compression stage in two parts. The first stage is identical to that presented by Mode 1, where process pressure is achieved, leaving a head space of gas at pressure in H2. However, once V6 has been opened in the new design and fuel has been fed to H3, a second stage of compression can take place similar to that observed in Mode 2 where H2 is filled to capacity and ultimately the volume of gas at pressure vented to the atmosphere is minimised. Therefore, Mode 3 presents itself as a combination of both Mode 1 and Mode 2 in order to minimise the amount of energy required for compression further. Mode 3 will be assessed alongside both Mode 1 and Mode 2 in the following sections.

3.4.2.2 Effect of fuel voidage

One factor that will change continuously from batch to batch of fuel fed is the voidage between the fuel in H2, which is directly linked to the amount of compression work required to operate the system. The larger the voidage is the more compression work is required due to a greater volume presented; however, this factor does not affect the HLH alone. It remains the same for conventional lock hoppers and therefore a direct comparison between the two can be drawn and the role that voidage has on compression efficiency can be determined.

Figure 3-6 highlights the energy saving generated from using the HLH over a conventional lock hopper of the same magnitude, assuming both systems operate isothermally (left) and adiabatically (right). In reality it is likely that the compression phase will lie somewhere between the two, and so Figure 3-6 displays both an isothermal and adiabatic process to provide an upper and lower limit. An operating pressure of 25 barg is assumed in all cases and a volume of H2=H4 is assumed for Mode 1, a volume of 1000*H2=H4+H3 is assumed for Mode 2 and a volume of H2=H4 and 1000*H2=H4+H3 is assumed for Mode 3.

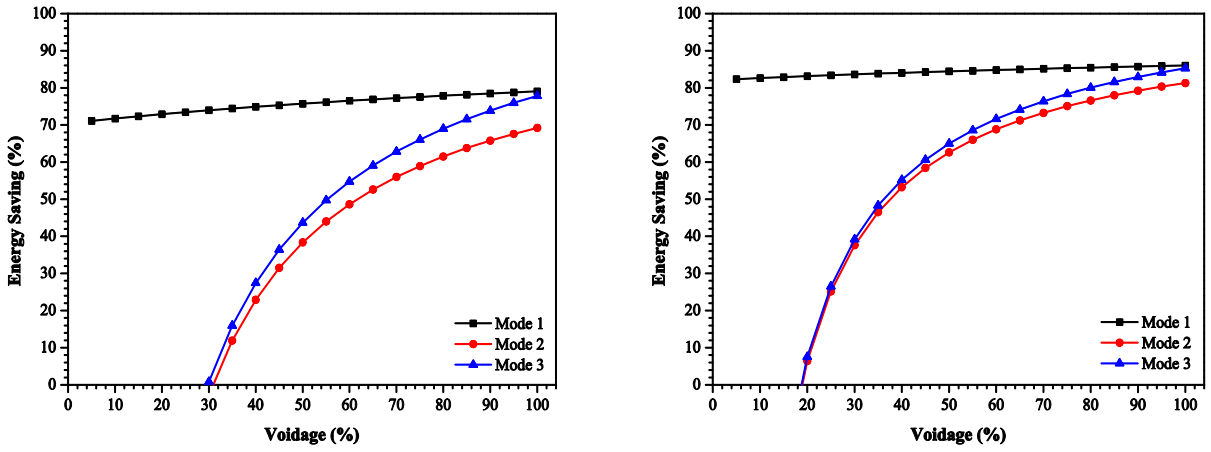

Figure 3-6: Compression energy savings generated by the HLH over a conventional lock hopper with varying degrees of fuel voidage (isothermal-left, adiabatic-right).

It is clear in all cases that as voidage increases so does the compression efficiency, and so it can be interpreted that for fuels presenting a large voidage such as straw, switchgrass and bagasse, the HLH will prove to be more efficient. Typical values for the voidage of monosized spheres having regular hexagonal and regular cubic packing are 26% and 48% respectively; however, voidages for non-spherical and irregular shaped solids are typically much higher (Woodcock and Mason, 1996). Efficiency gains created by the HLH in this case can therefore be calculated to be approximately equal to 76%, 38% and 44% for an isothermal compression in Mode 1, Mode 2 and Mode 3 respectively where a voidage of 50% is assumed.

3.4.2.3 Effect of operating pressure

Another important parameter to take into account in addition to fuel voidage is the operating pressure of the process. Figure 3-7 highlights the energy savings generated by the HLH over a conventional lock hopper assuming an isothermal compression (left) and an adiabatic compression (right). A voidage of 50% is assumed in all cases and a volume of H2=H4 is assumed for Mode 1, a volume of 1000*H2=H4+H3 is assumed for Mode 2 and a volume of H2=H4 and 1000*H2=H4+H3 is assumed for Mode 3.

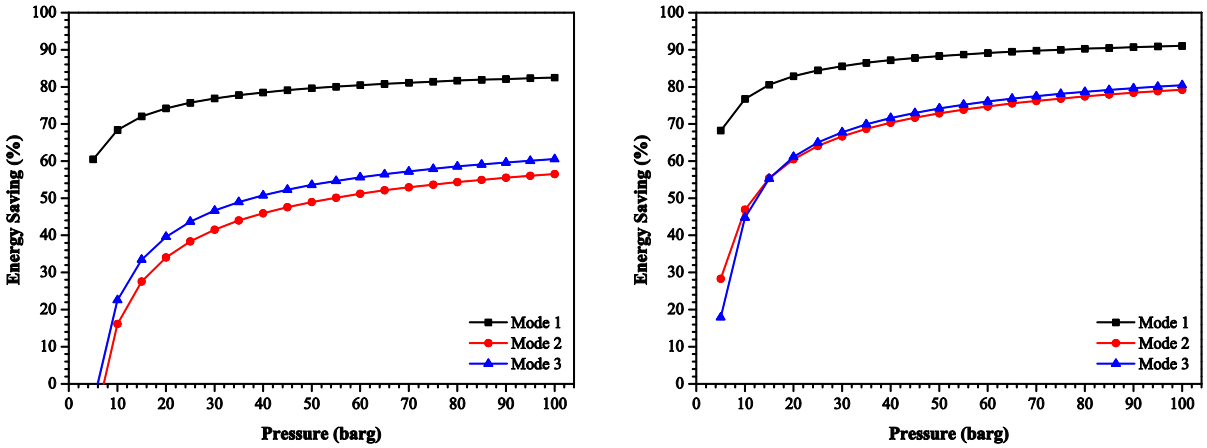

Figure 3-7: Compression energy savings generated by the HLH over a conventional lock hopper at varying operating pressures (isothermal-left, adiabatic-right).

Again, it is likely that both systems will operate somewhere between being isothermal and adiabatic and so an experimental value will lie somewhere between the two plots presented in Figure 3-7. However, regardless of how the compression takes place, a clear trend of increasing energy saving with increasing operating pressure can be observed. Therefore, from the theoretical calculations presented in Figure 3-6 and Figure 3-7 it can be stated that the design principle of the HLH maximises its efficiency where high voidage fuels and high operating pressures prevail. Calculations based on an isothermal compression indicate that energy savings are generated in all modes of operation where the operating pressure is ≥8 barg. Analysing Mode 1 further highlights the theoretical volume of water that is required to be pumped to bring about compression at varying operating pressures.

Pressure (barg)	Water Volume per Volume of H2 (%)	Pressure (barg)	Water Volume per Volume of H2 (%)
1	24.84	10	45.40
2	33.19	20	47.59
3	37.38	50	49.01
4	39.89	100	49.50
5	41.58	1000	49.95

Table 3-3: Volume of water required for compression at varying operating pressures in Mode 1 (voidage=50%).

Table 3-3 displays the volume percentage that water takes up in H2 after compression has taken place at varying operating pressures. The values stated are calculated assuming a fuel voidage of 50% and that H2 is equal in volume to H4. It can be observed that as operating pressure increases, the volume percent of water required for compression approaches that of the voidage. It can therefore be estimated that at operating pressures exceeding 100 barg the volume percentage of water required for compression to take place is equal to that of the voidage.

3.4.2.4 Overall comparison

Examining factors such as the volume fraction of H2 to H3, operating pressure and fuel voidage highlights the principal operating conditions that favour the HLH compared to a conventional lock hopper. Theoretical work highlights inflated energy savings for Mode 1 where H3 is equal to H2 and is in turn the basis for adding an intermediate chamber H4 to the design as displayed in Figure 3-8.

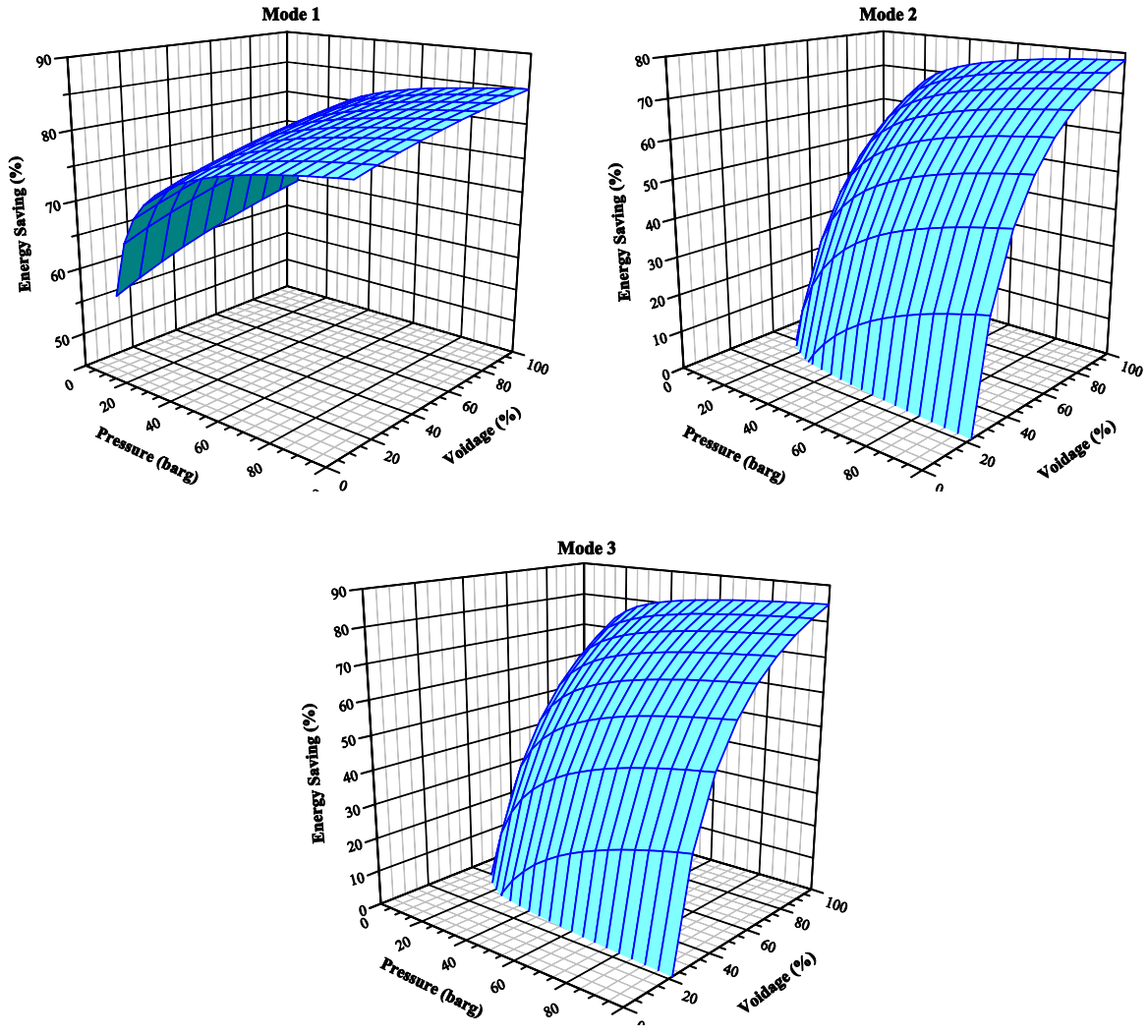

Figure 3-8: Energy saving of the HLH compared to a conventional lock hopper both operating isothermally at varying operating pressures and fuel voidages.

Removing the factor of volume fraction of H2 to H3 leaves the remaining factors: operating pressure and fuel voidage. Analysing both factors in terms of energy saving compared to a conventional lock hopper generates the graphs displayed in Figure 3-8 where energy savings are displayed at varying operating pressures and fuel voidages for Mode 1, Mode 2 and Mode 3. Both the HLH and conventional lock hopper are assumed to operate isothermally in the figures shown in order to highlight a minimum energy saving scenario.

It is clear from the cases computed that the HLH performs best where high operating pressures and high fuel voidages prevail. Mode 1 is shown to outperform both Mode 2 and Mode 3 in terms of energy saving in all cases due to the smaller amount of mechanical work that is required, and energy savings generated by Mode 3 are found to approach those generated by Mode 1 as both fuel voidage and operating pressure increase. It is anticipated that energy savings generated by Mode 2 and Mode 3 will become more competitive with those generated by Mode 1 where high levels of lock gas contamination with syngas are present. However, purely on the basis of compression work, Mode 1 is found to be the most efficient, followed by Mode 3 and then Mode 2.

3.5 Gas solubility

As the HLH incorporates water in the compression stage of its operation and high pressure gases are inherently present, gas absorption will invariably take place. While this doesn't pose a significant problem in the case of inert gases such as carbon dioxide and nitrogen, it is important to review the solubility of valuable product gases such as hydrogen and carbon monoxide as their absorption and subsequent removal through the liquid phase presents an energy penalty on the system. The level of gas dissolved in a given liquid can be determined using Henry's law as stated in Equation 3-10.

$$P_A = \mathcal{H} C_A$$

Equation 3-10

Where P_A is the partial pressure of component A (atm), H is the Henry's coefficient (atm/mol fraction) and C_A is the concentration of component A in the liquid (mol fraction) (Shinoda and Becher, 1978, Richardson et al., 2002). Fundamentally, Henry's law states that the solubility of a gas in a liquid is directly proportional to the partial pressure of the gas in contact with that liquid. Therefore, as water is introduced into H2 during the compression stage, gas species will become dissolved in the water and will be released during the depressurisation stage.

3.5.1 Effect of temperature on solubility

Although pressure is the main driving force for the dissolution of a gas in a liquid, gas solubility is also greatly affected by temperature. It is generally found that gas solubility decreases with increasing temperature and the Henry's coefficient changes accordingly. Equation 3-11 along with Table 3-4 provides a relationship between temperature (T) and the Henry's coefficient (H) for a range of gas species at a constant pressure of 1 atm (Coker, 2010), and Figure 3-9 highlights the effect of temperature on the solubility of carbon dioxide in water.

$$\log_{10} \mathcal{H} = A + B/T + C \log T + DT$$

Equation 3-11

Gas	A	B	C	D	T_{min}	T_{max}	H at 25 °C
CO_2	69.42	-3796.46	-21.67	0	273.15	353.15	1635.20
N_2	78.86	-3744.98	-24.80	0	273.15	350.15	87143.10
CO	74.60	-3603.30	-23.34	0	273.15	353.15	57978.50
H_2	54.69	-2400.98	-16.89	0	273.15	345.15	70832.10
CH_4	146.89	-5768.34	-51.91	0.02	273.15	360.95	39240.10

Table 3-4: Effect of temperature on the Henry's coefficient for a range of gas species in water (Coker, 2010).

Due to the large thermal mass that water presents, gas and liquid temperature is not likely to change dramatically during the compression stage of the HLH, and therefore temperature can be assumed to stay broadly constant and ambient during compression. Carbon dioxide is well known for its solubility in water and Figure 3-9 indicates carbon dioxide to be readily dissolved in water at fairly modest partial pressures, with around 9 litres of carbon dioxide being absorbed per litre of water at 10 atm and 18 °C. Where gasification is concerned, this does not pose a major problem energetically; however, the uncontrolled release of carbon dioxide presents a drawback from an environmental standpoint.

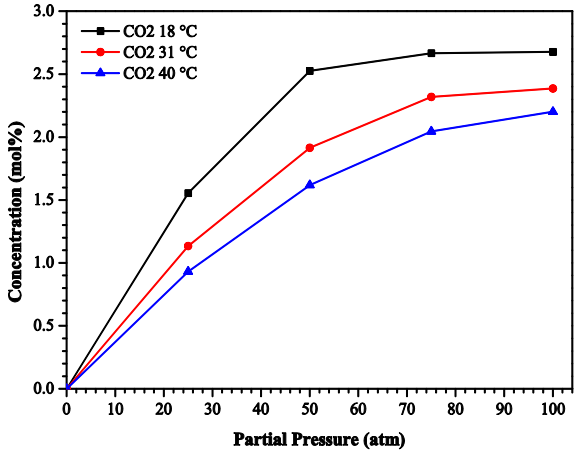

Figure 3-9: Effect of pressure and temperature on the solubility of carbon dioxide in water (Perry et al., 1997).

3.5.2 Solubility of product gas species

While carbon dioxide will invariably be present in some part in the product stream emerging from a gasifier, concentrations are typically low due to the desired incomplete conversion of the carbon containing feedstock. Carbon dioxide absorption does not pose a major concern compared to the absorption and removal of the valuable constituents of the product gas (hydrogen, carbon monoxide and methane). Their absorption and removal does not just pose a problem in terms of efficiency, but a major hazard due to their combustibility. Figure 3-10 provides an overview of the solubility of the main constituents of syngas in water at various partial pressures.

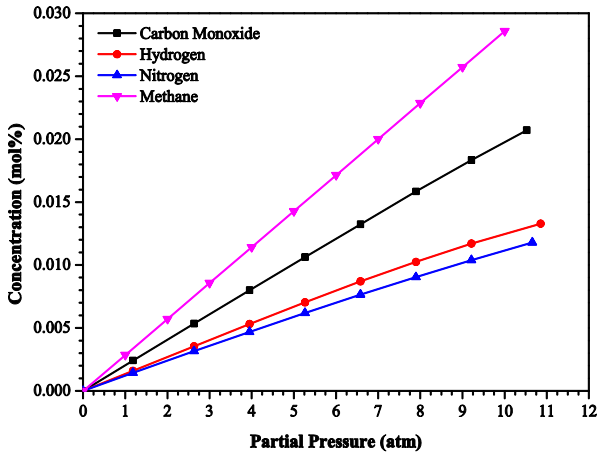

Figure 3-10: Effect of pressure on the solubility of a range of gas species in water (19 °C) (Perry et al., 1997).

It is clear from Figure 3-10 that all of the gaseous components typically making up a product syngas are soluble in water; however, it is observed that the solubility's of such gases are far lower than that of carbon dioxide. Where partial pressures of 10 atm prevail concentrations as low as 0.012 mol% in the case of hydrogen are brought about and 0.019 mol% in the case of carbon monoxide. Such concentrations do not present a significant drawback of the system and given the time scale of the compression stage and the surface area of the gas-liquid interface, it is anticipated that absorption will not take place to completion as given by Henry's law.

3.6 Designing a system for pressure

Stress analysis largely governs the design of any vessel under pressure (internal or external) and is principally used to determine the required material thickness to ensure an economical and safe design. It is not necessary to determine every stress present in a piece of equipment, but to know the principal stresses governing the design to ensure adequate process safety (Moss, 2004).

In the context of thin walled pressure vessels ($R/t_w > 10$), where R is the component radius (mm) and t_w is the associated wall thickness (mm), the wall is assumed to provide no resistance to bending. This

means that wall/membrane stresses are the only stresses acting and responsible for the containment of pressure; this differs from thick walled pressure vessels ($R/t_w < 10$) where bending stresses occur in addition. The three principal stresses of interest related to pressure vessel design are longitudinal stress (σ_l), circumferential (hoop) stress (σ_{hp}) and radial stress (σ_r) (Bednar, 1991, Moss, 2004), each of which will be discussed in the following sections.

3.6.1 Stress analysis

Cylinders, spheres and cones are three of the most common forms of pressure vessel used either in composite or in singular arrangements. The principal components concerned with this work take the form of cylinders and cones, and therefore stress analysis will be discussed with respect to these geometries. The longitudinal stress can be examined by examining the plane normal to the axis of a cylinder. Figure 3-11 highlights the resulting longitudinal stress in a cylinder under internal pressure where, P_i is the internal pressure (Pa), r_m is the mean radius (mm) and t_w is the wall thickness (mm).

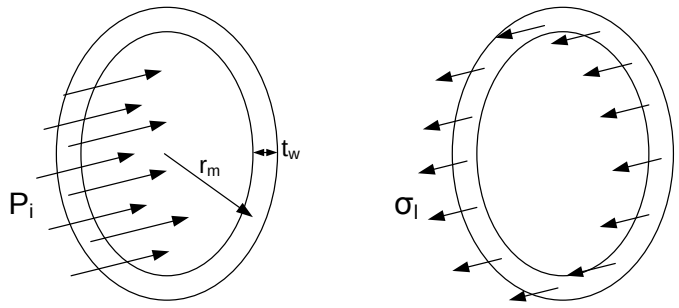

Figure 3-11: Longitudinal stress arising in a cylinder under internal pressure.

For equilibrium to occur there must be a force counteracting the internal pressure. Where thin walled vessels are concerned it is assumed that membrane action takes place (all stresses act parallel to the surface). Therefore, the only stress that can result in this plane is the longitudinal stress as highlighted. A force equilibrium generates Equation 3-12.

$$\sigma_l = \frac{P_i r_m}{2t_w}$$

Equation 3-12

The hoop stress can be determined by examining the plane parallel with the axis of a cylinder. Figure 3-12 highlights the resulting hoop stress in a cylinder under internal pressure where, l is the length of a given portion of a cylinder (mm).

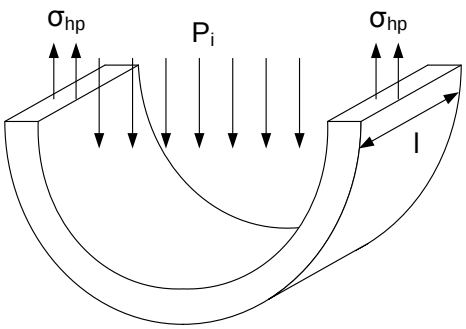

Figure 3-12: Hoop stress arising in a cylinder under internal pressure.

The only stress that can result in this plane is the hoop stress as highlighted. A force equilibrium generates Equation 3-13.

$$\sigma_{hp} = \frac{P_i r_m}{t_w}$$

Equation 3-13

Further to both the longitudinal and hoop stress is the radial stress. Analysis assumes that the radial stress exerted by the wall varies with length/distance through the wall with a linear relationship and that it is at its maximum on the inside wall of the pressure vessel and equal to the pressure (negative for compression). This is a reasonable approximation for thin walled pressure vessels and thus at its maximum σ_r is equal to $-P_i$. Comparing the maximum radial stress to the hoop stress in a thin walled pressure vessel where $R/t_w > 10$ must hold generates Equation 3-14.

$$\sigma_{hp} = \frac{P_i r_m}{t_w} = 10P_i = 10\sigma_r$$

Equation 3-14

As a result, the radial stress is commonly neglected when dealing with thin walled pressure vessels as at its maximum it is equal to a tenth of the hoop stress (Moss, 2004). The state of stress in a thin walled pressure vessel is therefore commonly assumed to be bi-axial. Similarly, it can be observed from the stress analysis conducted that the hoop stress is twice that of the longitudinal stress and therefore the hoop stress can be deemed the determining factor when calculating vessel wall thickness.

Further to the stresses present in cylinders are those present in cones. By examining the plane parallel to the axis of a cone, the conical longitudinal stress (σ_{lc}) can be examined. Figure 3-13 highlights the resulting longitudinal stress in a cone under internal pressure where, α is the conical half angle (°).

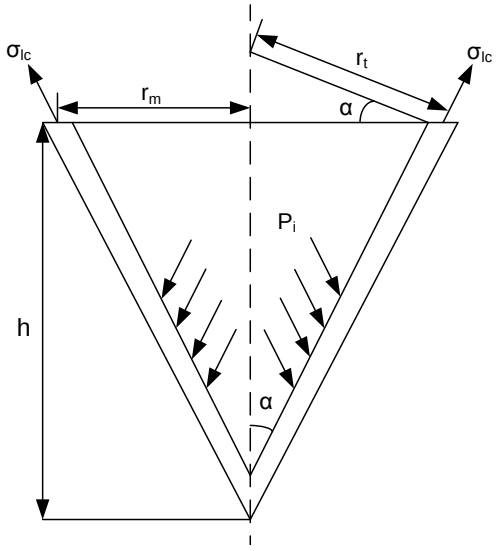

Figure 3-13: Longitudinal stress arising in a cone under internal pressure.

The stress highlighted is the longitudinal conical stress which acts against the internal pressure. As a result of the conical structure the radius is taken as the tangential radius of curvature (r_t) rather than the mean radius (r_m) as is taken in cylindrical elements. A force equilibrium generates Equation 3-15.

$$\sigma_{lc} = \frac{P_i r_m}{2t_w} \cdot \frac{1}{\cos\alpha}$$

Equation 3-15

$$r_t = r_m / \cos\alpha$$

Equation 3-15a

Similarly, by examining the plane parallel with the axis of the cone the conical hoop stress (σ_{hc}) can be examined to be:

$$\sigma_{hc} = \frac{P_i r_m}{t_w} \cdot \frac{1}{\cos\alpha}$$

Equation 3-16

The stress analysis for both cylindrical and conical elements stated above forms the basis for the relationships between component geometry/internal pressure and wall thickness as presented in the standard EN 13445. EN 13445 specifies the requirements for the construction, inspection and testing of unfired fusion welded pressure vessels, and provides a comprehensive procedure to design as well as reviewing a broad range of materials for construction (EN13445, 2009). The following section highlights the equations used for the design of vessels subject to high internal pressures.

3.6.2 Equations related to pressure vessel design

Further to the relationships derived from stress analysis between the principal stresses and the component geometry/internal pressure is the design protocol and equations stated in the standard EN 13445 which provides a comprehensive guide to determining the minimum wall thickness required for a vessel under internal pressure.

C is a design constant (0.41 for bolted cover with full face gasket)
d is the diameter of an opening into a vessel (mm)
D_c is the inside diameter of a cylinder at a junction with a cone (mm)
D_e is the nominal plate diameter (= the bolt circle diameter and taken as 15% above D_i) (mm)
D_i is the inside diameter of a cylinder ***or*** the inside diameter of a cone at the point (mm)
e is the minimum wall thickness for a conical shell (mm)
e_c is the minimum wall thickness required for a cylindrical shell (mm)
e_h is the minimum head thickness for a flat unstayed head (mm)
e_j is the thickness of a knuckle required where a cylindrical and conical section meet (mm)
e_p is the minimum head thickness used when $d/D_e < 0.5$ (mm)
e_1 is the minimum thickness of a cylindrical shell at a junction (mm)
e_2 is the minimum thickness of a conical shell at a junction (mm)
f is the nominal design stress (not exceeding $R_m/5$) (N/mm^2)
l_1 is the length of a knuckle along a cylindrical section (mm)
l_2 is the length of a knuckle along a conical section (mm)
p is the design pressure (10% above P_i) (N/mm^2)
P_i is the internal pressure (N/mm^2)
r is the inside radius of curvature of a knuckle ($r \leq 0.3D_c$) (mm)
R is the distance from the centre of a circular end (mm)
R_m is the tensile strength (400 N/mm^2 for mild steel EN3A / 070M20)
α is the half angle of a conical section (degrees)

Minimum wall thickness required for a cylindrical shell:

$$e_c = \frac{pD_i}{2f - p}$$

Equation 3-17

Minimum wall thickness for a conical shell:

$$e = \frac{pD_i}{2f - p} \cdot \frac{1}{\cos \alpha}$$

Equation 3-18

Minimum head thickness for a flat unstayed head:

$$e_h = CD_e\sqrt{p/f}$$

Equation 3-19

Where $d/D_e < 0.5$, the minimum head thickness is increased to provide reinforcement:

$$e_p = e_h\sqrt{\frac{D_e}{D_e - d - R}}$$

Equation 3-20

Further to the equations used to calculate the minimum thickness required for the shell walls and head are the following equations used to determine the thickness of a knuckle required where a cylindrical and conical section meet:

$$e_j = \frac{pD_c\beta}{2f\gamma}$$

Equation 3-21

$$\beta = \frac{1}{3}\sqrt{\frac{D_c}{e_j}}\cdot\left(\frac{\tan\alpha}{1 + 1/\sqrt{\cos\alpha}}\right) - 0.15$$

Equation 3-21a

$$\gamma = 1 + \frac{\rho}{1.2\left(1 + \frac{0.2}{\rho}\right)}$$

Equation 3-21b

$$\rho = \frac{0.028r}{\sqrt{D_c e_j}}\cdot\frac{\alpha}{1 + \frac{1}{\sqrt{\cos\alpha}}}$$

Equation 3-21c

The value for e_j is acceptable if it is not lower than that assumed for both Equation 3-21a and Equation 3-21c. The minimum thickness of the cylindrical shell at the junction where the cylindrical shell and the conical section meet (e_1) should be the greater of the two values obtained from Equation 3-17 for the cylindrical shell wall thickness (e_c) and Equation 3-21 for e_j. Similarly, the minimum thickness of the conical shell at the junction where the cylindrical shell and the conical section meet (e_2) should be the greater of the two values obtained from Equation 3-18 for the conical shell wall thickness (e) and Equation 3-21 for e_j.

The thickness e_1 should be maintained for at least $1.4l_1$ from the junction and $0.5l_1$ from the cylinder tanline. Similarly, the thickness e_2 should be maintained for at least $1.4l_2$ from the junction and $0.7l_2$ from the conical tanline where:

$$l_1 = \sqrt{D_c e_1}$$

Equation 3-22

$$l_2 = \sqrt{\frac{D_c e_2}{\cos \alpha}}$$

Equation 3-23

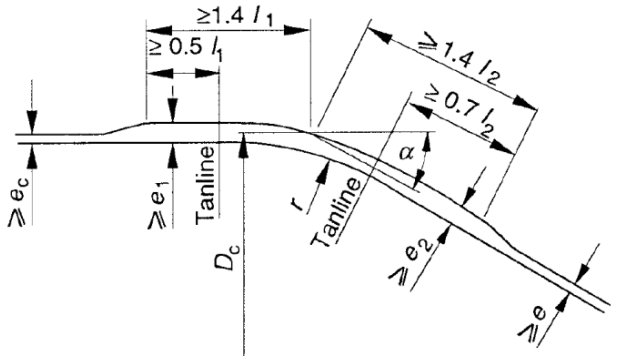

Figure 3-14: Geometry of a knuckle and the required measurements.

3.7 Summary

This chapter primarily details the design of a new feed system capable of feeding solid materials to high pressure environments. The proposed feed system, named the Hydraulic Lock Hopper (HLH) takes the form of a new lock hopper that utilises water as an incompressible fluid. Water is used to displace gas at high pressure, and the only energy required by the HLH is that to pump water against a back pressure. The system disposes with conventional gas compressors and does not require a supply of transport gas for pressurisation. The design presented is particularly attractive from an industrial standpoint, as the integration of the HLH can be brought about by retrofit at a relatively small cost. All that is required is a supply of water, high pressure pipe work and fittings, and a high pressure water pump.

Three modes of operation were proposed. One whereby a minimum amount of mechanical work is required for compression but a portion of gas at pressure is left and subsequently vented to the atmosphere, and two modes which minimise/negate the volume of gas at pressure vented but require additional compression work. The HLH seeks to address common operational problems encountered with conventional lock hoppers, but primarily seeks to counter issues regarding energy efficiency. Calculations relating solely to the amount of energy required for compression indicate that energy

savings compared to conventional lock hoppers as high as 84%, 64% and 65% for Mode 1, Mode 2 and Mode 3 respectively can be attained. Such figures assume that compression takes place adiabatically at a pressure of 25 barg and that there is a fuel voidage of 50%. Calculations also indicate that energy savings in excess of these can be attained, with higher energy savings being calculated for higher operating pressures and for fuels with larger voidages.

In addition to this, pressure vessel design was reviewed and stress analysis relating to the principal stresses found in common vessel configurations relating to the HLH was undertaken. The standard EN 13445 which provides a comprehensive guide to determining the minimum wall thickness required for vessels under internal and external pressure was reviewed and the equations immediately relating to the design of the HLH were analysed.

4

CHARACTERISATION OF SOLID FUELS

4.1 Introduction

The assessment of a material's properties is of paramount importance when handling bulk solids. In recent years, material feeding and handling systems have been cited as one of the most common causes of process downtime (Bonk and Hay, 1995, Clayton et al., 2002). More often than not, problems arise due to inadequately designed and sized equipment and where bulk solids have been assumed to behave in a convenient and stable manner like their fluid counterparts. Gasification is an industry where problems have been particularly prevalent due to the requirement for handling new and emerging fuels. But it is not just new fuels that cause problems. Proven and widely deployed fuels can cause significant setbacks where handing systems have been inadequately designed and the appropriate material tests have not been undertaken. It is for this reason that material tests should form the basis of all design work relating to handling systems and should be considered an integral part of the technical front end engineering design (FEED) stage of a proposed project.

This chapter aims to provide an overview of a range of bulk solid materials, detail their key material properties, how they are determined and how the materials in question are used in conjunction with the proposed feed system – the Hydraulic Lock Hopper.

4.2 Solid fuels

Six fuels were assessed as part of this study and each is shown in Figure 4-1. The materials selected provide a broad range in terms of particle size and material stability, and thus provide a good comparison between like and unlike fuels. The fuels assessed were:

- Wood pellets
- Torrefied spruce pellets
- Coarsely ground anthracite grains
- Torrefied spruce wood chips
- Milled wood pellets
- Pulverised bituminous coal

Figure 4-1: Wood pellets, torrefied spruce pellets, coarsely ground anthracite grains (first row, left to right), milled wood pellets, torrefied spruce wood chips and pulverised bituminous coal (second row, left to right).

The wood pellets are 6 mm in diameter and were produced from chemically untreated residues from the wood processing industry. The pellets were made available by CPL Distribution Ltd and comprise a physically stable, low-ash pellet conforming to the standard ENplus A1. The pellets described were used as the starting material for the milled wood pellets and were milled using a 1.1 kW Glen Creston hammer mill fitted with a trapezoidal screen of size 1.5 mm.

Both the torrefied spruce chips and pellets were made available by the Energy Centre of the Netherlands (ECN) and were torrefied at a temperature of 260 °C for approximately 40 minutes. The torrefied pellets are 8 mm in diameter and the torrefied wood chips are irregular in shape varying between 20 mm and 50 mm in size.

The coarsely ground anthracite grains were supplied by CPL Distribution Ltd and have an average particle size of approximately 9 mm. The coal grains are characteristic of anthracite and display a sub-metallic lustre. The pulverised bituminous coal was made available from the University of Sheffield and is sized approximately at 250 μm. The pulverised coal was as received and required no further processing.

4.3 Material properties

Due to the HLH taking the form of two hoppers equal in volume, the material tests directly relating to hopper design are of key importance. The approach used for hopper design in this instance was adapted from that proposed by Andrew Jenike for conical hopper design (Jenike, 1964, Rhodes, 2008, Schulze, 2008). The two principal tests required for hopper design according to this procedure are the material shear test and the wall friction shear test. Such tests are used to determine the following properties:

- Unconfined yield stress (σ_c)
- Material flow function
- Angle of internal friction (φ)
- Effective angle of internal friction (δ)
- Kinematic angle of wall friction (ϕ_w)

From these properties, a hopper is able to be reliably designed and the discharge rate from the hopper assessed. The semi-included angle of the hopper slope (θ) and the hopper flow factor (ff) are determined from the effective angle of internal friction and the kinematic angle of wall friction. The stress corresponding to the critical condition for flow or no flow (σ_{crit}) is determined from the material flow function and hopper flow factor. The minimum hopper outlet diameter (B) is determined from the critical flow condition, the semi-included hopper angle and the bulk density (ρ_b) of the material.

Further to the tests required to ensure the flow of material through a hopper are tests relating directly to the material being handled – tests for the particle density (ρ_p) and bulk density. Combining these two properties allows the void space present between the bulk solid being handled to be assessed, which is of pivotal importance where the HLH is concerned. When operating in Mode 1, the volume of water required to be pumped in the compression stage is approximately equal to the void space contained between the material being fed. Therefore, assessing both the bulk and particle density allows this value to be determined, and in turn the efficiency gain of the HLH to be calculated. The following sections provide an overview of each of the material properties stated.

4.3.1 Particle density

The particle density is defined as the volume a given mass of substance occupies and has SI units of kg/m^3. The particle density refers specifically to an individual element of a material and can also be referred to as the true or solid density. Particle density can be written as:

$$\rho_p = \frac{M_p}{V_p}$$

Equation 4-1

Where M_p is the mass of an individual particle of a bulk solid (kg) and V_p is the volume that particle occupies (m^3).

4.3.2 Bulk density

The bulk density differs to the particle density in the sense that it is a property of the bulk material. The bulk density is defined as the ratio between the mass of a given bulk solid and the volume it occupies. Like particle density, bulk density has an SI unit of kg/m^3.

A parameter inherently associated with the bulk density, and responsible for the bulk density being less than the particle density, is the material voidage, void space or porosity (ε). This refers to the volume of voids contained within the bulk material and is expressed as:

$$\varepsilon = \frac{V_{Voids}}{V}$$

Equation 4-2

Where V_{Voids} is the volume of voids (m^3) and V is the total volume of the bulk solid inclusive of voids (m^3). The bulk density can therefore be written as:

$$\rho_b = (1 - \varepsilon) \cdot \rho_p + \varepsilon \cdot \rho_f$$

Equation 4-3

Where ρ_f is the density of the fluid occupying the void space (kg/m^3). If the fluid occupying the void space is a gas, the second term of Equation 4-3 can usually be neglected due to the first term being far greater in magnitude.

Unlike particle density (where the particle contains no internal voids), the bulk density is observed to change when a stress is applied. An example of this is where materials are stored in and discharged from hoppers and so it is relevant to assess how the bulk density of a material changes with increasing stress. Knowing the relationship between an applied stress and the material bulk density allows the mass of the contents of a hopper or storage vessel to be accurately assessed.

4.3.3 Unconfined yield stress

The unconfined yield stress (σ_c) can be defined as the stress at which a material fails and begins to flow. This is of particular interest in a hopper as the unconfined yield stress governs when flow or no flow from the hopper outlet is generated. For flow to occur, the stress developed in the material contained in the free surface of the arch at the hopper outlet has to be greater than that of the unconfined yield stress (Rhodes, 2008). Therefore it can be said that where the stress developed in the material (σ_D) is greater than the unconfined yield stress, material will flow – $\sigma_D > \sigma_c$.

The unconfined yield stress is typically measured using the uniaxial compression test in a system consisting of a hollow cylinder and a series of loads. The hollow cylinder is filled with material and a series of loads are applied vertically compressing the material. The stress acting on the material is referred to as the consolidation stress (σ_1). The greater the increase in bulk density, the more compressible the material is. It can also be observed that the strength of the material increases as the consolidation stress increases. After the material has been consolidated, the hollow cylinder and loads are removed and the material is allowed to stand freely. A series of increasing loads are then applied to the free standing cylinder of material. When the stress developed in the material reaches a given point, the material will fail and the cylinder will collapse. It is this stress that is considered to be the unconfined yield stress. Figure 4-2 highlights the three key stages in the uniaxial compression test.

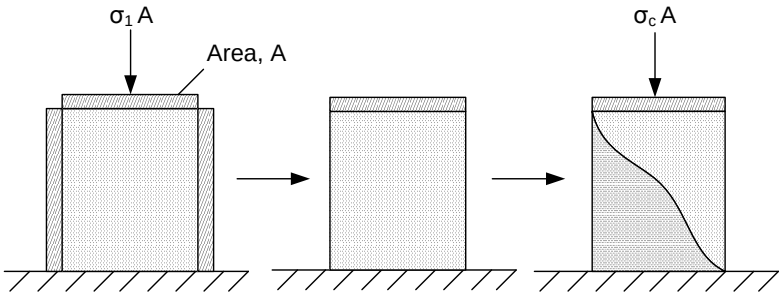

Figure 4-2: Three stages of the uniaxial compression test (Schulze, 2008).

The point of material failure is referred to as the point of incipient flow, as at failure the material starts to flow freely (Schulze, 2008). Incipient flow can be considered a type of plastic deformation which brings about a decrease in the overall bulk density of a material when its yield limit is reached. Unlike many materials (e.g. metals and plastics), bulk solids do not have a singular value for their yield limit. Where bulk solids are concerned, the yield limit is directly related to and dependent on its stress history. Generally it is found that as the consolidation stress increases, both the bulk density and the unconfined yield stress also increase.

4.3.4 Material flow function and hopper flow factor

The material flow function relates directly to the unconfined yield stress and is generated by plotting pairs of values for the unconfined yield stress and the associated consolidation stress. Figure 4-3 highlights a typical material flow function plotted alongside varying classifications of flowability (ff_c).

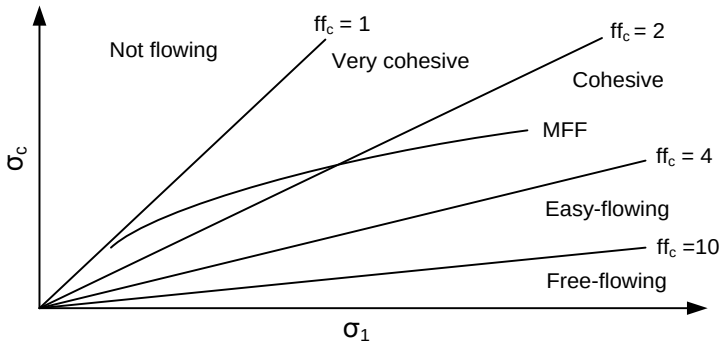

Figure 4-3: Illustration of the material flow function alongside classifications of flowability (Schulze, 2008).

The line labelled MFF highlights a typical material flow function. The range of lines plotted as ff_c highlight the differing classifications of flowability. Flowability is determined using the following relationship:

$$ff_c = \frac{\sigma_1}{\sigma_c}$$

Equation 4-4

Where σ_1 is the consolidation stress (Pa) and σ_c is the unconfined yield stress (Pa). It can be observed that as the unconfined yield stress diminishes in comparison to the consolidation stress, the material becomes more free-flowing.

The hopper flow factor (ff) presents a similar parameter to that of flowability (ff_c) and is broadly defined in the same way. However, the hopper flow factor is determined experimentally using plots developed by Jenike, incorporating the effective angle of internal friction and the kinematic angle of wall friction. An example of such a plot is displayed in Figure 4-4, which shows the hopper flow factor boundaries for a conical-shaped hopper with a material's effective angle of internal friction equal to 40°. Jenike obtained values for both conical and wedge-shaped hoppers for values of the effective angle of internal friction ranging between 30° and 70° (Jenike, 1964).

The hopper flow factor is plotted on the same axis as the material flow function and is used to determine the critical condition for flow, or the critical stress for flow. Plotting a line with a gradient 1/ff alongside the material flow function, the critical condition is considered to be the point where the two lines intersect. Referring to Figure 4-3, it can be seen that this is the case for a value of ff or ff_c

equal to 2. It can therefore be said that material will flow when the stress developed in the material is equal to or greater than the corresponding unconfined yield stress on the y-axis at the critical point.

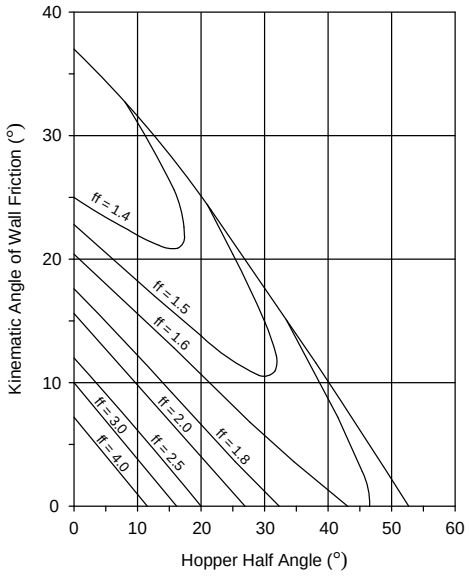

Figure 4-4: Graphical relationship for the hopper flow factor for a conical hopper, $\delta = 40°$ (Arnold et al., 1982).

Such relationships between the two lines plotted can be used to determine whether flow or no flow occurs. Using the hopper flow factor line of gradient 1/2 (i.e. ff or $ff_c = 2$) as a basis, it can be seen that any line plotted as the material flow function which lies below this (i.e. ff or $ff_c > 2$) indicates that the material will flow. Comparatively, any line plotted as the material flow function which lies above this (i.e. ff or $ff_c < 2$) indicates that the material will not flow.

4.3.5 Effective angle of internal friction and angle of internal friction

Neither the angle of internal friction (φ) nor the effective angle of internal friction (δ) are angles of friction in the true sense. That is, neither is a product of the arctan of the ratio of normal stress to shear stress applied to and recorded by the material in question. Both parameters are in fact associated with the plot of the yield locus of the material. This is comprised of a series of points made up from an applied normal stress to a material and the subsequent shear stress recorded by the material. The shear stress corresponds to the load required for a plane of material to flow freely on itself.

To determine such parameters, a series of normal loads are applied to the material, bringing about compression and an increase in bulk density. After the loads have been applied, the material is then sheared; this is carried out either linearly in a single direction or as a rotation. The loads and shearing motion are brought about in such a way that failure occurs within the material, thus the material shears and begins to flow on itself. Repeating this process with increasing or decreasing normal loads

enables a series of normal stress/shear stress pairs to be generated and a yield locus to be plotted. It is from this that both the angle of internal friction and effective angle of internal friction are determined. However, before both parameters are defined in terms of the yield locus, it is important to state the stress analysis required and how such stress analysis is applied to the yield locus.

If a given bulk solid is assumed to have an infinite height and be surrounded by a frictionless wall, the stresses exerted by and on the bulk solid can be reviewed. Unlike a Newtonian fluid where the horizontal stress (σ_h) and vertical stress (σ_v) are found to be the same in all places, the horizontal stress developed in a bulk solid is found to be a result of the vertical stress. It is always found to be less than the vertical stress. The ratio of both stresses can be referred to as the stress ratio (K), which typically varies between 0.3 and 0.6 (Schulze, 2008):

$$K = \frac{\sigma_h}{\sigma_v}$$

Equation 4-5

However, stresses are not just found in the horizontal and vertical direction. In a bulk solid, stresses can be found in different cutting planes regardless of whether the bulk solid is in motion. Making the same assumptions as stated previously, it can be said that no shear stresses act on the top or bottom of a bulk solid and, due to the walls being assumed to be frictionless, no shear stresses are acting laterally. Taking a triangular element of a bulk solid, two equations can be setup which allow a normal stress (σ_α) and shear stress (τ_α) to be calculated with a varying angle (α) of the triangular element taken from the bulk solid. Such equations are referred to as the transformation equations and can be written as:

$$\sigma_\alpha = \frac{\sigma_v + \sigma_h}{2} + \frac{\sigma_v - \sigma_h}{2} \cdot \cos 2\alpha$$

Equation 4-6

$$\tau_\alpha = \frac{\sigma_v - \sigma_h}{2} \cdot \sin 2\alpha$$

Equation 4-7

When the two equations are used in conjunction with each other, they allow all possible normal and shear stresses in an element of a bulk solid to be calculated. When plotted as a normal (x-axis) shear (y-axis) stress plot, it is found that they create a circular plot with a centre based on the x-axis; such a plot is referred to as a Mohr stress circle (Rhodes, 2008, Schulze, 2008). However, Equations 4-6 and 4-7 can be taken further taking into account local shear stresses present in both the vertical and lateral direction. Therefore, a new case assuming that shear stresses are present due both to non-frictionless walls and to a shearing force being applied to the top and bottom of a given element of a bulk solid generates Equation 4-8 and Equation 4-9.

$$\sigma_\alpha = \frac{\sigma_h + \sigma_v}{2} + \frac{\sigma_h - \sigma_v}{2} \cdot \cos 2\alpha + \tau_{vh} \cdot \sin 2\alpha$$

Equation 4-8

$$\tau_\alpha = \frac{\sigma_h - \sigma_v}{2} \cdot \sin 2\alpha - \tau_{vh} \cdot \cos 2\alpha$$

Equation 4-9

As Equation 4-8 and Equation 4-9 translate to a Mohr stress circle about the x-axis, it can be seen that two stress combinations exist where the shear stress is equal to zero. Such normal stresses are referred to as the principal stresses and are of vital importance regarding the yield locus of a bulk solid. The major principal stress corresponds to the larger of the two values, and the minor principal stress to the smaller.

As Mohr circles are used where normal stress and shear stress combinations are present, it is convenient to use such analysis in conjunction with the yield locus of a bulk solid generated from a material shear test. As a Mohr circle displays all combinations of normal and shear stresses in an element of a bulk solid, Mohr stress circles can be drawn tangential to the yield locus and with a centre based on the x-axis. Technically, a wide range of Mohr stress circles can be drawn tangential to the yield locus; however, there are two that play a vital role in determining key material properties. They are the "small" Mohr stress circle which is drawn passing through the origin, and the "large" Mohr stress circle which is drawn passing through the last point plotted on the yield locus, also known as the pre-shear point. A graphical representation of both Mohr stress circles is shown in Figure 4-5.

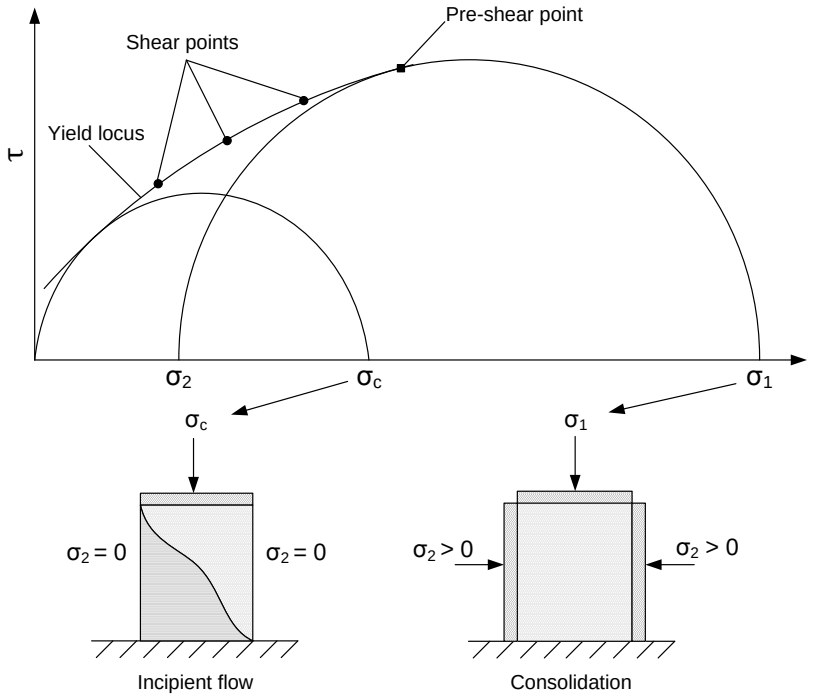

Figure 4-5: Graphical representation of both Mohr stress circles and their physical meaning (Schulze, 2008).

The two Mohr stress circles provide a comprehensive overview of all of the possible normal and shear stress pairs in a given bulk solid, but the two stresses of most importance are the principal stresses (shear stress = 0). The major principal stress determined from the large Mohr circle represents the consolidation stress (σ_1 or σ_v) applied vertically to the bulk solid, and the minor principal stress corresponds to the horizontal stress (σ_2 or σ_h). Comparatively, the major principle stress determined from the small Mohr circle corresponds to the unconfined yield stress (σ_c). This is due to the small Mohr circle passing through the origin and thus the minor principal stress being set equal to zero as no horizontal stress is applied. Such a stress point represents the condition at a hopper outlet where a free arched surface of material is present. As a side note, it is often found that the unconfined yield stress and the consolidation stress are determined this way in preference to the uniaxial compression test as stated in Section 4.3.3 due to a greater level of accuracy.

From this stress analysis, both the angle of internal friction and effective angle of internal friction can be determined. The angle of internal friction is defined as the gradient of the yield locus. However, it is often found that the yield locus takes the form of a curve and so has a constantly changing gradient. This in turn means that the angle of internal friction changes with increasing normal stress. In the majority of cases it is acceptable and convenient to take the angle of internal friction as a constant, plotting a line running tangential to both the small and large Mohr circles. The angle of internal friction is defined as the gradient of this line.

The effective angle of internal friction is defined as the gradient of the line plotted through the origin and running tangential to the large Mohr circle. Because the large Mohr circle represents the stresses associated with a flow condition at steady state, the effective angle of internal friction quantifies the internal friction present at a state of steady flow.

In addition to the definitions stated above, a series of equations developed by Jenike can be used to determine parameters such as the unconfined yield stress, consolidation stress, angle of internal friction and effective angle of internal friction. The equations require experimental material shear tests to generate a material yield locus and are written as:

$$m = \frac{\tau_E - \tau_a}{\sigma_E - \sigma_a}$$

Equation 4-10

$$K = m + \sqrt{(1 + m^2)}$$

Equation 4-11

$$\sigma_1 = \sigma_E + K\tau_E$$

Equation 4-12

$$\sigma_c = 2K(\tau_E - \sigma_E m)$$

Equation 4-13

$$\varphi = \tan^{-1} m$$

Equation 4-14

$$\delta = \sin^{-1}\left[\frac{(K^2+1)\tau_E}{2K\sigma_E + (K^2-1)\tau_E}\right]$$

Equation 4-15

Where σ_E and τ_E make up the normal stress shear stress pair where the yield locus meets the large Mohr circle (Pa), and σ_a and τ_a make up the normal stress shear stress pair where the yield locus meets the small Mohr circle (Pa). In turn, m is the gradient of the yield locus running tangential to both the small and large Mohr circle and K is a mathematical parameter determined from the gradient of the yield locus (m). σ_1 is the major principal stress (Pa), σ_c is the unconfined yield stress (Pa), φ is the angle of internal friction (°) and δ is the effective angle of internal friction (°) (Jenike, 1964).

4.3.6 Kinematic angle of wall friction

The kinematic angle of wall friction (ϕ_w) or the angle of wall friction is broadly defined as the angle at which a material will begin to flow on a given surface. The angle of wall friction is similar to the angle of internal friction in the sense that it corresponds to the gradient of a yield locus. The yield locus in this case, referred to as the wall yield locus, is generated by applying a series of loads to a sample of material and shearing the sample against a surface. The shear force is recorded and plotted against the normal force generated by the series of normal loads applied. As the angle of wall friction is directly related to hopper design, the surface is made from the same material used for constructing the hopper. Therefore, the angle of wall friction is not an inherent property of the bulk solid material and changes with changing wall material.

Comparatively to both the angle of internal friction and the effective angle of internal friction, the angle of wall friction is a true friction angle and is defined as the arctan of the ratio of shear stress to normal stress. The angle of wall friction can be written as:

$$\Phi_w = \tan^{-1}\frac{\tau_w}{\sigma_w}$$

Equation 4-16

Where ϕ_w is the angle of wall friction (°), τ_w is the wall shear stress (Pa) and σ_w is the wall normal stress (Pa). Where the yield locus is found to be a straight line passing through the origin, the angle of wall friction can be said to be constant and independent of normal stress. However, where the yield locus is found to take the form of a curve, the angle of wall friction can be said to be dependent on normal stress and changes with increasing/decreasing normal stress applied.

4.3.7 Particle size and particle size distribution

Particle size can be defined on three scales: volume, mass or length. It is most common in the field of bulk solids handling to define particle size on a length scale, and therefore particle size is defined as the length of an individual element of a bulk solid. Comparatively, particle size distribution (PSD) is not a material property but a property of a given quantity of a material. It is important to take the PSD into account as it plays an integral role in how a bulk solid flows.

Particle size largely determines how a bulk solid flows due to its close relationship to adhesive force. Adhesive forces are created via a number of mechanisms; however, it is often found that van der Waals and electrostatic interactions are the most common. Particle size is directly related to adhesive forces created, and it is found that adhesive forces are greater for smaller particle sizes. But particle size is not responsible for the magnitude of adhesive forces alone; in the case of van der Waals interactions, adhesive forces are also shown to be directly related to the relative inter-particle and surface-particle distance. Therefore, as particles approach both each other and a given surface, adhesive forces are seen to increase. For example, van der Waals interactions are shown to be very large at small distances; however, as distance increases (~1 μm) adhesive forces are shown to decrease dramatically. Therefore, for such interactions to affect flowability, inter-particle and surface-particle distances need to approach zero.

Where moist bulk solids are concerned, an additional phenomenon contributes to the creation of adhesive forces – liquid bridges. Liquid bridges are formed where a liquid of sufficiently low viscosity meets an inter-particle space. The liquid is able to be seated between the two particles and forms a contact with a given angle. The surface tension of the liquid acts to create an adhesive force and the particles in question are attracted to each other. However, it is not just surface tension that promotes adhesion, capillary pressure acts in addition to this. Where the capillary pressure is lower than that of the local pressure, the capillary pressure acts to increase the adhesive force. Like interactions due to van der Waals forces, the adhesive force generated through the presence of liquid bridges is affected by distance, and as distance increases, the adhesive force generated decreases. However, unlike van der Waals interactions, at a given distance the adhesive force becomes non-existent. This is due to the separation of the liquid and the failure of the liquid bridge. The adhesive forces generated through the creation of liquid bridges are often greater than those generated by either van der Waals or electrostatic interactions, and are often the main cause of flow problems where moist bulk solids are being handled. Contrary to both van der Waals interactions and liquid bridges, adhesive forces generated due to electrostatic interactions are not shown to decrease as dramatically with distance. Although initially they are shown to be lower in magnitude, it can be said that as inter-particle and surface-particle distances increase, adhesive forces due to electrostatic interactions dominate.

Adhesive forces are perhaps of most concern where particle size is small as forces generated due to particle mass are not sufficiently great to affect inter-particle and surface-particle adhesive forces. However, where large particle sizes are concerned (>100 μm), the effect of gravity becomes greater and the particle weight becomes the dominant force. It can therefore be said that where large particle sizes are concerned, adhesive forces are irrelevant. Figure 4-6 highlights the relative magnitude of each of the forces discussed, and that weight is proportional to the third power of the particle diameter.

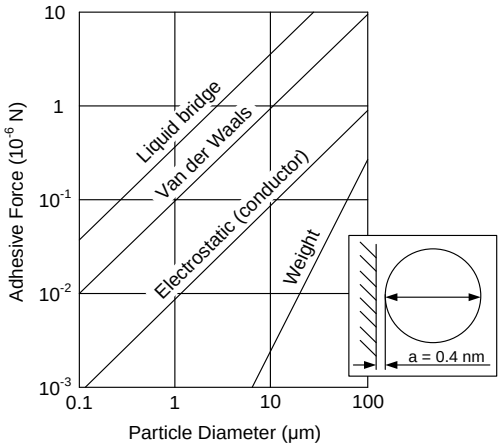

Figure 4-6: Effect of particle size on adhesive force (Schulze, 2008).

The tensile strength of a bulk solid increases with decreasing particle size as per:

$$\sigma_t \propto \frac{1}{d}$$

Equation 4-17

Where σ_t is the tensile strength of a bulk solid and d is the particle diameter. Therefore, the strength of a bulk solid is shown to increase with decreasing particle size, and in turn the flowability is reduced. This relationship to flowability is generally true; however, the use of flow agents acts to increase flowability by decreasing the average particle size. Typically flow agents are added in the region of 1 wt% (Schulze, 2008) and act to increase the roughness of a particle's surface. This in turn increases inter-particle and surface-particle distances and therefore decreases the adhesive forces generated.

Flow agents are typically used where smaller particles are concerned as adhesive forces dominate their flow behaviour. Where larger particles are concerned, material weight is the dominant force and so flow agents do not act to improve the flowability of the material. In fact, where fines (small particles) are present along with larger particles, the flowability of the bulk solid is observed to decrease. Table 4-1 highlights the effect of increasing fines content on the flowability of a coarse bulk solid.

It can be seen from Table 4-1 that as the percentage of fines present in a coarse bulk solid increases, the unconfined yield stress increases and in turn the flowability decreases. The reason for reduced

flowability with increasing fines content is twofold. Firstly, the fine material acts to increase inter-particle friction of the larger particles, and secondly, the fine material acts to give the bulk solid as a whole a greater cohesive strength. Further to the general trend of decreasing flowability with increasing fines content, it can be seen that as the fines content increases past 40-50%, changes in the flowability decrease. This is due to the fines becoming the dominant component of the bulk solid, and instead of the fines flowing through the larger bulk solid particles, the larger particles begin to flow through the fine material. Therefore, where coarse bulk solids are required to be fed, it can be said that it is the fine material that governs the flowability (Jenike, 1964, Schulze, 2008).

Fines (%)	σ_1 (Pa)	σ_c (Pa)	ff_c
5	3948	767	5.1
10	3991	914	4.4
15	4015	1082	3.7
20	4090	1229	3.3
25	4208	1352	3.1
30	4210	1541	2.73
35	4232	1693	2.50
40	4261	1840	2.32
45	4158	1893	2.20
50	4288	1976	2.17

Table 4-1: Effect of fines content on the flowability of a coarse bulk solid (Schulze, 2008).

4.3.8 Discharge rate

Discharge rate is defined as the mass or volume of material leaving an outlet per unit time and has the SI unit kg/s or m^3/s respectively. In the case of bulk solids, the discharge rate refers specifically to the mass of material leaving a device per unit time; in the case of the HLH, the device is a hopper. The discharge rate is not an inherent material property, but a property specific to that material and the device being discharged from. The importance of the discharge rate is felt when assessing the mass flow rate of a system, and in particular the mass flow rate of large devices, as the flow of material becomes the dominant step when compared to ancillary equipment activity such as valve operations.

Where discharge rate is applied to a bulk solid flowing from a hopper, it is important to review how the material flows. There are three main categories in which the flow or discharge of bulk solids from a hopper can be split: mass flow, funnel flow and expanded flow, and each is shown in Figure 4-7 (Jacob, 2000, Chase, 2010). Mass flow assumes that all material bodies contained within the hopper are moving during operation. Funnel flow assumes that only material bodies in the centre of the hopper are moving with stagnant or non-flowing regions present at the hopper wall. Expanded flow constitutes a scenario whereby both mass and funnel flow are taking place simultaneously in separate parts of the hopper.

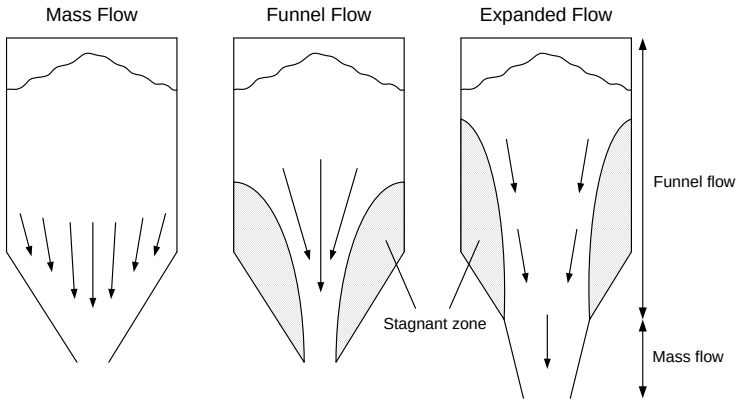

Figure 4-7: Examples of mass, funnel and expanded flow (Jenike and Johanson, 2010).

Typically when dealing with powders, funnel flow is undesirable due to the formation of stagnant regions and mass flow is the preferred flow mode. However, when dealing with coarse materials that are free flowing and non-degradable, the funnel flow mode is well-suited in addition to the mass flow mode (Marinelli and Carson, 1992). An approximate relationship between hopper height and diameter used to prompt mass flow is considered to be:

$$H \geq 0.75D \qquad \textit{Equation 4-18}$$

Where D is the inlet diameter of the cylindrical section of the hopper (m) and H is the height of the cylindrical section of the hopper (m) (Jacob, 2000, Chase, 2010).

There are numerous ways in which the discharge rate from a hopper can be determined theoretically, with many relationships between material properties and the rate of discharge being available in the literature (Beverloo et al., 1961, Woodcock and Mason, 1996, Jacob, 2000, Holdich, 2002, Rhodes, 2008, Chase, 2010). However, two relationships that are most commonly used to determine the discharge rate for coarse particles (d_p >500 μm) in terms of mass flow rate are the Johanson equation and the Beverloo equation written as Equation 4-19 and Equation 4-20 respectively.

$$m = \rho_b \frac{\pi B^2}{4} \sqrt{\frac{Bg}{4 \tan \theta}}$$

Equation 4-19

$$m = 0.58 \rho_b g^{0.5} \left(B - k d_p\right)^{2.5}$$

Equation 4-20

Where m is the mass flow rate (kg/s), ρ_b is the particle bulk density (kg/m^3), B is the diameter of the outlet (m), g is the gravitational acceleration (9.81 m/s^2), θ is the hopper half angle (°), k is the Beverloo shape coefficient (typically 1.4) and d_p is the average particle diameter (m).

Although the Johanson equation is not dependent on particle size, it is not commonly used when assessing the mass flow rate of fine particles (d_p <500 μm) and is reserved only for use where coarse particles are concerned. However, a variation of the Beverloo equation is used to assess the mass flow rate of fine particles taking into account the gas pressure in the discharge device. That is, the pressure gradient (dp/dz) that acts once the discharge of material begins. Once material starts flowing from the outlet of a closed discharge device, a pressure gradient is established between the outlet of the device and the surrounding atmosphere. This pressure gradient acts against the outlet creating a flow of gas contained in the surrounding atmosphere acting upwards on the material being discharged. The flow of gas acts to oppose the gravity force and thus impedes the flow of material and reduces the mass flow rate. This pressure gradient is commonly neglected where coarse materials are concerned as the porosity of the material is sufficiently large that a strong pressure gradient is not able to be created. The new Beverloo equation taking into account this pressure gradient is written as:

$$m = 0.58\rho_b \sqrt{g + \frac{1}{\rho_b}\frac{dp}{dz}} \left(B - kd_p\right)^{2.5}$$

Equation 4-21

Where dp/dz is the local pressure gradient written as $\Delta P/r_o$ for gas flows with low Reynolds numbers (kg/m^2s^2). Where ΔP is the pressure difference (Pa) and r_o is the distance from the virtual apex of the hopper to the hopper outlet (m) (Nedderman et al., 1983, Schulze, 2008). The discharge rate in all cases embodies all of the material properties previously discussed in Section 4.3, as all are required in the design procedure for the hopper.

4.4 Material tests

4.4.1 Particle density test

In the case of the coarse materials (wood pellets, torrefied wood pellets, ground anthracite grains and torrefied wood chips), the particle density was determined by displacement using oil and a 1-litre Florence flask. The mass of the Florence flask full of oil was first determined and the flask emptied. A given mass of a bulk material was then added to the flask, filled with oil and weighed. The difference in mass between both measurements, minus the mass of the bulk material was then determined, and the volume occupied by the bulk material determined using the known density of the oil. Mass readings were taken accurate to the nearest 0.1 g.

The particle density for both the milled wood pellets and the pulverised bituminous coal were unable to be assessed using this method due to their small particle size. In its place, a helium gas pycnometer was used. Material was weighed using an analytical mass balance, charged into a 1 cm^3 vessel, filled

with helium gas, and the volume of helium gas was measured. As with the previous method, the volume that the bulk material occupied was determined from the difference between the recorded volume of helium gas and the volume of an empty vessel. Mass readings were taken accurate to the nearest 0.1 mg.

4.4.2 Bulk density test

The bulk density was assessed using a volumetric cylinder and a mass balance. In the case of the wood pellets, torrefied wood pellets, torrefied wood chips and ground anthracite, a mass balance accurate to 0.1 g and a volumetric cylinder with a capacity of approximately 9 litres was used. In the case of the milled wood pellets and pulverised bituminous coal, a smaller volumetric cylinder with a capacity of approximately 30 ml was used in conjunction with a mass balance accurate to 1 mg.

Where both the bulk density and particle density are known, the material voidage can also be determined. Due to the fluid contained in the void space between the bulk solid materials being air, the mass of such a volume was neglected from the overall mass reading.

4.4.3 Material shear test

The material shear test was used to generate a material yield locus. From this, the unconfined yield stress, material flow function, angle of internal friction and effective angle of internal friction were determined. A 1 m diameter annular shear cell was used to assess the wood pellets, torrefied wood pellets, torrefied wood chips and ground anthracite. A Brookfield Powder Flow Tester (PFT) was used to assess the milled wood pellets and pulverised bituminous coal. Both shear testers take the form of annular shear cells and are displayed in Figure 4-8.

Figure 4-8: Ø1 m annular shear tester (left) and Brookfield PFT (right).

Both shear cells operate in the same manner and consist of an annular tray, a cupped lid and a torque sensor/load cell. Material is loaded into the annular tray, evenly levelled and then a cupped lid of known mass is applied. In the case of the Ø1 m annular shear cell, torque arms are connected to the shear cell lid via a load cell to measure the shear stress generated. The Brookfield PFT is able to measure the shear stress generated via a reaction torque sensor attached to the stationary lid. All components stated are shown in Figure 4-9.

Figure 4-9: Annular shear cell (left) and Brookfield PFT (right). Shear cell, lid and torque sensor (top to bottom).

A load is applied to the shear cell lid which acts to consolidate the material to a known and repeatable bulk density. Material is then sheared to failure through the rotation of the annular tray round a central point at a constant velocity. The shear stress generated is recorded to increase with time until a steady state is reached; it is at this point that a shear plane is generated and the material exhibits incipient flow. Once this point has been reached, the rotational direction is reversed and the material is returned back to its original state. This initial shearing procedure of material is referred to as pre-shear and is repeated after each subsequent load has been applied and the material has been sheared. Repeating the pre-shear procedure allows a reliable and known bulk density to be attained before shearing under each subsequent normal load.

After the measurement of the pre-shear point has been carried out, the load on the shear cell lid is reduced, the material is sheared and the shear stress required to generate incipient flow is recorded. The rotation of the annular tray is then reversed as with the measurement of the pre-shear point to return the material back to its original condition. The material is reconsolidated using the pre-shear load and then sheared to failure. This process is repeated with a number of normal loads in order to generate a yield locus made up of normal stress and shear stress points.

Pre-shear Consolidation Stress (kPa)	
Milled Wood Pellets	**Pulverised Coal**
0.85	0.55
1.72	1.10
3.94	2.25
8.10	4.57
15.20	9.38

Table 4-2: Pre-shear consolidation stresses generated using the Brookfield PFT.

Pre-shear Consolidation Stress (kPa)			
Wood Pellets	**Torrefied Wood Pellets**	**Ground Anthracite**	**Torrefied Wood Chips**
1.14	1.15	1.16	1.00
2.10	2.11	2.12	1.97
4.05	4.06	4.08	3.92

Table 4-3: Pre-shear consolidation stresses generated using the Ø1 m annular shear tester.

A reliable result can be generated with as few as three normal loads. That is, if the normal loads are sufficiently spaced apart to generate shear planes in different regions of the bulk material. Essentially, the greater the normal load applied, the further down into the bulk material the shear plane will be generated. Therefore, using loads that are sufficiently spaced apart ensures new shear planes are created under each normal load applied. Using normal loads that are only marginally spaced will generate shear planes in broadly the same region. The pre-shear consolidation stresses generated for all materials are detailed in Table 4-2 and Table 4-3.

4.4.4 Wall friction shear test

The wall friction shear test was used to generate a wall yield locus for a range of wall materials and in turn the kinematic angle of wall friction was determined for each wall material. Similarly to the material shear test, a Brookfield PFT was used to assess the milled wood pellets and pulverised bituminous coal, and a linear wall friction tester was used to assess the wood pellets, torrefied pellets, torrefied chips and ground anthracite. Both wall friction shear testers are displayed in Figure 4-10.

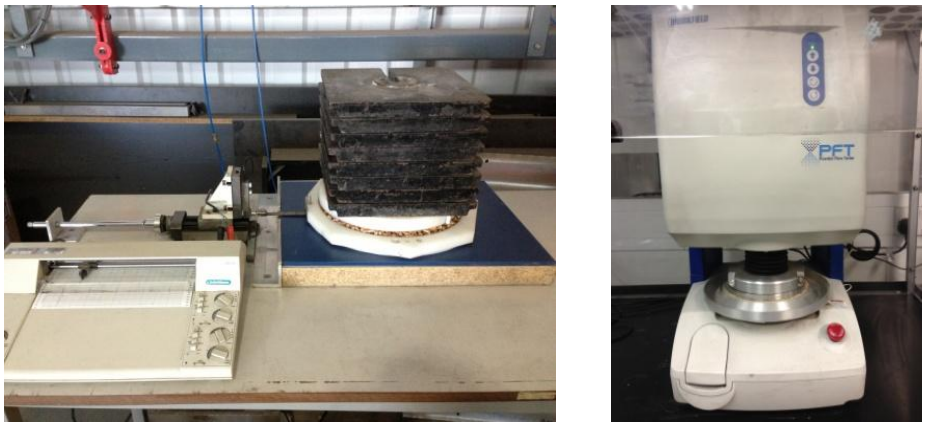

Figure 4-10: Linear wall friction shear tester (left) and Brookfield PFT (right).

The principle of both wall friction shear testers is the same; however, they differ slightly in how they are operated. In the case of the Brookfield PFT, the operational procedure is similar to that carried out for the material shear test. However, in place of the cupped lid used to measure the inter-particle friction, an annular sample of wall material is fitted. Material is loaded into the same annular shear cell used for the material shear tests shown in Figure 4-9, levelled and the annular sample of wall material is applied to the material at a known load. The shear cell containing the bulk solid is rotated at a constant velocity and the material is sheared by the sample of wall material. The material is said to be sheared when an approximately constant shear stress value is recorded. The shear stress in this case refers to the shear stress generated between the bulk solid and the wall material for a given normal stress. This process is repeated for a series of decreasing normal loads to generate a wall yield locus made up of normal stress and shear stress points.

The linear wall friction tester is used for larger particle sizes and shears the bulk solid in a single direction contrary to the Brookfield PFT. It is comprised of a circular ring and lid, a bracket and a mechanical shearing arm. The bracket and shearing arm are connected and attached to the circular ring via a load cell, which measures the shear stress generated. All components are displayed in Figure 4-11. The circular ring is placed on top of a sample of wall material and a known mass of a bulk solid is placed inside the ring. A lid of known mass is then placed on top of the bulk solid and a normal load is applied to the lid to create a stress normal to the bulk solid. The shearing arm is engaged and the bulk solid is sheared against the sample of wall material. This process is repeated for a series of normal loads.

The general wall shear principle detailed above can be used for a broad range of wall materials. In this study, the kinematic angle of wall friction was determined for the following materials: stainless steel, mild steel and TIVAR 88. The normal stresses generated by the normal loads applied are detailed in Table 4-4.

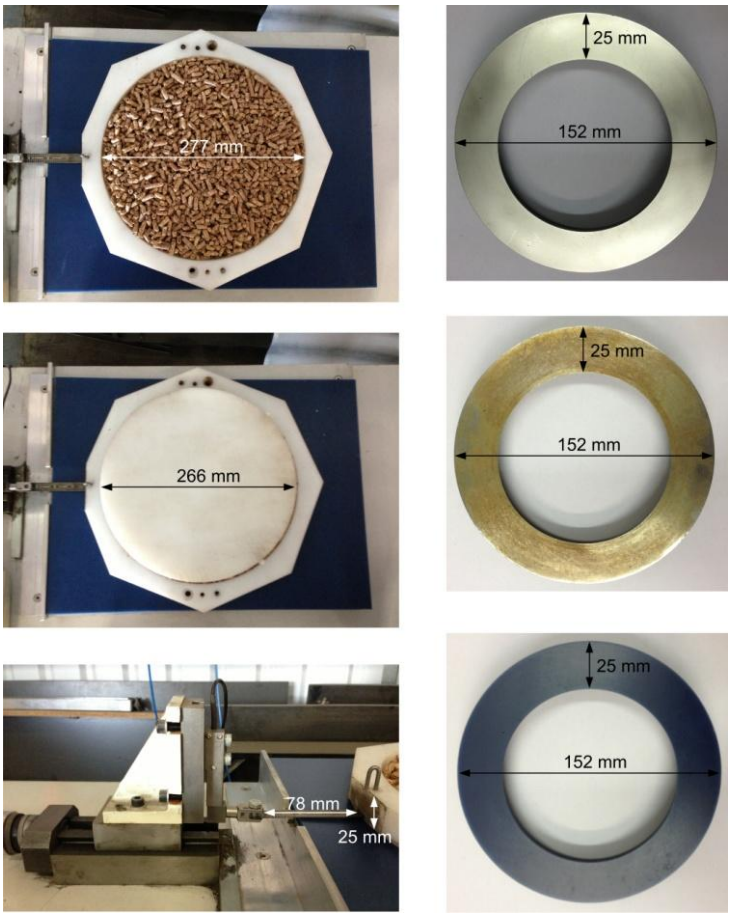

Figure 4-11: Components for the linear wall friction tester (left) and wall friction samples for the Brookfield PFT (right). Stainless steel, mild steel and TIVAR 88 (top to bottom).

Normal Stress (kPa)	
Brookfield PFT	**Linear Wall Friction Tester**
0.48	0.26
0.97	1.91
1.45	3.56
1.93	5.21
2.41	6.86
2.89	8.52
3.37	10.17
3.86	11.82
4.34	13.47
4.82	-

Table 4-4: Normal stresses generated by both the Brookfield PFT and the linear wall friction tester.

4.4.5 Particle size distribution test

A series of particle sieve trays were used to determine the distribution of particle sizes in a given bulk solid, and in the case of the coarser materials, assess the presence of fines. The sieving procedure was

carried out to comply with the standard EN 15149-2 and all sieve trays used were in accordance with the requirements of ISO 3310-1/-2. The frame of the sieve trays and the given loading were such that free movement of the sample was facilitated during the sieving procedure.

In the case of the wood pellets, torrefied pellets, torrefied wood chips and ground anthracite, three sieve trays of decreasing size aperture were used. The mesh sizes used were: 3.15 mm round holes, 2.36 mm square holes and 1.00 mm square holes. In this case any element sized at less than or equal to 1 mm was classified as a material fine. A representative sample of each of the coarse materials was achieved using a spinning riffler, which consisted of a wedge shaped hopper, a variable amplitude vibratory feeder and a rotating turntable on which ten collection vessels stood. Once the material had been split equally, the material contained in one of the ten collection vessels was then placed into the primary sieve tray (3.15 mm) of the sieve stack and mechanically shaken for 10 minutes using an Octagon mechanical sieve shaker. After sieving, the sieve trays containing material were then weighed using a mass balance accurate to 0.01 g.

A similar but more rigorous process was used to assess the PSD of both the milled wood pellets and the pulverised bituminous coal. A Gradex particle sieve analyser containing nine sieve trays of decreasing mesh size was used. All sieve trays contained square holes and had apertures of the following sizes: 850 μm, 600 μm, 425 μm, 300 μm, 212 μm, 150 μm, 106 μm, 75 μm and 56 μm. A spinning riffler was used to generate a representative sample of both materials. Mass readings for all sieve trays were carried out using a mass balance accurate to 0.1 g.

4.4.6 Density compressibility test

Density compressibility was assessed for all materials using a volumetric cylinder, a mass balance and a Hounsfield tensile tester as shown in Figure 4-12.

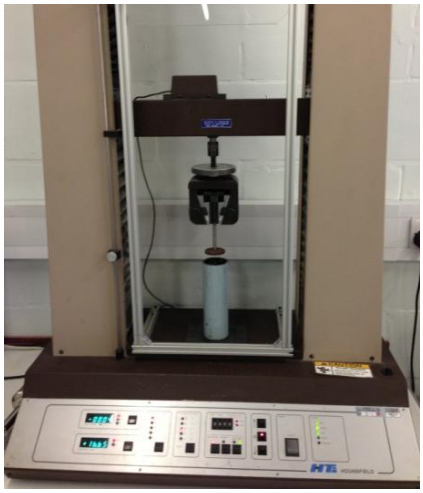

Figure 4-12: Hounsfield tensile tester fitted with a plunger to measure changes in bulk density.

A 415 ml volumetric cylinder was placed on a mass balance and filled with material to determine both the mass and the bulk density of the bulk solid at the initial condition. The material was then placed inside the Hounsfield tensile tester fitted with a plunger with a surface area 22 cm^2 and subjected to a compressive load with a constant extension/displacement. The corresponding force generated by the advancing plunger was recorded up to a maximum of 3.75 kN. The change in bulk density was determined via the relative extension of the plunger.

4.5 Material test results and discussion

4.5.1 Particle density, bulk density and material voidage

Table 4-5 shows that the milled wood pellets and pulverised coal are the densest materials, and the torrefied wood chips are the least dense. Relating the particle density to the bulk density generates the material voidage. Table 4-5 indicates all materials to have a voidage varying between 45% and 78%.

Fuel	Particle Density (kg/m^3)	Bulk Density (kg/m^3)	Voidage (%)
Wood pellets	1262 ± 6	651 ± 4	48.4 ± 0.4
Torrefied wood pellets	1267 ± 4	677 ± 2	46.5 ± 0.2
Ground anthracite	1353 ± 4	731 ± 1	46.0 ± 0.1
Torrefied wood chips	428 ± 5	170 ± 1	60.4 ± 0.8
Milled wood pellets	1530 ± 5	344 ± 7	77.5 ± 1.7
Pulverised coal	1505 ± 10	542 ± 7	64.0 ± 1.0

Table 4-5: Particle density, bulk density and voidage for all materials.

Relating material voidage to the amount of compression work required by the HLH as calculated in Section 3.4 indicates that an energy saving compared to a conventional lock hopper operating at 25 barg is approximately equal to 76% for operation in Mode 1. Energy savings are found to vary more dramatically for operation in Mode 2 and Mode 3 with energy savings being calculated to increase with increasing void space. Milled wood pellets are predicted to be the most efficient fuel to feed and the ground anthracite grains the least efficient.

	Energy Saving (%)		
Fuel	Mode 1	Mode 2	Mode 3
Wood pellets	75.6	36.3	41.5
Torrefied wood pellets	75.5	33.7	38.8
Ground anthracite	75.4	33.0	38.0
Torrefied wood chips	76.5	49.0	55.1
Milled wood pellets	77.7	60.3	67.6
Pulverised coal	76.8	51.9	58.3

Table 4-6: Theoretical energy saving generated using the HLH at 25 barg.

4.5.2 Material compressibility

It is important to quantify the extent to which a material compresses where feed systems are concerned as compression brings about a change in a materials bulk density and affects the mass flow rate. Where the HLH is concerned, compressibility also affects the volume of water required to be pumped in the compression stage, and in turn the efficiency of the device. Figure 4-13 highlights how bulk density varies with increasing vertical stress for each of the materials.

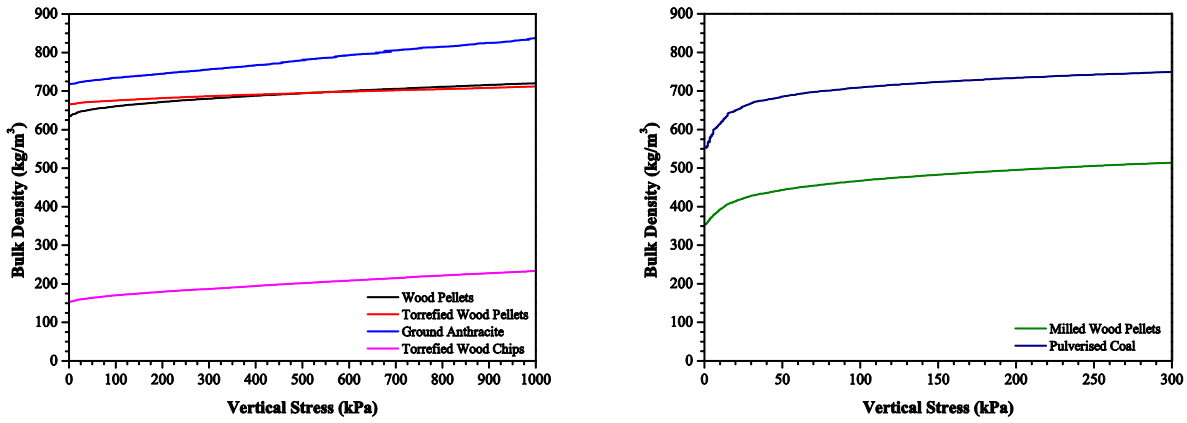

Figure 4-13: Effect of vertical stress on bulk density.

The bulk density of each material was found to increase as the vertical stress was increased. It is noted that for each of the coarse materials, the initial bulk density reading differs marginally to those presented in Table 4-5. This is brought about due to the smaller diameter of the apparatus used (53 mm) compared to that previously used to measure bulk density (277 mm), and in turn the formation of inter-particle bridges. Slight differences are observed for the milled wood pellets and pulverised coal; however, such differences are negligible compared to each of the coarse materials.

One of the key differences between the coarse materials and the fine materials is that a significantly higher pressure or vertical stress has to be generated to bring about the same displacement. Figure 4-14 highlights the differences in relative compressibility based on extension/displacement. The milled wood pellets are shown to be the most compressible material followed by the pulverised coal and torrefied wood chips. However, an interesting phenomenon is experienced with the remaining three materials. At lower vertical stresses, the wood pellets are shown to be the next most compressible material followed by the torrefied wood pellets and lastly the ground anthracite. However, where stresses are found in excess of approximately 620 kPa, the compressibility of the wood pellets is seen to reduce significantly, the compressibility of the ground anthracite increases and the compressibility of the torrefied wood pellets broadly stays the same.

Such trends can be explained by the physical strength of each of the materials. During the bulk density testing, all materials were observed to be initially receptive to the normal loads applied,

deforming elastically with increasing vertical stress. However, in the case of the harder materials, namely the ground anthracite, torrefied wood pellets and torrefied wood chips, visible and audible plastic deformations were observed. That is, all materials were shown to break at higher stress levels. This was not observed to be the case for the milled wood pellets or pulverised coal, and to a lesser extent in the case of the standard wood pellets. It is therefore supposed that an increase in extension is recorded at higher stress levels for both the torrefied wood pellets and ground anthracite compared to initial lower stress levels due to the plastic deformation and material breakage of both materials. The breakage gives rise to an overall smaller average particle size and thus allows void space otherwise present to be filled. The wood pellets are shown to be more compressible initially at lower stresses due to the material being softer (less hard) compared to both the torrefied pellets and ground anthracite. However, the onset of material breakage facilitates further compressibility which is not representative of the material with a given starting particle size. Therefore, the stress extension relationship displayed in Figure 4-14 should only be noted at lower stress levels – typically where stresses are less than 400 kPa. Further to the cases presented for the ground anthracite and torrefied pellets, a similar phenomenon was observed when compressing the torrefied wood chips. However, due to the larger particle size of the wood chips and their lower bulk density compared to all of the other materials, compression and material breakage facilitated a far greater extension to take place than for more appropriate cell dimensions.

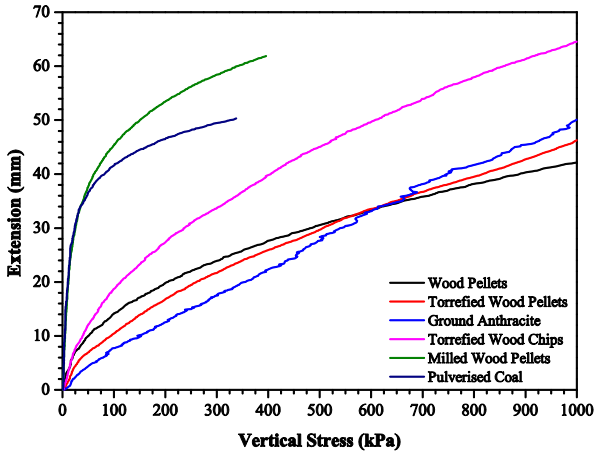

Figure 4-14: Material compressibility.

In addition to the results relating to the coarse materials, similar trends were observed for both the milled wood pellets and pulverised coal. Due to the particle size being sufficiently small that material breakage does not or is less likely to take place, materials are shown to curve upward until a constant extension/bulk density is attained; thus no change is recorded with further increasing the vertical stress. This highlights the ability for smaller particle sizes to pack more easily, interacting with each other and filling void spaces otherwise present where no stress is applied. Due to the milled wood

pellets attaining a plateau at a larger extension, the milled wood pellets can be said to be more compressible than the pulverised coal.

To provide context, the vertical stress experienced in a hopper due to the containment of material can be estimated using the Janssen equation, which states:

$$\sigma_v = \frac{g\rho_b A}{K \tan \phi_w U} \cdot [1 - \exp(-K \tan \phi_w Uz/A)]$$

Equation 4-22

Where g is the gravitational acceleration (m/s^2), ρ_b is the material bulk density (kg/m^3), A is the area of the cylindrical section of the hopper (m^2), ϕ_w is the kinematic angle of wall friction (°), U is the circumference of the cylindrical section of the hopper (m) and z is the height of the cylindrical section of the hopper (m) (Jacob, 2000, Schulze, 2008). K is the lateral stress ratio which can be written as:

$$K = \sigma_h/\sigma_v$$

Equation 4-23

$$K = 1 - \sin \varphi$$

Equation 4-24

Where σ_h is the horizontal stress component (Pa), σ_v is the vertical stress component (Pa) and φ is the angle of internal friction (°). Values for K typically range between 0.3 and 0.6 for most bulk solids (McGlinchey, 2008, Schulze, 2008). The Janssen equation assumes a constant vertical stress acting across the cross-section of the hopper and a constant bulk density of the material. Although the assumption of a constant bulk density is not strictly true, where a relationship between vertical stress and change in bulk density is known or determined experimentally, this is able to be factored into the Janssen equation iteratively.

It can be seen from the Janssen equation that the vertical stress generated is not strongly dependent on the height of the hopper. Moreover, it is strongly dependent on the diameter as A/U = D/4 where D is the diameter of the cylindrical section of the hopper (m). This is predominantly the reason why hoppers are designed and manufactured to be tall and narrow rather than short and wide. Figure 4-15 shows the implementation of the Janssen equation for a hopper of a constant height of 10 m with varying diameter, and a hopper of a constant diameter of 2 m with varying height to highlight this. A material with a bulk density of 650 kg/m^3 and an angle of internal friction of 33.4° (K = 0.45) is assumed in all cases.

Taking the case computed for a kinematic angle of wall friction of 30° it can be seen that increasing the hopper height in excess of 10 m does not generate an increase in vertical stress. For the same conditions (i.e. hopper height of 10 m), if the diameter of the hopper is increased in excess of 2 m (the

value kept constant in the previous calculation), a substantial increase in vertical stress is generated. Therefore, if a larger volume of material is required to be stored, increasing the hopper height looks to solve design issues relating to stress.

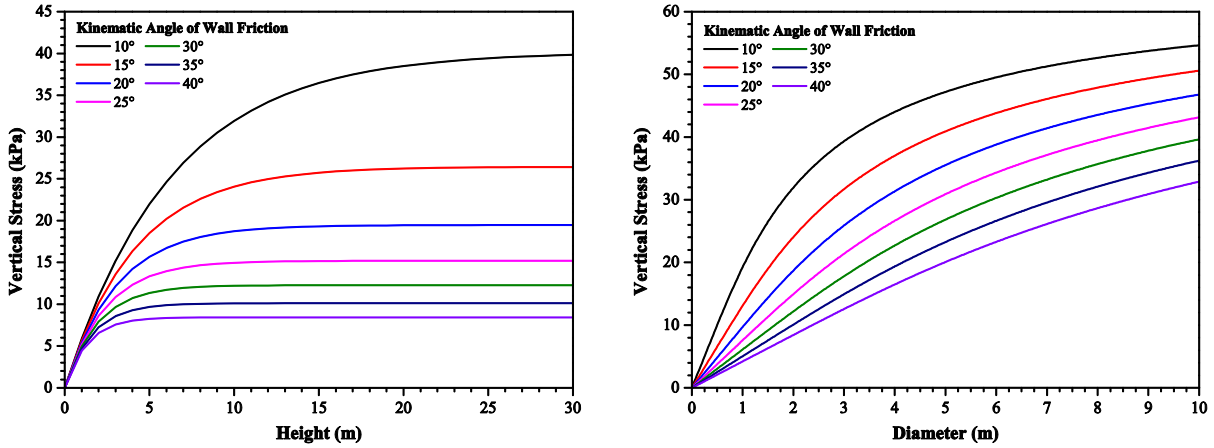

Figure 4-15: Effect of hopper height (left) and diameter (right) on vertical stress.

Figure 4-15 shows that stresses in the range of 10-40 kPa are experienced for the hypothetical hopper with a diameter of 2 m. By increasing the hopper diameter to 10 m it can be seen that vertical stresses peak around 32-55 kPa. Such stresses are substantially lower than those generated by the Hounsfield tensile tester in the bulk density compressibility test shown in Figure 4-13. Although the numbers stated assume a bulk density of 650 kg/m^3 and K = 0.45, stresses do not increase dramatically past this point for denser materials and smaller K values. It can therefore be said that the bulk density of large coarse materials does not vary dramatically when stored in a hopper as the stress generated is not sufficiently large. This is not found to be the case where materials with smaller particle sizes are handled. Figure 4-13 shows that at a vertical stress level of 50 kPa, approximately 51% of the recorded change in bulk density is achieved for milled wood pellets and 66% for pulverised coal. Comparing this to the remaining materials: 17% for wood pellets, 11% for torrefied wood pellets, 13% for torrefied wood chips and 6% for ground anthracite, it can be seen that the bulk density varies far more greatly at lower stress levels for smaller particle sizes. Therefore, when examining the average mass of materials with a small average particle size contained in a hopper, it is important to review the vertical stress generated and account for the change in bulk density.

4.5.3 Material shear test

A linear relationship of increasing shear stress with increasing normal stress can be seen in Figure 4-16 for all materials tested. This trend is observed due to the bulk strength of each of the materials increasing when the normal load applied is increased. However, a distinction can be made between

the coarse materials (wood pellets, torrefied pellets, ground anthracite and torrefied wood chips) and the fine materials (milled wood pellets and pulverised coal). As the consolidation stress increases, the stress required to shear both of the fine materials increases where the same normal load is applied. This is not found to be the case when shearing the bulk of the coarse materials and thus, where the consolidation stress is increased, the stress required to shear the materials is maintained broadly constant where the normal load applied is also maintained constant.

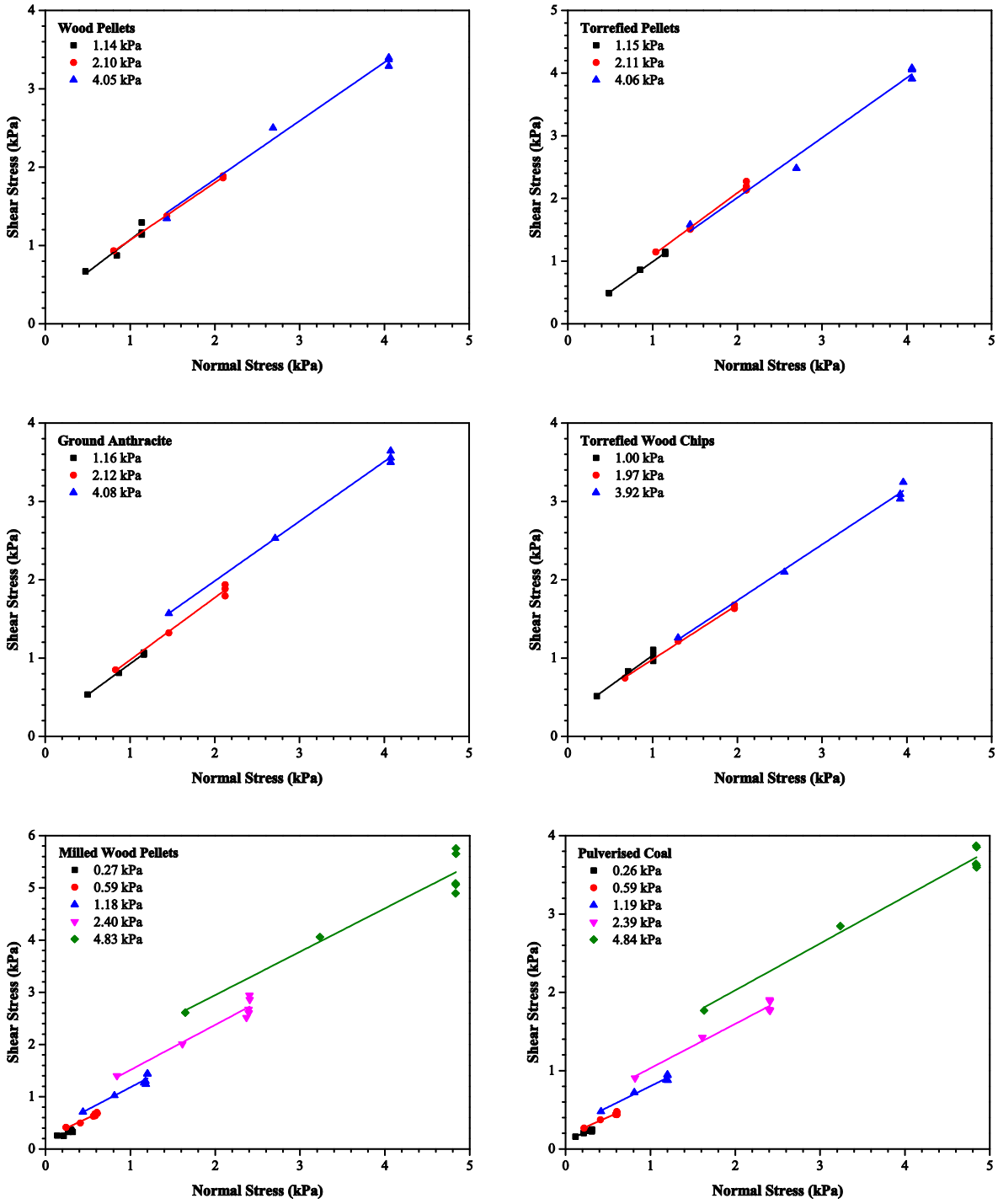

Figure 4-16: Family of yield loci for wood pellets, torrefied pellets, ground anthracite, torrefied wood chips, milled wood pellets and pulverised coal at varying consolidation stress.

Although this trend is found in the main for the coarse materials, the ground anthracite highlights an anomaly, specifically for a consolidation stress of 4.08 kPa. It can be seen in Figure 4-16 that when the consolidation stress is increased from 2.12 kPa to 4.08 kPa, an increase in shear stress is recorded for a normal stress of 1.46 kPa. A less pronounced increase in shear stress is also recorded for a normal stress of 0.85 kPa where the consolidation stress is increased from 1.16 kPa to 2.12 kPa.

The reason for both fine materials requiring a larger shear stress to shear the material where the consolidation stress is increased is due to an increased level of cohesivity. Cohesivity is generally found to increase as mean particle size decreases due to inter-particle forces representing the dominant forces in the bulk material (Rhodes, 2008, Schulze, 2008). Such inter-particle forces are found to be greater than competing gravitational and inertial forces and act to increase material cohesion. As discussed previously, inter-particle forces are largely present in the form of electrostatic forces and van der Waals forces, although forces due to liquid bridges and adsorbed liquids also play a large role where liquid contaminants are present (Rhodes, 2008).

Due to the large mean particle size of the anthracite grains (9 mm) it is thought that its exhibition of cohesivity takes place for a different reason. Observing the shape and surface of the ground anthracite and comparing it to the remaining coarse materials, it can be seen that the anthracite represents a more uniform shape. That is, it approaches a sphere more than either of the pelleted or chipped materials. Further to this, the ground anthracite represents a harder material than the remaining coarse materials and has a more even surface finish. It is supposed that both of these factors lead to the ground anthracite being more prone to inter-particle bridges forming once consolidated. Individual particles are allowed to fit more easily together than the pelleted or chipped materials, and the roughness increases inter-particle friction. Therefore, it is believed that it is this mechanism that leads to an increase in shear stress being required when the consolidation stress is increased.

Fuel	Flowability (ff_c)	Category
Wood pellets	6.12	Easy-flowing
Torrefied wood pellets	24.0	Free-flowing
Ground anthracite	6.37	Easy-flowing
Torrefied wood chips	6.49	Easy-flowing
Milled wood pellets	2.91	Cohesive
Pulverised coal	3.72	Cohesive

Table 4-7: Flowability of wood pellets, torrefied pellets, ground anthracite, torrefied wood chips, milled wood pellets and pulverised coal.

Analysing the data in Figure 4-16 further and applying Mohr stress analysis generates Figure 4-17, which allows pairs of values of the unconfined yield stress and the consolidation stress to be measured. In turn, these values can be plotted to generate material flow functions for each material

which are shown in Figure 4-18. Plotting these points through the origin generates a line of flowability most appropriate for the material flow function. The line of flowability is largely used to determine whether a material is free-flowing ($ff_c > 10$), easy-flowing ($4 < ff_c < 10$), cohesive ($2 < ff_c < 4$), very cohesive ($1 < ff_c < 2$) or does not flow ($ff_c < 1$) (Schulze, 2008).

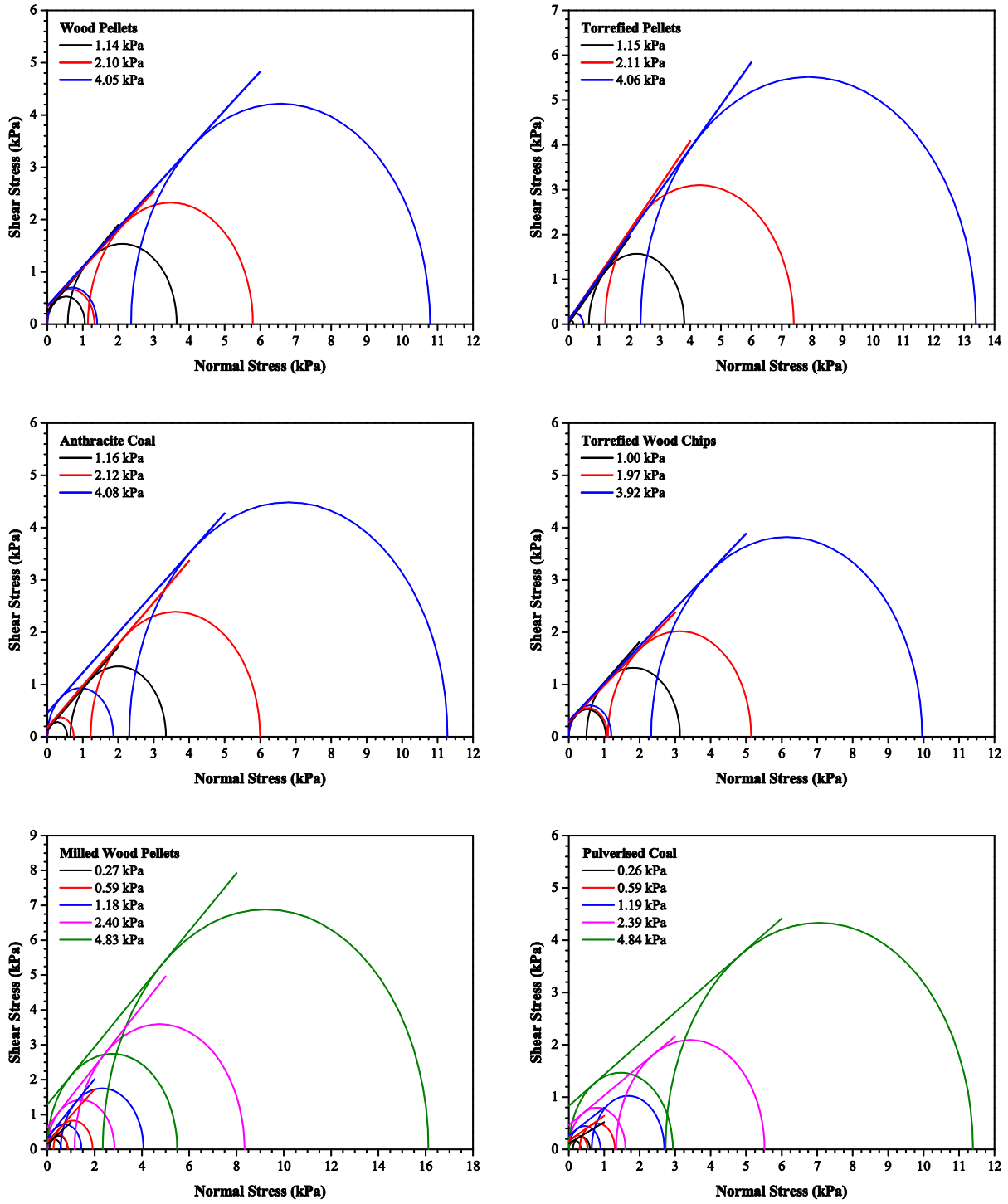

Figure 4-17: Mohr stress circle analysis for wood pellets, torrefied pellets, ground anthracite, torrefied wood chips, milled wood pellets and pulverised coal with varying consolidation stress.

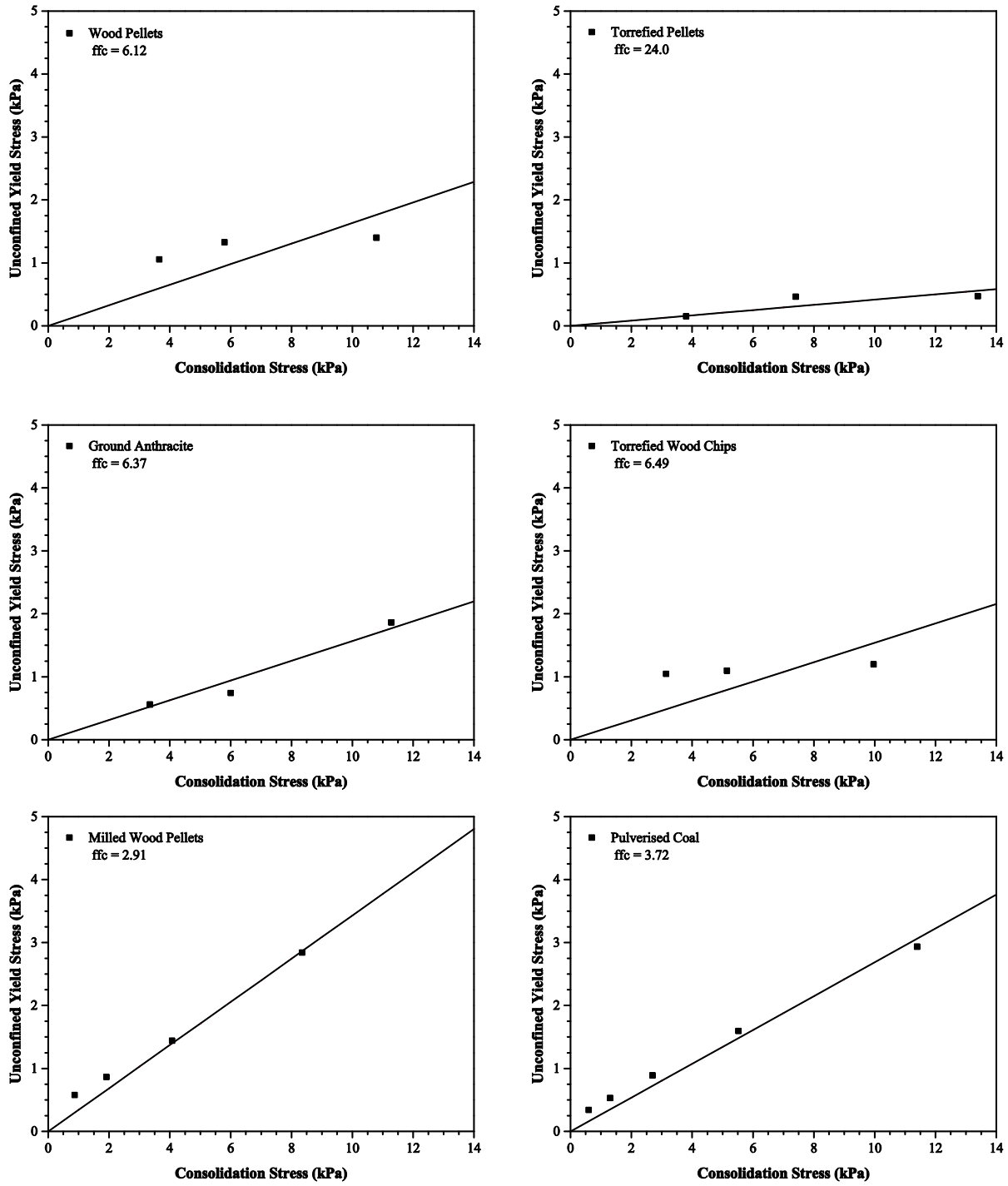

Figure 4-18: Material flow function for wood pellets, torrefied pellets, ground anthracite, torrefied wood chips, milled wood pellets and pulverised coal.

Broadly speaking, coarse materials can be considered to be easy-flowing when dry. This is due to inertial and gravitational forces being dominant in the bulk material. Figure 4-18 and Table 4-7 fortify this assertion and indicate all of the coarse materials tested to be either free-flowing or easy-flowing materials. The lines of flowability indicate that low stresses are required to generate incipient flow

and deformation of the material even after significant consolidation loads have been applied. For the majority of the coarse materials, a line of flowability between 6 and 6.5 is observed. The only exception is presented by the torrefied pellets, which indicates a free-flowing bulk solid with a line of flowability of 24. This is due to a low unconfined yield stress level being recorded at all consolidation stresses.

Generally it is found in most bulk solids that as the consolidation stress is increased, the unconfined yield stress also increases. This trend is found most notably in cohesive materials and is particularly pronounced for both the milled wood pellets and pulverised coal; however, it is also displayed in the case of the ground anthracite and torrefied pellets. The two exceptions are the wood pellets and torrefied wood chips. Both materials indicate that the unconfined yield stress is not greatly dependent on the consolidation stress. Plotting the individual unconfined yield stress/consolidation stress pairs through the origin generates a lower ff_c value for lower consolidation stresses. That is to say, both the wood pellets and torrefied wood chips are less free-flowing where lower stresses are present.

In the case of both the milled wood pellets and pulverised coal, a strong linear relationship between consolidation stress and unconfined yield stress is observed. Both materials are indicated to be cohesive, with the milled wood pellets being shown to be more so than the pulverised coal. Referring to Table 4-14 in Section 4.5.6, this can be attributed to the relative particle size variation and the respective particle shape. In the case of the milled wood pellets, both a broader range of particle sizes and a broader range of particle shapes are present. The milled wood pellets are largely made up of needle-like structures interspersed with finer material. It is thought that it is these needle-like structures that interact to form more stable bulk structures, which require a larger stress to create a deformation. The pulverised coal is seen to be broadly uniform in size and flows easily when handled compared to the milled wood pellets.

In addition to the flow function, Mohr stress circle analysis shown in Figure 4-17 can be used to determine both the effective angle of internal friction and the angle of internal friction, both of which are shown in Figure 4-19. It can be seen for all materials that as the consolidation stress increases, the effective angle of internal friction decreases. This trend is only slight and thus doubling the consolidation stress typically brings about a change of the order of a couple of degrees. As the consolidation stress increases past a given point, little or no change in the effective angle of internal friction takes place.

There is a direct relationship between the effective angle of internal friction and the hopper half angle. As the effective angle of internal friction increases, a smaller hopper half angle is required and thus the slope of a hopper is required to be steeper to prompt flow. Although the hopper half angle also requires the kinematic angle of wall friction to be determined, it is observed that where the kinematic angle of wall friction is kept constant and the effective angle of internal friction is varied, an increase

in the effective angle of internal friction generates a steeper hopper slope. The angle of internal friction is not used in the hopper design procedure, and is regarded as the gradient of the yield locus. Figure 4-19 shows the angle of internal friction to change in line with the effective angle of internal friction for all of the coarse materials tested, and to be a few degrees less in magnitude in each case.

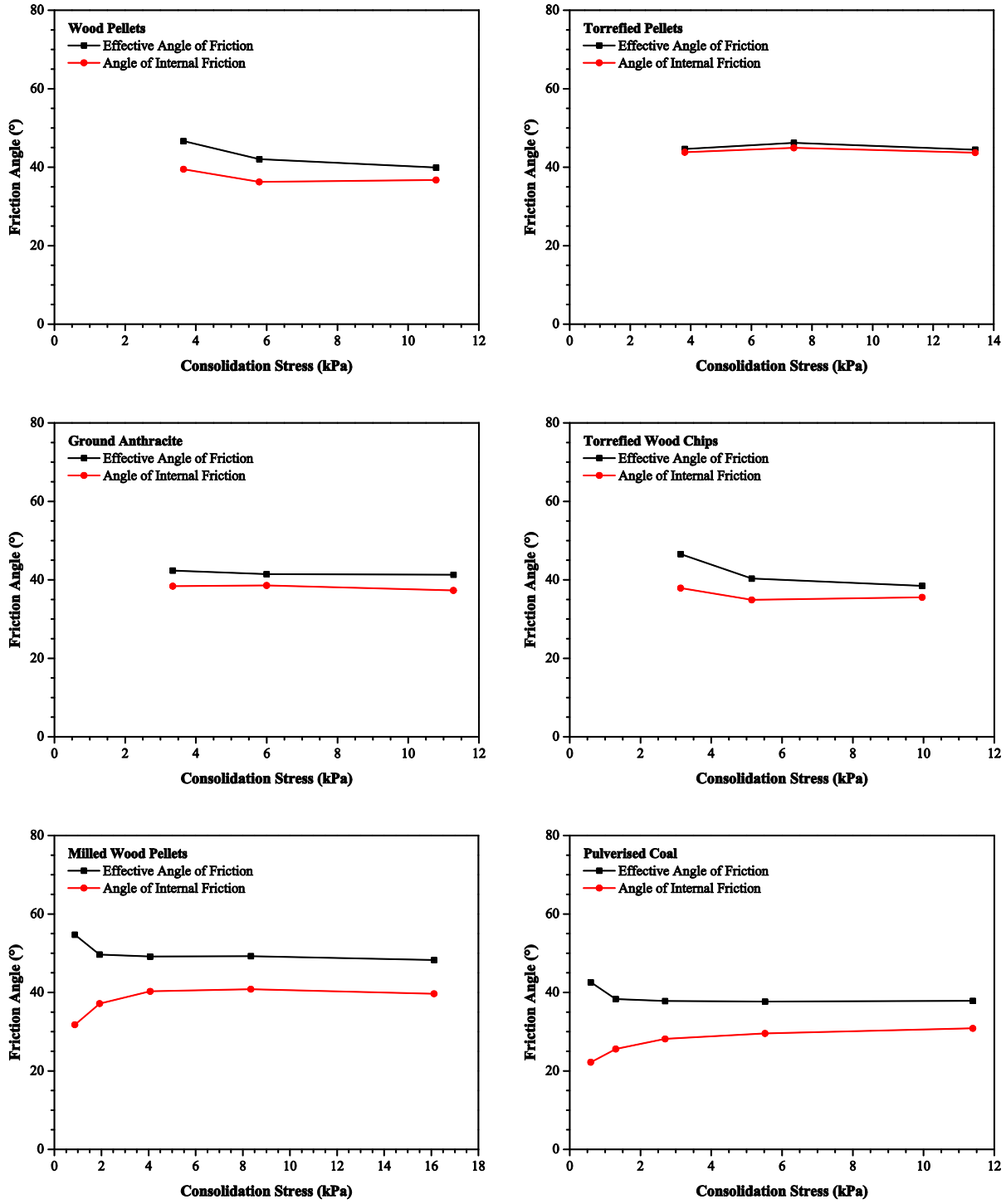

Figure 4-19: Angle of internal friction and effective angle of internal friction for wood pellets, torrefied pellets, ground anthracite, torrefied wood chips, milled wood pellets and pulverised coal.

In the case of both fine materials, the angle of internal friction is seen to increase in line with the decrease observed by the effective angle of internal friction. As with the effective angle of internal friction, the angle of internal friction is seen to stay broadly constant past a sufficiently large consolidation stress. It can therefore be said that as the stress built up in a hopper increases past a given point, the angle of the hopper slope is not required to be changed dramatically to prompt flow. It can also be said that for all materials where a small stress prevails, the hopper half angle is required to be steeper to prompt flow.

4.5.4 Wall friction shear test

Three wall materials were tested: TIVAR 88, stainless steel and mild steel. TIVAR 88 (a low friction plastic lining material) was used in this case as a comparison for the two steel samples which were present in the form of steel plate with a cold rolled finish. Due to the HLH incorporating water during its operation, and mild steel being used to construct the HLH in this study, the mild steel sample was tested when both dry and when wet.

Figure 4-21 highlights a general trend of decreasing friction angle with increasing normal stress where low normal stresses prevail (<2 kPa). Where higher normal stresses are generated (>2 kPa), the kinematic angle of wall friction is seen to stay broadly constant for all materials and with all wall material samples. Figure 4-21 therefore indicates that where low normal stresses prevail, a steeper hopper is required to prompt the flow of material for all materials. A general trend relating to the mild steel wall material sample is shown for all bulk materials. Where the mild steel wall material sample is wetted, a greater shear force is required to displace the bulk material and in turn a larger wall friction angle is recorded.

In the majority of cases either the TIVAR 88 or mild steel sample require the smallest shear force to generate displacement. Therefore, hoppers constructed from either of these materials are required to be the least steep when compared to the remaining materials. It is observed from Figure 4-21 that for both of the fine materials, little distinction can be made between either the stainless steel or mild steel (dry) samples. Both materials generate a wall friction angle of approximately 10° in the case of the milled wood pellets and 30° in the case of the pulverised coal. Further to this, a similar wall friction angle is recorded for the TIVAR 88 in the case of the pulverised coal. Comparatively, the milled wood pellets require a far larger wall friction angle when used in conjunction with the TIVAR 88. This is likely to be due to enhanced electrostatic forces being present. During testing, electrostatic forces between both the TIVAR 88 sample and the milled wood pellets were apparent. During the application of the TIVAR 88 sample to the Brookfield PFT and the subsequent lowering of the wall material disc into the annular shear cell, small portions of the sample were seen to be attracted prior to

the start of the wall friction test. It is supposed that larger wall friction angles are recorded for TIVAR 88 in the case of the milled wood pellets due to this phenomenon.

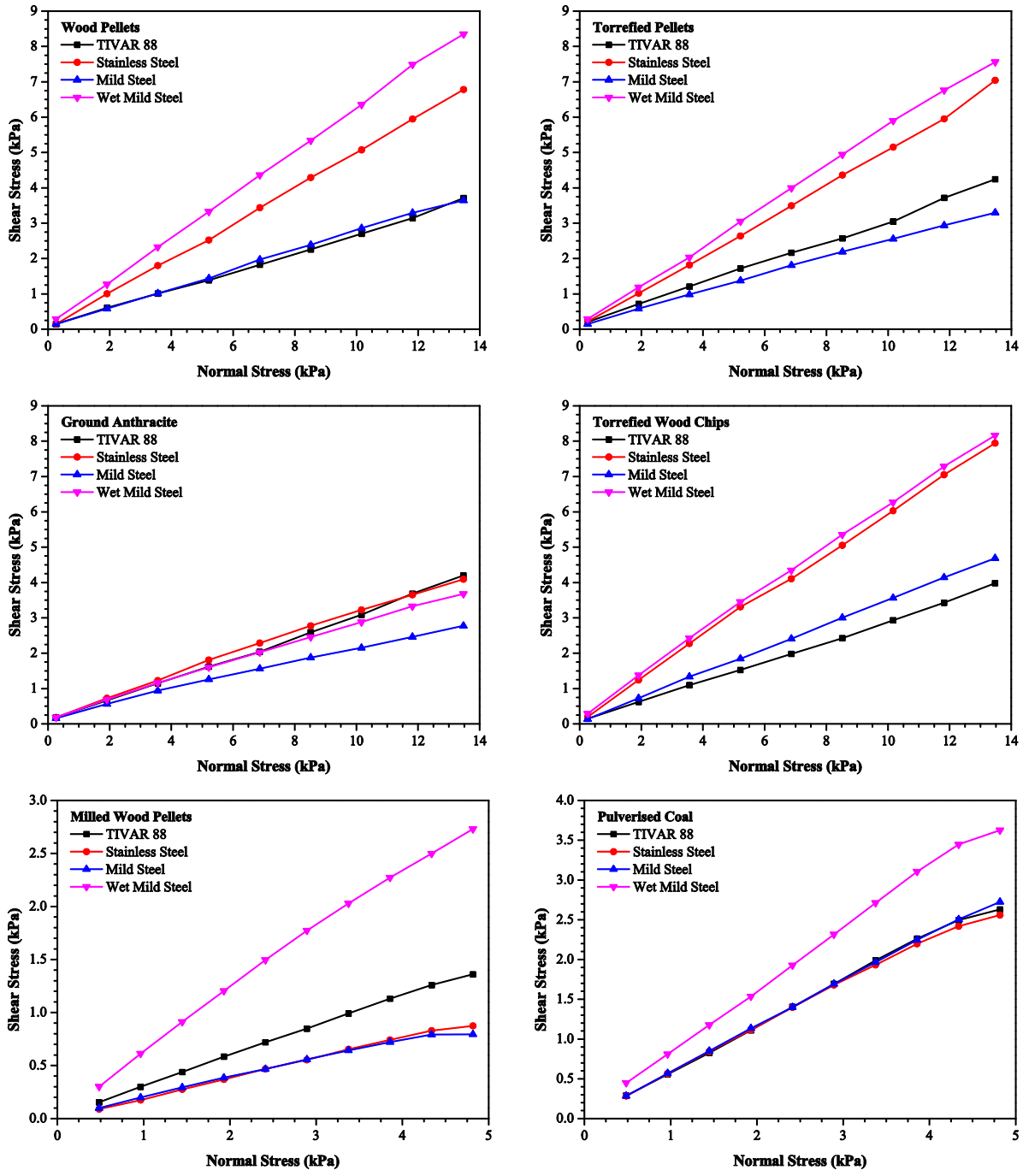

Figure 4-20: Family of wall friction loci for wood pellets, torrefied pellets, ground anthracite, torrefied wood chips, milled wood pellets and pulverised coal.

The wood pellets, torrefied pellets and torrefied wood chips display similar wall friction angles for all wall material samples. Values of approximately 30° are recorded for both wet mild steel and stainless steel and between 15° and 20° for dry mild steel and TIVAR 88, where normal stresses in excess of 2

kPa are generated. Ground anthracite presents an anomaly, recording lower friction angles with all wall material samples. The anthracite coal has a metallic surface and thus inherently has a lower coefficient of friction than any of the remaining coarse materials. Further to this, as its particle size is significantly larger than the pulverised coal, the bulk solid is able to hold its shape more readily and slide freely over the wall material.

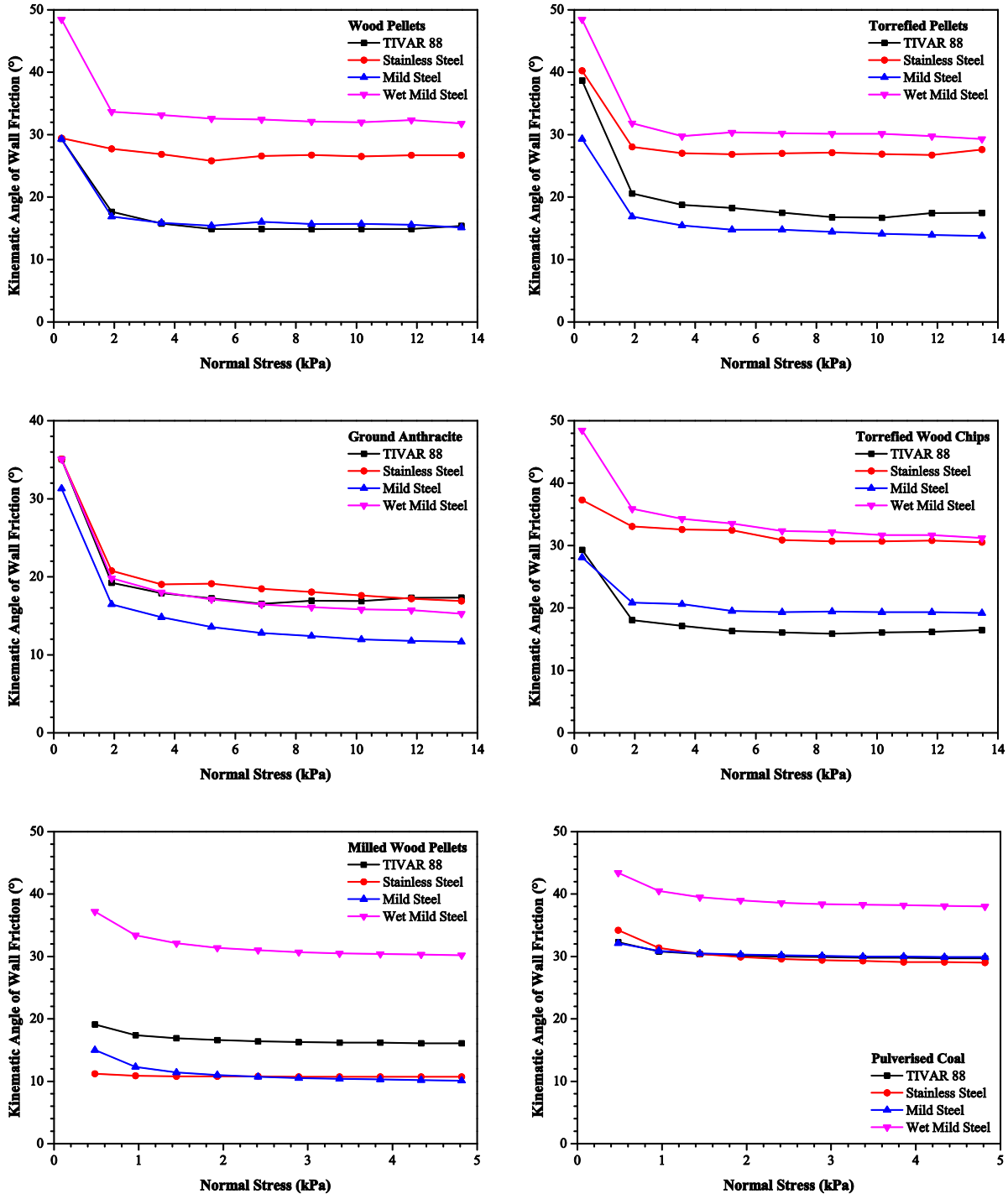

Figure 4-21: Kinematic angle of wall friction for wood pellets, torrefied pellets, ground anthracite, torrefied wood chips, milled wood pellets and pulverised coal.

Comparing the milled wood pellets with the pulverised coal, it can be seen from Figure 4-21 that a far steeper hopper angle is required to prompt flow when handing the pulverised coal. Comparing values for mild steel and stainless steel, a difference of approximately 20° is observed. Such differences take place due to the respective particle size of the materials. As the particle size of a material decreases, more particles are allowed to interact with the wall material. An approximate relationship between the number of particle contacts and particle diameter is:

$$n_p \propto A/{d_p}^2$$

Equation 4-25

Where n_p is the number of particle contacts, A is a given area (m^2) and d_p is the particle diameter (m) (Schulze, 2008). Taking this relationship further and assuming the failure force is equal to the sum of the adhesive forces between particles, it can be shown that the tensile strength of a bulk solid is proportional to the inverse of the particle diameter (Schulze, 2008). Thus, as particle size decreases, an increase in tensile strength of the material is observed. In the case of the pulverised coal and the wall friction shear test, a decrease in particle size not only brings about an increase in the tensile strength, but an increase in friction due to the increase in the number of particle contacts. Therefore, it is the decrease in particle size that leads to the increase in the kinematic angle of wall friction compared to the milled wood pellets.

As an aside, it is important to state that where both of the steel wall samples are concerned, the results generated correspond to a cold rolled finish. The surface finish of the steel used to construct the HLH in this study differs from this and corresponds to a machined finish, as both the top hopper and the bottom hopper are machined from mild steel rounds. This means that the hopper half angles required to generate flow will be different to those reported in Table 4-9 for the HLH constructed in this study due to the associated changes in local friction. Although this somewhat invalidates the results generated for both steels (when dry) for use with the HLH in its current form, they go a considerable way to aid the design of industrial scale units. That being said, it is anticipated that any increase in local friction brought about by changing the surface finish from cold rolled to machined will be dwarfed by the presence of water on the wall material surface. Therefore, it is imagined that the results relating to the wet mild steel sample reported in Figure 4-20 and Figure 4-21 will be valid for use in conjunction with the HLH in its current form, and will act as upper limits for wall friction.

4.5.5 Hopper flow factor, half angle and minimum opening diameter

The Jenike hopper design procedure follows that once the effective angle of internal friction and the kinematic angle of wall friction have been determined, the hopper flow factor, hopper half angle and the minimum hopper outlet diameter can be assessed. As all of the materials tested have an effective

angle of internal friction approximately between 40° and 50°, the plots in Figure 4-22 determined by Jenike can be used to determine the hopper flow factor and the hopper half angle for a conical hopper.

Once the hopper flow factor has been determined, the inverse of the hopper flow factor can be plotted alongside each of the material flow functions shown in Figure 4-18 to determine the critical stress at which flow occurs. Where the two lines intersect is defined as the critical stress, and the minimum hopper outlet diameter for a conical hopper can in turn be determined using Equation 4-26:

$$B = \frac{H(\theta)\sigma_{crit}}{\rho_b g}$$

Equation 4-26

$$H(\theta) = 2.0 + \theta/60$$

Equation 4-26a

Where B is the minimum hopper outlet diameter (m), θ is the hopper half angle (°), σ_{crit} is the critical stress (N/m^2), ρ_b is the bulk density (kg/m^3) and g is the gravitational acceleration (9.81 m/s^2).

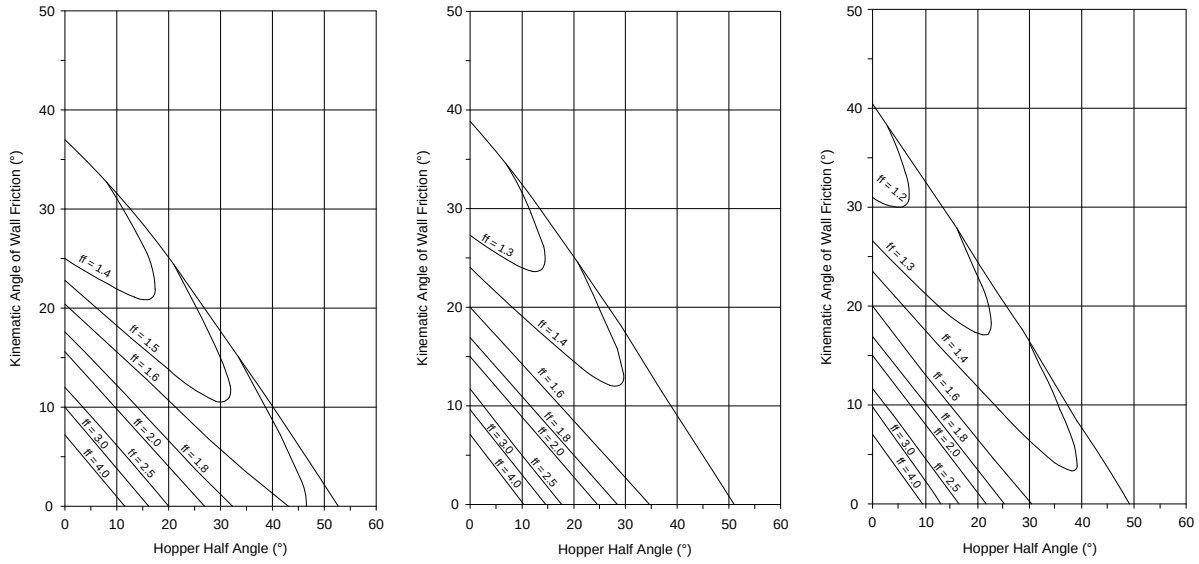

Figure 4-22: Conical hopper flow factor values for an effective angle of internal friction of 40°, 45° and 50° (left to right) (Arnold et al., 1982).

Table 4-9 shows that TIVAR 88 and mild steel require a similar hopper half angle for all bulk solids. Pulverised coal is observed to require the steepest hopper slope in all wall material cases, and ground anthracite is broadly shown to require the same hopper half angle regardless of wall material type. All bulk solids highlight that where the mild steel wall material sample is wetted, a steeper hopper slope is required. From Table 4-10 it can be seen that the hopper flow factor ranges from 1.3 to 1.8 and does not vary dramatically for all cases. Plotting lines of gradient 1/ff for all wall material cases on the plots generated for the material flow function shown in Figure 4-19 generates a critical stress for flow.

		Kinematic Angle of Wall Friction (°)			
Fuel	**Effective Angle of Friction (°)**	**TIVAR 88**	**Stainless Steel**	**Mild Steel**	**Wet Mild Steel**
Wood pellets	39.9	15.4	26.7	15.1	31.8
Torrefied wood pellets	44.5	17.5	27.6	13.8	29.3
Ground anthracite	41.3	17.3	16.9	11.6	15.3
Torrefied wood chips	38.5	16.5	30.5	19.2	31.2
Milled wood pellets	48.3	16.1	10.7	10.1	30.2
Pulverised coal	37.9	29.7	29.0	29.9	38.0

Table 4-8: Friction angles at maximum normal stress for wood pellets, torrefied pellets, ground anthracite, torrefied wood chips, milled wood pellets and pulverised coal.

	Hopper Half Angle (°)			
Fuel	**TIVAR 88**	**Stainless Steel**	**Mild Steel**	**Wet Mild Steel**
Wood pellets	33	17	34	10
Torrefied wood pellets	29	17	34	15
Ground anthracite	31	31	38	34
Torrefied wood chips	32	12	28	11
Milled wood pellets	31	37	38	14
Pulverised coal	13	14	13	0

Table 4-9: Hopper half angle for wood pellets, torrefied pellets, ground anthracite, torrefied wood chips, milled wood pellets and pulverised coal with varying wall material type.

	Hopper Flow Factor (ff)			
Fuel	**TIVAR 88**	**Stainless Steel**	**Mild Steel**	**Wet Mild Steel**
Wood pellets	1.6	1.5	1.6	1.5
Torrefied wood pellets	1.6	1.4	1.6	1.4
Ground anthracite	1.6	1.6	1.8	1.6
Torrefied wood chips	1.6	1.5	1.6	1.5
Milled wood pellets	1.4	1.6	1.6	1.3
Pulverised coal	1.5	1.5	1.5	1.3

Table 4-10: Hopper flow factor for wood pellets, torrefied pellets, ground anthracite, torrefied wood chips, milled wood pellets and pulverised coal with varying wall material type.

It can be seen from Figure 4-23 that an intersection of the material flow function with the hopper flow factor does not occur in the stress range measured for all of the coarse materials. This is due to the easy-flowing nature of the coarse bulk solids. As a consequence, a critical stress for flow cannot be determined, and in turn, neither can a minimum outlet diameter for a conical hopper. Therefore, an approximation and general rule is to be applied in order to generate a minimum outlet diameter that facilitates flow. It is generally considered that a value of 10 to 12 times the average particle diameter (d_p) is sufficient to prompt flow unaided (Jacob, 2000, Berry, 2013). In the case of the coarse bulk

solid materials, sizing the outlet as such primarily seeks to counter flow problems caused by the formation of mechanical bridges (arching). Table 4-11 provides an overview of the minimum outlet diameter required for a conical hopper and for all materials based on this general rule. In the case of the wood pellets, torrefied wood pellets, ground anthracite and torrefied wood chips, the midpoint between the average particle diameter and particle length is used in place of the average particle diameter.

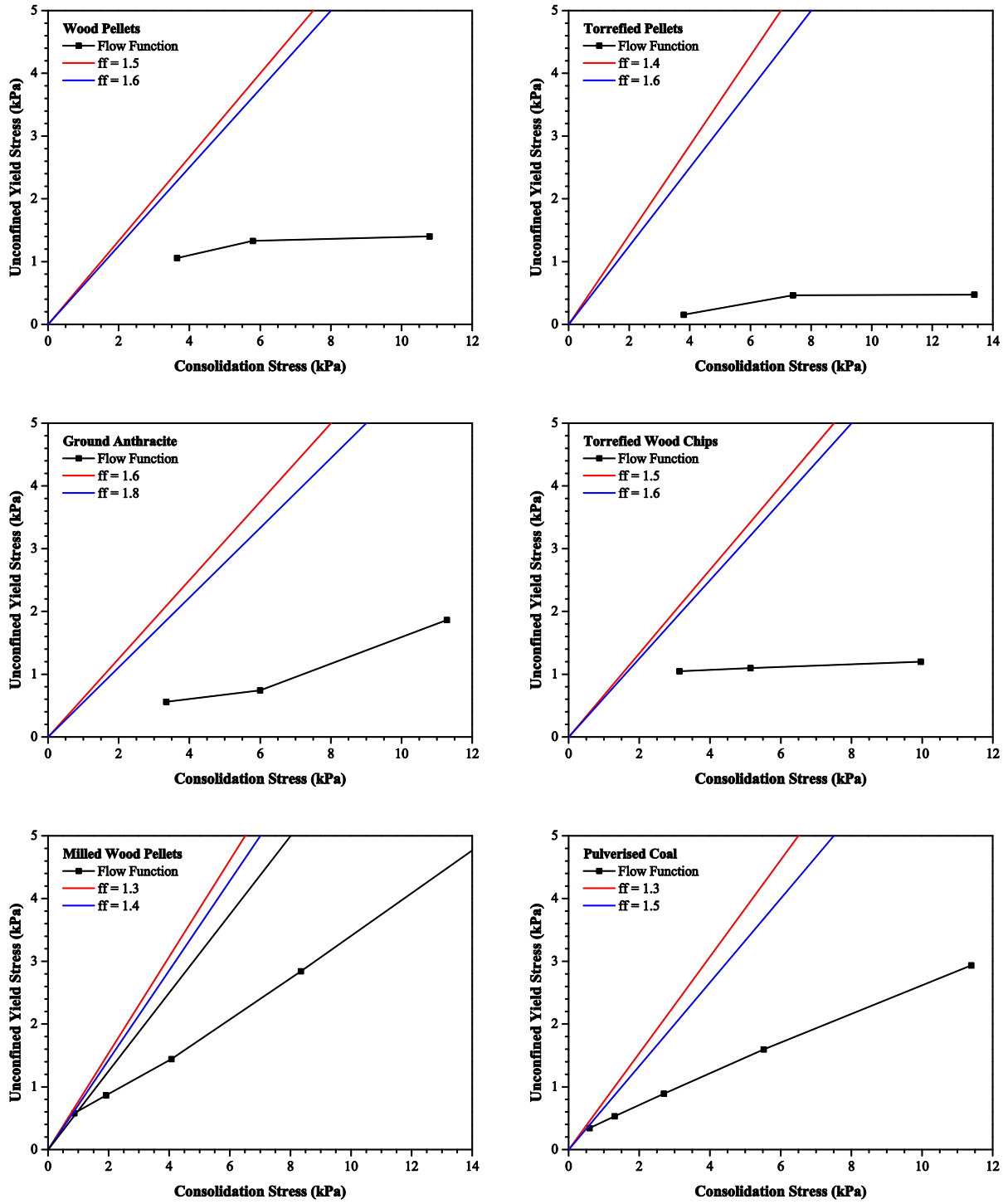

Figure 4-23: Determination of the critical stress for flow.

Figure 4-23 shows that for both the milled wood pellets and the pulverised coal, the respective material flow functions intersect with each of the hopper flow factors plotted. Therefore, a critical stress for flow can be determined and the outlet of a conical hopper can be sized according to Equation 4-26. The minimum outlet required for both the milled wood pellets and the pulverised coal based on the critical stress is shown in Table 4-12.

	Minimum Hopper Outlet Diameter (mm)			
Fuel	**TIVAR 88**	**Stainless Steel**	**Mild Steel**	**Wet Mild Steel**
Wood pellets	102	102	102	102
Torrefied wood pellets	107	107	107	107
Ground anthracite	89	89	89	89
Torrefied wood chips	272	272	272	272
Milled wood pellets	10	10	10	10
Pulverised coal	4	4	4	4

Table 4-11: Minimum hopper outlet diameter for feeding wood pellets, torrefied pellets, ground anthracite, torrefied wood chips, milled wood pellets and pulverised coal with varying wall material type.

	Minimum Hopper Outlet Diameter (mm)			
Fuel	**TIVAR 88**	**Stainless Steel**	**Mild Steel**	**Wet Mild Steel**
Milled wood pellets	295	332	334	251
Pulverised coal	128	135	128	109

Table 4-12: Minimum hopper outlet diameter for feeding milled wood pellets and pulverised coal with varying wall material type based on the critical stress.

It is observed from Table 4-12 that the required minimum outlet diameter is significantly larger where the Jenike hopper design procedure is used compared to the general rule applied regarding the average particle diameter. It therefore goes that for smaller particle sizes, the Jenike hopper design procedure is particularly appropriate. This is to be expected, not least due to the bulk of Jenike's work taking place with materials with a small particle size. Both the hopper half angle and minimum outlet diameter seek to mitigate flow problems caused by high levels of inter-particle and wall-particle friction. Where large particles are concerned, gravity is the dominant force and therefore the main aim when sizing the hopper outlet is to minimise the formation of mechanical bridges. Therefore, the values stated in Table 4-12 are sufficient when sizing the outlet of a conical hopper containing coarse materials.

4.5.6 Particle size distribution

The PSD of each material was determined using particle sieves to provide context for the inter-particle and wall-particle friction values stated in Section 4.5.3 and Section 4.5.4. Table 4-13 provides an

overview of the average particle sizes for the wood pellets, torrefied wood pellets, ground anthracite and torrefied wood chips. Table 4-14 provides an overview of the average particle sizes for both the milled wood pellets and pulverised coal.

In the case of the coarse materials, it is found that the majority of the particle sizes exceed the maximum sieve aperture of 3.15 mm and present a low concentration of fines, less than 0.1 wt% in the case of the wood pellets, torrefied wood pellets and ground anthracite. Torrefied wood chips present a higher degree of fine material in a concentration of approximately 1.4 wt%. Both pelleted materials are shown to contain the highest portions of the parent material, followed by the ground anthracite and torrefied wood chips. Approximately 6.8 wt% of material sized at less than 3.15 mm was found in the case of the torrefied wood chips, where in each of the sieve graduations used (2.36 mm, 1.00 mm and tray) needle-like structures were found as the predominant species. In the case of the remaining materials, sphere-like particles were found.

	Concentration (wt%)			
Mesh Size (mm)	**Wood Pellets**	**Torrefied Wood Pellets**	**Ground Anthracite**	**Torrefied Wood Chips**
3.15	99.96	99.89	98.96	93.23
2.36	0.00	0.03	0.21	0.63
1.00	0.01	0.05	0.75	4.78
Tray	0.03	0.03	0.08	1.36

Table 4-13: PSD of wood pellets, torrefied wood pellets, ground anthracite and torrefied wood chips.

	Concentration (wt%)	
Mesh Size (μm)	**Ground Wood Pellets**	**Pulverised Coal**
850	28.05	0.00
600	28.70	0.06
425	16.88	0.12
300	10.54	3.40
212	11.14	92.09
150	4.24	3.90
106	0.21	0.10
75	0.13	0.14
56	0.11	0.13
Tray	0.00	0.06

Table 4-14: PSD of milled wood pellets and pulverised coal.

For both of the fine materials it can be seen that the majority of particles are sub-millimetre in size, with the pulverised coal indicating all particles to be less than 850 μm. In the case of the milled wood pellets the largest portion of particles is found to prevail in the 600 μm < X < 850 μm category, with the majority of particles having a particle size in excess of 600 μm. Where the pulverised coal sample

is concerned, the largest portion of particles is found in the 212 μm < X < 300 μm category in which approximately 92 wt% of the material is classified. The milled wood pellets highlight a far broader range in particle sizes when compared to the pulverised coal and have a larger mean particle size. However, one of the key differences between the two materials is that the milled wood pellets contain needle-like structures. Due to the fibrous nature of biomass materials, when milled they tend to form needle-like structures which are not easily classified by sieve trays. Analysing the sieve trays after separation, it can be seen that the majority of the needle-like structures are contained in the 425 μm, 600 μm and 850 μm sieve trays while in all of the sub-450 μm trays predominantly spherical or sphere-like structures are found. This is contrary to the pulverised coal which predominantly showcases sphere-like structures which are easily quantified by sieving. Results shown regarding the PSD of the milled wood pellets in Table 4-14 can therefore be classified in terms of particle length rather than diameter in the case of the 450 μm, 600 μm and 850 μm sieve trays. Tests were repeated in all cases and an error of approximately 3% was found for all three sieve trays in question relating to the milled wood pellets.

The tests regarding PSD look to provide a more detailed account of the materials being handled. It is well known that as the quantity of fines in a bulk material increases, the flowability decreases (Jenike, 1964, Schulze, 2008). This is especially true for larger coarse materials containing fines, as the cohesive fine material can be said to transition from passively flowing between the larger bulk solid particles, to presenting the predominant material. Thus, in such cases the larger bulk solid can be said to be flowing through the fine material which inherently presents higher degrees of inter-particle friction. Quantifying the presence of fines therefore seeks to provide context for the material tests carried out regarding flowability.

4.5.7 Discharge rate

Following the solid fuel characterisation tests, a prototype test hopper was constructed from cardboard to assess the flowability of each material in a real a device. Although not strictly the same in terms of wall friction effects, a prototype provides a good approximation to how a material will flow, especially in the case of the coarse materials where gravitational and inertial forces dominate.

Where the dimensions of the hopper were concerned, constraints were imposed on the design by the valves available for use and the space available to construct the experimental rig. Due to an economic constraint, the diameter of the valves used was limited to 3-inch bore, and as such the outlet diameter of the hopper was limited to approximately 75 mm. Due to the space available for the construction of the experimental rig, the height of the rig was limited to around 2 m, and in turn, a constraint was imposed on the hopper half angle of each of the hoppers. Due to the construction material for the hoppers being mild steel, an average value for the hopper half angle associated with each of the fuels

and mild steel was used (approximately 30 degrees). Although a hopper half angle associated with wet mild steel would ideally be used as to minimise flow problems, the value associated with wet mild steel (approximately 15 degrees) was deemed to be too steep given the available height for the construction of the experimental rig. Incorporating such a value for the hopper half angle would negatively impact the associated dimensions of the hopper and in turn, would significantly reduce the mass per batch of each fuel being able to be held by each hopper. Consequently, a prototype test hopper was constructed with the dimensions shown in Figure 4-24.

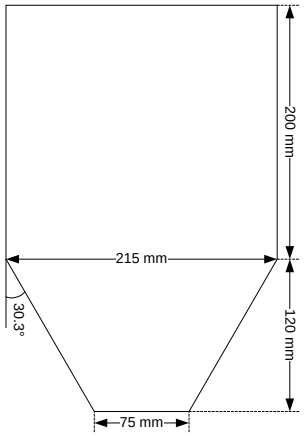

Figure 4-24: Dimensions of the prototype test hopper.

The prototype hopper was tested in conjunction with all of the fuels detailed previously; however, only the wood pellets, torrefied pellets, ground anthracite and pulverised coal were found to flow unaided. The milled wood pellets were not found to flow due to a mixture of inter-particle friction effects and the formation of mechanical bridges over the hopper outlet, and similarly mechanical bridges were found to form when feeding the torrefied wood chips due to large particle sizes. As the outlet diameter of the hopper is fixed by the diameter of the valves used, feeding with the torrefied wood chips and the milled wood pellets was retired at this stage.

Figure 4-25: Flow of wood pellets from the prototype test hopper.

The hoppers used in the HLH were constructed with broadly similar dimensions to those shown in Figure 4-25. The hopper half angle was reduced from 30.3 degrees to 28.5 degrees, the diameter of the cylindrical section was reduced from 215 mm to 200 mm and the total height of the hopper was reduced from 320 mm to 300 mm. The hoppers were milled from mild/carbon steel rounds and painted internally in order to minimise corrosion encountered through contact with water. Differences between the dimensions of the constructed hoppers and the prototype hopper came about due to discrepancies in the manufacturing procedure.

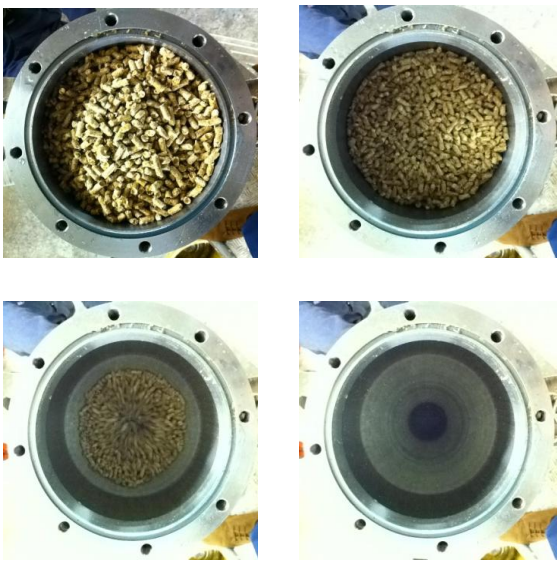

Figure 4-26: Flow of wood pellets from one of the hoppers used to make up the HLH.

The discharge rate was assessed on a mass basis measuring the mass of material leaving one of the hoppers used to make up the HLH per unit time. Varying quantities of material were loaded in to the hopper and the time taken to discharge the hopper completely to a collection vessel mounted on a mass balance was measured. The results for each material are shown in Table 4-15.

Material	Mass per Batch (kg)	Discharge Rate (kg/s)
Wood pellets	4.00	0.789 ± 0.006
Torrefied pellets	4.25	0.805 ± 0.014
Ground anthracite	4.75	1.039 ± 0.032
Torrefied wood chips	1.00	No flow
Milled wood pellets	2.00	No flow
Pulverised coal	3.50	Partial discharge

Table 4-15: Discharge rate of materials from a hopper used to make up the HLH.

As with the tests carried out with the prototype test hopper, the wood pellets, torrefied pellets and ground anthracite were found to flow freely. Problems were found again when feeding both the torrefied wood chips and milled wood pellets, and in addition to this, when feeding the pulverised

coal. Local regions of material were found to remain on the hopper walls and slope when feeding the pulverised coal, and significant force was required to dislodge it. A clear example of funnel flow was demonstrated, with stagnant regions being found above the hopper slope, and the presence of moisture was found to exacerbate problems with flow. Although the material was able to be dislodged through mechanical means, feeding was ceased with the pulverised coal as with the torrefied wood chips and milled wood pellets.

Inputting the hopper dimensions and material properties into both the Johanson and Beverloo equations stated in Section 4.3.8 allows theoretical mass flow rates to be calculated and compared to those determined experimentally. Theoretical flow rates for all materials are shown in Table 4-16. Two values are calculated using the Beverloo equation as it is reliant on particle size. Both the average particle diameter and average particle length are used in this case.

	Discharge Rate (kg/s)		
Flow type	**Johanson Equation**	**Beverloo Equation (Diameter)**	**Beverloo Equation (Length)**
Wood pellets	1.56	1.25	0.95
Torrefied wood pellets	1.63	1.17	1.05
Ground anthracite	1.76	1.42	1.20
Torrefied wood chips	0.41	0.16	0.06
Milled wood pellets	1.18	1.23	1.23
Pulverised coal	1.22	1.31	1.31

Table 4-16: Theoretical mass flow rates from a hopper used to make up the HLH.

The mass flow rate of material recorded experimentally is seen to be considerably lower than either of the predicted values stated in Table 4-16 generated by the Johanson and Beverloo (diameter) equations in all cases. However, examining the mass flow rate calculated using the average particle length in the Beverloo equation shows that experimental results correlate reasonably well with theoretical work.

Two key reasons why the mass flow rate is seen to be significantly lower than values calculated using the Johanson equation and Beverloo equation based on the average particle diameter are that each fuel is fed as a batch and all of the materials fed are not made up of uniform spherical particles. The non-spherical and non-uniform particle size means that the flow of material is unlikely to be uniform due to the formation and removal of inter-material obstructions impeding and promoting flow charges. As each of the fuels is fed as a batch, flow inconsistencies are brought about and this leads to the funnel flow mode being favoured in the latter stages of the discharging of the hopper. A continuous process whereby fuel is fed *from* and *to* the hopper maintaining a constant material head facilitates a constant stress or pressure acting on the material adjacent to the hopper outlet. This constant pressure is a vital factor affecting the formation of a stable arch. If the pressure acting on the arch is sufficient and greater than the stress created by the arch, then the arch will fail and flow will be promoted. However,

if the inverse of this is true, then the arch will be maintained and no flow will be observed. In a continuous process the pressure due to the material head is able to be maintained and thus the formation of a stable arch curtailed, allowing continuous flow and an increased flow rate. In a batch process, the pressure head is continuously changing due to the flowing material. This increases the probability of a stable arch being formed and thus reduces the flow rate if there is a succession of arch formations and destructions.

However, it can be seen from Table 4-16 that where the Beverloo equation is used in conjunction with the average particle length (i.e. the maximum particle dimension), a reasonably accurate estimation of the real mass flow rate is made. The Beverloo equation based on the average particle length generates a discharge rate greater by a factor of 1.20, 1.30 and 1.15 in the case of the wood pellets, torrefied pellets and ground anthracite respectively. However, the Beverloo equation used in this case assumes a constant for k equal to 1.4. The shape coefficient k is dependent on the particle shape and the hopper half angle and thus varies from material to material. Ultimately, the shape coefficient seeks to account for where particles do not flow fully at the perimeter of the hopper outlet. Typically, values for k range between 1 and 2.9; however, a value of 1.4 is usually assumed where a k value for a specific material is not known (Mankoc et al., 2007, Chase, 2010). Substituting the recorded mass flow rates into the Beverloo equation, a k value for each of the materials can be determined. In the case of the wood pellets, torrefied pellets and ground anthracite, a k value of 1.77, 1.99 and 1.78 was determined respectively. Such values fit well within the expected boundary previously stated and thus can be used as corrective measures when estimating the discharge rate of the materials exiting the HLH.

4.6 Summary

A broad range of materials with varying particle size and shape were tested: wood pellets, torrefied wood pellets, ground anthracite grains, torrefied wood chips, milled wood pellets and pulverised bituminous coal. The particle density, bulk density, voidage, unconfined yield stress, material flow function, angle of internal friction and effective angle of internal friction were determined for all materials. Further to this, the kinematic angle of wall friction was assessed for a range of wall materials: TIVAR 88, stainless steel and mild steel. Results from such tests were used in conjunction with the Jenike hopper design procedure to determine the required hopper half angle and minimum hopper outlet diameter to ensure the flow of material out of a conical hopper. Thus, the results from such tests were recorded for design and scale-up purposes for the HLH.

Tests showed all of the coarse materials (wood pellets, torrefied pellets, ground anthracite and torrefied wood chips) to be either free-flowing or easy-flowing, and both of the fine materials (milled wood pellets and pulverised coal) to be cohesive. Such assessments correspond well with work

detailed in the literature. The flow of coarse materials (>500 μm) is typically dominated by the gravitational force, and the flow of fine materials is largely governed by inter-particle and wall-particle forces. Coarse materials are generally found to be free-flowing for this reason, whereas fine materials are typically more cohesive.

TIVAR 88 and mild steel were found to generate the lowest wall friction values, and comparatively wet mild steel was observed to generate the highest wall friction values in all cases, with the exception of the ground anthracite. The kinematic angle of wall friction was also observed to increase for all materials where the mild steel wall sample was wetted. Results indicate that the design procedure for the HLH should use wetted wall materials to establish the required hopper half angle to reliably prompt flow during operation.

Critical stress values to prompt the flow of material were determined using the Jenike hopper design procedure for both the milled wood pellets and pulverised coal, and such values were used to size the minimum outlet diameter of a conical hopper. Values ranging between 250 mm and 335 mm were determined in the case of the milled wood pellets and values ranging between 105 mm and 135 mm in the case of the pulverised coal. Contrary to both of the fine materials, a critical stress to prompt the flow of all coarse materials was unable to be determined using the Jenike hopper design procedure. This was because all of the material flow functions lay far below the lines of constant hopper flow factor plotted. Sizing was therefore brought about by applying a general rule found in the literature, which states that the outlet diameter should correspond to 10 to 12 times the average particle diameter of the material being fed. Such a rule acts to minimise the formation of mechanical bridges during feeding. Therefore, conical hopper outlet diameters required to facilitate flow were determined to be equal to 102 mm, 107 mm, 89 mm and 272 mm for the wood pellets, torrefied wood pellets, ground anthracite grains and torrefied wood chips respectively.

In addition to material tests, a prototype hopper was constructed and tested alongside each of the materials mentioned. A constraint was imposed on the outlet diameter of the hopper due to the valves proposed to be used in the HLH, and consequently only the wood pellets, torrefied pellets and the ground anthracite were found to flow freely from the hopper. The torrefied wood chips and milled wood pellets were found to form mechanical bridges over the outlet of the hopper, and the pulverised coal was found to flow intermittently in the funnel flow mode, leaving stagnant pockets of material in the hopper. Discharge rates were assessed for the wood pellets, torrefied pellets and ground anthracite, and were found to be broadly in line with values determined using the Beverloo equation when the particle diameter was substituted for the average particle length. Shape coefficients (k) of 1.77, 1.99 and 1.78 were determined as corrective values for the wood pellets, torrefied pellets and ground anthracite grains respectively, to allow an estimation of each of the material's discharge rates to be carried out.

5

EXPERIMENTAL PROGRAMME PART 1 DEVELOPMENT OF THE HYDRAULIC LOCK HOPPER

5.1 Introduction

As stated in Chapter 3, the proposed high pressure solids feed system takes the form of a new lock hopper that incorporates water during the compression stage. The purpose of using water is to reduce the energy requirement associated with conventional lock hoppers and in turn dispose of the need for a pressurised transport gas. This chapter provides an overview of the experimental setup of the HLH, the components constructed, the operating procedures and the results relating to its operation. Parameters such as the mass flow rate, energy requirement and air leakage will be assessed, in addition to the effect the new system has on the moisture content of the fuel being fed. Results relating to energy use determined experimentally will also be compared to those calculated in Chapter 3.

5.2 Experimental setup

5.2.1 Hydraulic Lock Hopper components

The experimental rig of the HLH consists of two hoppers (equal in volume) and a cylindrical collection vessel connected in series. Both hoppers are connected by an external pipe (DN15) containing a 1/2 inch ball valve but are separated primarily by a 3 inch ball valve (DN80). Both

hoppers were constructed in accordance with the dimensions specified in Chapter 4, Section 4.5.7 and therefore both have a height of 300 mm (cylindrical section height = 183 mm and conical section height = 117 mm), an inlet internal diameter of 200 mm, an outlet internal diameter of 73 mm, and a hopper half angle of 28.5 degrees. Both hoppers were milled from mild steel rounds (EN3A/070M20) to a wall thickness of approximately 15.5 mm and contain a separate hopper lid which was milled to a thickness of 16 mm and bolted with high tensile cap screws (M12) fixed to a pitch circle diameter of 212 mm. Each hopper lid contains a central circular orifice corresponding to a diameter of 95 mm in which a cylindrical central connection is seated which has a wall thickness of 11 mm and an internal diameter of 73 mm. The cylindrical section is threaded and connected to the respective ball valve further to being fusion welded to the underside of the hopper lid. A 4 mm nitrile cord O-ring seal is located inside of the pitch circle diameter at an internal diameter of approximately 186 mm to ensure a seal against air leakage.

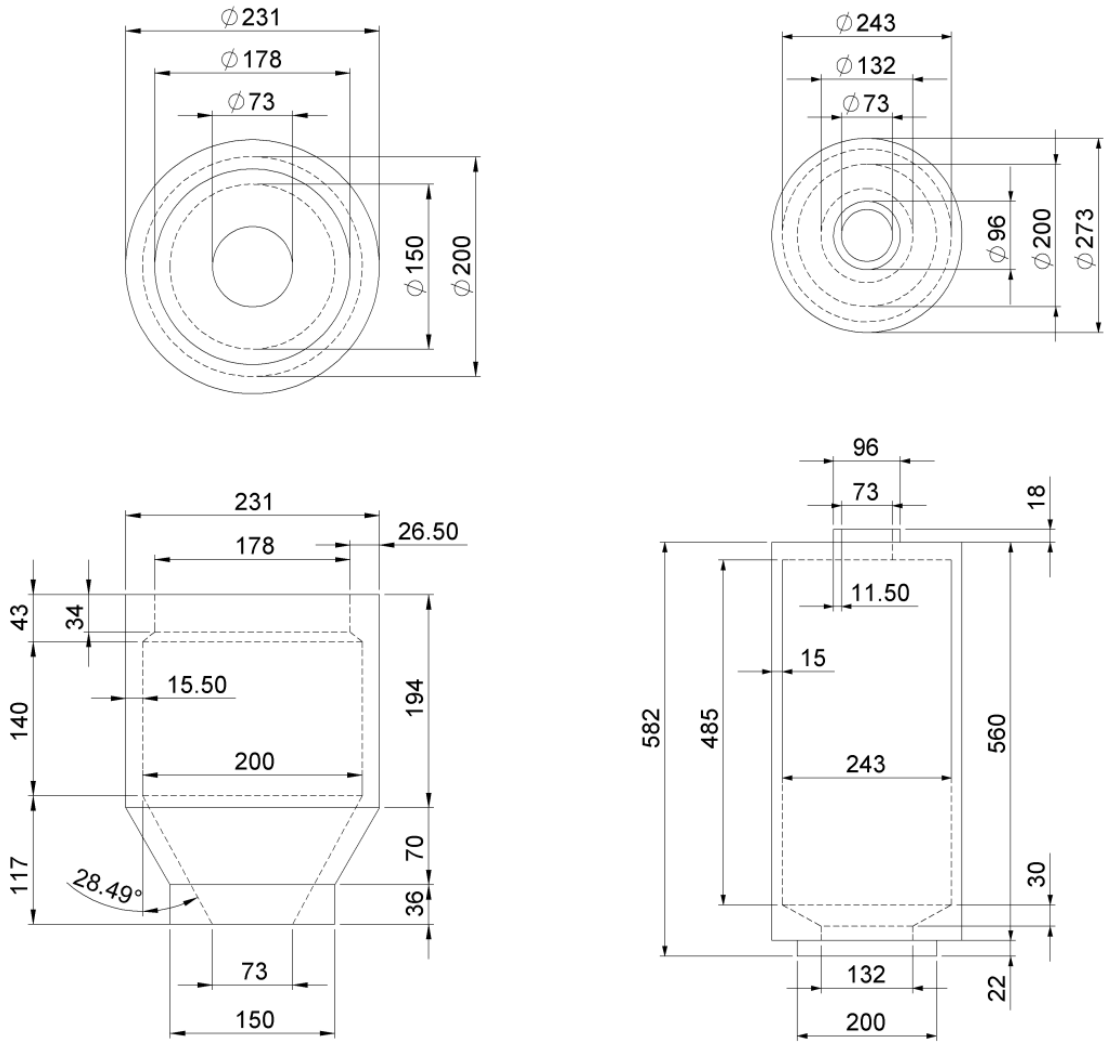

Figure 5-1: Geometry and dimensions of each of the hoppers (left) and the collection vessel (right) in mm.

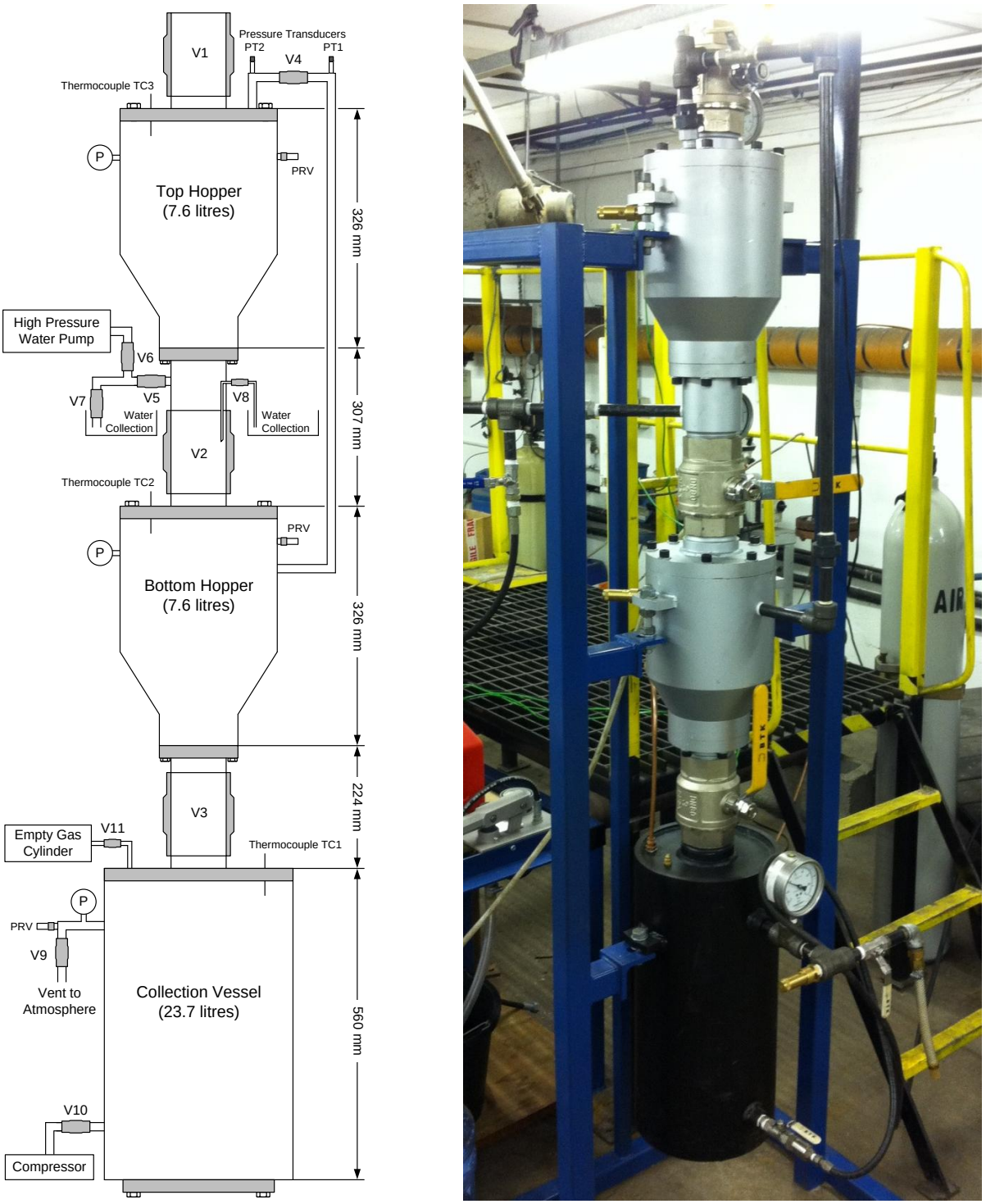

Figure 5-2: Schematic diagram of the HLH (left) and constructed experimental rig (right).

The collection vessel consists of a section of mild steel pipe (EN3A/070M20) with an internal diameter of 243 mm, a wall thickness of 15 mm and a length of 560 mm. A mild steel head is fusion welded to the top of the pipe and similarly to each of the hoppers, the collection vessel head contains a central circular orifice corresponding to a diameter of 96 mm in which a cylindrical central connection is seated which has a wall thickness of 11.5 mm and an internal diameter of 73 mm. Again, the

cylindrical section is threaded and connected to the respective ball valve further to being fusion welded to the underside of the collection vessel head. The bottom of the collection vessel contains a conical Perspex taper to allow ease of fuel unloading after the collection vessel is full. The outlet diameter of the collection vessel is 132 mm and is sealed with a mild steel face with a diameter of 200 mm and a thickness of 22 mm. Similar to each of the hopper lids, the outlet face is bolted with high tensile cap screws (M12) fixed to a pitch circle diameter of 167 mm. A 4.5 mm nitrile cord O-ring seal is also located inside of the pitch circle diameter at an internal diameter of approximately 145 mm.

The primary purpose of the collection vessel is for it to act as a high pressure destination for the fuel to be fed to. It therefore goes that as fuel is fed to the vessel the volume it presents is reduced over time. In reality the feed system will be feeding to a volume far exceeding that of the feed system itself and in order to simulate this, an empty gas cylinder is attached to the collection vessel via a shut-off valve with the sole purpose of presenting a larger volume for the fuel to be fed to. A schematic and picture of the constructed HLH is shown in Figure 5-2. One thermocouple is located in the lid of each hopper and the lid of the collection vessel (three total) and two pressure transducers are located in the external pipe connecting the two hoppers, separated by a 1/2 inch ball valve. All thermocouples and pressure transducers are connected to a data logger for data acquisition.

5.2.2 Compressor and high pressure water pump

A Niedermeier three stage compressor (VZER 90c-2) rated at 1.5 kW (3400 psi) was selected to pressurise the collection vessel (complete with empty gas cylinder) and the bottom hopper prior to fuel feeding, and a Rothenberger water pump (RP PRO III) rated at 1.3 kW, with a maximum operating pressure and flow rate of 40 bar and 6 litres/min respectively was used in the compression stage of the feeding process. The compressor was connected to the collection vessel via a high pressure hose (DN10) containing a 1/2 inch ball valve, and the water pump was primarily connected to a T-junction located prior to the base of the top hopper via a high pressure hose (DN8) also containing a 1/2 inch ball valve. The T-junction is constructed from pipe size DN15 and contains a further two 1/2 inch ball valves for water *in*/*out* and for isolation. The isolation valve poses as the primary boundary for the top hopper preventing either water *in* or *out*.

Further to this is a siphon which is comprised of a pipe (6.6 mm) containing a 1/4 inch ball valve (DN8). The siphon is designed to minimise the residual water left in the top hopper after the compression stage and is attached to the base of the top hopper and fitted flush with the 3 inch ball valve connecting the top hopper with the bottom hopper. Further to the compressor air *in* line is a separate air *out* line/vent to atmosphere also formed from a pipe (DN15) containing a 1/2 inch ball valve.

Figure 5-3: Niedermeier three stage compressor (left) and Rothenberger RP PRO III water pump (right).

5.2.3 Vacuum pump and collection vessel

A vacuum pump and collection vessel was also employed to ensure the top hopper was fully emptied before the start of each cycle. An Edwards 8 (E2M8) rotary vane two stage vacuum pump rated at 0.5 hp (0.37 kW) was selected with an operating pressure and flow rate of 0.001 mbar and 170 litres/min respectively. The pump was connected to a collection vessel which in turn was connected to a 10 mm diameter Perspex pipe, approximately 1 m in length. The pipe was used to clean the 3 inch ball valve of any residual fuel remaining in the top hopper to minimise valve failure and to ensure accuracy of results regarding moisture uptake.

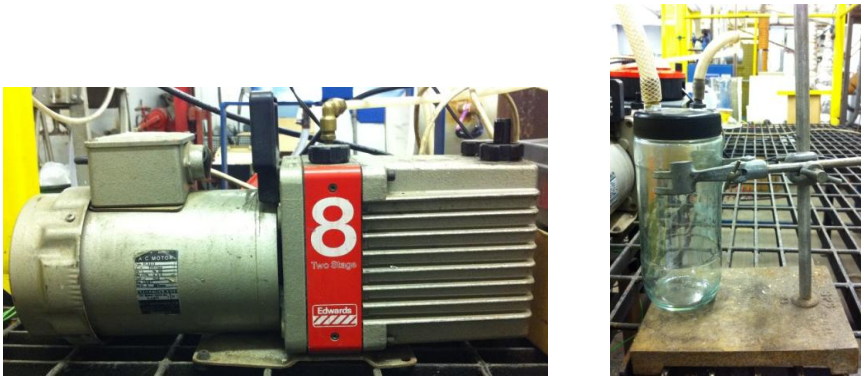

Figure 5-4: Edwards rotary vane two stage vacuum pump (left) and solids collection vessel (right).

5.2.4 Data acquisition

Two Omega PXM410 pressure transducers were used to measure the pressure in each of the hoppers used to make up the HLH. Both transducers were set to read pressures between 0 barg and 30 barg with a supply and output voltage of 13-30 Vdc and 0-5 Vdc respectively. As the pressure transducers used are moisture sensitive, both transducers were located in the external pipe separating the top hopper from the bottom hopper to minimise contamination with water. One transducer was situated either side of the 1/2 inch valve located in the external pipe.

Three K-type, nickel-chromium/nickel-aluminium thermocouples were used to measure the air temperature in the HLH and were positioned in the lid of each of the vessels. Thermocouples were located off-centre and approximately 50 mm into each of the vessels in order to minimise interference with fuel during feeding. All thermocouples and pressure transducers were connected to a Graphtec GL800 midi data logger set to continuously take readings at 1 second intervals.

In addition to temperature and pressure measurements, an Electrocorder AL-2VA single phase voltage and current data logger was used in conjunction with a Prodigit Electronics Co. Ltd. 2000MU logger to assess the energy requirement of the HLH. The Electrocorder AL-2VA facilitates the measurement of the root mean square (RMS) voltage and current at 1 second intervals, and the Prodigit Electronics Co. Ltd. 2000MU logger allows the power factor of a single phase appliance to be continuously assessed through a real time display.

5.2.5 Ancillary equipment

Ashcroft T5500 pressure gauges rated at 0-70 barg as well as Goetze GOE-810 pressure relief valves set to relieve at 30 barg were added to each of the primary vessels. The feed system was designed to withstand a pressure of up to 30 bar using the equations detailed in Chapter 3, Section 3.6.2 and was manufactured in excess of this specification. A maximum operating pressure was set at 25 barg and therefore the pressure relief valves were fitted as a failsafe. Water was stored at atmospheric pressure in a 15 litre container located above the high pressure water pump and was pumped to the top hopper during operation. Water was drained from the hopper to a separate 15 litre water container situated on a Mettler mass balance to allow the measurement of water used during operation, and fuel was weighed using a Precisa junior 5000D mass balance before and after feeding to assess any water taken up by the fuel.

5.3 Measurement accuracy and associated errors

5.3.1 Pressure measurement

The transducers selected allow pressure to be continuously measured between 0-30 barg linearly to an output voltage varying between 0-5 Vdc. The transducers have a non-linearity/hysteresis of less than ±0.25% full scale output (FSO), repeatability of less than ±0.1% FSO, long term stability of less than ±0.2% FSO/6 months and a maximum overpressure of approximately 200%.

As the pressure transducers are moisture sensitive, they were not directly calibrated using a dead weight tested due to the use of hydraulic oil (OW-20). However, the Ashcroft pressure gauges used (rated at 0-70 barg) were directly calibrated using a Budenberg dead weight tester at pressures of 100

psi, 200 psi and 300 psi (9.89 bar, 13.79 bar and 20.68 bar). In turn, the Ashcroft gauges were used to calibrate the pressure transducers supplied by Omega Engineering Ltd. Results from the dead weight testing proved both pressure transducers to be in accordance with the supplied literature, whereas two of the three Ashcroft pressure gauges were shown to read approximately 0-5 psi less than the required pressure and the third shown to read approximately 20 psi less than the required pressure. All three pressure gauges inaccuracies were noted and factored into any readings taken manually.

5.3.2 Temperature measurement

The K-type thermocouples used conform to tolerance class 2 specified by the IEC 584-2 (International Electrotechnical Commission: Thermocouple reference table) and thus temperature can be continuously measured between -40 °C and 1200 °C with an accuracy of ±2.5 °C or ±0.0075.T, where T is the actual temperature (°C) (Labfacility, 2012).

Energy transfer between the thermocouple bead and the medium can take place either by conduction, convection and/or radiation. The majority of errors associated with thermocouples are caused due to the temperature of the thermocouple bead not being at the same temperature of the medium being measured. When measuring air temperatures that are quickly fluctuating and changing, temperature lag will occur; that is, the temperature measurement will differ from the actual air temperature. Lag is due in large part to the time taken for energy to be transferred to the centre of the thermocouple bead from the surroundings when being heated, and similarly, the time taken for energy to be transferred from the centre of the thermocouple bead to the surroundings when being cooled. This phenomenon isn't directly observed as a step change as temperature measurements are smoothed as a result of this lag. One way in which to reduce the error due to temperature lag is by selecting a thermocouple with a lower mass (Shannon and Butler, 2003). The thermocouples selected in this instance have an external diameter of 1.5 mm and a length of 150 mm. This choice was made as a compromise as sufficient robustness is required during fuel feeding.

5.3.3 Energy measurement

Single phase energy monitors were selected to be the most accurate way in which to measure the energy consumption and power drawn from mains appliances. Current clamps were investigated; however, in order to assess energy requirement, a constant voltage has to be assumed. This method presents additional inaccuracies to those presented by the current clamp itself, as mains voltage can vary up to ±10% (Swithenbank, 2012). The energy monitor selected is able to measure both voltage and current, and allows voltage measurements with an accuracy of ±1% of the reading, and current measurements with an accuracy of ±5% of the reading.

5.3.4 Mass and water measurement

The mass of the fuel being fed was weighed before and after feeding in order to gauge moisture uptake. Mass was measured using a calibrated Precisa mass balance measuring accurately to the nearest 0.1 g. Similarly, water *out* was measured using a calibrated Mettler mass balance measuring accurately to the nearest 1 g to assess and compare the volume of water required for compression to take place per batch of fuel fed. A nickel-chromium/nickel-aluminium K-type thermocouple attached to a digital display accurate to the nearest 1 °C was used to assess the water temperature and in turn the density and volume of the water used per batch of fuel fed.

5.4 Operating procedures

5.4.1 Mode 1: Start-up and operating procedure

1. Ensure all valves are closed and all vessels are sealed.
2. Open V3 connecting the collection vessel to the bottom hopper and V11 connecting the collection vessel to the empty gas cylinder.
3. Turn the compressor on and open V10 to pressurise the collection vessel, bottom hopper and the gas cylinder to system pressure.
4. Turn the compressor off and close V10.
5. Close V3 connecting the collection vessel to the bottom hopper.
6. Open V1 to allow the feeding of a batch of fuel to the top hopper.
7. Close V1 once the batch of fuel has been fed.
8. Open V2 connecting the top hopper to the bottom hopper to allow pressure equalisation between the two hoppers and the feeding of fuel to the bottom hopper.
9. Close V2 once the fuel has been fed.
10. Open V4 located in the external pipe connecting the top hopper to the bottom hopper.
11. Open V6 and turn the water pump on to allow water pressure to build up in the connecting pipe.
12. Once the water pressure has been established and is equal to or exceeds the pressure in the top hopper, open V5 to allow water to be pumped into the top hopper.
13. Close V5 and turn the water pump off once the pressure in the top hopper and the bottom hopper has been restored to system pressure.
14. Close V6 to isolate the water pump.
15. Close V4 to isolate the top hopper from the bottom hopper.
16. Open V3 connecting the collection vessel to the bottom hopper to allow the fuel to be fed to the collection vessel.
17. Close V3 connecting the collection vessel to the bottom hopper.
18. Open V5 and V7 to allow the water contained in the top hopper to be drained to the water collection container.

19. Close V5 and V7 and open V8 in the siphon pipe to allow any remaining water contained in the top hopper to be drained.
20. Close V8.
21. The process starts anew from **step 6.**

5.4.2 Mode 1: Shut-down procedure

1. Ensure the water pump and the compressor are both turned off and unplugged.
2. Vent any high pressure gas to the atmosphere by opening V3, V4, V9 and V11.
3. Drain any water from the top hopper by opening V5, V7 and V8.
4. Open all remaining valves.

5.4.3 Mode 2: Start-up and operating procedure

In this mode of operation the bottom hopper acts to increase the volume presented by the collection vessel and the empty gas cylinder. The operating procedure will refer to this volume as the bottom hopper/collection vessel as there is no separation between the two chambers.

1. Ensure all valves are closed and all vessels are sealed.
2. Open V3 connecting the collection vessel to the bottom hopper and V11 connecting the collection vessel to the empty gas cylinder.
3. Turn the compressor on and open V10 to pressurise the bottom hopper/collection vessel and the gas cylinder to system pressure.
4. Turn the compressor off and close V10.
5. Open V1 to allow the feeding of a batch of fuel to the top hopper.
6. Close V1 once the batch of fuel has been fed.
7. Open V2 connecting the top hopper to the bottom hopper/collection vessel to allow pressure equalisation between the two vessels and the feeding of fuel to the bottom hopper/collection vessel.
8. Close V2 once the fuel has been fed.
9. Open V4 located in the external pipe connecting the top hopper to the bottom hopper/collection vessel.
10. Open V6 and turn the water pump on to allow water pressure to build up in the connecting pipe.
11. Once the water pressure has been established and is equal to or exceeds the pressure in the top hopper, open V5 to allow water to be pumped into the top hopper.
12. Close V5 and turn the water pump off once the top hopper has been filled to capacity with water. A slight net increase in system pressure should be observed after this step.
13. Close V6 to isolate the water pump.
14. Close V4 to isolate the top hopper from the bottom hopper/collection vessel.
15. Open V5 and V7 to allow the water contained in the top hopper to be drained to the water collection container.

16. Close V5 and V7 and open V8 in the siphon pipe to allow any remaining water contained in the top hopper to be drained.
17. Close V8.
18. The process starts anew from **step 5.**

5.4.4 Mode 2: Shut-down procedure

1. Ensure the water pump and the compressor are both turned off and unplugged.
2. Vent any high pressure gas to the atmosphere by opening V4, V9 and V11.
3. Drain any water from the top hopper by opening V5, V7 and V8.
4. Open all remaining valves.

5.4.5 Mode 3: Start-up and operating procedure

In this mode of operation the compression stage takes place in two stages. It bares similarities to Mode 2, as it minimises the volume of gas at pressure vented to the atmosphere. However, it aims to be more efficient by breaking the compression stage up into two stages. Steps 1-13 are identical to those found in **Mode 1**.

1. Ensure all valves are closed and all vessels are sealed.
2. Open V3 connecting the collection vessel to the bottom hopper and V11 connecting the collection vessel to the empty gas cylinder.
3. Turn the compressor on and open V10 to pressurise the collection vessel, bottom hopper and the gas cylinder to system pressure.
4. Turn the compressor off and close V10.
5. Close V3 connecting the collection vessel to the bottom hopper.
6. Open V1 to allow the feeding of a batch of fuel to the top hopper.
7. Close V1 once the batch of fuel has been fed.
8. Open V2 connecting the top hopper to the bottom hopper to allow pressure equalisation between the two hoppers and the feeding of fuel to the bottom hopper.
9. Close V2 once the fuel has been fed.
10. Open V4 located in the external pipe connecting the top hopper to the bottom hopper.
11. Open V6 and turn the water pump on to allow water pressure to build up in the connecting pipe.
12. Once the water pressure has been established and is equal to or exceeds the pressure in the top hopper, open V5 to allow water to be pumped into the top hopper.
13. Close V5 and turn the water pump off once the pressure in the top hopper and the bottom hopper has been restored to system pressure.
14. Open V3 connecting the collection vessel to the bottom hopper to allow the fuel to be fed to the collection vessel.
15. Turn the water pump on for a second time to allow water pressure to build up in the connecting pipe.

16. Once the water pressure has been established and is equal to or exceeds the pressure in the top hopper, open V5 to allow water to be pumped into the top hopper.
17. Close V5 and turn the water pump off once the top hopper has been filled to capacity with water. A slight net increase in system pressure should be observed after this step.
18. Close V6 to isolate the water pump.
19. Close V4 to isolate the top hopper from the bottom hopper.
20. Close V3 connecting the collection vessel to the bottom hopper.
21. Open V5 and V7 to allow the water contained in the top hopper to be drained to the water collection container.
22. Close V5 and V7 and open V8 in the siphon pipe to allow any remaining water contained in the top hopper to be drained.
23. Close V8.
24. The process starts anew from **step 6.**

5.4.6 Mode 3: Shut-down procedure

1. Ensure the water pump and the compressor are both turned off and unplugged.
2. Vent any high pressure gas to the atmosphere by opening V3, V4, V9 and V11.
3. Drain any water from the top hopper by opening V5, V7 and V8.
4. Open all remaining valves.

5.5 Experimental results and discussion: HLH characterisation

Although it was shown in Chapter 4 that three of the six fuels assessed are compatible with the HLH (wood pellets, torrefied pellets and ground anthracite grains), the HLH was initially characterised using wood pellets **only**. Wood pellets were selected in this case as they present the least stable of the three fuels and are best suited to assessing moisture uptake levels brought about during operation. Wood pellets were used as the feedstock for the results presented in this section unless otherwise stated.

Before the results from the HLH are analysed in more detail, it is important to state why results relating to Mode 3 are absent from this section. Prior to characterising the HLH, preliminary tests were carried out in all modes of operation to assess the basic energy requirement of the HLH. Tests highlighted Mode 3 to be the most energy intensive mode of operation, followed by Mode 2 and then Mode 1 (Figure 5-5). Mode 3 was originally developed to increase the efficiency of Mode 2 by splitting the compression stage into two stages, and was calculated in Chapter 3 to have a lower energy requirement. However, preliminary tests revealed the energy requirement of Mode 3 to exceed that of Mode 2.

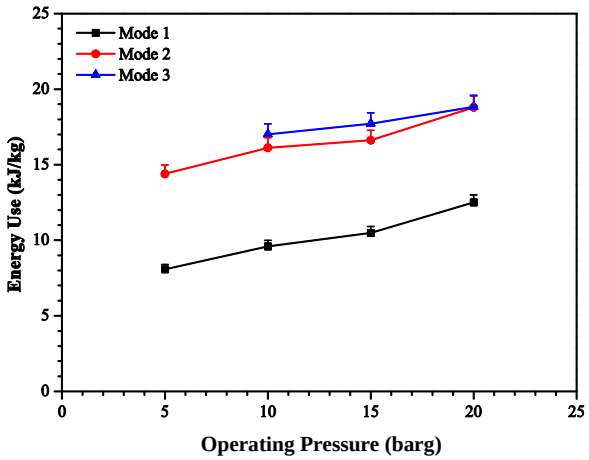

Figure 5-5: Preliminary results regarding the energy requirement of the HLH.

The increase in energy required by Mode 3 can be accounted for by examining the operating procedure of the HLH and the high pressure water pump used in the compression stage. The compression stage of Mode 3 is carried out in two stages, whereas the compression stage of Mode 2 (and Mode 1) is carried out in a single stage. The pump used is required to be primed and started from atmospheric pressure with the delivery valve fully open, and only once the pump has been engaged can the delivery valve be closed and in turn the desired pressure brought up. Due to the two stage compression of Mode 3, the priming of the pump has to be carried out twice. As energy is consumed during the pump priming stage, this increases the amount of electrical energy used per cycle and in turn accounts for the increase in energy recorded by Mode 3 over Mode 2. Both Mode 1 and Mode 2 only require the priming stage once per cycle and in turn the relative electrical energy wasted during this stage is minimised. Operation in Mode 3 was retired after the preliminary tests were completed as a consequence of this finding.

The results presented in the following sections therefore aim to provide an overview of the main parameters associated with the HLH operating in both Mode 1 and Mode 2. Temperature and pressure variations in each of the primary vessels are discussed, the mass flow rate of the system is assessed, and the energy requirement is analysed in detail. In addition to this, the effect the HLH has on the moisture content of the fuel being fed is assessed, as well as the reliability of the system.

5.5.1 Cycle analysis and operation

Like a conventional lock hopper, the HLH is a batch feed system and therefore the geometry of the system governs the mass flow rate and how the system is operated. A maximum of three batches of fuel can be fed across the pressure boundary during one *complete* cycle (defined as system pressurisation, fuel feeding, system depressurisation) using the HLH, and therefore results relating to

cycle operation are presented as such. The reason for a three batch *complete* cycle is related to the geometry of the feed system and is as follows.

The total volume of the collection vessel to which fuel can be fed to is calculated to be approximately 23.5 litres. Using wood pellets as an example with an average bulk density of 651 kg/m^3, this presents a maximum capacity of 15.3 kg. The hopper volume determines the mass of each batch of fuel fed and in turn the number of batches that can be fed to the collection vessel. Based on a hopper volume of approximately 7.6 litres, the maximum mass of wood pellets per hopper/batch is determined to be approximately 4.9 kg. This means that a maximum of three batches of wood pellets can be fed across the pressure boundary before the collection vessel has to be emptied and the *complete* cycle to be started anew. The following sections provide an overview of the temperature and pressure variations encountered in each vessel during a *complete* cycle while operating the HLH in Mode 1 and Mode 2. For Figure 5-6 and Figure 5-7, TC1, TC2 and TC3 refer to the temperature in the collection vessel, bottom hopper and top hopper respectively (°C), and PT1 and PT2 refer to the pressure in the bottom hopper and top hopper respectively (barg).

5.5.1.1 Mode 1 cycle analysis

Figure 5-6 shows the thermocouple TC1 located in the collection vessel to record a constant temperature around 16 °C throughout operation. This temperature correlates well with that of the ambient temperature and a constant reading indicates a constant pressure throughout the operation of the HLH. A temperature rise recorded by TC3 is observed with a pressure rise at PT2 in the top hopper due to the immediate compression taking place on opening V2 connecting the top hopper to the bottom hopper. Similarly, a temperature decrease at TC2 is observed with a pressure decrease at PT1 in the bottom hopper due to the respective expansion taking place. In the time taken for the water pump to be primed and started, both a temperature decrease is recorded by TC3 and an increase by TC2 in the top and bottom hopper respectively. Both PT1 and PT2 record an equal pressure at this stage and a slight increase in pressure is observed immediately prior to water being pumped to the top hopper. As water is pumped to the top hopper, compression of both the top hopper and bottom hopper takes place which is signified by both an increase in pressure recorded by PT1 and PT2, and by an increase in temperature recorded by TC2 and TC3. The temperature of the top hopper recorded by TC3 is seen to be noticeably higher than that of the bottom hopper recorded by TC2 in all cases. This is due to thermal losses from the non-insulated pipe work separating the two thermocouples and the respective positions of both of the thermocouples (50 mm into the lid of each hopper). After the compression stage has taken place, TC2 records a temperature decrease approaching that of ambient temperature found in the collection vessel, and TC3 records a large temperature decrease due to the expansion of the gas contained within the top hopper back to atmospheric pressure. Immediately

following the completion of the expansion stage, TC3 records a temperature rise back up to that of ambient temperature, approximately equal to that recorded by TC1 and TC2.

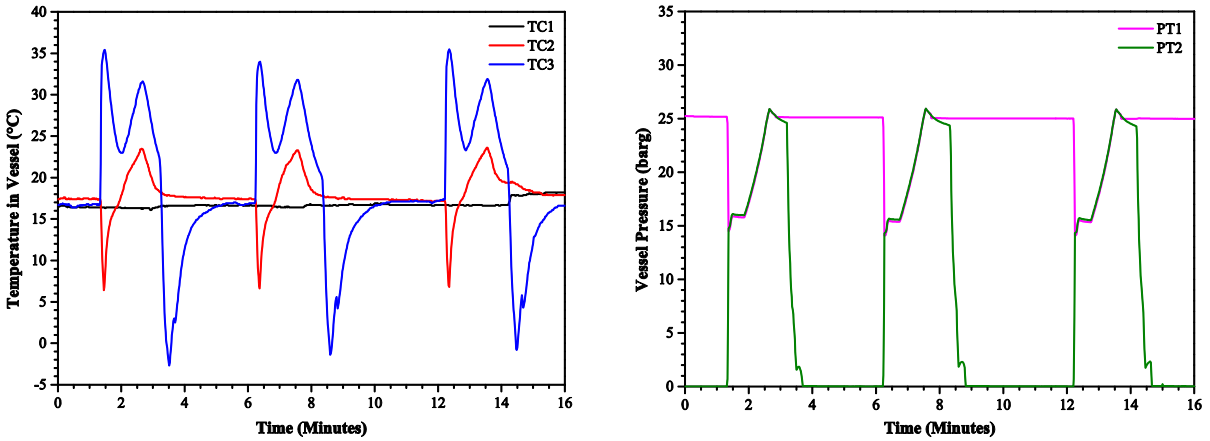

Figure 5-6: A typical *complete* cycle of the HLH operating in Mode 1 at a system pressure of 25 barg.

The temperature changes observed in both the top hopper and the bottom hopper are due to the compression and expansion of gas. The expansion and compression in this instance represents a polytropic process approximating an overall isothermal process as a temperature change is observed with little net change in the overall temperature. The respective temperature increases and decreases are only observed for relatively short periods of time, typically around 30-40 seconds which therefore technically constitutes the process to be polytropic as it neither wholly fulfils conditions for an isothermal or adiabatic process. However, as temperature changes are observed for relatively short periods of time, the system can be approximated to an overall isothermal process. Significant temperature changes are only observed due to the immediate compression and expansion of gas present in each of the vessels. Further to this, thermal losses take place due to the materials used for construction which are insufficiently insulated and so do not maintain any temperature increases or decreases brought about by respective compressions or expansions.

5.5.1.2 Mode 2 cycle analysis

One of the main differences between Mode 1 and Mode 2 is that temperature variations are observed in all vessels. Mode 1 showcases a constant temperature (and pressure) in the collection vessel throughout operation, whereas Mode 2 highlights both a temperature decrease and increase in the collection vessel at the start of each cycle and during the compression stage respectively. The length of time required for the compression stage to take place is also observed to be different and greater in Mode 2 than when running in Mode 1 due to the larger volume of water required to be pumped. Mode 1 requires approximately half the volume of the hopper to be filled with water for compression to take

place, whereas Mode 2 minimises any waste of process gas at pressure and thus requires a volume of water approximately equal to that of the hopper volume. The compression stage is highlighted in Figure 5-7 by the increase in pressure recorded by PT1 in the bottom hopper/collection vessel and PT2 in the top hopper.

Figure 5-7 displays a step increase in system pressure recorded by PT1 after each cycle has been completed, with the total system pressure increasing by approximately 0.6 bar after each cycle. This is characteristic of Mode 2 as a minimum amount of process pressure is wasted by filling the top hopper to capacity with water. This characteristic was found to be most pronounced where higher operating pressures prevailed and is observed due to the volume taken up by the fuel contained in the collection vessel. This step increase in system pressure is contrary to Mode 1 where a stable pressure reading is maintained after each cycle has been completed.

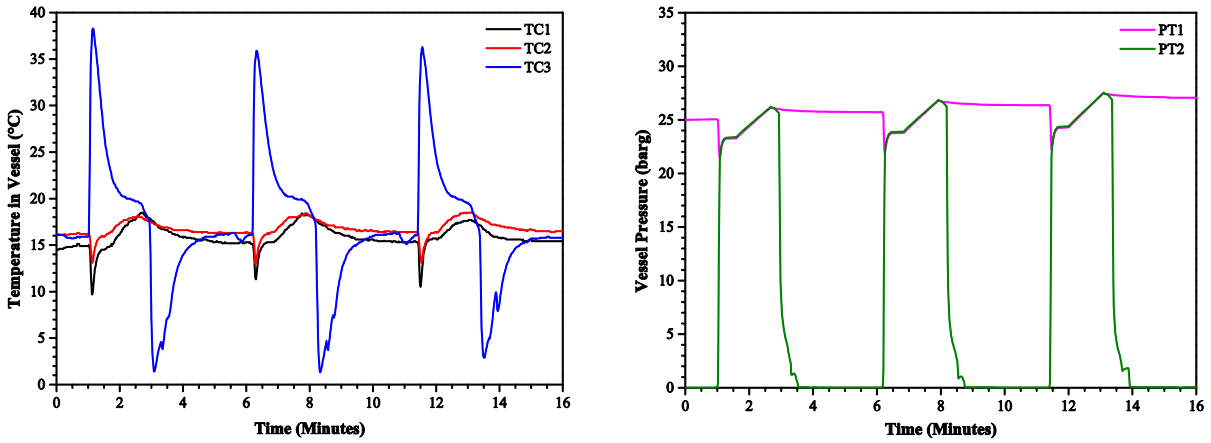

Figure 5-7: A typical *complete* cycle of the HLH operating in Mode 2 at a system pressure of 25 barg.

As with Mode 1, notable temperature fluctuations primarily take place in the top hopper. A large temperature increase is recorded by TC3 during the pressure equalisation stage, and a large temperature decrease is recorded during the water drainage stage due to the expansion of the small portion of gas contained in the head space above the water level. A double temperature peak is not observed while operating in Mode 2 as it is in Mode 1, as the pressure increase associated with the compression stage takes place throughout the system as a whole and is not confined to the top and bottom hopper as it is in Mode 1. The net change in pressure brought about during the pressure equalisation stage is also observed to be far smaller than that encountered in Mode 1 for the same reason. Further to this, a small temperature drop is observed towards the end of the compression stage in the top hopper and is contrary to the slight rise in temperature recorded by TC1 and TC2 in the collection vessel and bottom hopper respectively. This is due to the water in the top hopper (typically at a temperature between 13-15 °C), cooling the compressed gas and countering the temperature increase associated with gas compression.

5.5.2 Mass flow rate and cycle time

In the context of high pressure solids feed systems, the mass flow rate is defined as the mass of material passing across the pressure boundary per unit time. As previously stated in Section 4.5.7, the system geometry largely governs the mass flow rate of the HLH due to the system taking the form of a batch feeder. In order for the HLH to maximise its mass flow rate, a maximum mass of fuel per batch must be assessed. This was previously determined to be equal to 4.9 kg; however, it is important to state that 4.9 kg per batch is considered to be the maximum mass per batch and is only sought where theoretical maximum flow rates are required. In reality there are operational problems linked to operating at maximum capacity, such as solids holdup and valve jamming which plague conventional lock hoppers (Schell, 1988). In order to minimise or avoid such problems, the mass per batch is set at below this theoretical maximum in order to allow for a sufficient head space to be present above the fuel. This seeks to minimise problems with solids interacting with the principal valves separating each vessel and allows for the non-uniform accumulation of solids in the hopper once fed (typically slightly domed towards the centre of the solids deposited).

Analysing the mass flow rate of wood pellets fed across the pressure boundary on the basis of the results shown in Figure 5-6 and Figure 5-7 suggests a mass flow rate far lower than that found in reality (of the order of 16 minutes per three batches). Taking the average mass of a batch as 4 kg generates a mass flow rate of approximately 12.5 g/s (1.08 tonnes/day). However, this examines the data in its raw form and is in turn comprised of errors relating to human activity. Errors relating to the time taken to manually prepare each batch of fuel, the time taken for manual valve operation and the time taken to assess the level of safety of the process at each stage of the feeding operation are present in the data when assessed in this form. In order to gain a more reliable and accurate insight into the mass flow rate, individual batch cycle times were analysed. Although this does not account for all elements relating to human activity, it eliminates the time taken between each batch of fuel fed. Table 5-1 highlights the average time taken to feed individual batches of wood pellets while operating in Mode 1 and Mode 2.

	Mass per Cycle (g)		**Cycle Time (s)**	
Pressure (barg)	**Mode 1**	**Mode 2**	**Mode 1**	**Mode 2**
10	4000.4 ± 0.2	4000.3 ± 0.2	138 ± 6	144 ± 4
15	4000.4 ± 0.3	4000.5 ± 0.2	145 ± 9	145 ± 9
20	4000.4 ± 0.3	4000.4 ± 0.2	151 ± 15	152 ± 2
25	4000.4 ± 0.3	4000.4 ± 0.2	154 ± 8	154 ± 4

Table 5-1: Average mass per batch and cycle time for feeding wood pellets in Mode 1 and Mode 2.

Both modes of operation show a general trend of increasing cycle time with increasing pressure and are shown to be broadly similar at each operating pressure. Analysing the time taken for compression

shown in Table 5-2 it can be deduced that any time saved by Mode 1 due to it only requiring a portion of the hopper to be filled with water compared to Mode 2 is lost due to a more complicated operational procedure. Table 5-2 indicates an average difference in compression time between Mode 1 and Mode 2 of approximately 17 seconds. When this is combined with the results for cycle time shown in Table 5-1, the time taken for further manual valve operations encountered in Mode 1 can be equated to this.

	Volume of Water (ml)		**Compression Time (s)**	
Pressure (barg)	**Mode 1**	**Mode 2**	**Mode 1**	**Mode 2**
10	5577 ± 112	7512 ± 16	55 ± 2	69 ± 1
15	5589 ± 45	7503 ± 25	55 ± 2	71 ± 1
20	5523 ± 92	7574 ± 20	54 ± 2	72 ± 1
25	5536 ± 58	7534 ± 43	56 ± 2	74 ± 1

Table 5-2: Volume of water required for compression and the associated time operating in Mode 1 and Mode 2.

A general trend of increasing compression time with increasing operating pressure is observed for Mode 2 and is shown in Table 5-2. Comparatively, Table 5-2 also shows that no appreciable difference in compression time is observed with varying operating pressure for Mode 1 and thus compression time is shown to be broadly constant taking into account the stated error. Although compression time is seen to increase with pressure for Mode 2, results are still seen to be fairly constant as compression time is shown to take on average between 69-74 seconds for operating pressures between 10 barg and 25 barg. Such a marginal increase in compression time with operating pressure indicates that the pump works almost independently of pressure. Further to this, it can be seen from Table 5-2 that the volume of water required in each mode of operation is approximately equal at all operating pressures, with a difference of 1975 ml on average between Mode 1 and Mode 2. Combined with the results for compression time in both modes of operation, these results suggest that compression time is not greatly affected by large increases in pressure. Increases in compression time of 2 seconds and 5 seconds for Mode 1 and Mode 2 are recorded respectively for increases in pressure of 15 bar in both cases. A larger time difference between 10 and 25 barg in Mode 2 (5 seconds) compared to Mode 1 (2 seconds) is due to the larger volume of water required during the compression stage and in turn the pump working for a longer period of time.

When the results for compression time and cycle time are combined, and it is assumed that all manual valve operations take place uniformly and at a constant rate, it can be said that any increase in cycle time with pressure, further to that brought about by compression time is due to the length of time taken for the water draining stage. However, this contradicts what would otherwise be predicted, as a reduced drainage time would be anticipated where higher operating pressures are encountered. Analysing temperature and pressure readings taken with time during each mode of operation shows this not to be the case and is highlighted in both Table 5-3 and Table 5-4.

Mode 1				
Pressure (barg)	**Gravity Feeding (s)**	**Water Compression (s)**	**Water Drainage (s)**	**Valve Activity (s)**
10	18 ± 2	55 ± 2	29 ± 1	36 ± 7
15	18 ± 2	55 ± 2	30 ± 3	42 ± 10
20	18 ± 2	54 ± 2	30 ± 1	49 ± 15
25	18 ± 2	56 ± 2	30 ± 1	50 ± 9

Table 5-3: Overall cycle analysis for operation in Mode 1.

Mode 2				
Pressure (barg)	**Gravity Feeding (s)**	**Water Compression (s)**	**Water Drainage (s)**	**Valve Activity (s)**
10	12 ± 1	69 ± 1	33 ± 2	30 ± 5
15	12 ± 1	71 ± 1	32 ± 2	30 ± 9
20	12 ± 1	72 ± 1	34 ± 2	34 ± 3
25	12 ± 1	74 ± 1	33 ± 1	35 ± 4

Table 5-4: Overall cycle analysis for operation in Mode 2.

There is no appreciable difference in the time taken to drain the top hopper of water as operating pressure is varied when the error of the stated values in either Table 5-3 or Table 5-4 are taken into account. Therefore, it can be said that any increase in cycle time after taking into account the increase in compression time with increasing operating pressure is due to manual valve operations and human activity. Combining the results for the cycle time and the average mass per batch of fuel fed generates Figure 5-8 which displays a slight trend of decreasing mass flow rate with increasing operating pressure for both modes of operation (when results are used which are inclusive of manual valve operation). Mass flow rates as high as 25 g/s have been demonstrated when feeding to gauge pressures as high as 25 bar in both Mode 1 and Mode 2.

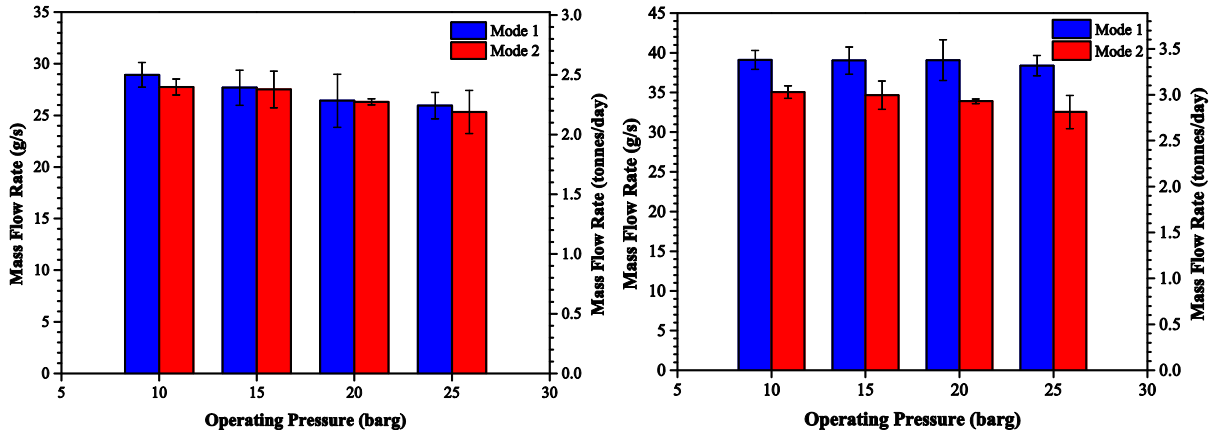

Figure 5-8: Effect of operating pressure on mass flow rate for operation in Mode 1 and Mode 2. Mass flow rate inclusive of manual valve operation (left) and exclusive of manual valve operation (right).

Interestingly, reviewing the results shown in Figure 5-8 which are exclusive of manual valve operation indicates the mass flow rate of the HLH when operating in both Mode 1 and Mode 2 to be independent of operating pressure. This can be explained by the results shown in Table 5-3 and Table 5-4 which show that the time taken for water compression, water drainage and gravity feeding are relatively constant regardless of operating pressure.

5.5.3 Energy requirement of the Hydraulic Lock Hopper

The energy required to operate the HLH was examined using an Electrocorder single phase voltage and current logger. The power drawn by the high pressure water pump was assessed from the voltage, current and power factor readings taken, and the energy requirement of the HLH was assessed by combining such readings with the readings taken for cycle and compression time. Table 5-5 highlights how the power drawn by the high pressure water pump varies with operating pressure, and Figure 5-9 highlights how the power drawn changes during the compression stage.

	Power (W)	
Pressure (barg)	**Mode 1**	**Mode 2**
10	927 ± 31	974 ± 19
15	998 ± 57	1012 ± 21
20	1091 ± 33	1061 ± 21
25	1104 ± 24	1123 ± 19

Table 5-5: Effect of operating pressure on the power drawn by the high pressure water pump.

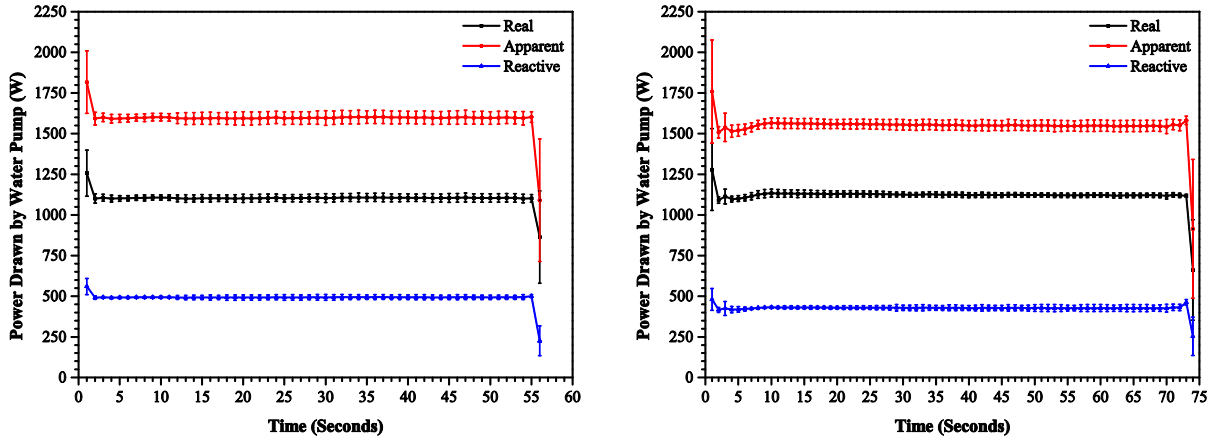

Figure 5-9: Apparent, reactive and real power drawn by the high pressure water pump operating at 25 barg in Mode 1 (left) and Mode 2 (right).

Figure 5-9 highlights the power drawn by the high pressure water pump to be maintained broadly constant during the compression stage, and Table 5-5 shows a clear trend of increasing power drawn with increasing operating pressure for both modes of operation. Comparing the results shown in Table

5-5 and Figure 5-9 regarding the power drawn by the high pressure water pump to those determined theoretically in Chapter 3 indicates a pump efficiency of approximately 17.5%. Combining the results shown in Table 5-5 with those shown in Table 5-2 generates Figure 5-10 which highlights how the energy requirement of the HLH varies with operating pressure.

As with the preliminary results shown in Figure 5-5 regarding the energy requirement of the HLH, a general trend of increasing energy use with increasing operating pressure is seen for both modes of operation. Mode 1 is shown to have a lower energy requirement than Mode 2 at all operating pressures and the results shown in Figure 5-10 are found to be broadly in line with those shown in Figure 5-5 for the preliminary tests. The primary reason why the results shown in Figure 5-10 slightly differ to those shown in Figure 5-5 is because of a change in the average mass per batch of fuel used. In the preliminary tests, the mass of each batch of fuel was varied between 4.2 kg and 4.3 kg; whereas, in all of the tests carried out subsequently, the mass per batch of fuel was maintained constant at 4 kg. As the results shown regarding energy use are expressed in terms of specific energy, the mass per batch directly affects the value determined.

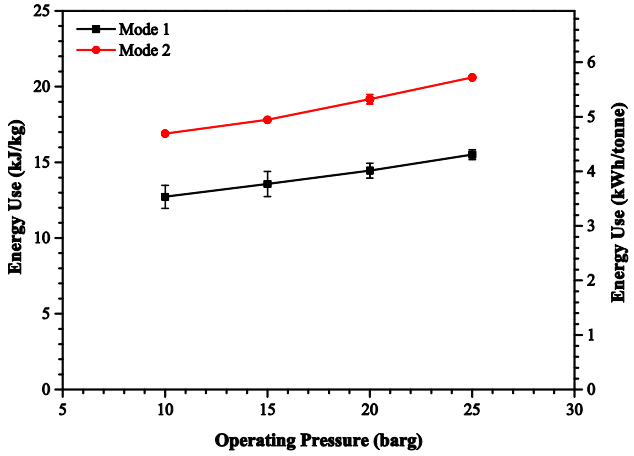

Figure 5-10: Effect of operating pressure on the energy requirement of the HLH operating Mode 1 and Mode 2.

In Chapter 3, it was proposed that the energy requirement of the HLH operating in Mode 1 was proportional to the void space contained in the top hopper containing fuel prior to feeding. Examining the volume of water pumped shown in Table 5-2, and the volume of the top hopper inclusive of piping and fittings proves this assertion to be correct. The volume of void space present in the top hopper containing a 4 kg batch of wood pellets prior to feeding is approximately equal to 5560 ml. Reviewing the figures shown in Table 5-2, it can be seen that the volume of water pumped during the compression stage of Mode 1 varies between 5500 ml 5600 ml for all operating pressures, and therefore indicates the volume of water required to be pumped to be broadly equal to that of the void space.

Comparatively, the volume of water pumped during operation in Mode 2 was not found to equal the total volume of the top hopper as was previously asserted. However, this was not due to failings on the HLH's part and was a conscious decision taken to ensure that water carryover into the bottom hopper/collection vessel was not brought about. The volume of water pumped during operation in Mode 2 was set at 7500 ml, which corresponds to approximately 86% of the volume of the top hopper. Such a value was deemed to be substantial enough to allow the majority of high pressure gas to be displaced and ensure that water carryover and fuel contamination with water did not take place.

5.5.4 Energy requirement of conventional lock hopper systems

In addtion to operating the HLH in Mode 1 and Mode 2, the HLH was run both as a conventional single and dual lock hopper in order to make a to-scale comparison. Compression was brought about using a three stage compressor and the energy requirement of both systems was assessed using the same single phase voltage and current logger used during the assessment of the HLH. The high pressure water pump was replaced with the compressor and compression was brought about via the pipe previously used for pumping/draining water to/from the top hopper. The compressor and associated fittings were assembled to allow toggling between the top hopper and the collection vessel.

As with the operation of the HLH in Mode 2, the pressure boundary was situated at V2 when operating the HLH as a conventional single lock hopper. V3 was left open at all times during operation, and in turn the bottom hopper was only present to increase the volume of the collection vessel. The operating procedure was as follows. A 4 kg batch of wood pellets was fed to the top hopper, the top hopper was then sealed and the compressor was engaged until the pressure in the top hopper was brought up to system pressure. V2 was then opened and the batch of wood pellets was fed to the collection vessel. Comparatively, when operating the HLH as a dual lock hopper, the pressure boundary was situated at a mixture of V2 and V3. Initially, system pressure was established in the bottom hopper and the collection vessel, and then V3 was closed. The operating procedure for a dual lock hopper was as follows. A 4 kg batch of wood pellets was fed to the top hopper and sealed, V4 was opened in the connecting pipe between the two hoppers to allow the batch of wood pellets to be initially pressurised, and V4 was then closed. V3 was opened, the compressor engaged, and the pressure in the bottom hopper and collection vessel was brought up to system pressure. The compressor was then toggled to the top hopper, engaged, and the pressure in the top hopper was then also brought up to system pressure. V2 was then opened and the batch of wood pellets was fed to the collection vessel.

Table 5-6 highlights the effect of operating pressure on both the power drawn by the compressor and the compression time while operating as a conventional single and dual lock hopper, and Figure 5-11

highlights how the power drawn changes during the compression stage. A 4 kg batch of wood pellets was maintained throughout the testing of both conventional lock hopper systems.

	Power (W)		Compression Time (s)	
Pressure (barg)	**Single Lock Hopper**	**Dual Lock Hopper**	**Single Lock Hopper**	**Dual Lock Hopper**
10	1514 ± 35	1554 ± 30	101 ± 3	45 ± 1
15	1524 ± 40	1521 ± 39	136 ± 7	61 ± 3
20	1600 ± 38	1534 ± 39	170 ± 2	83 ± 7
25	1590 ± 32	1528 ± 32	215 ± 3	112 ± 6

Table 5-6: Effect of operating pressure on the power drawn by the compressor and the compression time.

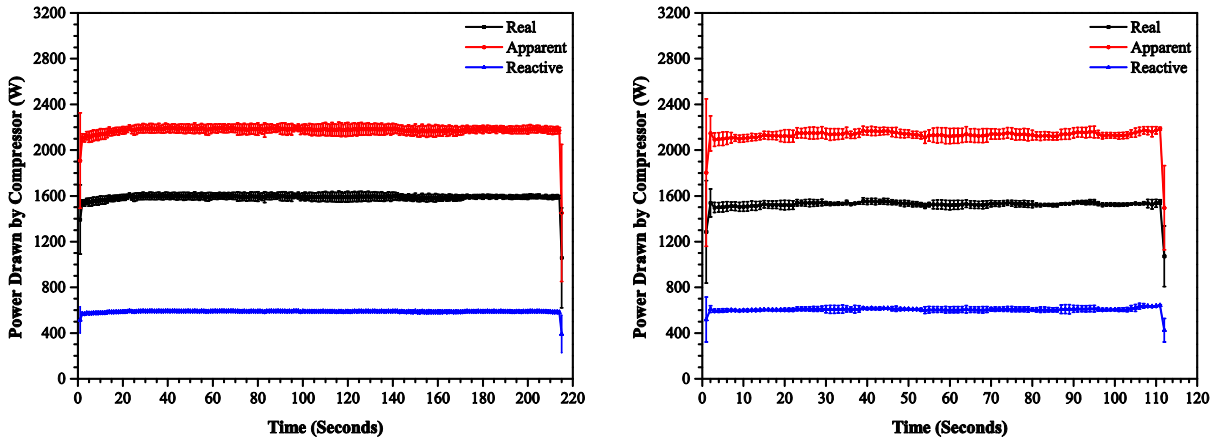

Figure 5-11: Apparent, reactive and real power drawn by the compressor operating as a conventional single lock hopper (left) and a dual lock hopper (right) at 25 barg.

It can be seen from Figure 5-11 and Table 5-6 that there is no clear relationship between the power drawn by the compressor and operating pressure for either a conventional single or a dual lock hopper. Power drawn is seen to be approximately constant regardless of pressure for both systems and ranges between 1500 W and 1600 W with an average of 1546 W. Comparing the results shown in Table 5-6 and Figure 5-11 regarding the power drawn by the compressor to those determined theoretically in Chapter 3 indicates an operating efficiency ranging between 14.5% and 24.0% where compression is assumed to take place isothermally and adiabatically respectively. Such efficiencies compare reasonably well with that determined for the high pressure water pump and in turn, indicate a reasonable comparison between the two systems can be made. Combining the results for compression time and power drawn by the compressor generates Figure 5-12 which highlights a trend of increasing energy requirement with increasing pressure.

The main advantage of the HLH is realised when looking at Figure 5-12. A far more dramatic trend of increasing energy use with increasing pressure is observed for both a conventional single and dual

lock hopper than for the HLH operating in either Mode 1 or Mode 2. Although a dual lock hopper is shown to use approximately 45-50% (10-25 barg) of the energy a conventional single lock hopper uses, energy savings of approximately 82% and 76% are recorded for the HLH operating at 25 barg in Mode 1 and Mode 2 respectively. At lower pressures (≤10 barg) a dual lock hopper is seen to become more competitive with the HLH, with an average energy use of 17.03 kJ/kg at 10 barg. This compares favourably to Mode 1 (12.73 kJ/kg) and Mode 2 (16.90 kJ/kg). However, as pressure is increased the energy use of the HLH is seen to be dramatically lower than a dual lock hopper. Energy savings of approximately 64% and 52% are observed for Mode 1 and Mode 2 operating at 25 barg respectively compared to a dual lock hopper, and savings compared to both conventional systems are projected to increase for higher operating pressures.

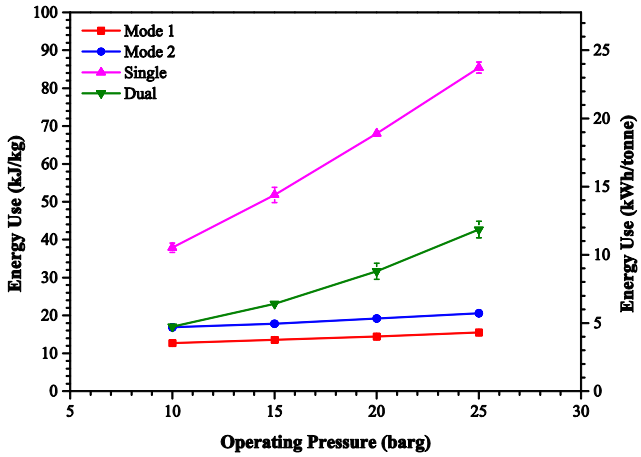

Figure 5-12: Energy requirement comparison between the HLH and a conventional single and dual lock hopper.

Since one of the immediate benefits of the HLH is that the volume of lock gas vented to the atmosphere is greatly reduced, it is timely to analyse the embodied energy use taking into account waste. By assuming varying percentage contaminations of lock gas with syngas and assuming that the lock gas is vented and not recovered allows inherent energy waste to be factored into the energy requirement of the feed system. Figure 5-13 highlights four cases where lock gas contamination with syngas takes place in concentrations of 5 vol%, 10 vol%, 25 vol% and 50 vol%.

Although Mode 2 of the HLH ultimately seeks to negate lock gas venting, in reality there is small volume that cannot be displaced with water during the compression stage. The average volume displaced by water for Mode 1 and Mode 2 was 5560 ml and 7530 ml respectively. With a total volume of the top hopper being equal to 8730 ml, the volume percentage of lock gas at pressure vented is 36.3% and 13.7% for Mode 1 and Mode 2 respectively. However, lock gas contamination affects a conventional single and dual lock hopper far more dramatically, with a conventional single lock hopper venting a full volume of gas at pressure after feeding. Figure 5-13 displays a combination

of the experimental data generated for Mode 1, Mode 2, a conventional single and a dual lock hopper with a theoretical energy waste due to venting. A medium calorific value syngas of 15 MJ/Nm³ is assumed in each case with a temperature of 1000 °C. Such a temperature assumes a gasification process where the feed system is located immediately adjacent to the gasifier. Although in reality, this may not be the case and significant pipe work and/or processes may separate the two systems (feed system and gasifier), assuming such a temperature allows a lower limit for the energy wasted through lock gas venting to be determined. Where the two systems are separated, gas cooling will inevitably take place, and in turn, the volume of gas vented at standard temperature and pressure (STP) will be larger. It is anticipated that energy waste through lock gas venting will be different for different process setups, and will be greatest where the product gas is allowed to cool before venting. The lock gas contaminated with syngas in this case is assumed to expand to STP and the volume at STP is calculated via a molar basis.

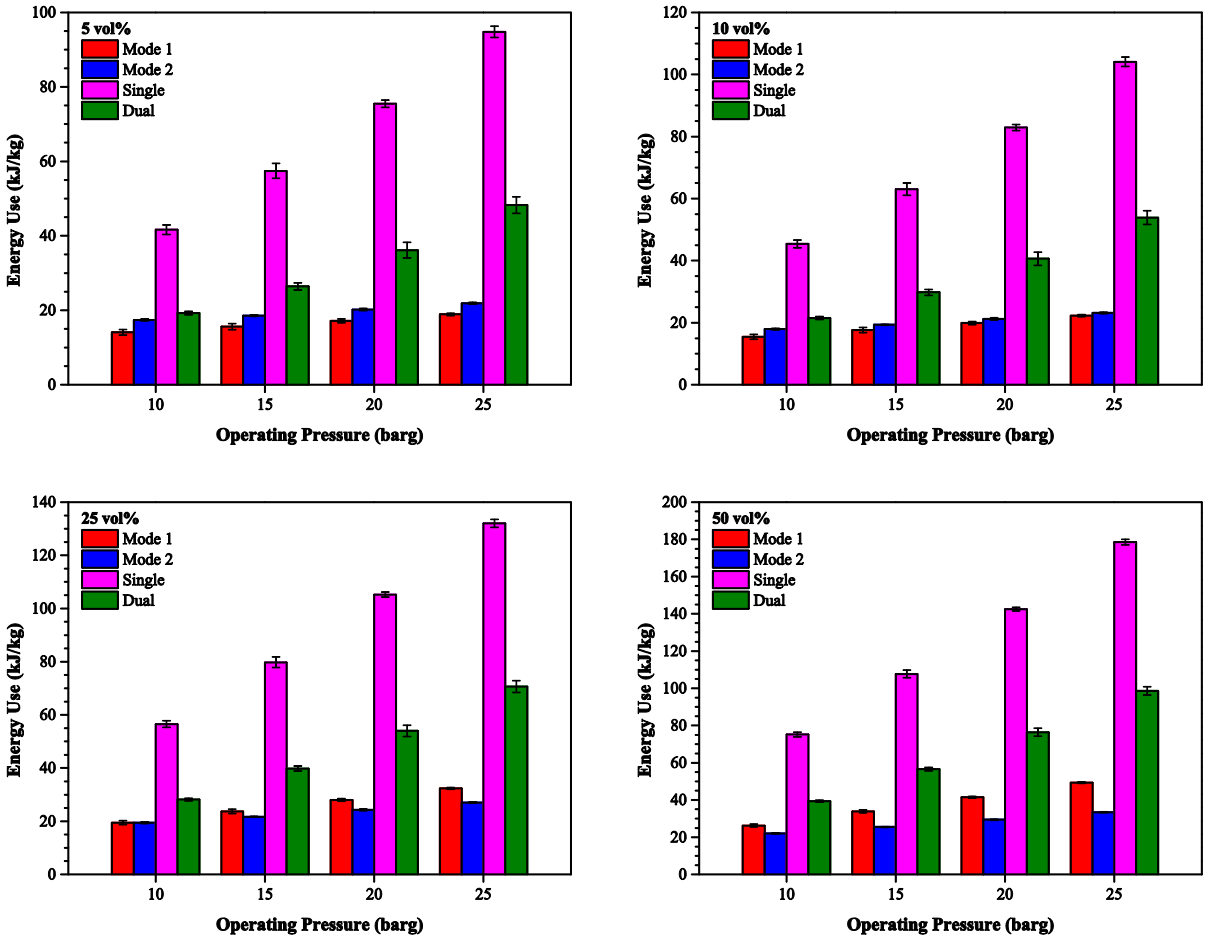

Figure 5-13: Energy use of the HLH operating in Mode 1 and Mode 2 compared to a conventional single and dual lock hopper with varying degrees of lock gas contamination with syngas.

Figure 5-13 indicates that as lock gas contamination increases, the energy use increases in all four cases. As expected, the HLH operating in Mode 2 is seen to be the least affected case as

contamination increases. At an operating pressure of 25 barg and where a lock gas contamination of 12 vol% takes place, the embodied energy use of Mode 1 is approximately equal to that of Mode 2. As lock gas contamination increases past this (>12 vol%), Mode 2 is seen to be the most efficient mode of operation followed by Mode 1, a dual lock hopper and lastly a conventional single lock hopper. It can be said that Mode 2 is the most favourable mode of operation where lock gas contamination with syngas takes place in high concentrations, and the breakeven concentration between Mode 1 and Mode 2 is found to decrease as syngas heating value is increased.

5.5.5 Comparison to theoretical energy saving

Having determined the energy requirement of the HLH and a conventional single and dual lock hopper, it is timely to compare the results determined experimentally to those calculated in Chapter 3. Figure 5-14 highlights a comparison between experimental and theoretical results relating to the energy saving generated by the HLH operating in both Mode 1 and Mode 2 compared to a conventional single lock hopper. An upper and lower limit for energy saving is calculated in both cases. The upper limit assumes the compression stage takes place adiabatically in both cases, and the lower limit assumes the compression takes place isothermally.

Figure 5-14 shows the results determined experimentally to correlate well with theory. Experimental results are shown to be equal to those calculated within the stated error at all operating pressures and for both modes of operation. Theoretical calculations suggest energy savings to increase with increasing pressure for both modes of operation, and energy savings as high as 91.9% and 86.8% are predicted for an operating pressure of 100 barg when operating in Mode 1 and Mode 2 respectively.

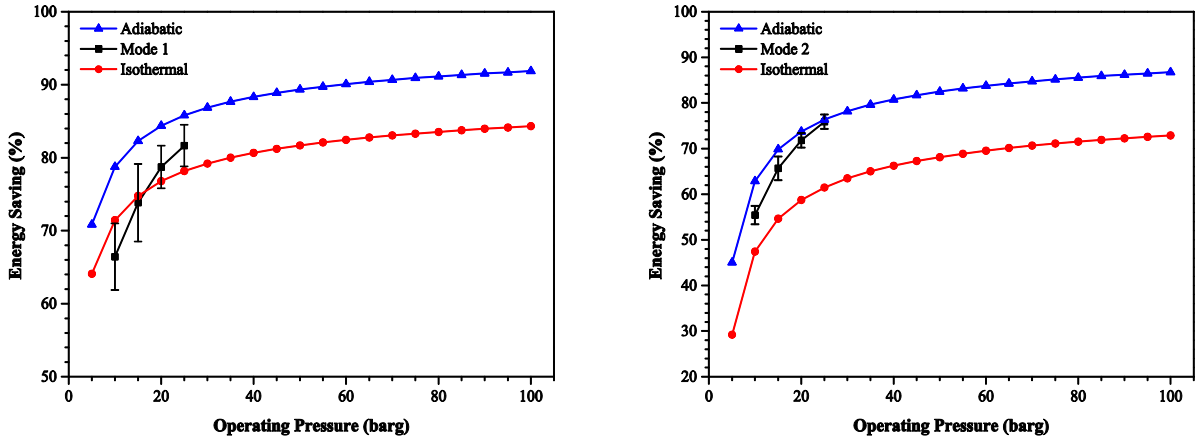

Figure 5-14: Comparison between theoretical and recorded energy savings generated by the HLH operating in Mode 1 (left) and Mode 2 (right) compared to a conventional single lock hopper.

5.5.6 Moisture content analysis

As water plays an intrinsic role in the compression stage of the HLH, it is important to examine the effect water has on the moisture content of the fuel after it has been fed across the pressure boundary. Where moisture unstable fuels are being fed, slight changes in moisture content can dramatically alter a fuel's physical properties and promote flow problems. Therefore, analysing the effect the HLH has on the moisture content of the fuel being fed allows an assessment to be made regarding the compatibility of the feedstock with the system.

Moisture content variation was analysed using wood pellets as the primary feedstock as wood pellets present an absorbent fuel able to most accurately monitor moisture uptake brought about during feeding. Moisture content was assessed assuming that any mass increase across the pressure boundary was due to the uptake of water by the pellets and so the mass of each batch of wood pellets was assessed before and after feeding was completed. To provide an assessment of the primary valves (V2 and V3) used to separate each of the three primary vessels of the HLH, moisture content analysis was carried out using two types of valve material – chrome-plated brass and stainless steel. Operating conditions were maintained constant for both types of valve; however, operation was ceased at 25 barg when using the chrome-plated brass valves due to 25 barg posing the pressure limit of that valve type. Table 5-7 provides an overview of the changes in moisture content recorded while operating the HLH fitted with both types of valve.

	Moisture Content Increase (%)			
Valve Material	**Chrome-plated Brass**		**Stainless Steel**	
Pressure (barg)	**Mode 1**	**Mode 2**	**Mode 1**	**Mode 2**
5	0.06 ± 0.04	2.70 ± 0.20	–	–
10	0.04 ± 0.02	1.74 ± 0.77	0.37 ± 0.25	0.54 ± 0.21
15	0.10 ± 0.08	3.39 ± 0.47	0.27 ± 0.03	0.81 ± 0.22
20	0.09 ± 0.07	4.00 ± 1.19	0.31 ± 0.12	0.22 ± 0.01
25	–	–	0.60 ± 0.07	0.50 ± 0.37

Table 5-7: Moisture content increase generated during operation in Mode 1 and Mode 2 with the HLH fitted with chrome-plated brass and stainless steel valves.

It can be seen from Table 5-7 that moisture content increases are relatively stable across both modes of operation where the stainless steel valves are fitted, and are recorded to be less than 1 wt% for all operating pressures. Moisture content increases of the same magnitude are recorded where the chrome-plated brass valves are fitted for operation in Mode 1; however, Mode 2 presents moisture content increases far in excess of those recorded for Mode 1. The trend observed with the chrome-plated brass valves may be due to Mode 2 involving a larger volume of water pumped during the compression stage; however, the results reported for the stainless steel valves do not agree with this

hypothesis. Reviewing the order in which the HLH was operated allows a better understanding of the results presented in Table 5-7.

In both cases, the HLH was run in Mode 1 prior to Mode 2. In the case of the chrome-plated brass valves, it is proposed that at the start of testing, any increase in moisture content is generated from the absorption of the residual moisture present on the inside of the top hopper after the compression and water drainage stages have been completed. It is also proposed that as testing continues, the primary valves used to pass solids are subject to wear and degrade over time. The degradation encountered compromises their sealing ability and in turn allows water to pass through the valves. Figure 5-15 seeks to quantify the level of degradation experienced through air leakage measurements.

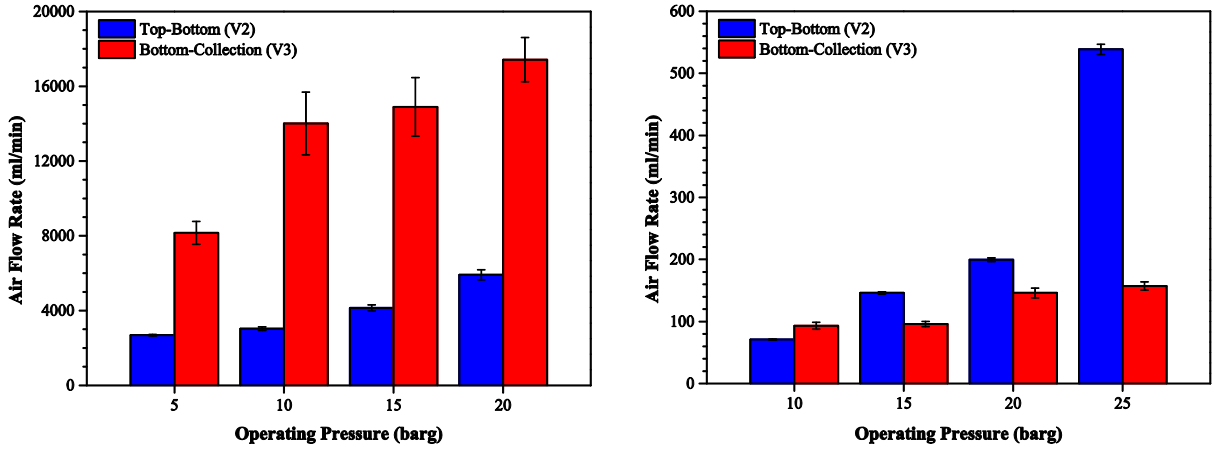

Figure 5-15: Air leakage through V2 and V3 for valves manufactured from brass (left) and stainless steel (right).

Air leakage rates were measured via the siphon pipe connected to the top hopper using a wet gas meter. V8 contained in the siphon pipe was opened and closed accordingly to let the air leaking from either V2 or V3 flow through the meter, and the time taken for each 250 ml rotation of the gas meter was measured to determine a volumetric flow rate of air. V1 separating the atmosphere from the top hopper was closed at all times, and V2 and V3 were opened or closed accordingly.

It is clear from Figure 5-15 that the chrome-plated brass valves are less stable than their stainless steel counterparts as they are shown to give rise to far greater levels of air leakage. The results shown in Figure 5-15 support the proposition of valve degradation giving rise to larger increases in moisture content, and indicate the stainless steel valves to be more resilient during operation. This is to be expected as stainless steel is a harder material than brass. Although the brass valves are chrome-plated and chrome has a high degree of hardness (739 HB) (BAL Seal, 2001) compared to brass (80-95 HB) (Rothbart, 1985), the thickness of the plate deposited is small, typically around 0.02-0.125 mm (BAL Seal, 2001). Therefore, when the valves are subject to harsh environments, the primary material is unable to provide a sufficient support for the plate material and thus the plate material is depressed

into the primary material and forms indentations as shown in Figure 5-16. The formation of indentations leads to further solids contamination and in turn allows further degradation of the valve to take place. Such degradation promotes leakage through the valve, and in the case of the HLH, leakage of both air and water which lead to pressure losses of the system and moisture content increases of the fuel being fed respectively.

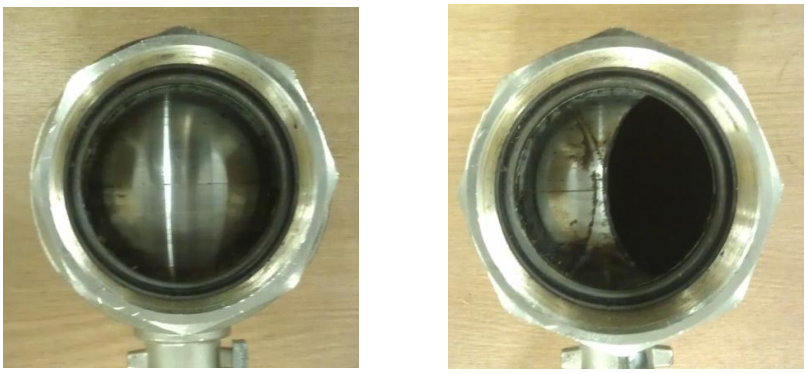

Figure 5-16: Degradation of the chrome-plated brass V2 separating the top hopper from the bottom hopper (closed-left, half bore-right).

The stainless steel valves present a higher degree of hardness (217 HB) (ASTM, 2012) than the chrome-plated brass valves, and in addition to this, facilitate the operation at pressures as high as 69 bar which is far in excess of the 25 bar limit that the chrome-plated brass valves allow. Minimal levels of degradation were experienced after testing with the stainless steel valves and this is reflected in the small levels of air leakage recorded and presented in Figure 5-15. As moisture content increases are recorded to be independent of operating pressure and are less than 1 wt% in all cases, it can be stated that any increase in moisture content is brought about through the fuel absorbing any residual moisture present on the inside of the top hopper prior to feeding.

Overall, the stainless steel valves were found to be the most resilient valve type. However, although moisture content increases do not indicate water to have started passing through the valves, air leakage was still recorded from both V2 and V3 at all operating pressures. Therefore, it can be said that the use of stainless steel valves does not pose a permanent solution to air leakage and fuel moisture content increase, as preliminary signs of degradation are observed through air leakage results. The results shown indicate that both types of valve are sacrificial, and that the chrome-plated brass valves are required to be replaced more frequently than their stainless steel counterparts.

5.6 Experimental results and discussion: Feedstock flexibility

Further to the characterisation of the HLH using wood pellets – torrefied pellets and ground anthracite grains were fed via the HLH in order to assess the flexibility of the device. The energy requirement to

feed such fuels was assessed and the energy saving compared to conventional lock hopper systems was determined. In addition to this, the effect the HLH has on the moisture content of the above stated fuels was analysed.

5.6.1 Energy requirement of the Hydraulic Lock Hopper

As the relationship between energy requirement and operating pressure has been established, the HLH was only run at an operating pressure of 25 barg with the torrefied pellets and ground anthracite grains. The power drawn by the high pressure water pump was recorded alongside the power factor, and in turn and the amount of energy required to a feed a batch of each material was determined. The power drawn by the high pressure water pump was observed to stay broadly constant throughout operation, and the average power drawn and compression time are shown in Table 5-8.

Fuel	Power (W)	Compression Time (s)
Wood pellets	1104 ± 24	56 ± 2
Torrefied pellets	1107 ± 51	54 ± 3
Ground anthracite	1096 ± 18	52 ± 2

Table 5-8: Power drawn and compression time for a range of fuels operating in Mode 1 at 25 barg.

The HLH was not operated in Mode 2 when feeding either the torrefied pellets or ground anthracite as the compression stage in Mode 2 stays constant regardless of the fuel being fed. A constant and predetermined volume of water is required to be pumped in Mode 2 and therefore the only variable affecting the energy required to feed is the mass per batch of fuel. As both fuels were observed to flow without problems in Mode 1, it is assumed that operation in Mode 2 does not present any problems relating to flowability. Results regarding the energy required to feed wood pellets to pressures as high as 25 barg can therefore be used for all new fuels and corrected accordingly with the mass per batch of the new fuel being fed. Figure 5-17 highlights both the results recorded when feeding the wood pellets, torrefied pellets and ground anthracite in Mode 1 as well as Mode 2 at 25 barg. Further to this, the volume of water pumped in the compression stage of the feeding operation and the time taken for compression were recorded and are shown in Table 5-9.

Figure 5-17 shows the energy requirement of Mode 2 to be greater than that of Mode 1 in all cases. Feeding the ground anthracite grains is shown to be the least energy intensive process followed by the torrefied pellets and then the standard wood pellets which are shown to be the most energy intensive fuel to feed. This outcome is to be expected as from Table 5-9 it can be seen that the mass per batch of fuel is the greatest in the case of the ground anthracite and similarly the batch of the torrefied pellets is greater than the wood pellets. Although both pelletised fuels present broadly similar bulk densities, a larger mass per batch was used in the case of the torrefied pellets due to an increase in mechanical

stability when in the presence of water. Standard wood pellets dramatically increase in volume when wetted, and so a head space above the fuel is allowed to accommodate for any changes in volume brought about through wetting. A larger mass per batch of fuel is used in the case of the ground anthracite grains for the same reason in addition to the anthracite presenting a larger bulk density.

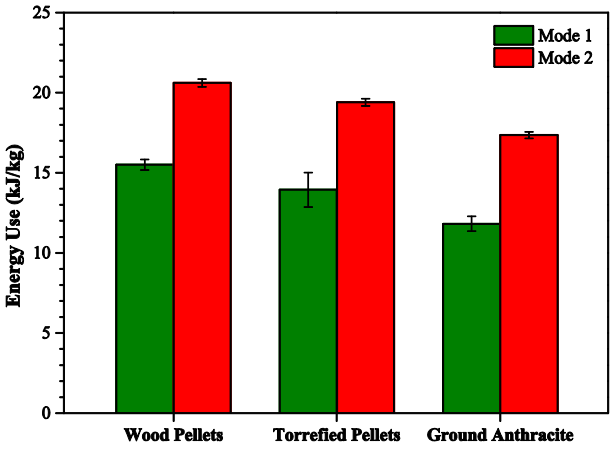

Figure 5-17: Energy requirement to feed at 25 barg using the HLH in Mode 1 and Mode 2.

Material	Mass per Batch (g)	Volume of Water (ml)	Compression Time (s)
Wood pellets	4000.4 ± 0.3	5536 ± 58	56 ± 2
Torrefied pellets	4250.4 ± 0.2	5304 ± 361	54 ± 3
Ground anthracite	4750.8 ± 0.1	5068 ± 314	52 ± 2

Table 5-9: Average mass per batch of fuel fed, volume of water pumped in the compression stage and the time taken for compression operating the HLH at 25 barg in Mode 1.

Table 5-9 highlights both the volume of water pumped by the high pressure pump and the time taken for compression to vary with each fuel fed. These trends can be explained by the void space present in the top hopper prior to the pressure equalisation stage and the feeding of fuel to the bottom hopper. Due to the increase in the mass per batch of fuel fed for both the torrefied pellets and ground anthracite, the void space present in the top hopper is reduced. Taking the total volume of the top hopper inclusive of pipe work and fittings to be approximately 8730 ml, the void space can be calculated using the particle density of each of the fuels. Calculations determine a void space of approximately 5560 ml, 5380 ml and 5220 ml for the wood pellets, torrefied pellets and ground anthracite respectively. Such values compare reasonably well to those presented in Table 5-9 for the volume of water pumped in the compression stage and indicate the same decreasing trend as the void space calculated. As the compression time and the volume of water required to be pumped for each fuel varies, and the power drawn by the pump is maintained broadly constant, it can be said that both

the mass per batch and the void space present in the top hopper are responsible for the trend shown in Figure 5-17.

5.6.2 Energy requirement of conventional lock hopper systems

In addition to operating the HLH in Mode 1, the HLH was operated both as a conventional single and a dual lock hopper when feeding the torrefied pellets and ground anthracite grains. The power drawn, power factor and compression time were recorded and are displayed in Table 5-10.

	Power (W)		Compression Time (s)	
Fuel	**Single Lock Hopper**	**Dual Lock Hopper**	**Single Lock Hopper**	**Dual Lock Hopper**
Wood pellets	1590 ± 32	1528 ± 32	215 ± 3	112 ± 6
Torrefied pellets	1574 ± 20	1540 ± 28	214 ± 3	111 ± 3
Ground anthracite	1559 ± 49	1529 ± 19	211 ± 1	108 ± 4

Table 5-10: Power drawn and compression time feeding wood pellets, torrefied pellets and ground anthracite using a conventional single and dual lock hopper at 25 barg.

Table 5-10 highlights broadly similar compression times for all fuels and when both operating as a conventional single and dual lock hopper. Compression time is seen to be the lowest in the case of the ground anthracite and the highest in the case of the wood pellets. This slight variation is observed due to the variation in the void space present in the top hopper prior to feeding. The power requirement by the three stage compressor is shown to stay broadly constant varying between 1500 W and 1600 W for all cases. Figure 5-18 highlights a comparison of the energy requirement per unit mass of fuel fed between both Mode 1 and Mode 2 of the HLH and both a conventional single and dual lock hopper, and Table 5-11 shows how such energy requirements translate to energy savings generated by the HLH over both conventional systems.

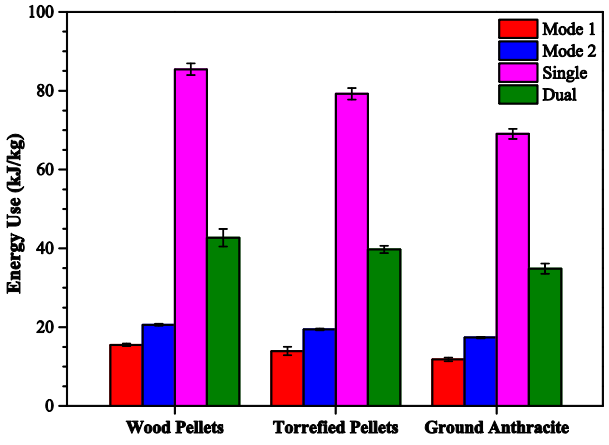

Figure 5-18: Energy requirement comparison between the HLH and both conventional lock hopper systems when feeding wood pellets, torrefied pellets and ground anthracite at 25 barg.

	Energy Saving (%)			
	Single Lock Hopper		Dual Lock Hopper	
Material	**Mode 1**	**Mode 2**	**Mode 1**	**Mode 2**
Wood pellets	81.9 ± 2.2	75.9 ± 1.6	63.7 ± 3.6	51.7 ± 2.7
Torrefied pellets	82.4 ± 6.5	75.5 ± 1.7	64.9 ± 5.2	51.2 ± 1.3
Ground anthracite	82.9 ± 3.6	74.9 ± 1.6	66.1 ± 3.5	50.2 ± 1.9

Table 5-11: Energy saving generated by the HLH operating in Mode 1 and Mode 2 at 25 barg compared to a conventional single and dual lock hopper.

Mode 1 is seen to generate a higher energy saving compared to Mode 2 in all cases, and the greatest energy saving comes when feeding the ground anthracite grains in Mode 1 compared to a conventional single lock hopper. This is followed by the torrefied pellets and then the standard wood pellets. This trend is observed due to the smaller void space present in the top hopper prior to feeding when operating with the ground anthracite compared to the two pelletised fuels, and in turn the lower energy requirement by the high pressure water pump operating in Mode 1. Although this also affects both types of conventional lock hopper as this means a smaller volume of gas has to be compressed, more energy is required per volume of void space by the high pressure water pump than the three stage compressor.

Comparatively, this benefit is not felt when both the conventional single and dual lock hopper is compared to Mode 2. As the energy required by the high pressure water pump remains constant for all fuels in Mode 2, it is only the mass per batch that affects the energy required per unit mass fed. The reduction is void space presented by the torrefied pellets over the standard wood pellets, and in turn the ground anthracite over the torrefied pellets does not constitute an advantage for Mode 2, whereas it does for both a conventional single and a dual lock hopper. Therefore, Table 5-11 shows energy savings to drop for both the torrefied pellets and the ground anthracite grains compared to the standard wood pellets due to the reduction in void space. It can be concluded from Table 5-11 that the greatest energy savings are generated in Mode 1 where the void space present between the fuel is minimised, and where the void space between the fuel is maximised in the case of Mode 2.

5.6.3 Projected energy requirement for feeding alternative fuels

Although the torrefied wood chips, milled wood pellets and pulverised coal are incompatible with the HLH, the energy requirement to feed these fuels can be projected using existing data regarding the wood pellets, torrefied pellets and ground anthracite grains. Figure 5-19 shows a plot of the energy requirement to feed these fuels against the void space present in the top hopper prior to feeding. It is the void space that is the key variable when feeding and the variable that determines the energy requirement to feed.

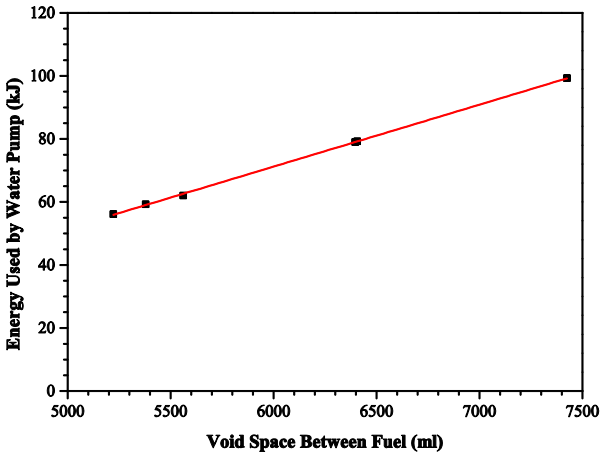

Figure 5-19: Relationship between void space and the energy required to feed in Mode 1 at 25 barg.

Figure 5-19 shows a linear relationship with a line of gradient 19.7. Using this relationship, the energy required to feed the remaining three fuels can be predicted and are also shown in Figure 5-19. It is clear from Figure 5-19 that the HLH performs the best where a densely packed fuel is selected and in turn the void space present in the top hopper prior to feeding is minimised. Taking the average mass per batch of fuel for the torrefied wood chips, milled wood pellets and pulverised coal, an average energy requirement per unit mass of fuel can be determined. Table 5-12 combines the results shown in Figure 5-19 with the readings made for the average mass per batch of fuel to predict the energy required to feed a batch of torrefied wood chips, milled wood pellets and pulverised coal at 25 barg in Mode 1. Similarly, results are shown for the HLH operating in Mode 2 to provide a comparison.

		Energy (kJ/kg)	
Fuel	**Mass per Batch (kg)**	**Mode 1**	**Mode 2**
Wood pellets	4.00	15.51	20.61
Torrefied pellets	4.25	13.94	19.40
Ground anthracite	4.75	11.82	17.35
Torrefied wood chips	1.00	79.03*	82.43*
Milled wood pellets	2.00	49.64*	41.22*
Pulverised coal	3.50	22.64*	23.55*

Table 5-12: Energy required to feed a batch of fuel at 25 barg in Mode 1 and Mode 2. *Projected values.

The values derived from the data plotted in Figure 5-19 provide a reasonable estimation for the energy use per unit of mass of fuel fed in most cases. However, it can be seen that in the case of the milled wood pellets, it is less energy intensive to operate the HLH in Mode 2 than in Mode 1. Clearly, this is not the case in reality, as Mode 2 acts to displace all of the gas at high pressure and ultimately imposes an upper limit for the energy use. It is anticipated that the energy requirement to feed the milled wood

pellets in Mode 1 will approach that of Mode 2 as it impossible for Mode 1 to exceed Mode 2. The relationship shown in Figure 5-19 and the subsequent prediction shown in Table 5-12 should therefore be taken as an approximation. Using the case of the milled wood pellets, it can be assumed that the estimations for the pulverised coal and the torrefied wood chips are also in excess of what is found in reality, and therefore the HLH operating Mode 1 will perform more efficiently than the proposed figures stated in Table 5-12.

5.6.4 Projected energy saving generated feeding alternative fuels

Using the same method as with the data obtained for the HLH operating in Mode 1, it is possible to estimate the energy use of both a conventional single and dual lock hopper operating with alternative materials. Figure 5-20 shows two plots of how the energy use of a conventional single and dual lock hopper varies with void space respectively. Both figures contain estimations for the energy use required to feed torrefied wood chips, milled wood pellets and pulverised coal.

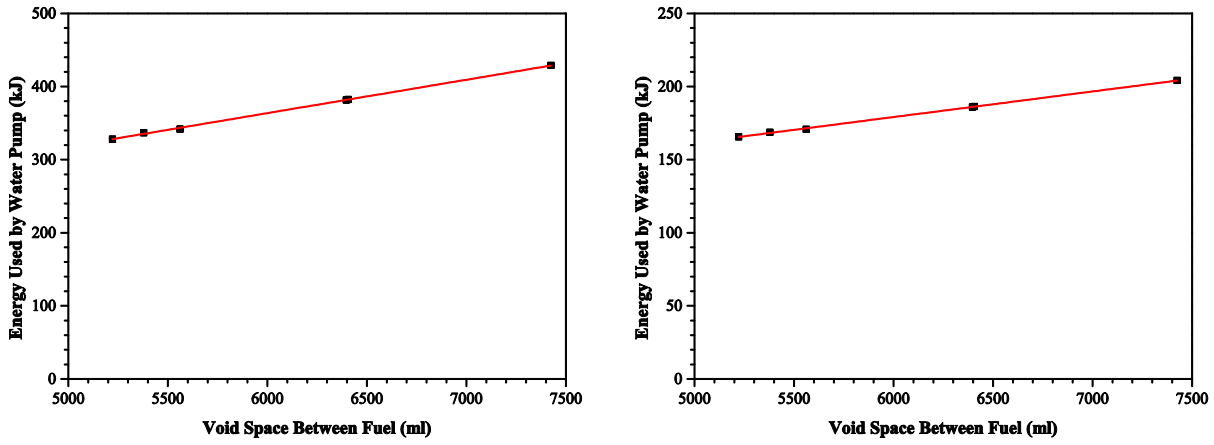

Figure 5-20: Relationship between void space and the energy requirement of a conventional single lock hopper (left) and dual lock hopper (right) operating at 25 barg.

Energy savings generated by the HLH operating in Mode 1 and Mode 2 can be estimated using Figure 5-19 and Figure 5-20 and are shown in Figure 5-21 for a conventional single and dual lock hopper. Figure 5-21 shows energy savings to vary between 74% and 83% for all modes and fuels compared to a conventional single lock hopper, and shows energy savings to vary between 50% and 66% for all modes and fuels compared to a dual lock hopper. Mode 1 is seen to generate a higher energy saving compared to Mode 2 when feeing all fuels with the exception of the milled wood pellets. As previously discussed in Section 5.6.3, this comes about due to an over estimation of the energy use of Mode 1 when feeding the milled wood pellets. In reality it is anticipated that the energy requirement of Mode 1 will be less than or equal to that of Mode 2.

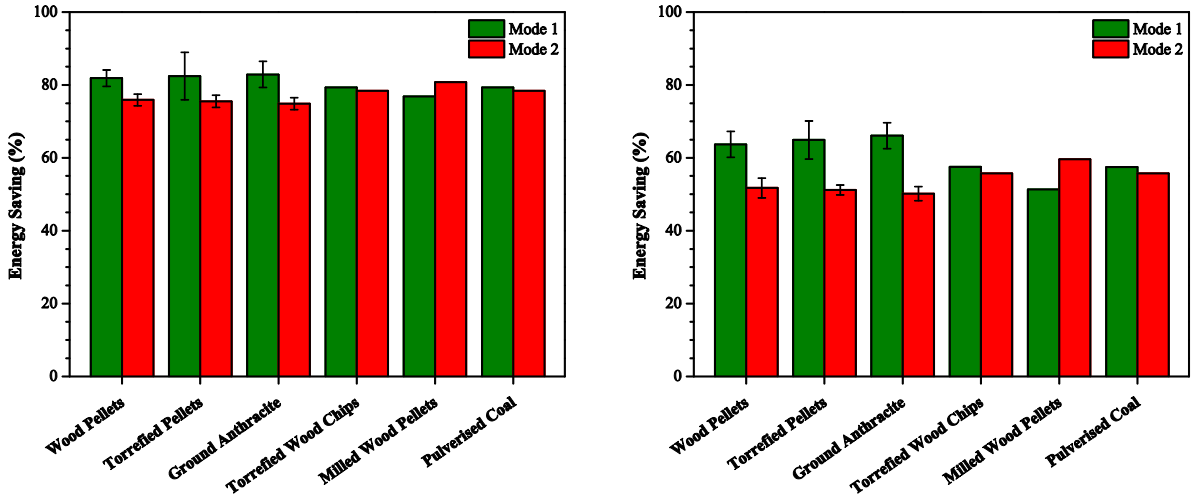

Figure 5-21: Energy saving generated by the HLH operating in Mode 1 and Mode 2 at 25 barg compared to a conventional single lock hopper (left) and dual lock hopper (right).

5.6.5 Moisture content analysis

The tests carried out regarding fuel moisture content increase were also undertaken for both the torrefied pellets and the ground anthracite grains. The feed system was run in Mode 1 at 25 barg and the mass of the material fed was recorded before and after to assess moisture uptake during feeding. Table 5-13 shows that the moisture content of each fuel increases marginally during feeding, increasing by less than 1 wt% in all cases. Torrefied pellets were found to be the least affected by the HLH, followed by the ground anthracite grains and then the standard wood pellets.

Fuel	Moisture Content Increase (wt%)
Wood pellets	0.60 ± 0.07
Torrefied pellets	0.21 ± 0.01
Ground anthracite	0.56 ± 0.05

Table 5-13: Percentage moisture content increase operating in Mode 1 at 25 barg feeding wood pellets, torrefied pellets and ground anthracite grains.

In the case of the torrefied pellets and the ground anthracite, moisture was observed to be present on the surface of the fuels after feeding, which is contrary to the feeding of the standard wood pellets where moisture was absorbed and taken up by the material. Both the torrefied pellets and ground anthracite grains constitute far more moisture stable fuels than standard wood pellets and exhibit good levels of hydrophobictity. Although increases in moisture content were recorded after feeding, the structural stability of both materials was shown to be unaffected. Although structural stability was broadly maintained when feeding the standard wood pellets, it is important to state that the standard wood pellets are less resilient to fluctuations in moisture content. Moisture content increases by

approximately 10-15 wt% can create noticeable changes in the structural stability of wood pellets and can cause them to break up and degrade over time.

5.7 Summary

This chapter provides an overview of the development of the HLH which has successfully demonstrated the feeding of a range of fuels to pressures as high as 25 barg. The HLH has demonstrated two modes of operation, and in addition to this, has been operated as a conventional single and dual lock hopper in order to gauge a small scale comparison to a conventional feed system.

A general trend of increasing energy requirement with increasing operating pressure was found during operation in both Mode 1 and Mode 2. Energy requirements for the HLH operating at 25 barg were found to be as low as 11.82 kJ/kg in Mode 1 and 17.35 kJ/kg in Mode 2 when feeding ground anthracite grains, and as high as 15.51 kJ/kg and 20.61 kJ/kg when feeding wood pellets. Such energy requirements were found to correspond to approximately 0.05% of the energy content of the fuel being fed in the case of the ground anthracite grains and 0.1% in the case of the wood pellets. Energy requirements for the HLH operating as a conventional single and dual lock hopper were also determined and were found to be equal to 69.06 kJ/kg and 34.84 kJ/kg respectively when feeding ground anthracite grains at 25 barg, and 85.47 kJ/kg and 42.70 kJ/kg when feeding wood pellets. The HLH was found to consistently generate energy savings between 81% and 83% compared to a conventional single lock hopper when operating in Mode 1, and between 74% and 76% when operating in Mode 2. Energy savings were found to be lower in all cases when compared to a dual lock hopper, with a dual lock hopper being found to require between 45% and 50% of the energy required to operate a conventional single lock hopper. In addition to this, results generated from experimental work were found to correlate well with the theoretical work carried out and detailed in Chapter 3. Energy savings generated experimentally were found to sit inside the upper and lower bound calculated for both modes of operation, and energy savings were shown to increase with increasing operating pressure.

Mode 1 was consistently found to require less energy than Mode 2 in all cases. However, assuming lock gas contamination with product syngas at various concentrations highlighted Mode 1 to become more energy intensive than Mode 2 for concentrations in excess of 12 vol% for an operating pressure of 25 barg. That is, where the high pressure gas contained in the head space above the water level was found to be contaminated with syngas in a concentration of 12 vol% or greater, Mode 2 was found to be the most efficient mode of operation. Calculations assumed a syngas with a heating value of 15 MJ/Nm^3, and lower breakeven concentrations were found to occur for product gases with lower heating values.

The mass flow rate of the HLH was found to stay broadly constant with operating pressure, varying between 25 g/s and 29 g/s for both Mode 1 and Mode 2. Although a slight decreasing trend of mass flow rate with increasing operating pressure was shown for both modes, this was found to be due to an increased level of manual valve activity as pressure increased. The high pressure pump was found to operate independently of pressure and in turn, compression time was found to stay broadly constant for both Mode 1 and Mode 2. Mode 1 was found to have a slightly larger mass flow rate than Mode 2 in all cases due to the larger volume of water required to be pumped during the compression stage, and the water drainage stage was found to stay broadly constant regardless of operating pressure.

As the HLH utilises water during the compression stage, moisture content was assessed throughout operation. The HLH was not found to significantly impact fuel moisture content and was found to increase moisture contents by less than 1 wt% in all cases when utilising stainless steel valves as the principal valves (V2 and V3). Increases in fuel moisture content were found to take place due to the uptake of residual moisture present in the top hopper after the water drainage stage had been completed when feeding all fuels. Moisture uptake was found to be most pronounced when feeding wood pellets followed by ground anthracite grains and then torrefied pellets. In addition to operating the HLH with stainless steel valves, the HLH was operated using chrome-plated brass valves. Initial moisture content variations were recorded to be in line with the stainless steel valves during operation in Mode 1; however, the chrome-plated brass valves were found to degrade more readily and in turn gave rise to higher degrees of air and water leakage. Moisture content increases of the order of 4 wt% were recorded after successive tests and significant air leakage was found to take place after testing had been completed.

6

EXPERIMENTAL PROGRAMME PART 2 MINIMISING AIR INGRESS

6.1 Introduction

Preventing the backflow of gas at pressure is fundamental to systems used to feed solids to high pressure processes. Results shown in Chapter 5 indicate the HLH to achieve this well, with low levels of air leakage being recorded after successive tests. However, it is timely to investigate the opposing side of this – preventing the forward flow of air at atmospheric pressure. Where gasification is concerned, the ingress of air at atmospheric pressure not only incurs a drop in process efficiency due to the subsequent combustion of the product gas, but presents a major hazard. This chapter aims to provide an overview of an adaptation made to the HLH which practically eliminates air ingress and details the benefits associated with this system.

6.2 Process safety relating to the handling of biomass

The number of biomass fed systems has increased dramatically in recent years and with this much has been learnt about the dynamics of operating such plants. Due to the apparent similarities to coal combustion plants, many mistakes have been made in the development and utilisation of biomass fuels for combustion, particularly where it comes to material handling and feeding. The same can also be said for gasification systems (Wiltsee, 2000, Van Loo and Koppejan, 2008). Early projects sought to use biomass-coal blends with modest biomass concentrations (4-5%) as an effective and low cost route to utilising biomass fuels in their systems (Mahr, 2011). However, today sees a wide range of

dedicated and co-fired biomass plants operating with a multitude of biomass feedstocks (Van Loo and Koppejan, 2008).

During the course of biomass plant development, some of the most valuable lessons have been learnt in the area of material handling and feeding, and not only with respect to process optimisation, but also to process safety. Unfortunately, lessons are still being learnt in this area today, with a number of incidents taking place in recent years. June 2011 saw an explosion in the world's largest pellet production plant in Georgia, USA (Renewables International, 2011). In February 2012, a fire took place in the biomass storage area of a power station in Tilbury, UK (Jones, 2012) and in April 2013, an explosion occurred at a combined heat and power plant (CHP) in Minnesota, USA (Schlossberg, 2013). All three incidents were related to inadequate handling practices with regard to the handling of dusty biomass and were thus preventable. To assess whether an environment presents an explosion hazard, a basic rule of thumb can be applied which is shown in Figure 6-1.

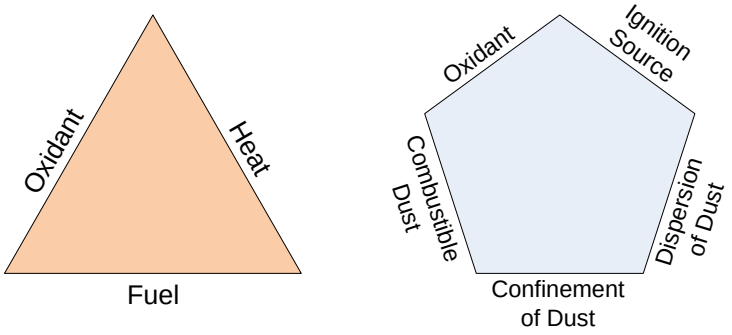

Figure 6-1: The fire triangle (left) and explosion pentagon (right) (Koppejan, 2011).

The explosion pentagon relates specifically to dusty environments and states the conditions needed for a dust explosion to take place. Generally it states that if a combustible dust is dispersed in a contained environment with a supply of oxygen and an ignition source, an explosion is likely to or will take place. Therefore, it can be stated that in order to prevent a dust explosion taking place, one or more of these elements has to be removed. Many modern biomass plants implement preventative and management measures to deal with such scenarios. Three key examples are measuring the composition of the atmosphere in the storage vessel, measuring the temperature at various points in a bulk solid, and preparing the storage base for inert gas injection (Wilén and Rautalin, 2001, Koppejan, 2011). Continuously measuring the atmosphere at various points in the storage vessel allows the detection of evolved gases, and in turn whether processes such as self-heating are taking place, and temperature measurements at various points in the bulk solid also aim to determine this.

Many of the large scale disasters relating to biomass have been routed with the storage and handling systems and where technologies used for handling coal have been applied to biomass materials.

Although fundamentally a solid fuel, biomass behaves dramatically differently to coal and has a far greater risk attached due to its higher reactivity (Huéscar et al., 2012, Huéscar et al., 2013). Table 6-1 highlights a comparison between wood dust, coal dust and dried sewage sludge in terms of their layer ignition temperature (LIT), minimum ignition temperature (MIT) and minimum ignition energy (MIE).

Material	LIT (°C)	MIT (°C)	MIE (mJ)
Coal dust	>400	670	>1000
Wood dust	330	420	50-60
Dried sewage sludge	280	460	100-500

Table 6-1: Flammability properties of coal dust, wood dust and dried sewage sludge (<63 μm) (Merritt, 2012).

Wood dust is far more likely to ignite than coal dust at lower temperatures and requires a far lower amount of energy for ignition. The parameters stated in Table 6-1 are of paramount importance where dust accumulation on hot surfaces takes place (LIT) and where hot environments are mixed with dusty environments (MIT); however, it is not these parameters alone that govern the reactivity of dusty fuels. Two further important parameters are the limiting oxygen concentration (LOC) and lower explosive limit (LEL) (Eckhoff, 2003). The LOC and the LEL seek to state a point where the oxygen content and the dust content of the atmosphere is insufficient to generate an explosion respectively. Table 6-2 provides an overview of LOC and LEL values for a number of different materials.

Material	Median Particle Size for LEL (μm)	LEL (g/m^3)	Median Particle Size for LOC (μm)	LOC (vol%)
Hard coal	17	60	17	14
Brown coal	43	60	63	12
Wood	60	60	27	10
Corn starch	15	60	17	9
Pea flour	<63	60	25	15

Table 6-2: Lower explosive limit and limiting oxygen concentration for a range of materials(Gosewinkel, 2008).

Wood presents a greater explosion risk than coal as a lower LOC is required to generate an explosion. It can also be seen that, generally, an explosive atmosphere will cease where dust concentrations lower than 60 g/m^3 are present. However, it is important to state that the LEL is an inherent property of the material in question and so is subject to change from material to material. For example, charcoal has a LEL of 30 g/m^3 for a particle size of less than 63 μm (Gosewinkel, 2008). Table 6-2 also shows that typically below an oxygen concentration of 9-15 vol% the atmosphere is said to contain enough inert material to suppress an explosion. However, as with the LEL, the LOC is an inherent property of the material in question and is subject to vary.

The LOC is perhaps one of the most important parameters when handling biomass. By ensuring that the atmosphere in which the biomass is contained is not explosive, handling can be carried out without an explosion risk. This is perhaps best exemplified by the deployment of inert gas injection systems in biomass storage sites. The injection of inert gas at high pressure effectively removes one of the sides of the explosion pentagon by reducing the atmospheric concentration of oxygen below the LOC level, where a self-sustained flame can no longer be propagated. Inert gases such as nitrogen and carbon dioxide are commonly used for this process (Eckhoff, 2003). In terms of high pressure solids feed systems, such a safety measure is inherently implemented in conventional lock hoppers, as such systems typically utilise inert gas to bring about pressurisation. It can therefore be said that lock hoppers present a safe, if not efficient route to feeding solid fuels to high pressure processes (Higman and Van der Burgt, 2008).

In its current state the HLH does not act to impede the forward flow of air into the system it is feeding to and thus presents an explosion risk where high temperature combustible gases prevail. The introduction of a vacuum precursor to the HLH seeks to address this by minimising air ingress and facilitating feeding without the need for any inert gas as is required by conventional lock hopper systems. While reducing the pressure does not lower the gaseous concentration of oxygen past the LOC, it ultimately deems an environment incombustible due to the reduced amount of oxygen available for combustion. The following sections detail the mechanics and the design considerations surrounding the addition of the vacuum precursor to the HLH, and provides in depth analysis of the results generated through experimental and theoretical work.

6.3 Operating principle and experimental setup of the vacuum precursor

The vacuum precursor utilises an Edwards 8 (E2M8) two stage rotary vane vacuum pump to create a vacuum in the top hopper containing fuel prior to feeding. A schematic diagram of the vacuum precursor is shown in Figure 6-2 and the fitted vacuum assembly is shown in Figure 6-3.

Alternative methods to create a vacuum in the top hopper were considered, namely using a stream of superheated steam and an external condenser. It was supposed that a vacuum could be created by feeding a stream of superheated steam into the top hopper containing fuel via a valve and allowing the steam to occupy the void space. The superheated steam would effectively displace the air in the top hopper by "blowing" it out of a steam outlet also contained in the top hopper. It was envisaged that, once the concentration of air in the top hopper had been minimised and steam occupied the void space between the bulk solid, the valve in the steam outlet could be closed, the flow of superheated steam stopped, and the valve in the inlet line also closed. The superheated steam would cool, condense, and

subsequently create a vacuum in the top hopper containing the fuel. A schematic diagram of the vacuum induced superheated steam arrangement is also shown in Figure 6-2.

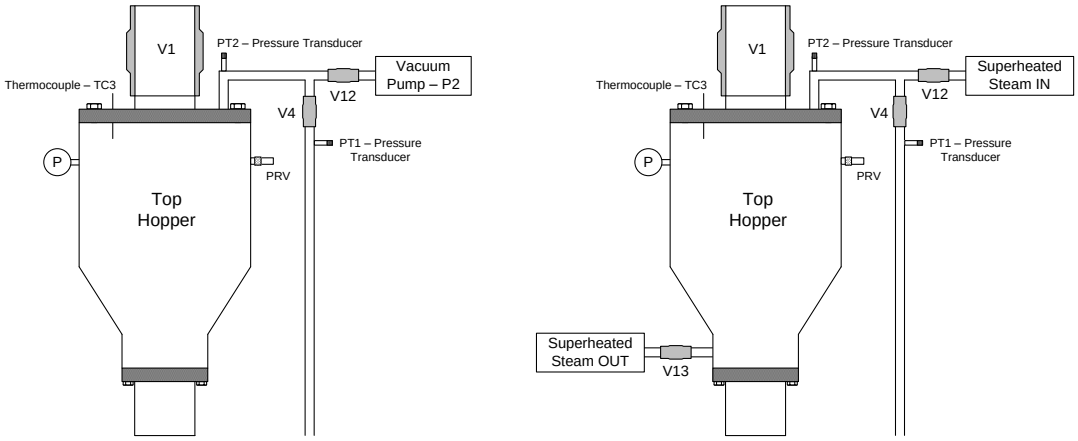

Figure 6-2: Schematic diagram of the HLH with the addition of a vacuum precursor using a vacuum pump (left) and superheated steam (right).

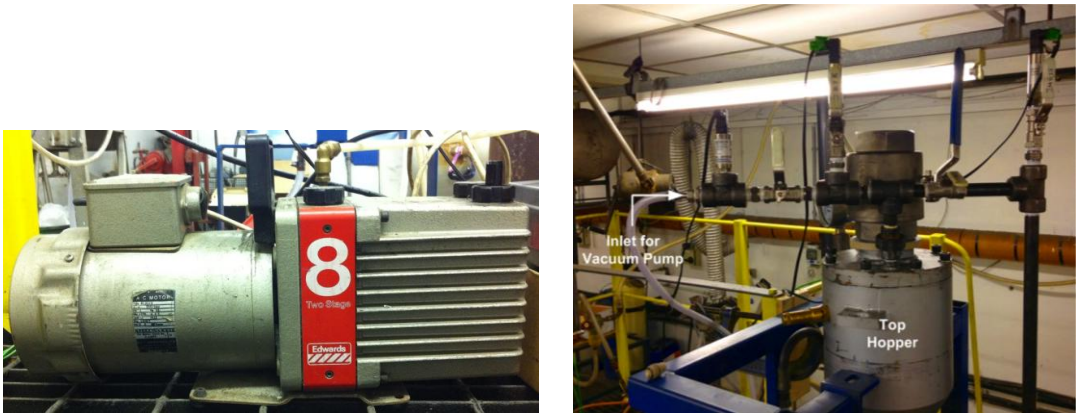

Figure 6-3: Two stage rotary vane vacuum pump (left) and the vacuum inlet for the HLH (right).

However, due to the inherent use of water, development of a system using superheated steam was not pursued due to the negative effect of water on the structural stability of some fuels – namely wood pellets. Although superheated steam is commonly used in industrial drying processes (with the superheated steam acting as both the heat source and the medium to carry away vaporised moisture), it creates a vacuum by condensing inside the vessel (Van Deventer and Heijmans, 2001, Van Deventer, 2004, Morey and Zheng, 2011). The liquid water produced can act to reduce fuel stability where moisture stable fuels are concerned. It can be said that such a system will be favourable where excess superheated steam is available on site and moisture stable fuels are being fed. The level of superheat required to create a vacuum will be low as only a slight margin is required over saturated conditions in order to minimise the level of condensation occurring in the vessel.

6.4 Vacuum precursor characterisation

6.4.1 Vacuum pump characterisation

In terms of process safety, it is preferable to evacuate the top hopper of air/oxygen entirely to ensure the possibility of dust explosions taking place is eliminated. However, the requirement of a perfect vacuum is impractical and costly, not least in terms of the energy required to create it. Most modern vacuum pumps are able to produce vacuums as low as $1x10^{-3}$ mbar; however, the inadequacy of seals in vessels often means that such pressures are not reached or maintained easily (Edwards, 2013). Therefore, it is important to assess the ability of the vacuum pump used to create and maintain a vacuum in the top hopper. Figure 6-4 shows how the pressure in the top hopper varies with time and with changing volume. The volume was varied by varying the mass of wood pellets contained in the top hopper between 0 kg and 4 kg.

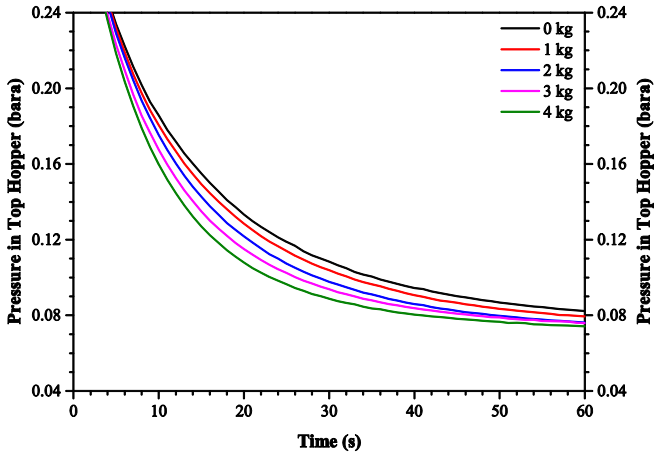

Figure 6-4: Vacuum formation in the top hopper containing varying batches of wood pellets.

Figure 6-4 shows that the pressure in the top hopper approaches a constant of approximately 0.073 bara, which constitutes the removal of approximately 92.7 vol% of air. As the volume of the top hopper increases due to a decreasing volume of wood pellets stored, a general trend shows the curve moving up and to the right. This indicates that more time is required to reach a given pressure as the volume of the top hopper increases. This is simply because the volume of gas evacuated by the vacuum pump is larger where there is a smaller mass of wood pellets in the top hopper. All of the curves shown in Figure 6-4 approach 0.073 bara after an extended period of time.

Figure 6-5 shows how the change in pressure varies with the change in time in the top hopper. The majority of the work done in terms of the pressure attained is achieved in the first few seconds of operation, and Figure 6-5 shows that for a 4 kg batch of wood pellets, approximately 73.7% of the final pressure is achieved after the first second of operation. Figure 6-5 also shows that as time passes, the difference in pressure consistently decreases over time, until a stable pressure is reached.

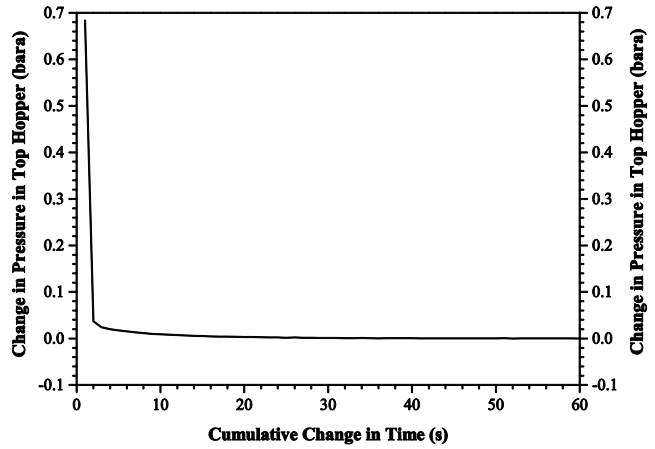

Figure 6-5: Change in pressure with change in time (cumulative) for a 4 kg batch of wood pellets.

Figure 6-6 shows how energy use varies with pressure, providing an overview of how efficient the vacuum pump is and displays a similar trend to that observed in Figure 6-4. As the mass of wood pellets is increased, and in turn the volume of the top hopper is decreased, the amount of energy required to reach a given pressure is decreased. This translates to the curve moving up and to the right as the mass in the top hopper is decreased.

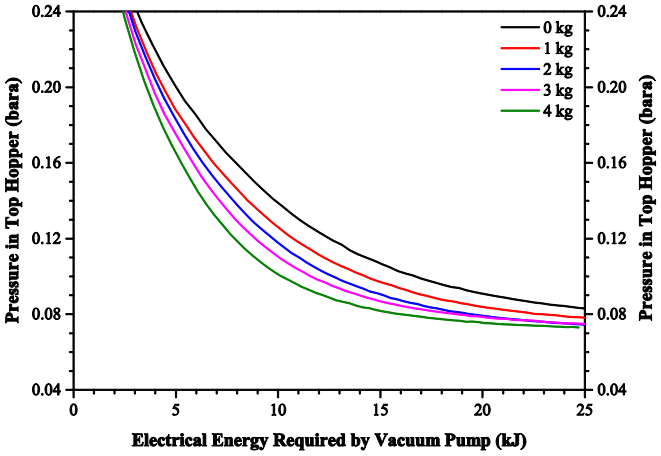

Figure 6-6: Energy required by the vacuum pump with varying batches of wood pellets in the top hopper.

Combining the results shown in both Figure 6-4 and Figure 6-6 indicates that the vacuum pump works most efficiently at the start of its operation, requiring a relatively small amount of energy to achieve the largest portion of the overall pressure drop.

6.4.2 Point of diminishing returns

Clearly there becomes a point where the decrease in pressure generated does not become worth the amount of energy supplied to bring about that change in pressure; this point can be viewed as the point

of diminishing returns. This point has been chosen arbitrarily as where the change in pressure generated from the previous state of pressure is equal to or less than 1% of the previous state of pressure. This can be written as:

$$0.01 \geq 1 - K_0$$

Equation 6-1

$$K_0 = \frac{P_2}{P_1}$$

Equation 6-1a

Where P_1 is the intake pressure (Pa), P_2 is the discharge pressure (Pa) and K_0 is the compression ratio. For a 4 kg batch of wood pellets this is realised at a pressure of 0.087 bara and after a time of 32 seconds. Table 6-3 provides an overview of the time taken to reach a given pressure that translates to diminishing returns for batches of wood pellets equal to 0 kg, 1 kg, 2 kg, 3 kg and 4 kg.

Mass of Batch (kg)	Volume in Top Hopper (ml)	Pressure (bara)	Time (s)	Diminishing Returns (%)
0	8730	0.094	41	0.67
1	7940	0.090	41	0.99
2	7145	0.088	38	0.90
3	6355	0.088	35	0.92
4	5560	0.087	32	0.98

Table 6-3: Effect of hopper volume on the time taken to reach the point of diminishing returns.

Although a value of 1% for the net pressure decrease over the initial pressure provides a good rule of thumb to determine the point of diminishing returns, it is more rational to treat the situation on an energy basis where gasification systems are concerned. There are two main energy components influencing gasification efficiency – electrical energy (used by the vacuum pump), and chemical energy (energy content of the syngas produced in the gasifier). Where the HLH operates without air evacuation, air ingress along with the fuel being fed is encountered. Air is predominantly comprised of two components – nitrogen (78.09 mol%) and oxygen (20.95 mol%), with trace amounts of other molecules (of which Argon is the most prevalent). Air ingress presents two issues – syngas dilution with inert nitrogen, and the waste of product syngas through combustion with oxygen. The issue relating to syngas dilution by nitrogen does not represent a major drawback. Nitrogen is commonly used as the pressurising agent in conventional lock hopper systems in far greater quantities than that present in the void space between the fuel in the lock at atmospheric pressure. Nitrogen is also commonly used as a transport medium for the pneumatic conveying of the fuel, and again in far greater quantities (Klinzing et al., 2010). Further to this, where gasification is operated in a combined cycle, nitrogen is often added to the product syngas stream with water as a measure for minimising NOx formation in the gas turbine. Its main role being to reduce the flame temperature and thus

minimise the formation of thermal NOx (Maurstad, 2005). The presence of oxygen in the lock prior to feeding on the other hand, does constitute a drawback by combusting the product syngas due its high temperature. Typically, temperatures between 600 °C and 1600 °C are encountered, but most commonly temperatures in excess of 1000 °C are found (Maurstad, 2005, Phillips, 2006, Higman and Van der Burgt, 2008).

The composition of the syngas stream produced depends on the operating temperature and pressure. Table 6-4 provides an overview of the composition of the syngas streams for seven cases, based on the operation of eight gasifier designs shown in Table 6-5. Cases 1-5 provide approximations to Shell, GE, E-Gas, PRENFLO and KBR type gasifiers where a coal feedstock is used, respectively Cases 6 and 7 provide approximations to a typical bubbling fluidised bed (BFB) and circulating fluidised bed (CFB) where a woody feedstock is used.

	Concentration (mol%)					
Case	**CO**	**H_2**	**CH_4**	**CO_2**	**H_2O**	**N_2**
1	55	30	0	3	7	5
2	15	15	0	10	60	0
3	29	30	1	15	25	0
4	60	22	0	3	0	15
5	15	15	5	10	25	30
6	10	15	10	25	0	40
7	20	21	4	15	0	40

Table 6-4: Composition of syngas for cases one to seven.

	Concentration (mol%)							
Component	**Shell**	**GE**	**E-Gas**	**PRENFLO**	**KBR**	**BFB**	**CFB**	**FB**
Fuel	Coal	Coal	Coal	Coal	Coal	Wood	Bark	MSW
Oxidant	O_2	O_2	O_2	O_2	O_2	Air	Air	O_2
CO	56.4	15.6	27.4	59.9	4-14	11.7	19.6	39.1
H_2	29.7	15.1	27.7	21.7	8-16	14.8	20.2	23.4
CH_4	-	-	0.094	<0.1	2-5	10.8	3.8	5.47
CO_2	1.4	7.3	16.5	2.9	12-14	22.4	13.5	24.4
H_2O	7	61	26.6	-	17-40	-	-	-
N_2	4.53	0.8	0.6	14.4	30-55	40.3	42.9	-

Table 6-5: Composition of syngas for a range of existing gasifiers (Spath et al., 1999, Ciferno and Marano, 2002, Maurstad, 2005, Guan et al., 2008, NETL, 2013).

It is interesting to analyse what effect the primary components of syngas have on both the heating value of the gas and on the amount of energy lost per mole of oxygen combusted. Figure 6-7 shows how the concentration of methane, hydrogen and carbon monoxide affect both of these parameters. In all three cases, 25 mol% of inert material is assumed which is broken up into 10 mol% carbon dioxide, 10 mol% water vapour and 5 mol% nitrogen. The two remaining combustible species from the specie

being varied are assumed to be present in equal concentrations. For example, if methane is being varied and assumed to be 5 mol%, carbon monoxide and hydrogen are present at a concentration of 35 mol% each.

Figure 6-7 shows that as the concentration of methane in the syngas increases, the heating value also increases. This is due to the higher enthalpy of combustion of methane compared to carbon monoxide and hydrogen. The enthalpies of combustion on a lower heating value basis for methane, carbon monoxide and hydrogen are -802.62 kJ/mol, -283 kJ/mol and -241.82 kJ/mol respectively (Yaws, 2003, DIPPR, 2012). However, when reviewing the same gas compositions in terms of the energy released per mole of oxygen consumed in the reaction, the opposite is found. As the methane concentration increases, the energy released decreases. This is simply due to the ratio of fuel to oxygen required by each of the primary components of the syngas. For both carbon monoxide and hydrogen a ratio of 2:1 is required, whereas for methane a ratio of 1:2 is required.

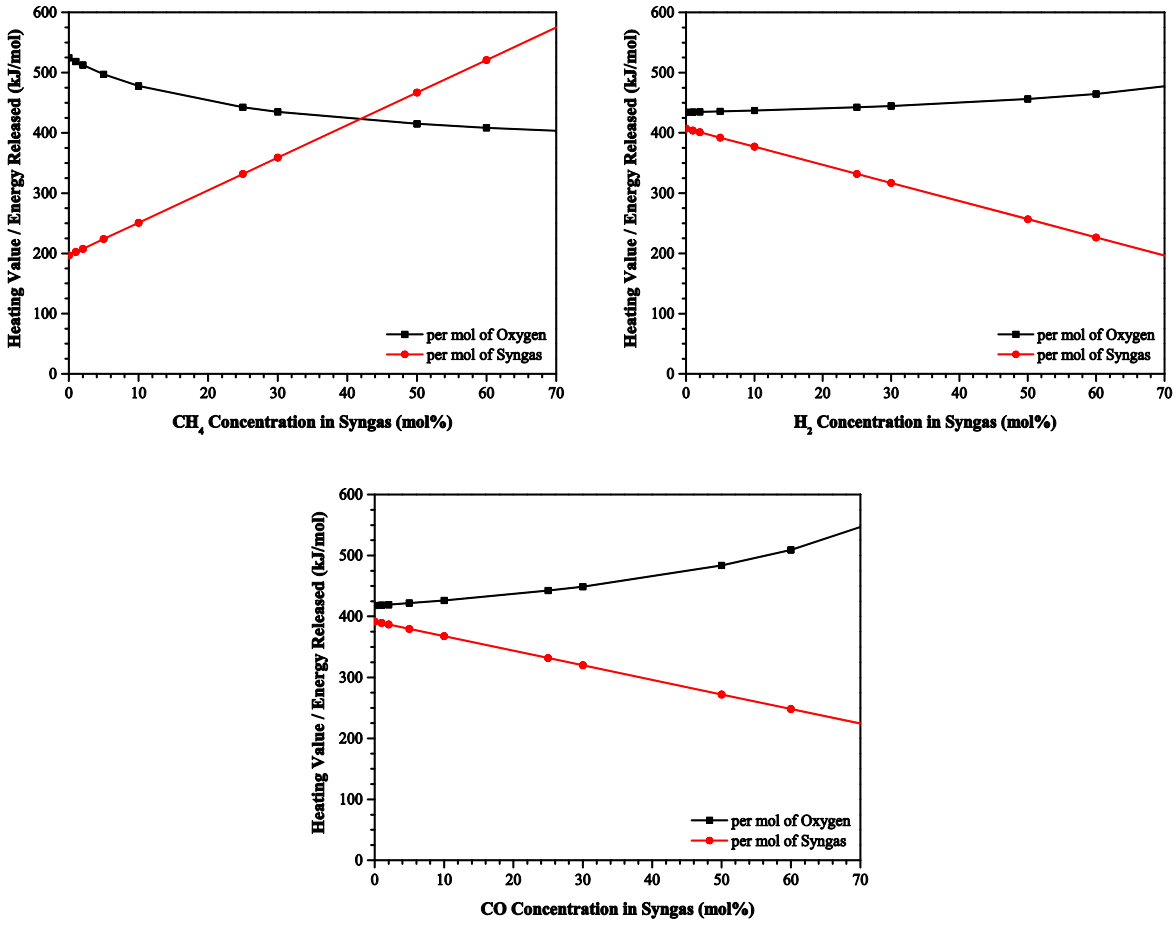

Figure 6-7: Heating value of syngas and energy released per mole oxygen combusted with varying methane, hydrogen and carbon monoxide concentration (left to right, top to bottom).

Figure 6-7 also highlights similar trends between hydrogen and carbon monoxide. As the concentration of each of these components is increased, the heating value of the syngas decreases;

however, the energy released per mole of oxygen combusted increases. Again, this is due to the respective enthalpies of combustion of each of the syngas components. As expected, the concentration of carbon monoxide has a greater effect than that of hydrogen on both the heating value of the syngas and the energy released per mole of oxygen combusted. This is due to the enthalpy of combustion of carbon monoxide (-283 kJ/mol) being slightly greater than that of hydrogen (-241.82 kJ/mol).

Strictly speaking, the syngas compositions presented in Table 6-4 and in Figure 6-7 do not represent accurate syngas compositions. Typically, syngas streams produced from gasification contain a multitude of different species in addition to those stated. Species such as argon, ammonia and hydrogen sulphide are commonly encountered in syngas streams; however, these are typically found in low concentrations. For the purpose of establishing the point of diminishing returns from the trade-off between the electrical energy required by the vacuum pump and the energy lost through syngas combustion, these components can be neglected. Figure 6-8 shows the amount of energy lost due to syngas combustion with the oxygen carried forward in the void space present in the top hopper.

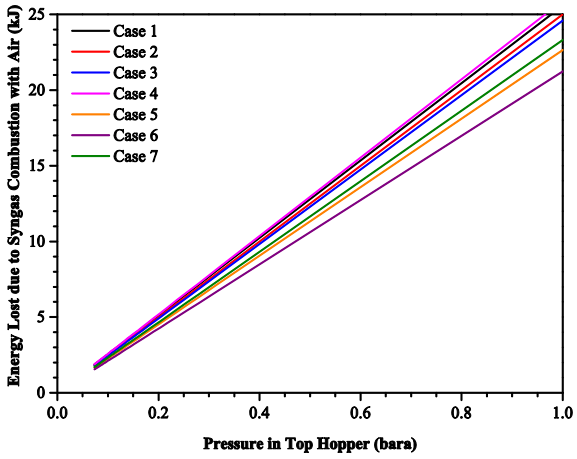

Figure 6-8: Energy lost due to syngas combustion with oxygen from the forward flow of air into the system.

Figure 6-8 displays a clear trend of decreasing energy lost with decreasing pressure in the top hopper. Where the pressure is reduced to a minimum of 0.073 bara, the energy lost due to syngas combustion is broadly equal between cases. A minimum energy lost of 1.55 kJ is found for Case 6 and a maximum energy lost of 1.89 kJ is found for Case 4 where the pressure in the top hopper is equal to 0.073 bara. Where no air evacuation takes place, the difference between cases is far larger. A maximum energy lost of 25.92 kJ is found for Case 4 and a minimum energy lost of 21.23 kJ is found for Case 6 where the pressure in the top hopper is equal to atmospheric pressure.

Figure 6-9 illustrates the trade-off between the energy required for air evacuation and the energy lost due to syngas combustion for Cases 1-7. This figure is obtained by combining the results for the energy required by the vacuum pump for a 4 kg batch of wood pellets (see Figure 6-6) and the results

for the energy lost due to syngas combustion (see Figure 6-8). All cases broadly highlight a minimum energy use where a pressure of approximately 0.25 bara is achieved. This constitutes a removal of approximately 75 vol% of the air contained in the top hopper. A general trend of decreasing overall energy use is observed with increasing pressure from case to case; however, this trend is slight and does not present a significant difference. A minimum overall energy use is observed in Case 6, with Case 6 < Case 5 < Case 7 < Case 3 < Case 2 < Case 1 < Case 4. This trend corresponds to the amount of energy released per mole of oxygen consumed.

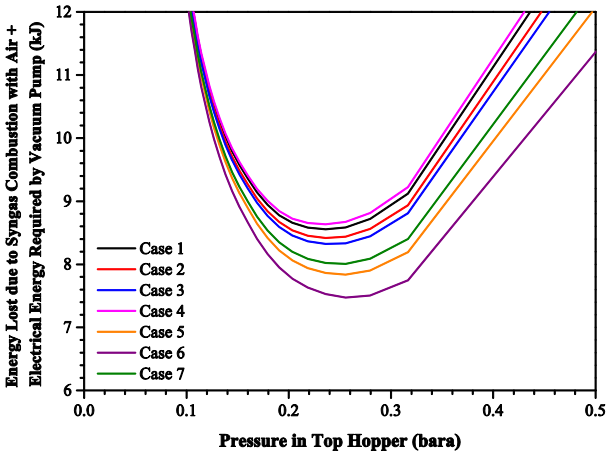

Figure 6-9: Trade-off between energy required for air evacuation and energy lost due to syngas combustion.

As the amount of energy released per mole of oxygen consumed increases, the total amount of energy used also increases. This is due in large part to the concentration of methane in the syngas stream and the ratio of carbon monoxide to hydrogen ($CO:H_2$). When the ratio of the sum of carbon monoxide and hydrogen to methane ($CO+H_2:CH_4$) is examined, it can be seen that as the ratio increases the total amount of energy used also increases. This is due to the respective stoichiometries of these reactions. Methane requires four more times the amount of oxygen that both carbon monoxide and hydrogen require on a mole for mole basis, which in turn means that for a methane-rich syngas, the amount of energy released is reduced where oxygen is the limiting reagent. Where methane is absent from the syngas stream, a trend of increasing total energy use is observed with increasing carbon monoxide to hydrogen ratio. In this case, the stoichiometry is equally paired. Therefore, in order to explain this trend, the enthalpy of combustion of each reactant is referred to. The enthalpy of combustion of carbon monoxide is greater than that of hydrogen by a small margin on a lower heating value basis. As the ratio of carbon monoxide to hydrogen increases, the energy per mole of oxygen consumed increases, as does the total energy used.

Table 6-6 provides an overview of the energy required to reach the point of diminishing returns for Cases 1-7. All cases roughly require 2 kJ of electrical energy to achieve a pressure of 0.25 bara, which

constitutes a minimum overall energy requirement of the process. The energy lost due to syngas combustion with the remaining oxygen present in the top hopper varies from case to case, with Case 5 and Case 1 presenting the lowest and highest case respectively.

Case	Vacuum Time (s)	Pressure (bara)	Syngas Energy (kJ)	Vacuum Energy (kJ)	Total Energy (kJ)
1	4	0.236	6.04	2.52	8.56
2	4	0.236	5.90	2.52	8.42
3	4	0.236	5.81	2.52	8.33
4	4	0.236	6.12	2.52	8.64
5	3	0.256	5.79	2.04	7.83
6	3	0.256	5.43	2.04	7.47
7	3	0.256	5.96	2.04	8.00

Table 6-6: Analysis of the energy required to reach the point of diminishing returns for Cases 1-7.

6.4.3 Safe initial pressure to minimise explosive environments

As previously stated, the impetus for the addition of the vacuum precursor was not to maximise process efficiency, but predominantly to maintain process safety. Figure 6-9 illustrates how process efficiency is maximised; however, it is important to review whether the attainment of such a low pressure presents a safe working limit in terms of dust explosion suppression.

As mentioned in Section 6.2, explosion suppression is chiefly enabled by the introduction of an inert gas to reduce the atmospheric oxygen concentration to a level where a self-sustained flame can no longer be propagated. It is important to state that creating a vacuum does not have the same effect as inerting; although the concentration of oxygen on a system volume basis is reduced through evacuation, the concentration of oxygen in the gas remains unchanged. Much work has been carried out regarding explosive environments at varying initial pressure (Dahoe et al., 1995, Wilén et al., 1998, Dennison, 1997, Conde Lázaro and García Torrent, 2000, Pilão et al., 2004, Amyotte et al., 1990, Walther and Schacke, 1986, Wiemann, 1987, Bartknecht, 1978, Pedersen and Wilkins, 1988). The main conclusion from such works is that the maximum final explosion pressure is related linearly to the initial pressure. Such a relationship can be written as:

$$P_{max} = \frac{P_{\max 0}}{P_0} \cdot P_a$$

Equation 6-2

Where P_a is the initial pressure (bara), P_{max} is the maximum explosion pressure at P_a (bara), P_0 is the known initial pressure (bara) and P_{max0} is the known maximum explosion pressure at P_0 (bara) (Wiemann, 1987). Wiemann indicates a constant (P_{max0}/P_0) of 8.76 for brown coal (Wiemann, 1987), Pedersen and Wilkins indicate a constant of 7 for sub-bituminous coal (Pedersen and Wilkins, 1988),

Conde Lazaro and Garcia Torrent indicate a constant of 8.07 for bituminous coal (Conde Lázaro and García Torrent, 2000), Bartknecht indicates a constant of 7.57 for starch (Bartknecht, 1978) and Walther and Schacke indicate a constant of 6.68 for benzoic acid (Walther and Schacke, 1986). Values for both the maximum explosion pressure and the maximum rate of pressure increase (K_{st}) are shown in Table 6-7 for a range of materials and for an initial pressure of 1 bara. K_{st} relates cubically to the enclosed volume ($K_{st} = V^{1/3}.dP/dt$) and as such, is presented with units "bar m/s". The K_{st} values reported thus correspond to an enclosed volume of 1 m^3 as $V^{1/3}$ becomes equal to 1 at such a volume, and in turn $K_{st} = dP/dt$ (Hauert, 2009, Explosion Hazard Testing Ltd, 2013).

Material	**K_{st} (bar m/s)**	**P_{max} (bara)**
Coal dust	85	6.4
Wood dust	224	10.3
Sewage sludge	102	8.1
Grain dust	89	9.3
Flour	63	9.7
Aluminium dust	515	11.2

Table 6-7: Overview of typical maximum pressures and maximum rate of pressure rises for an initial pressure of 1 bara (Explosion Hazard Testing Ltd, 2013).

Analysis of Equation 6-2 indicates that if the initial pressure is sufficiently low, the resultant maximum pressure generated will be lower than or equal to atmospheric pressure. Therefore, it can be stated that the damage potential from an explosion at this pressure does not exist (FM Global, 2013). The P_{max}/P_0 constant is in the range of 5-10 for most dusts. This means that, if the damage potential from an explosion is to be minimised to nil, an initial pressure between 0.1-0.2 bara is required.

As a side note to this, it is generally found that most dusts will not burn if the atmospheric pressure is reduced below 50 mbar (Birtwistle, 2003, FM Global, 2013). However, it is important to state that this is considered a severe precautionary measure and, in most cases, an initial pressure of less than 100 mbar is considered a safe working initial pressure. It is also quite common to introduce inerting systems where a high vacuum is used as the explosion mitigation method. Such systems provide a secondary route to explosion suppression where vacuum is lost (Eckhoff, 2003, FM Global, 2013).

By taking into account the initial pressure required to minimise the potential of explosion damage, a broadly similar pressure where a 1% decrease in pressure was imposed for the purposes of diminishing returns is obtained (Table 6-3). Therefore, Table 6-6 for syngas Cases 1-7 can be recalculated to take into account this new pressure limit (Table 6-8). Table 6-8 shows that the amount of energy lost due to syngas combustion has a far lower bearing on the total amount of energy where a pressure of 0.1 bara is achieved. Again, Case 6 embodies the lowest amount of energy and Case 4 the highest.

However, the difference between the two is far lower than the values previously reported in Table 6-6. Previously, Case 4 embodied approximately 15.8% more energy than Case 6, whereas now it only embodies 3.5% more energy. This is due to a larger reliance on the vacuum pump used to generate a sufficiently low pressure (0.1 bara). It can therefore be stated that the heating value of the syngas or the amount of energy lost due to syngas combustion with oxygen does not play a major role in terms of the energy requirement or energy lost.

Case	Vacuum Time (s)	Pressure (bara)	Syngas Energy (kJ)	Vacuum Energy (kJ)	Total Energy (kJ)
1	23	0.1	2.57	10.14	12.71
2	23	0.1	2.51	10.14	12.65
3	23	0.1	2.47	10.14	12.61
4	23	0.1	2.60	10.14	12.74
5	23	0.1	2.27	10.14	12.41
6	23	0.1	2.13	10.14	12.27
7	23	0.1	2.34	10.14	12.48

Table 6-8: Electrical energy required to achieve a vacuum of 0.1 bara and the energy lost due to syngas combustion for Cases 1-7.

6.5 Experimental results and discussion

6.5.1 Cycle analysis and operation

The addition of the precursory vacuum stage does not significantly alter the operation of the HLH. After a batch of fuel has been fed to the top hopper and V1 has been closed, V12 is opened and the vacuum pump is engaged (see Figure 6-2). After the pressure in the top hopper has been sufficiently lowered, V12 is closed and the vacuum pump is disengaged. The operating cycle of the HLH is now able to proceed unchanged in either Mode 1 or Mode 2. Figure 6-10 shows how the temperature and pressure of each vessel varies during operation at a gauge pressure of 25 bar in Mode 1.

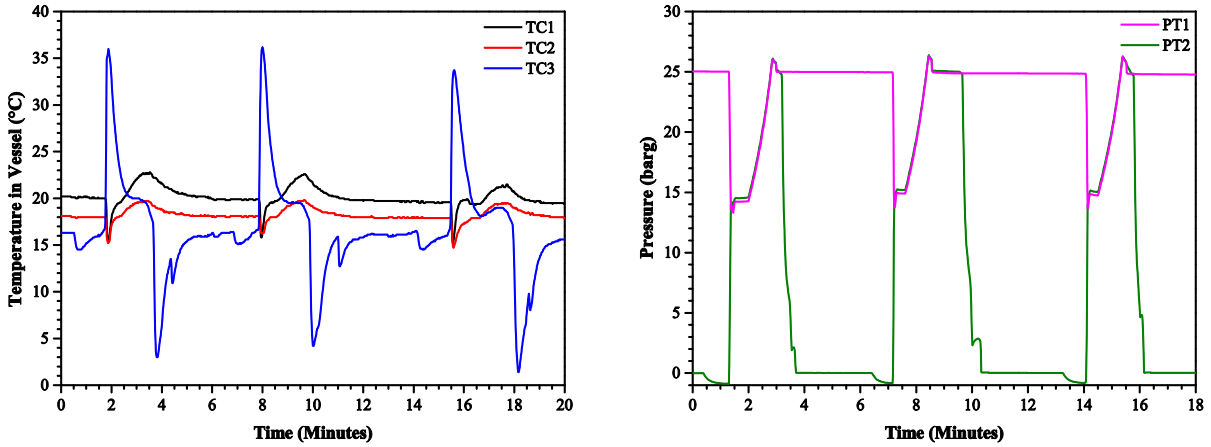

Figure 6-10: Temperature and pressure variations operating at 25 barg in Mode 1 with the vacuum precursor.

Figure 6-10 indicates that temperature and pressure variations do not differ greatly from those previously reported in Section 5.5.1.1 for the HLH operating in Mode 1 without the vacuum precursor. Peak temperatures are in line with compression phases and temperature lows are in line with expansion phases. TC1 presents a stable and fairly constant reading for the temperature in the collection vessel throughout operation, and peak temperatures are recorded by TC3 in the top hopper.

Although temperature and pressure variations are seen to be broadly similar to those previously reported, there are subtle differences between the two data sets. One of the key differences to the results reported previously is that at the point of pressure equalisation when both V2 and V4 are opened. The pressure reached in both the top and bottom hopper is recorded to be lower where the vacuum precursor is introduced. The pressure brought about through equalisation and the feeding of fuel from the top hopper to the bottom hopper is approximately 0.5-1 bar less than for previous results and is due to the level of vacuum achieved previous to feeding (0.1 bara). As with the other expansion phases of the feeding operation, a temperature decrease of the order of 2-3 °C is recorded in the top hopper during the vacuum precursory stage. However, this small temperature decrease has little effect on the considerably larger temperature increase recorded immediately after, during the pressure equalisation between the top and bottom hopper. In addition to operation in Mode 1, the vacuum precursor was also run in conjunction with Mode 2 at an operating pressure of 20 barg to investigate potential handling problems.

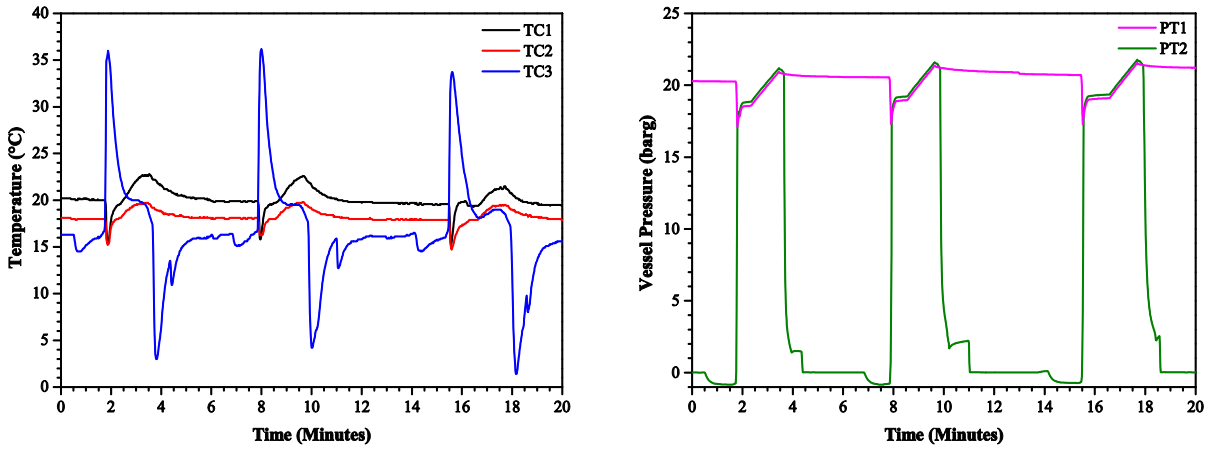

Figure 6-11: Temperature and pressure variations operating at 20 barg in Mode 2 with the vacuum precursor.

The pressure variations for operation in Mode 2 were not shown to be dramatically different from the results previously stated where operation without the vacuum precursor takes place (Figure 5-7). This is due to the larger increases in pressure observed in the top hopper after the opening of V2 and V4 and, in turn, the feeding of fuel to the bottom hopper/collection vessel. Due to pressure variations not varying dramatically from those previously recorded, further operation in Mode 2 with the vacuum precursor was ceased. In Mode 2 without the vacuum precursor, net increases in pressure were

recorded in the collection vessel after each batch of fuel had been fed. This was found to be due to the relatively small volume ratio between the collection vessel and the top hopper, and the top hopper being filled to capacity with water during the compression stage. This phenomenon is still observed where Mode 2 is operated with the vacuum precursor and is shown in Figure 6-11. Therefore, it can be said that results regarding both temperature and pressure variation, and the energy requirement of the high pressure water pump are not appreciably sensitive to the introduction of the vacuum precursor.

6.5.2 Mass flow rate and cycle time

The introduction of the vacuum precursor clearly has an effect on the overall cycle time and mass flow rate of the HLH. In the case of Mode 1, this is not only realised through the time required to bring about a vacuum, but also in the additional time taken to reach the required operating pressure in the compression stage and the time taken to drain the top hopper of water. In the case of Mode 2, the compression time is unchanged as the volume of water pumped in this stage is maintained constant regardless of the integration of the vacuum precursor. Therefore, the cycle time and mass flow rate in Mode 2 is only affected by the time taken to bring about a vacuum in the top hopper. Table 6-9 provides an overview of the results generated for the vacuum precursor to reach 0.1 bara for varying batches of wood pellets contained in the top hopper.

Mass (kg)	Volume (ml)	Time (s)
0	8730	35
1	7940	32
2	7145	29
3	6355	26
4	5560	23

Table 6-9: Effect of volume on the time taken to achieve 0.1 bara in the top hopper.

The key trend is that, as the mass of wood pellets in the top hopper increases and the available volume decreases, the time taken to bring about a pressure of 0.1 bara also decreases. Batches of 0 kg, 1 kg, 2 kg and 3 kg provide comparison cases to the 4 kg batch which is fed in reality. Such a relationship can be applied where higher voidage fuels are being fed. The results generated for the 4 kg case will be carried forward and used in further analysis of both the mass flow rate and the overall energy use of the HLH.

Table 6-10 provides an overview of how the three main parameters affect the cycle time of Mode 1 when operating with the vacuum precursor. Comparing these results to those previously reported where the vacuum precursor is omitted, it can be seen that the compression time marginally increases where the vacuum precursor is applied, and the time taken for water drainage is shown to marginally

decrease. The increase in compression time is expected due to the lower pressure generated where pressure equalisation between the top and bottom hopper takes place, and therefore a larger amount of water is required to be pumped to generate the operating pressure. This effect is substantiated further by reviewing the volume of water required in the compression stage (Table 6-10). Comparing these results to those previously stated for Mode 1 operating without the vacuum precursor shows an average difference of approximately 440 ml. That is, 440 ml more water is required to be pumped where Mode 1 operates with the vacuum precursor. The water drainage stage is shown on average to take less time where the vacuum precursor is added; however, the error stated in this case is larger than that stated for previous results without the vacuum stage. It is expected that the drainage stage takes longer where the vacuum precursor is added due to the larger volume of water drained. However, this has been shown not to be the case. Due to the error stated in both cases and the variability due to the use of manual valves, the time taken for drainage can be said to be unaffected by the addition of the vacuum precursor.

Pressure (barg)	Vacuum Precursor (s)	Water Compression (s)	Water Drainage (s)	Volume of Water (ml)
10	23 ± 0	57 ± 1	28 ± 3	6050 ± 77
15	23 ± 0	57 ± 2	27 ± 2	6014 ± 106
20	23 ± 0	56 ± 2	28 ± 3	5973 ± 163
25	23 ± 0	58 ± 2	28 ± 4	5937 ± 150

Table 6-10: Key parameters affecting the overall cycle time for operation in Mode 1 with the vacuum precursor and the volume of water required for compression.

Therefore, the only factor significantly affecting the overall cycle time and thus the mass flow rate of the HLH operating in Mode 1 with the vacuum precursor, is the time taken to reach a suitable vacuum in the top hopper. Figure 6-12 shows the adapted mass flow rate taking into account this time for both Mode 1 and Mode 2.

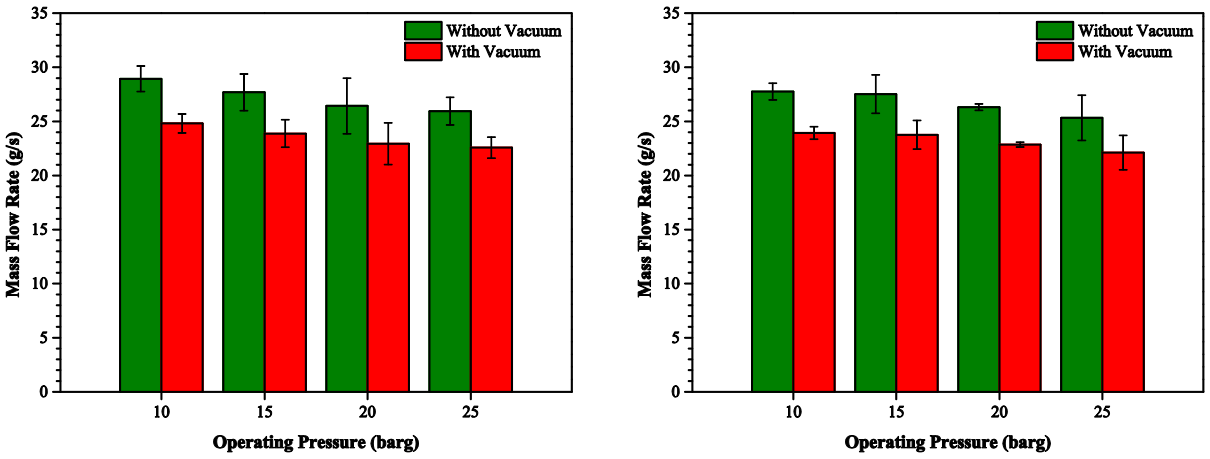

Figure 6-12: Mass flow rate of Mode 1 (left) and Mode 2 (right) with and without the vacuum precursor.

Figure 6-12 highlights a general trend of decreasing mass flow rate with increasing operating pressure for both modes of operation. As previously stated, this is due to manual valve activity. Gravity feeding, compression time and drainage time are all shown to be broadly constant, and manual valve activity is found to be the main variable. Chiefly, Figure 6-12 shows what effect the vacuum precursor has on the mass flow rate of both Mode 1 and Mode 2, and highlights the mass flow rate to decrease by approximately 3.3-4.2 g/s and 3.2-3.8 g/s for Mode 1 and Mode 2 respectively.

6.5.3 Energy requirement

In addition to decreasing the mass flow rate, the introduction of the vacuum precursor increases the overall amount of energy required to feed each batch of fuel. Table 6-11 and Figure 6-13 provide an overview of how the vacuum pump works to achieve a pressure of 0.1 bara by varying the mass of wood pellets per batch.

Mass (kg)	Volume (ml)	Power (W)
0	8730	452 ± 58
1	7940	419 ± 50
2	7145	419 ± 56
3	6355	431 ± 60
4	5560	414 ± 63

Table 6-11: Effect of volume on the power drawn by the two stage vacuum pump.

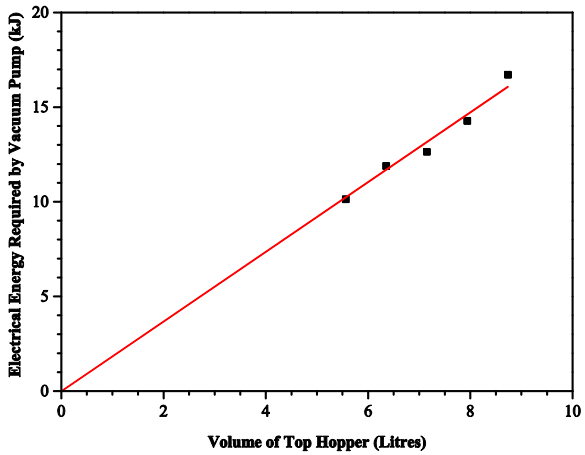

Figure 6-13: Relationship between volume and the energy requirement to attain 0.1 bara.

Table 6-11 shows that the vacuum pump works at a reasonably constant rate. It can be seen from Figure 6-13 that, as the mass per batch of fuel contained in the top hopper increases and the volume available decreases, the amount of energy required to bring about a pressure of 0.1 bara also decreases

at a fairly constant rate. As the mass per batch is increased, the available volume in the top hopper decreases, and so the volume required to be evacuated and reduced in pressure is decreased. Plotting these points and fitting a line that passes through the origin indicates a linear relationship with a slope of approximately 1.84. Such a relationship indicates that the energy required to bring about a pressure of 0.1 bara in the top hopper prior to feeding is minimised where low voidage fuels are used. For the purpose of this work, the energy required by the vacuum pump to achieve a pressure of 0.1 bara to feed a 4 kg batch is approximately equal to 10.14 kJ. In terms of the amount of energy per mass of fuel fed, this translates to approximately 2.54 kJ/kg.

However, the additional energy required where the vacuum precursor is enabled is not only felt through the electrical energy required by the vacuum pump. In the case of Mode 1, an additional strain is imposed on the high pressure water pump due to a greater pressure drop being encountered during the pressure equalisation stage. This was shown in Table 6-10 which highlighted a marginal increase in compression time where the vacuum precursor was used, and also a larger volume of water to be pumped during the compression stage. Table 6-12 provides a comparison between the energy required by the high pressure water pump operating with and without the vacuum precursor in place.

	Energy Use (kJ/kg)	
Pressure (barg)	**Mode 1 (No Vacuum)**	**Mode 1 (Vacuum)**
10	12.73 ± 0.77	12.93 ± 0.32
15	13.57 ± 0.83	13.77 ± 0.44
20	14.46 ± 0.50	14.59 ± 0.37
25	15.51 ± 0.33	15.69 ± 0.44

Table 6-12: Energy required by the high pressure water pump for operation in Mode 1 with and without the vacuum precursor.

It is clear from Table 6-12 that the high pressure water pump requires a larger amount of energy where the vacuum precursor is in place. However, the increase is slight and translates to approximately 1-1.5% more energy than if the pressure in the top hopper was left at atmospheric levels. As previously stated, the vacuum precursor is assumed to have no effect on the compression time and the energy required by the high pressure water pump when operating in Mode 2. This is simply due to the volume of water required in the compression stage of Mode 2 to be independent of the pressure drop encountered. A volume of approximately 7500 ml is required in the compression stage regardless of the pressure drop. Further to this, the results regarding energy use for Mode 2 did not strictly indicate energy requirements at set pressures as slight net increases of pressure were recorded during this mode of operation without the vacuum precursor. These net pressure increases were also observed for operation in Mode 2 with the vacuum precursor and are shown in Figure 6-11.

Combining the results recorded for the energy use of the vacuum precursor with those recorded for the high pressure water pump generates Figure 6-14. The same general trend of increasing energy use with increasing pressure is observed with the same gradient for each mode of operation. The vacuum precursor only adds a constant amount of energy to each respective point at pressure. It can be seen that in terms of the energy requirement of the HLH, the vacuum precursor has a greater effect on Mode 1 due to it initially having a lower energy requirement. Further to this, it can be seen that the vacuum precursor will be felt most in terms of energy use at lower operating pressures. For an operating pressure of 10 barg, the total energy use inclusive of the vacuum precursor is approximately 21.5% and 15% greater than without for Mode 1 and Mode 2 respectively. Comparatively, for an operating pressure of 25 barg, the total energy use inclusive of the vacuum precursor is approximately 17.5% and 12.3% greater than without for Mode 1 and Mode 2 respectively. Therefore, results suggest that, as operating pressures increase, the effect the vacuum precursor has on the total energy requirement will be diminished.

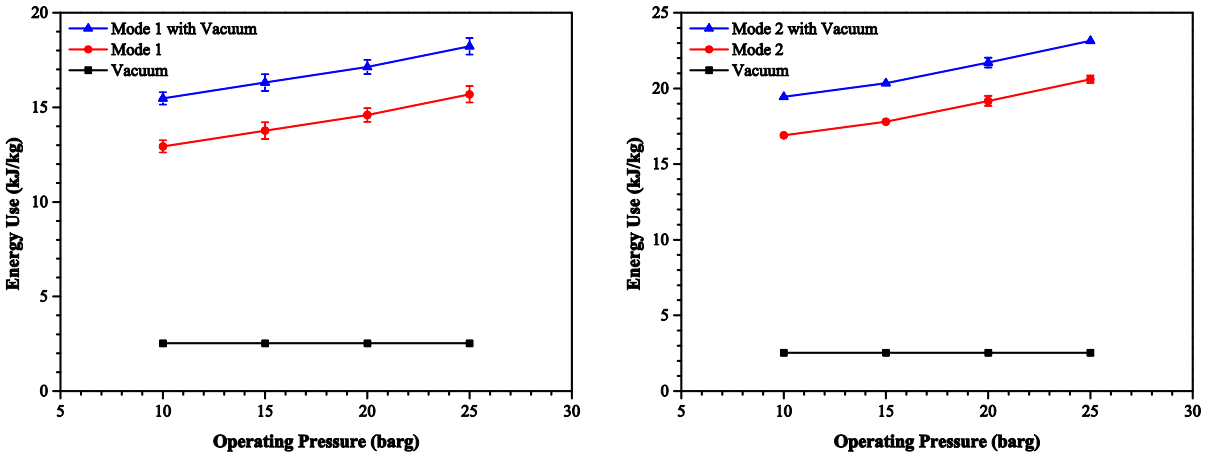

Figure 6-14: Energy requirement operating in Mode 1 (left) and Mode 2 (right) with the vacuum precursor.

In addition to reviewing how the energy use compares to previous results where the HLH has been operated without the vacuum precursor, Figure 6-15 shows how it compares to a conventional single and dual lock hopper. The HLH operating in Mode 1 with the vacuum precursor outperforms both a conventional single and dual lock hopper at all pressures. This is also true of Mode 2, with the exception of the 10 barg case where a dual lock hopper requires approximately 12.4% less energy per unit mass. As with previous results, the energy saving of the HLH increases with increasing operating pressure. Examining the 25 barg case, the HLH operating with the vacuum precursor is found to generate an energy saving of approximately 78.7% and 72.9% compared to a conventional single lock hopper for Mode 1 and Mode 2 respectively. Similarly, energy savings compared to a dual lock hopper at 25 barg of approximately 57.3% and 45.8% are recorded for Mode 1 and Mode 2 respectively.

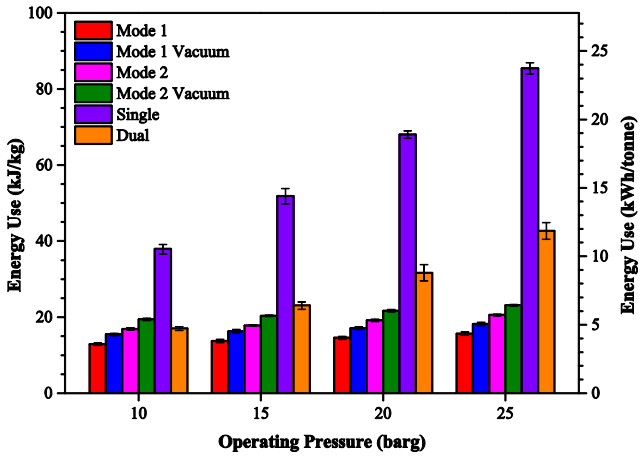

Figure 6-15: Energy use of the HLH operating with and without the vacuum precursor compared to a conventional single and dual lock hopper.

6.5.4 Energy requirement when feeding alternative fuels

Using Figure 6-13 which displays the relationship between volume and the energy required by the vacuum pump to generate a pressure of 0.1 bara, energy requirements to feed alternative fuels can be assessed. Table 6-13 highlights the mass per batch of each fuel fed, the respective void space present in the top hopper prior to feeding and the energy required by the vacuum pump.

Fuel	Mass per Batch (kg)	Void Space (litres)	Vacuum Energy (kJ)	Vacuum Energy per Mass (kJ/kg)
Wood pellets	4.00	5.56	10.15	2.54
Torrefied pellets	4.25	5.38	9.91	2.33
Ground anthracite	4.75	5.22	9.61	2.02
Torrefied wood chips	1.00	6.40	11.78	11.78
Milled wood pellets	2.00	7.42	13.66	6.83
Pulverised coal	3.50	6.41	11.80	3.37

Table 6-13: Energy requirement of the vacuum precursor for a range of fuels.

Taking the energy requirement of the vacuum precursor and combining it with the measured and predicted energy requirements for feeding the fuels stated in Section 5.6.3 (Table 5-12) generates Table 6-14 and Table 6-15 which present an overview of the energy requirements to feed when operating in Mode 1 and Mode 2 respectively with and without the vacuum precursor.

Although in the main the addition of the vacuum stage does not introduce a major energy penalty, it can be seen that a significant addition is made to the total energy requirement when feeding both the torrefied wood chips and the milled wood pellets. However, it is important to state that the vacuum precursor represents on average 13.5% (±0.9%) and 11.9% (±1.3%) of the total energy requirement for Mode 1 and Mode 2 respectively, and is maintained broadly constant regardless of the material being

handled. Therefore, it can be said that the variation in magnitude of the energy requirement of the vacuum stage is relative to the base energy requirement of the HLH for both modes of operation.

	Energy (kJ/kg)		
Fuel	**Mode 1**	**Vacuum**	**Total**
Wood pellets	15.51	2.54	18.05
Torrefied pellets	13.94	2.33	16.27
Ground anthracite	11.82	2.02	13.84
Torrefied wood chips	79.03*	11.78	90.81*
Milled wood pellets	49.64*	6.83	56.47*
Pulverised coal	22.64*	3.37	26.01*

Table 6-14: Energy required to feed fuels in Mode 1 at 25 barg inclusive and exclusive of the vacuum precursor. *Projected values.

	Energy (kJ/kg)		
Fuel	**Mode 2**	**Vacuum**	**Total**
Wood pellets	20.61	2.54	23.15
Torrefied pellets	19.40	2.33	21.73
Ground anthracite	17.35	2.02	19.37
Torrefied wood chips	82.43*	11.78	94.21*
Milled wood pellets	41.22*	6.83	48.05*
Pulverised coal	23.55*	3.37	26.92*

Table 6-15: Energy required to feed fuels in Mode 2 at 25 barg inclusive and exclusive of the vacuum precursor. *Projected values.

Reviewing energy savings generated by the HLH over conventional lock hopper systems, it can be seen that the reduction in energy saving brought about through adding the vacuum precursor is broadly constant across all fuels for operation in Mode 2. Energy savings are observed to drop by around 3% (±0.1%) for all fuels compared to a single lock hopper and by around 6.2% (±0.3%) compared to a dual lock hopper. Comparatively, decreases in energy savings where Mode 1 is concerned are not found to be as constant between fuels. Energy savings are observed to decrease by between 2% and 3% compared to a conventional single lock hopper when the vacuum precursor is introduced, and by between 4% and 6% compared to a dual lock hopper. The energy saving generated when feeding the standard wood pellets is seen to be the most affected by the addition of the vacuum precursor, whereas the milled wood pellets are seen to be the least affected. Although drops in energy saving are recorded for all fuels, energy savings are still significant and are greater than 50% in all cases.

6.5.5 Operational problems involving the vacuum precursor

During the characterisation of the vacuum precursor, the problem of solids holdup was repeatedly encountered when feeding standard wood pellets. After the pressure reduction to 0.1 bara in the top

hopper, wood pellets were repeatedly observed to not flow from the top hopper to the bottom hopper unless aided by external means (vibration). Similarly, holdup problems were encountered after the compression stage of the feeding process, as batches of wood pellets were observed to flow inconsistently from the bottom hopper to the collection vessel.

It is supposed that solids holdup takes place while operating with the vacuum precursor due to the extended time each batch of wood pellets spends in the top hopper prior to feeding to the bottom hopper, and subsequently the collection vessel. The time taken for a pressure of 0.1 bara to be reached was recorded to take on average 23 seconds. Problems due to solids holdup were observed consistently to take place during the feeding of batches two and three during a three batch cycle. It is supposed from this that solids holdup takes place due to the wood pellets having a longer time to absorb any residual water present in the top hopper, and the pellets losing their physical stability. Figure 6-16 shows results for the percentage moisture content increase of the wood pellets fed operating with and without the vacuum precursor in Mode 1.

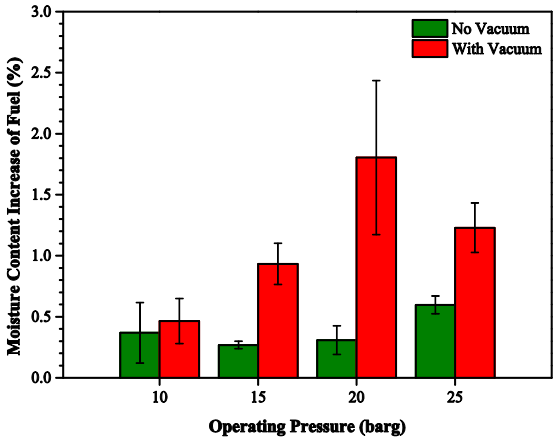

Figure 6-16: Moisture content increase operating with and without the vacuum precursor in Mode 1.

The moisture content of the wood pellets fed where the vacuum precursor is enabled increases more than where it is not enabled at each operating pressure. Figure 6-16 therefore indicates that solids holdup takes place due to the extended overall cycle time brought about by the introduction of the vacuum precursor. It is this, coupled with the residual moisture present in the top hopper after the water drainage stage, and the use of a moisture sensitive fuel that generates solids holdup. It is envisaged that moisture stable fuels such as ground coal grains and torrefied wood would not encounter such holdup problems due to their increased physical stability and hydrophobicity.

6.6 Summary

This chapter details the work undertaken with the HLH to facilitate its operation without the ingress of air. Such a development seeks to reduce hazardous conditions brought about when operating in

conjunction with gasification units, and increase process efficiency through minimising the energy penalty imposed by syngas combustion.

The forward flow of air was minimised through the addition of a vacuum pump to the top hopper. The pump was engaged prior to feeding each batch of fuel to allow the removal of air, and thus, hazardous conditions were minimised through the removal of oxygen. In order to assess the energy penalty incurred through the ingress of air, and in turn, syngas combustion, seven real-life syngas compositions were considered. Energetically, a pressure of around 0.25 bara was determined to be the most efficient pressure to achieve by the vacuum pump in all seven cases, taking into account the energy requirement of the vacuum pump and energy lost through syngas combustion. However, reviewing the conditions for explosion suppression, such a pressure was overruled and a pressure of 0.1 bara was deemed to be a safe initial pressure. Achieving such a pressure was found to require around four times that of the energy lost through syngas combustion, and brought about a specific energy requirement of approximately 2.54 kJ/kg for a 4 kg batch of wood pellets.

The introduction of the vacuum precursor was found to decrease the mass flow rate of the HLH by approximately 3.3-4.2 g/s and 3.2-3.8 g/s for Mode 1 and Mode 2 respectively. Only the time taken to engage and operate the vacuum pump was found to decrease the mass flow rate of both modes of operation, which was found on average to take 23 seconds when feeding a 4 kg batch of wood pellets. The time taken for the water compression stage of the feeding operation was found to be unaffected in the case of Mode 2 and marginally increase in Mode 1 due to a slightly larger volume of water required to be pumped. Mass flow rates varying between 22 g/s and 25 g/s were demonstrated for both modes of operation.

A slight increase in energy requirement was found for operation in Mode 1, whereas the energy requirement of Mode 2 was found to be unaffected. A larger drop in pressure in the bottom hopper was observed during operation in Mode 1 due to the lower initial pressure of the top hopper, and in turn, a larger amount of energy and water and was found to be required in the compression stage. However, increases in the energy requirement of the high pressure water pump were found to be eclipsed by that of the vacuum pump, and in turn, the vacuum pump was found to be the largest contributor to the increase in energy requirement of the HLH. Energy requirements of approximately 18.22 kJ/kg and 23.15 kJ/kg were found when feeding wood pellets at 25 barg in Mode 1 and Mode 2 respectively, which were found to translate to increases in energy requirements by around 16.2% and 12.3% compared to the HLH operating without the vacuum precursor.

In addition to the mass flow rate and energy requirement, the effect the vacuum precursor had on the moisture content of fuel was assessed. Although the vacuum pump was not found to introduce moisture into the system directly, the time taken to engage and operate the vacuum pump meant that each batch of fuel was stored in the top hopper for a longer period of time than if the HLH was

operating without the vacuum stage. This increase in time was found to allow each batch of fuel to absorb a greater portion of the residual moisture present in the top hopper. Moisture content increases were recorded to be greater at each operating pressure when handling wood pellets; however, moisture content increases were found to be less than 2 wt% in all cases. Although the HLH fitted with vacuum precursor was found to increase the moisture content of the fuel being fed by a greater proportion than when operating without it, moisture content increases were still observed to be relatively minor.

7

INDUSTRIAL OPTIMISATION AND ECONOMIC ANALYSIS

7.1 Introduction

Much has been stated about the gains in efficiency the HLH presents over conventional systems. However, unknowns still remain where the system is required to operate alongside a working process. This chapter primarily aims to optimise the HLH for use on site in a working plant. It details the changes required to be made to the HLH in its current form, and specifies the additional equipment and processes required for scale-up. In addition to this, the efficiency gains demonstrated by the HLH over competing lock hopper designs will be assessed for an industrial scale unit, and the effect they have on energy, cost and carbon savings will be analysed. An economic assessment of a HLH unit required to feed to a 10 MW, 50 MW, 100 MW, 175 MW and 250 MW gasification plant will be undertaken, and an economic comparison will be made with a conventional single lock hopper system. The effect that operating pressure has on the economics of both types of feed system will be analysed, in addition to plant capacity.

7.2 Optimisation for an industrial setting

7.2.1 Valves

One of the factors limiting the scale-up of the HLH in its current form is the use of ball valves. For the purpose of this work, ball valves were selected due to their manual ease of use and their high

pressure rating compared to alternative valves. However, the use of ball valves on a large scale is often found to be economically unfavourable compared to competing valve designs due to their size and the vulnerability of their sealing element.

The key problem found with conventional valves when feeding solid materials to pressurised environments is degradation. Solids are found to interact with the sealing element and the seat of the valve and cause deformities which compromise the sealing ability of the valve. This phenomenon is common among the majority of valves, and in this respect ball valves are no different and pose a suitable choice. However, compared to competing valve designs, the sealing element in ball valves is far more costly to replace when damaged due to the complexity of its construction and manufacture. In addition to this, where high feed rates are required, the size of the valve is required to be far larger than competing valves due to the sealing element taking the form of a bored sphere and the height of the valve being approximately equal to the diameter. Where a seal is required to be made by a valve in a system that feeds solid materials, the valve component will always be sacrificial due to degradation. Therefore, simpler designs are favoured for economic reasons.

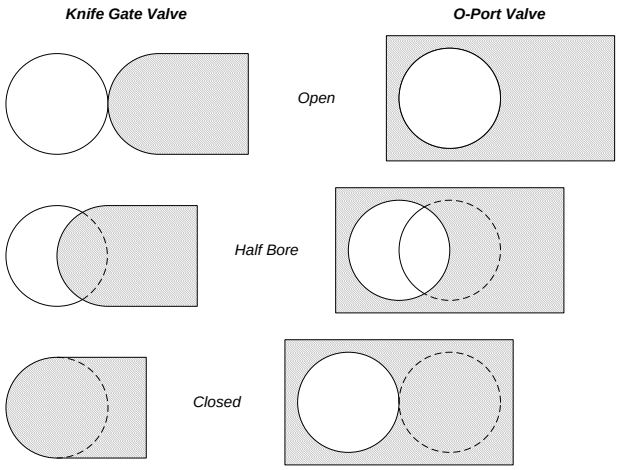

Figure 7-1: Configuration of a knife gate and an O-Port valve.

Two valve designs more appropriate for use in an industrial setting for use with solids are knife gate valves and O-Port valves. Knife gate valves present a more resilient configuration of a gate valve and utilise a sealing element with a sharp leading edge to reduce the build up of solids in the seat of the valve. O-Port valves are similar to conventional gate valves; however, the sealing element does not fit directly into the seat of the valve as with knife gate valves. Moreover, an O-Port valve creates a void space within the seat of the valve once closed and provides a place where any contaminant can be contained when the valve is sealed. Where contaminants are present in conventional gate valves, the contaminant reduces the sealing ability of the valve as it acts as a barrier between the sealing element and the seat of the valve. In an O-Port valve configuration, the contaminant specie is freed once the

valve is reopened. Figure 7-1 highlights both a knife gate valve and an O-Port valve in an open, half bore and closed configuration.

Knife gate valves have previously been demonstrated in commercial designs of conventional lock hopper feed systems. Most notably is in the design developed by T. R. Miles Consulting Engineers (Guzdar and Harvey, 1982, Cummer and Brown, 2002). No formal accounts of O-Port valves being used in conjunction with lock hoppers have been made; however, O-Port valves are commonly used in systems where solid materials, suspended solids and slurries are handled (Cowan Dynamics, 2013, DeZURIK, 2014, Stainless Valve Co., 2014).

7.2.2 Hopper geometry and continuous operation

Hopper geometry is governed by inter-particle and wall-particle friction effects, and as such, the geometry of a hopper is subject to change from material to material. Section 4.4 details the material tests required to determine the hopper geometry for a given material and Table 4-9 and Table 4-11 (Table 4-12) provide an overview of the hopper half angle and hopper outlet diameter required to obtain flow respectively for a range of solid materials and for a range of materials used for hopper construction. Figure 4-21 highlights that where wall materials are wetted, wall friction effects are heightened. This in turn affects the required hopper half angle to obtain flow, and it can be seen in Table 4-9 that in some cases the hopper angle is reduced to zero.

In addition to this, when operating the HLH in conjunction with moisture unstable materials, namely wood pellets, flow problems have been found to take place. When operating the HLH, flow was found to be hampered by surface moisture present on the hopper walls. Furthermore, where water drainage was incomplete via the siphon and an appreciable volume of water remained, wood pellets were found to expand and cause blockages, limiting the flow of material. Such problems were not observed when feeding either the torrefied wood pellets or the ground anthracite coal grains; fuels with higher degrees of hydrophobictity.

With both of these factors in mind, it is proposed that future configurations of the HLH dispose of the hopper geometry developed in this study and incorporate straight walled lock vessels either in a parallel or flared arrangement as shown in Figure 7-2. Such configurations will act to minimise solids holdup where moisture unstable materials are being fed and will ensure total discharge when feeding. Where continuous operation is necessitated, one of two systems can be deployed. Either a screw conveyor can be deployed in the collection vessel of the HLH and a head of material greater than the volume of each lock vessel can be allowed to build up, or a pneumatic conveying system can be fitted. Both designs have been developed in previous works and made commercial by T. R. Miles Consulting Engineers and Macawber Engineering Inc. respectively. A schematic incorporating both feed systems

is highlighted in Figure 7-2. Where pneumatic conveying is deployed, operation may be costly due to the pressure required to convey in a system at elevated pressure. It is therefore proposed that the system takes advantage of the elevated pressure of the system and feeds to a vessel at a pressure in excess of the system required to be fed to downstream; thereby taking advantage of the natural pressure gradient setup.

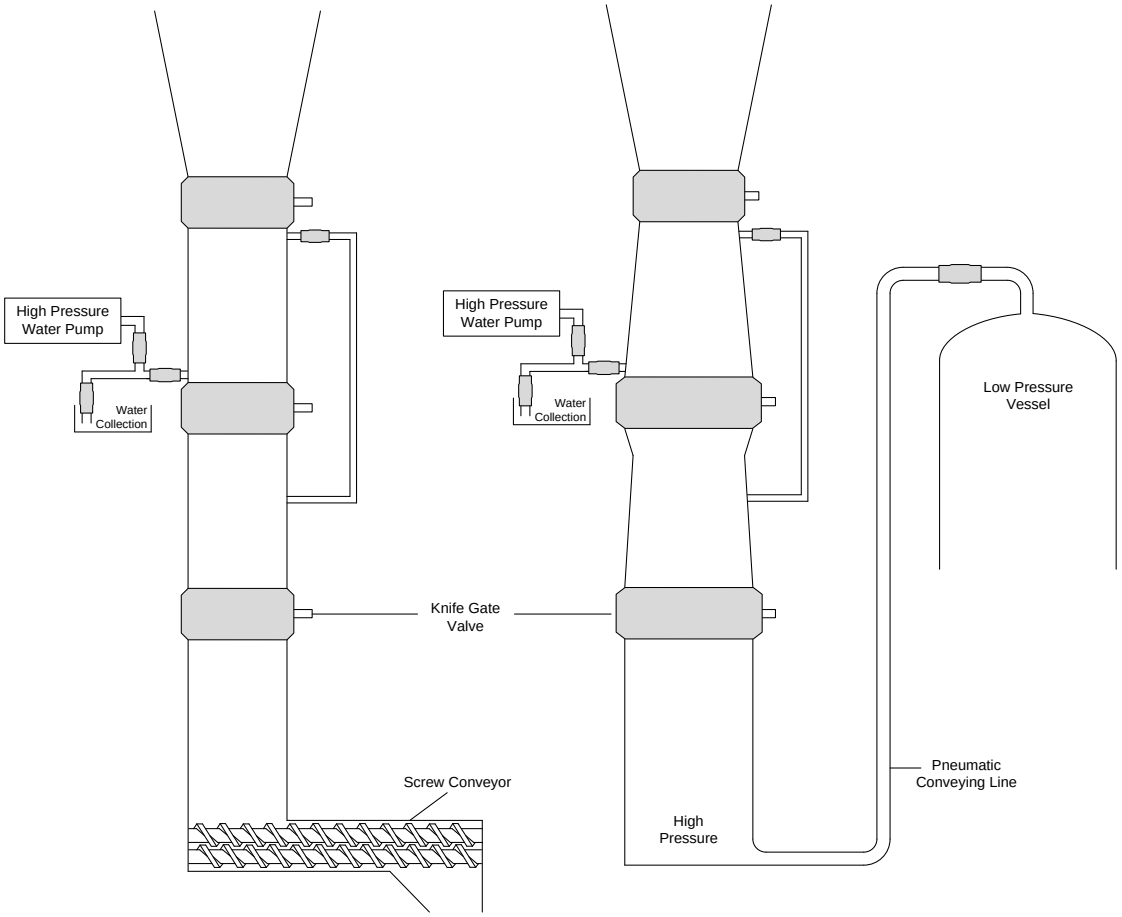

Figure 7-2: Straight and flared HLH configurations fitted with a screw feeder and pneumatic conveying line (left to right).

Although the designs proposed and shown in Figure 7-2 will minimise solids holdup where moisture unstable materials are being fed, it is important to state that such hopper/vessel geometries will require valves with considerable diameters when used on an industrial scale. This, coupled with the requirement to operate at high pressures brings about a considerable cost. Data obtained from Orbinox suggests a price of around £11,500 for a knife gate valve with a diameter of 0.6 m (PN10) (Parrett, 2014). Taking the same valve model (ET) with a smaller diameter and reviewing its associated cost, it is possible to determine a rough exponent for use in Equation 7-7 to estimate valves with larger diameters. Undertaking such an assessment generates an exponent of around 1.49. It is anticipated that for large scale systems, vessel geometry will be dictated by the cost of the associated valve.

7.2.3 Water treatment cycle

An element that has not been assessed in this study is that of water use, and more specifically, water treatment and storage. While operating the HLH, suspended solids were consistently found in the used water after depressurisation and drainage. In this study, water has been used in batches and supplied fresh from mains during each cycle. Where the HLH is scaled-up, water will be required in larger volumes and therefore it is appropriate for the water used to be recycled in a closed loop. Such a system requires two key elements to operate effectively – a storage tank and a solid-liquid separation device. Figure 7-3 displays a schematic of such a configuration.

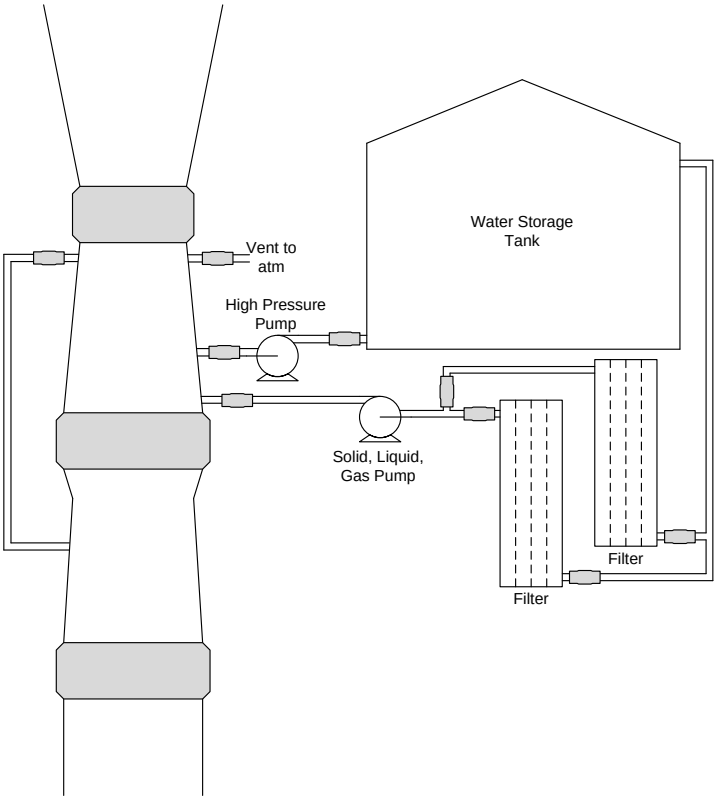

Figure 7-3: HLH incorporating water re-use.

When selecting a solid-liquid separation device, two parameters are of primary concern – the concentration of solids and the particle size. Where gasification is concerned, particle size is largely governed by the gasifier type, with entrained flow gasifiers requiring tighter specification and smaller particle sizes than fixed or fluid bed systems. Fuel type also effects particle size and it is generally found that biomass species are more reactive than coal species due to their higher volatile content, and therefore coal species require smaller particle sizes to ensure complete conversion. Taking a bituminous coal fed entrained flow gasifier as an example, a particle size of the order of 50-100 μm is assumed (Van der Drift et al., 2004). In terms of the concentration of solids in the water used for compression in the HLH, contamination was generally found to be low and is estimated at no more

than 1 wt% solids. Reviewing Figure 7-4 it can be seen that such criteria indicate that either a filter or centrifuge is best suited to handle the contaminated water stream.

Where continuous operation is required, filters must be able to be isolated and fitted in parallel to allow for downtime, removal of the filter cake built up and regeneration. The frequency of switching between the two filters is reliant on the scale of the HLH and similarly the scale of the filter. Typically filter cakes are found to build up to around 30-50 mm in thickness before being removed (Wakeman and Tarleton, 2006). However, as in most situations there lies an optimum. In this case, the optimum filter cake thickness is a product of the pressure drop generated by the filter cake, the efficiency of the pump and the time taken to regenerate the filter. Equations 7-1 to 7-4 can be used to assess the filter cake thickness and the pressure drop encountered for a given volumetric flow rate, time and filter area.

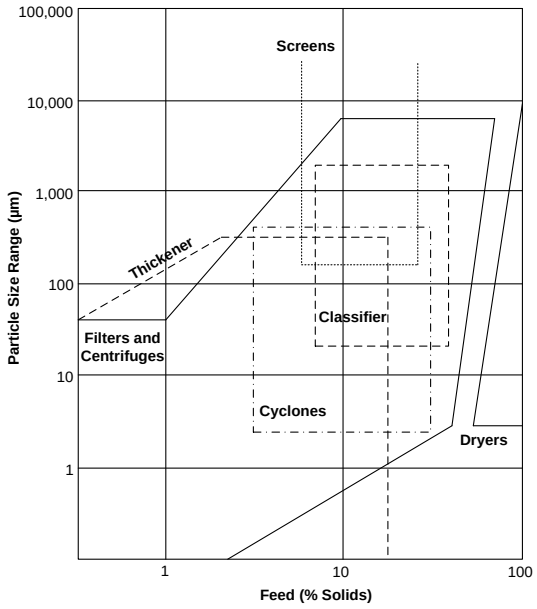

Figure 7-4: Solid-liquid separation systems based on particle size and concentration (Sinnott, 2007).

$$l_{\mathrm{fc}} = \frac{J\, V_{\mathrm{f}}\, \rho_{\mathrm{fi}}}{A_{\mathrm{fc}}[(1-J)(1-e_{\mathrm{fc}})\rho_{\mathrm{s}} - J e_{\mathrm{fc}}\, \rho_{\mathrm{fi}}]}$$

Equation 7-1

$$v_{\mathrm{fc}} = \frac{J\rho_{\mathrm{fi}}}{(1-J)(1-e_{\mathrm{fc}})\rho_{\mathrm{s}} - J e_{\mathrm{fc}}\, \rho_{\mathrm{fi}}}$$

Equation 7-2

$$r_{\mathrm{fc}} = \frac{5(1-e_{\mathrm{fc}})^2 S^2}{{e_{\mathrm{fc}}}^3}$$

Equation 7-3

$$V_f^2 + \frac{L_{fc}\, A_{fc}}{\upsilon_{fc}} V_f = \frac{A_{fc}^2 (-\Delta P)}{r_{fc}\, \mu_f\, \upsilon_{fc}} t$$

Equation 7-4

Where l_{fc} is the filter cake thickness (m), J is the mass fraction of solids in the liquid stream, V_f is the volume of filtrate (m^3) that has passed in time t (s), A_{fc} is the cross-sectional area of the filter cake (m^2), e_{fc} is the voidage of the filter cake, ρ_s is the density of the solids (kg/m^3), ρ_{fi} is the density of the filtrate (kg/m^3), υ_{fc} is the volume of the filter cake deposited by unit volume of filtrate, r_{fc} is the specific resistance of the filter cake (m^{-2}), S is the specific surface area of the solid particles, μ_f is the viscosity of the filtrate (Ns/m^2) and ΔP is the applied pressure difference (N/m^2). L_{fc} is the filter cloth resistance expressed in terms of filter cake thickness (m) (Richardson et al., 2002).

As the pressure drop is a function of the volume of filtrate passed through the filter, a clear relation can be made between the number of cycles the HLH goes through and the filter cake thickness. In turn, the number of cycles the HLH goes through before the filter is required to be regenerated can be defined. Table 7-1 highlights the operating conditions for a filter sized to treat the water stream generated by the HLH detailed in this study. The filter in this case utilises a filter cloth with a resistance equivalent to 10 cm of filter cake and is comprised of 10 units, 10 cm squared giving a total filter area of 0.1 m^2.

Variable	Mode 1	Mode 2
Water per hopper (litres)	5.5	7.5
Drainage time (s)	30	33
Mass fraction	0.01	0.01
Particle size (μm)	200	200
Voidage	0.5	0.5
Filter cake thickness (cm)	3	3
Pressure drop (Pa)	2149	2664
Number of cycles	40	30

Table 7-1: Operating conditions for a 0.1 m^2 filter sized to remove pulverised coal from a water stream.

The pump prior to the filter unit must be selected so that it is able to overcome the pressure drop generated by the build up of filter cake on the filter cloth. It can be seen from Table 7-1 that for the conditions computed, this ranges between a head of 0.2 m and 0.3 m. Such a pressure does not present a significant problem and this by and large owes to the modest material voidage presented by the pulverised coal filter cake. Material voidage is the primary factor that affects the pressure drop encountered across a filter, and therefore it is crucial that this parameter is known when assessing a pump to overcome the pressure difference presented by a filter and the associated filter cake.

Due to the pumping of water taking place in batches during the drainage stage, the pump must be capable of pumping three phases. Although this is primarily due to the water slurry not being

continually drained, it is also anticipated that gas will be released from the slurry after depressurisation in accordance with Henry's law. Although this phenomenon is minor in the case of most gases associated with gasification, carbon dioxide is found to dissolve strongly in water at pressure and must be taken into account where carbon dioxide partial pressures are high. Where gasification is concerned, the concentration of carbon dioxide should not be sufficiently great to present a significant problem; however, where pump selection is concerned, it is important to take this phenomenon into account to minimise damage to the pump.

Further to the pump and filter configuration, a suitable store for the water must be introduced. For the purpose of the HLH this can take the form of a conical roofed liquid storage tank. It is proposed that the tank volume should be of the order of three to five times the volume of the HLH to allow for water treatment and recirculation to the tank. The primary load to be considered where liquid storage tanks are concerned is the hydrostatic pressure presented by the liquid being stored. Equation 7-5 can be used to assess the minimum tank thickness required to hold a given volume of liquid.

$$e_s = \frac{\rho_L H_L g}{2 f_t J} \frac{D_t}{10^3}$$

Equation 7-5

Where e_s is the tank thickness (mm) at a depth of liquid H_L (m), ρ_L is the liquid density (kg/m^3), f_t is the tank material design stress (N/mm^2), J is the joint factor and D_t is the tank diameter (m) (BSEN14015, 2005, Sinnott, 2007). The design stress is typically equal to two thirds of the yield strength of the tank material but should not exceed 260 N/mm^2. When calculating the wall thickness, the joint factor should be set equal to 1 (BSEN14015, 2005).

7.3 Economic and environmental implications for industry

The economic implications of using the HLH in place of conventional pressurised feed systems are great. What is most notable about the HLH when compared to conventional systems is the reduction in energy required to feed, and savings can be assessed either in terms of the fuel saving, or in terms of the energy price to operate the system. Where power generation is concerned, it is most convenient to assess the energy requirement of the feed system in terms of the energy content of the fuel being fed, as the energy requirement can also be expressed in terms of energy per unit mass. Taking the HHV of an average biomass fuel to be 18.90 MJ/kg (Neves et al., 2011), the energy requirements of Mode 1, Mode 2 and a conventional lock hopper can be translated to be equal to approximately 0.082%, 0.11% and 0.45% the energy content of the fuel respectively. Similarly, it can be found that the respective energy requirements translate to approximately 0.048%, 0.064% and 0.27% of the energy content of an average bituminous coal where a HHV of 32 MJ/kg is assumed (Higman and Van der Burgt, 2008).

Taking such requirements and applying them to a working plant allows fuel, energy and carbon savings to be assessed.

Table 7-2 and Table 7-3 highlight savings generated by gasification plants utilising the HLH over a conventional and a dual lock hopper respectively per MW output. Two cases are computed for each comparison, one that assumes a biomass feed and the other a coal feed; and two separate cases are computed for the HLH, one incorporating the vacuum precursor and one without. Plant efficiency is assumed to stay constant at 48% (Higman and Van der Burgt, 2008) for each case, and an onsite electricity price is assumed to be 40 £/MWh (Peralta-Solorio, 2013). CO_2 savings assume a fuel fixed carbon content of 48 wt% for biomass (Neves et al., 2011) and 78 wt% for coal (Higman and Van der Burgt, 2008).

	Comparison to a Conventional Single Lock Hopper				
Fuel	**HLH Configuration**	**Fuel kg/day per MW**	**Electricity kWh/day per MW**	**CO2 kg/day per MW**	**Cost £/day per MW**
Bituminous Coal 32 MJ/kg	Mode 1	25.6	109.3	73.3	4.4
	Mode 1 Vac.	24.6	105.1	70.4	4.2
	Mode 2	23.8	101.3	67.9	4.1
	Mode 2 Vac.	22.8	97.4	65.3	3.9
Biomass 18.9 MJ/kg	Mode 1	73.4	185.1	129.3	7.4
	Mode 1 Vac.	70.6	177.9	124.2	7.1
	Mode 2	68.1	171.6	119.8	6.9
	Mode 2 Vac.	65.4	164.9	115.2	6.6

Table 7-2: Daily fuel, electricity, CO_2 and cost savings generated by using the HLH in place of a conventional single lock hopper per MW output of a coal and biomass fed gasification plant.

	Comparison to a Conventional Dual Lock Hopper				
Fuel	**HLH Configuration**	**Fuel kg/day per MW**	**Electricity kWh/day per MW**	**CO2 kg/day per MW**	**Cost £/day per MW**
Bituminous Coal 32 MJ/kg	Mode 1	10.0	42.5	28.5	1.7
	Mode 1 Vac.	9.0	38.2	25.6	1.5
	Mode 2	8.1	34.5	23.1	1.4
	Mode 2 Vac.	7.2	30.6	20.5	1.2
Biomass 18.9 MJ/kg	Mode 1	28.5	71.9	50.2	2.9
	Mode 1 Vac.	25.7	64.7	45.2	2.6
	Mode 2	23.2	58.4	40.8	2.3
	Mode 2 Vac.	20.5	51.7	36.1	2.1

Table 7-3: Daily fuel, electricity, CO_2 and cost savings generated by using the HLH in place of a dual lock hopper per MW output of a coal and biomass fed gasification plant.

Table 7-2 and Table 7-3 indicate savings to increase for lower calorific value fuels. This is primarily due to lower calorific value fuels requiring higher throughputs to attain the same power rating as when higher calorific value fuels are used. A larger number of cycles are required by the feed system and in turn savings are found to increase.

7.4 Calculation procedure and economic assumptions

Having assessed the economic implications of implementing the HLH compared to a conventional single lock hopper in terms of operating efficiency, it is appropriate to assess the capital cost of such a system and compare it to its conventional counterpart. At this stage in the development of the HLH, a preliminary estimate in the capital cost will be made using ratio and proportionate estimating. Specifically costs will be estimated using costs indices and the "rule of six-tenths". Such methods provide satisfactory cost estimates where approximate costs are required and generally generate a value within an accuracy of plus or minus 30% (Sinnott, 2007).

7.4.1 Cost indices

Cost indices are assessed using the relationship shown in Equation 7-6. Where C_c is the current cost of a piece of equipment (£), C_0 is the base cost of the same piece of equipment (£), I is the current cost index and I_0 is the base cost index (Sinnott, 2007).

$$C_c = C_0 \left(\frac{I}{I_0}\right)$$

Equation 7-6

Numerous cost indices are available; however, the cost index used in this study is the Chemical Engineering Plant Cost Index (CEPCI) which has been in existence since the early 1960s and uses the period of 1957-1959 as a base of 100 (Vatavuk, 2002). The CEPCI is broadly split into four sub-indexes with respective weightings attached. These are equipment, construction labour, buildings and engineering supervision (Vatavuk, 2002). The two key indexes that make up the CEPCI are equipment and construction labour which comprise 51% and 45% of the overall index respectively (Vatavuk, 2002). Care should be taken when using cost indices, especially over extended periods of time as changes both in the technological and social landscape can dramatically affect costing. A limit for the effective use of cost indices is typically set at five years, with higher degrees of error being found where indices greater than this are used. Although a limit of five years is usually used, cost indices can still be reliably used over longer periods of time where there have been few technological advancements and legislative changes to the equipment or process in question. Table 7-4 provides an overview of the CEPCI from the year 2000.

Year	CEPCI	Year	CEPCI
2013	567.3	2006	499.6
2012	584.6	2005	468.2
2011	585.7	2004	444.2
2010	550.8	2003	402.0
2009	521.9	2002	395.6
2008	575.4	2001	394.3
2007	525.4	2000	394.1

Table 7-4: Historic overview of the CEPCI.

7.4.2 Rule of six-tenths

The rule of six-tenths is stated in Eqiuation 7-7. Where C_B is the capital cost of a piece of equipment (£) of size or capacity S_B, and C_A is the capital cost of a piece of equipment (£) of size or capacity S_A (Sinnott, 2007).

$$C_B = C_A \left(\frac{S_B}{S_A}\right)^n$$

Equation 7-7

The index n is the exponent associated with the type of equipment in question, but it is commonly taken as 0.6 where data is unavailable and as such gives rise to the namesake of Equation 7-7 (Sinnott, 2007). Table 7-5 provides an overview of exponents associated with various pieces of equipment and the range where they can be reliably used.

Component	Unit	Range	Exponent
Conical roofed tank	m^3	450-27,000	0.57
Drum dryer	m^2	0.9-37	0.52
Electrostatic precipitator	m^3/s	37.8-472	0.81
Belt conveyor	m^2	5.6-18.6	0.50
Screw conveyor	m.mm	390-780	0.46
Atmospheric vessel	m^3	0.4-76	0.30
Pressure vessel (150 psi)	m^3	0.4-302	0.62
Centrifugal pump	kW	30-300	0.67
Plate and frame filter	m^2	0.9-93	0.55
Pressure leaf filter	m^2	2.8-140	0.57
Reciprocating compressor	kW	0.75-1490	0.84
Centrifuge	m^2	0.65-7.43	0.65
AC induction motor	kW	18.6-149	0.77

Table 7-5: Exponents associated with process equipment (Perry et al., 1997).

7.4.3 Assumptions for capital cost estimations

Where the feed system for a process is concerned, it is appropriate to assess the front end as a whole in addition to the feed system as a standalone component. This primarily means incorporating a fuel

store and an appropriate method for delivering the fuel to the feed system. The process boundary therefore lies at the point of delivery to the plant, and costing for the HLH will take into account both of these components in addition to the components required to construct the HLH as a standalone device.

Five cases are estimated with capacities capable of feeding to gasification plants with electric outputs of 10 MW, 50 MW, 100 MW, 175 MW and 250 MW. Costing for each of the systems makes a number of assumptions for both the process as a whole and for each individual piece of equipment required to make up the HLH. The assumptions made are stated in the following sections.

7.4.3.1 Overall process assumptions

The process takes the form of a wood pellet fired gasifier with a cold gas efficiency of 80%. Turbine system efficiency is rated at 60% to generate an overall plant efficiency of 48%, and the operating pressure of the gasification plant is 25 barg. The fuel used has a heating value of 18.35 MJ/kg, a bulk density of 651 kg/m^3 and a voidage of 48.4%.

7.4.3.2 Fuel storage and delivery assumptions

The fuel storage unit takes the form of a conical roofed storage tank. The tank is constructed from carbon steel and is sized to contain fuel required for one day of operation. A belt conveyor is used to convey the fuel from the storage tank to the atmospheric hopper of the HLH, and the belt used is 50 m in length and varies between 0.5 m and 1 m in width depending on the capacity of the plant. The power requirement for the motor required to operate the belt conveyor is calculated using Equations 7-8 to 7-10.

$$F_U = \mu_T g \left(m_b + \frac{m_B}{2}\right) + \mu_R g \left(\frac{m_B}{2} + m_R\right)$$

Equation 7-8

$$P_A = F_U v$$

Equation 7-9

$$P_M = P_A / \eta$$

Equation 7-10

Where F_U is the effective pull of the conveyor (N), μ_T is the friction coefficient when running over the table support, g is the acceleration due to gravity (m/s^2), m_b is the total mass of the material contained on the belt (kg), m_B is the mass of the belt (kg), μ_R is the friction coefficient when running over a roller and m_R is the mass of all rotating drums excluding the mass of the drive drum (kg). P_A is the

mechanical power calculated for the drive drum (W), v is the velocity of the belt (m/s), P_M is the mechanical motor power for the drive drum (W) and η is the drive efficiency (CEMA, 2007, Forbo, 2009). Equation 7-8 assumes a friction coefficient of 0.33 for the table support and 0.033 for the rollers. It assumes the belt material to have a mass of 2.5 kg/m^2, the total mass of the drums used excluding the driving drum to be 500 kg and the drive efficiency is assumed to be 80%.

7.4.3.3 Vessel and conveying assumptions

The HLH is comprised of four vessels. An atmospheric feeding hopper, two vertical straight walled pressure vessels equal in volume, and a secondary feeding chamber sized at twice that of the pressure vessels equal in volume located upstream. The secondary vessel is sized such that a head of material is always present and allows continuous operation of the screw feeder arrangement contained in the vessel.

A cycle time of 5 minutes is assumed in all cases and each of the vessels is sized to accommodate 1/288th of the daily feed rate with the exception of the secondary feeding chamber which is sized to accommodate 1/144th of the daily feed rate. Each vessel is designed to have a head space of 5 vol% to minimise flow problems.

The screw feeder arrangement varies depending on the capacity of the plant. Screw conveyors are sized to be 5 m in length and have a diameter varying between 0.3 m and 0.5 m with a shaft diameter 0.1 m and 0.2 m respectively. A standard screw is assumed with a pitch equal to the screw diameter. The power rating of the motor required to operate the screw conveyor is calculated using Equations 7-11 to 7-13.

$$HP_f = \frac{LNF_dF_b}{1000000}$$

Equation 7-11

$$HP_m = \frac{Lq\rho_bF_fF_mF_p}{1000000}$$

Equation 7-12

$$HP = \frac{(HP_f + HP_m)F_o}{\eta}$$

Equation 7-13

Where L is the screw length (ft), N is the rotational rate (rpm), F_d is the diameter factor, F_b is the bearing factor, q is the volumetric flow rate (ft^3/hour), ρ_b is the bulk density of the material (lb/ft^3), F_f is the screw flight factor, F_m is the material factor, F_p is the paddle factor, F_o is the overload factor, η is the drive efficiency, HP_f is the power requirement to run an empty conveyor (hp), HP_m is the power

requirement to solely convey the material (hp) and HP is the total power requirement to convey the material (hp) (Thomas Conveyor Co., 2014). Equation 7-11 assumes a diameter factor of 55 for a 0.3 m screw diameter and 165 for a 0.5 m screw diameter. The bearing factor, flight factor and paddle factor are all assumed to be equal to 1, and the material factor and overload factor are assumed to be equal to 0.5 and 3 respectively. A drive efficiency for the motor is assumed to be 88%.

7.4.3.4 Pressurisation assumptions

Pressurisation brought about through the pumping of water is assumed to take 1 minute using a centrifugal pump, and the power requirement of the pump is determined using Equation 7-14.

$$\mathrm{P_p} = m\left(g\Delta h + \frac{\Delta P}{\rho} - \frac{\Delta P_f}{\rho}\right)$$

Equation 7-14

Where P_p is the power required to pump (W), m is the mass flow rate of water (kg/s), g is the acceleration due to gravity (m/s^2), Δh is the change in elevation (m), ΔP is the difference in system pressure (Pa), ρ is the density of water (kg/m^3) and ΔP_f is the pressure drop due to friction (Pa) (Sinnott, 2007). No change in elevation and no pressure drop due to friction is assumed in all of the cases computed.

The pump is sized for use in Mode 2 and therefore assumes a mass flow rate equal to the volume of the pressure vessel being fed to per minute. Where air evacuation is necessitated, a two-stage vacuum pump is assumed with a cycle time of 1 minute.

Where a conventional lock hopper is concerned, pressurisation and compression is assumed to take place isothermally using a reciprocating compressor. The power requirement for the compressor is determined using Equation 7-15.

$$W = P_2 V_2 \ln\left[\frac{P_2}{P_1}\right]$$

Equation 7-15

Where W is the energy required for compression (J), P_2 is the pressure required for feeding (Pa), V_2 is the volume of gas at pressure P_2 (m^3) and P_1 is the initial pressure of the gas being compressed (Pa) (O'Neill, 1993). As with the HLH, the time taken for pressurisation is assumed to be equal to 1 minute.

7.4.3.5 Water storage and recycling assumptions

The water storage tank takes the form of a vertical cylinder. The volume of the tank is assumed to be three times the volume of the pressure vessel required to be pressurised using the water pump to allow for the time taken for water treatment. Suspended solids contaminating the water stream are removed using either a plate and frame filter or a pressure leaf filter, and the area of the filter required is determined using Equation 7-1 from Section 7.2.3. Water drainage from the pressure vessel during the depressurisation stage is assumed to take 1 minute and the water is assumed to have a solids content of 1 wt%. The particle size is assumed to be 200 μm and the material is assumed to have a density of 1500 kg/m^3. The filter is assumed to be cleaned after a filter cake thickness of 5 cm has been achieved and the voidage of the filter cake built up is assumed to be 50%. Where a plate and frame filter is assumed to be used, cleaning is assumed to be carried out manually twice a day. Where a pressure leaf filter is used, cleaning is assumed to be carried out automatically every two hours. Two filters are assumed in each case to enable continuous operation.

The pressure drop generated by the filter cake is calculated using Equation 7-4 stated in Section 7.2.3 and in turn is used to calculate the power requirement of the pump. In addition to the pressure drop brought about by the filter cake, there is the head required to be overcome by the height of the water storage tank. In each case a total pressure drop of 2.5 barg is assumed to be overcome which constitutes a pressure in excess of any vessel height and filter cake pressure drop combination calculated. The power requirement of the pump is calculated using Equation 7-14.

7.5 Economic analysis

7.5.1 Capital cost estimation for the Hydraulic Lock Hopper

Table 7-6 to Table 7-10 show capital cost estimations for both a HLH and a conventional singe lock hopper. Cost estimations were unable to be made for a dual lock hopper system in this case due to time constraints on the study. However, it is envisaged that the capital cost for a dual lock hopper system will not be significantly different to that for a single lock hopper arrangement due to the only difference between the two systems being the provision of an extra lock vessel, plus high pressure pipe work and fittings.

The systems assessed in Table 7-6 to Table 7-10 are sized to feed wood pellets to gasification plants with electrical outputs of 10 MW, 50 MW, 100 MW, 175 MW and 250 MW. All tables show a cost estimation for the HLH using a pressure leaf filter in the water treatment process and assume the filter is regenerated once every two hours. Estimations do not take into account the cost for piping and valve fittings, other than the principal valves through which solids are fed. Such costs are predicted to be greater for the HLH due to the presence of the water treatment process. Cost estimates are based on

data obtained from the following sources: (Garrett, 1989, Perry et al., 1997, Loh et al., 2002, Parrett, 2014).

Tables 7-6 to 7-10 indicate both systems to be broadly comparable in cost and a conventional lock hopper to be marginally less expensive than a HLH at each plant capacity computed. Prices vary between the two systems by on average $74,500. Where plant capacities are increased, the difference in cost between the two systems is found to decrease, especially when compared to the overall price of the system. For example, a HLH with a 250 MW capacity is only found to be around 4.3% more in price than a conventional lock hopper of the same capacity. As prices are found to be broadly comparable, it can be inferred from the data shown in Figure 7-5 that the capital cost of the compressor for the conventional lock hopper is broadly equal to the cost of the high pressure water pump, the water treatment plant and the extra principal valve required by the HLH, as the remaining equipment costs are equal in both cases.

10 MW Feed System			**HLH**	**Conventional**
Component	**Unit**	**Size**	**Price ($)**	**Price ($)**
Storage and Conveying				
Fuel storage tank	m^3	151	46,629	46,629
Belt conveyor	m^2	25	16,352	16,352
Belt Motor	kW	0.3	3,019	3,019
Vessels				
Atmospheric hopper	m^3	0.55	2,751	2,751
Pressure vessel 1	m^3	0.55	3,877	3,877
Pressure vessel 2	m^3	0.55	3,877	
Pressure vessel 3	m^3	1.10	5,959	5,959
Principal valves	m	0.62	60,205	40,137
Screw conveyor	m x mm	1500	23,816	23,816
Screw Motor	kW	0.2	2,406	2,406
Pressurisation				
Vacuum pump	m^3/min	0.28	11,652	
HP Water pump	kW	25	3,418	
Pump Motor	kW	25	35,933	
Compressor	kW	38		44,610
Water Treatment				
Water storage vessel	m^3	1.7	3,859	
LP Water pump	kW	2.5	1,713	
Pump Motor	kW	2.5	9,897	
Pressure leaf filter 1	m^2	3.6	14,733	
Pressure leaf filter 2	m^2	3.6	14,733	
TOTAL			264,829	189,556

Table 7-6: Capital cost estimate for a HLH and a conventional lock hopper feeding to 10 MW gasification plant.

50 MW Feed System			HLH	Conventional
Component	**Unit**	**Size**	**Price ($)**	**Price ($)**
Storage and Conveying				
Fuel storage tank	m^3	754	116,610	116,610
Belt conveyor	m^2	25	16,352	16,352
Belt Motor	kW	1.4	7,153	7,153
Vessels				
Atmospheric hopper	m^3	2.75	4,458	4,458
Pressure vessel 1	m^3	2.75	11,622	11,622
Pressure vessel 2	m^3	2.75	11,622	
Pressure vessel 3	m^3	5.50	17,861	17,861
Principal valves	m	1.05	133,902	89,268
Screw conveyor 1	m x mm	1500	23,816	23,816
Screw Motor 1	kW	0.6	4,451	4,451
Screw conveyor 2	m x mm	1500	23,816	23,816
Screw Motor 2	kW	0.6	4,451	4,451
Pressurisation				
Vacuum pump	m^3/min	1.40	27,673	
HP Water pump	kW	115	8,753	
Pump Motor	kW	115	52,935	
Compressor	kW	187		170,123
Water Treatment				
Water storage vessel	m^3	8.25	6,199	
LP Water pump	kW	12	2,742	
Pump Motor	kW	12	23,822	
Pressure leaf filter 1	m^2	17.75	36,579	
Pressure leaf filter 2	m^2	17.75	36,759	
TOTAL			571,576	489,981

Table 7-7: Capital cost estimate for a HLH and a conventional lock hopper feeding to 50 MW gasification plant.

100 MW Feed System			**HLH**	**Conventional**
Component	**Unit**	**Size**	**Price ($)**	**Price ($)**
Storage and Conveying				
Fuel storage tank	m^3	1507	173,045	173,045
Belt conveyor	m^2	25	16,352	16,352
Belt Motor	kW	2.7	10,333	10,333
Vessels				
Atmospheric hopper	m^3	5.5	5,489	5,489
Pressure vessel 1	m^3	5.5	18,165	18,165
Pressure vessel 2	m^3	5.5	18,165	
Pressure vessel 3	m^3	11	27,917	27,917
Principal valves	m	1.33	188,929	125,953
Screw conveyor 1	m x mm	2500	30,125	30,125
Screw Motor 1	kW	1	5,924	5,924
Screw conveyor 2	m x mm	2500	30,125	30,125
Screw Motor 2	kW	1	5,924	5,924
Pressurisation				
Vacuum pump	m^3/min	2.8	43,694	
HP Water pump	kW	230	13,927	
Pump Motor	kW	230	90,269	
Compressor	kW	375		305,213
Water Treatment				
Water storage vessel	m^3	16.5	7,631	
LP Water pump	kW	23	3,333	
Pump Motor	kW	23	34,294	
Pressure leaf filter 1	m^2	35.5	54,302	
Pressure leaf filter 2	m^2	35.5	54,302	
TOTAL			832,245	754,565

Table 7-8: Capital cost estimate for a HLH and a conventional lock hopper feeding to 100 MW gasification plant.

175 MW Feed System			**HLH**	**Conventional**
Component	**Unit**	**Size**	**Price ($)**	**Price ($)**
Storage and Conveying				
Fuel storage tank	m^3	2637	238,050	238,050
Belt conveyor	m^2	50	23,126	23,126
Belt Motor	kW	4.5	13,754	13,754
Vessels				
Atmospheric hopper	m^3	9.65	6,497	6,497
Pressure vessel 1	m^3	9.65	26,318	26,318
Pressure vessel 2	m^3	9.65	26,318	
Pressure vessel 3	m^3	19.3	40,448	40,448
Principal valves	m	1.60	249,463	166,309
Screw conveyor 1	m x mm	2500	30,125	30,125
Screw Motor 1	kW	1.75	8,105	8,105
Screw conveyor 2	m x mm	2500	30,125	30,125
Screw Motor 2	kW	1.75	8,105	8,105
Pressurisation				
Vacuum pump 1	m^3/min	2.45	40,782	
Vacuum pump 2	m^3/min	2.45	40,782	
HP Water pump 1	kW	200	12,682	
Pump Motor 1	kW	200	81,059	
HP Water pump 2	kW	200	12,682	
Pump Motor 2	kW	200	81,059	
Compressor	kW	655		487,596
Water Treatment				
Water storage vessel	m^3	29	9,038	
LP Water pump	kW	40	4,314	
Pump Motor	kW	40	23,474	
Pressure leaf filter 1	m^2	62.5	74,962	
Pressure leaf filter 2	m^2	62.5	74,962	
TOTAL			1,156,230	1,078,558

Table 7-9: Capital cost estimate for a HLH and a conventional lock hopper feeding to 175 MW gasification plant.

250 MW Feed System			**HLH**	**Conventional**
Component	**Unit**	**Size**	**Price ($)**	**Price ($)**
Storage and Conveying				
Fuel storage tank	m^3	3,770	291,843	291,843
Belt conveyor 1	m^2	50	23,126	23,126
Belt Motor 1	kW	3.25	11,463	11,463
Belt conveyor 2	m^2	50	23,126	23,126
Belt Motor 2	kW	3.25	11,463	11,463
Vessels				
Atmospheric hopper	m^3	13.75	7,225	7,225
Pressure vessel 1	m^3	13.75	33,665	33,665
Pressure vessel 2	m^3	13.75	33,665	
Pressure vessel 3	m^3	27.50	51,739	51,739
Principal valves	m	1.80	297,812	198,541
Screw conveyor 1	m x mm	2500	30,125	30,125
Screw Motor 1	kW	1.65	7,842	7,842
Screw conveyor 2	m x mm	2500	30,125	30,125
Screw Motor 2	kW	1.65	7,842	7,842
Screw conveyor 3	m x mm	2500	30,125	30,125
Screw Motor 3	kW	1.65	7,842	7,842
Pressurisation				
Vacuum pump 1	m^3/min	3.5	54,618	
Vacuum pump 2	m^3/min	3.5	54,618	
HP Water pump 1	kW	287	16,154	
Pump Motor 1	kW	287	107,048	
HP Water pump 2	kW	287	16,154	
Pump Motor 2	kW	287	107,048	
Compressor	kW	935		657,505
Water Treatment				
Water storage vessel	m^3	41.5	10,064	
LP Water pump	kW	57.5	5,501	
Pump Motor	kW	57.5	31,042	
Pressure leaf filter 1	m^2	88.75	91,547	
Pressure leaf filter 2	m^2	88.75	91,547	
TOTAL			1,484,369	1,423,597

Table 7-10: Capital cost estimate for a HLH and a conventional lock hopper feeding to 250 MW gasification plant.

Component	Unit	10 MW	50 MW	100 MW	175 MW	250 MW
Fuel Storage Tank						
Capacity	tonnes/day	98.1	490.5	981.0	1,716.6	2,452.3
Height	m	4	6.5	8	9.5	11
Diameter	m	7.5	12.5	16	18	21.5
Belt Conveyor						
Length	m	50	50	50	50	50
Width	m	0.5	0.5	0.5	1	1
Velocity	m/s	0.12	0.58	1.16	1.02	0.73
Atmospheric Hopper						
Capacity	kg	341	1,703	3,406	5,961	8,515
Height	m	1.27	1.78	2	2.18	2.29
Opening diameter	m	0.86	1.73	2.37	3.07	3.63
Hopper half angle	°	5.4	10.8	14.6	18.7	21.8
Pressure Vessel 1 and 2						
Capacity	kg	341	1,703	3,406	5,961	8,515
Height	m	1.86	3.15	4	4.8	5.4
Diameter	m	0.62	1.05	1.33	1.60	1.80
Pressure Vessel 3						
Capacity	kg	682	3,406	6,812	11,922	17,030
Height	m	1.86	3.15	4	4.8	5.4
Diameter	m	0.87	1.5	1.88	2.26	2.55
Screw Conveyor						
Length	m	5	5	5	5	5
Diameter	m	0.3	0.3	0.5	0.5	0.5
Pitch	m	0.3	0.3	0.5	0.5	0.5
Rotational speed	rpm	5.6	13.9	6.3	11.1	10.6
Vacuum Pump						
Capacity	m^3/min	0.28	1.40	2.80	2.44	3.50
HP and LP Pump						
Capacity	m^3/min	0.55	2.75	5.50	4.81	6.87
Pressure Leaf Filter						
Capacity	m^3/min	0.55	2.75	5.50	9.62	13.74
Area	m^2	3.55	17.75	35.50	62.12	88.74
Cycles per change	-	24	24	24	24	24
Pressure drop	m	0.36	0.36	0.36	0.36	0.36
Water Storage Tank						
Height	m	1.39	2.37	2.99	3.60	4.05
Diameter	m	1.23	2.11	2.65	3.20	3.60
Compressor						
Capacity	m^3/min	0.28	1.40	2.80	4.89	6.99

Table 7-11: Equipment specification for the data shown in Table 7-6 to 7-10.

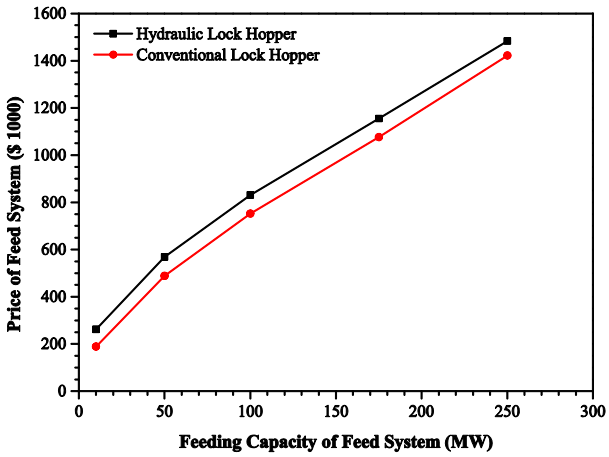

Figure 7-5: Capital cost estimate comparison between a HLH fitted with a pressure leaf filter regenerated every two hours and a conventional lock hopper.

7.5.2 Effect of the filtration process on the capital cost of the Hydraulic Lock Hopper

Figure 7-5 displays cost estimates for a HLH implementing a pressure leaf filter which is regenerated every two hours. In addition to these estimates, Figure 7-6 and Figure 7-7 display cost comparisons between a HLH and a conventional lock hopper where alternative filtration processes are used. Figure 7-6 assumes a plate and frame filter is used and regenerated twice a day, and Figure 7-7 assumes a pressure leaf filter is used which is also regenerated twice a day to provide a direct comparison between the two processes.

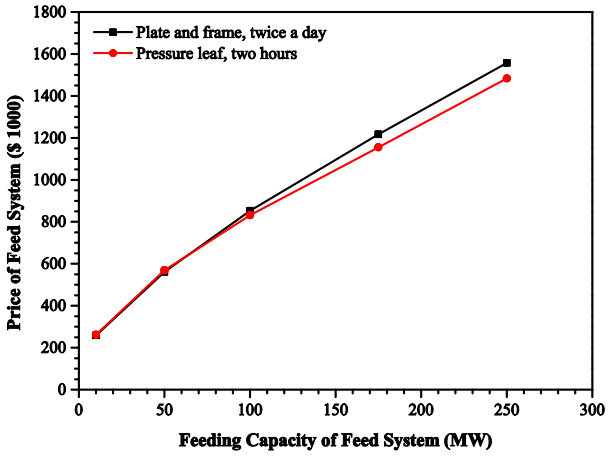

Figure 7-6: Capital cost estimate comparison between a HLH fitted with a pressure leaf filter regenerated every two hours and a HLH fitted with a plate and frame filter regenerated twice a day.

Figure 7-6 shows that substituting the pressure leaf filter which is regenerated ever two hours with a plate and frame filter sized to be regenerated twice a day has little effect on the overall cost of the system. Both systems are found to be broadly the same in cost, particularly where smaller plant

capacities are concerned. The plate and frame filter arrangement is seen to be more costly than using a pressure leaf filter at larger plant capacities and is estimated to cost around 5.0% more where a plant capacity of 250 MW is required to be fed to. On the basis of Figure 7-6, a pressure leaf filter is preferred as it is both more practical, as it does not require manual cleaning, and is less costly. However, the upfront capital cost of a pressure leaf filter is far greater per square metre than a plate and frame filter and in turn the price is a product of the cleaning or regenerating frequency (Perry et al., 1997). Figure 7-7 highlights a case where a pressure leaf filter is sized to be regenerated twice a day and is compared to a conventional lock hopper. It can be seen that the capital cost estimate for the HLH is far in excess of the conventional lock hopper and roughly costs around 48.7% more than a conventional lock hopper for a gasification plant with a capacity of 250 MW.

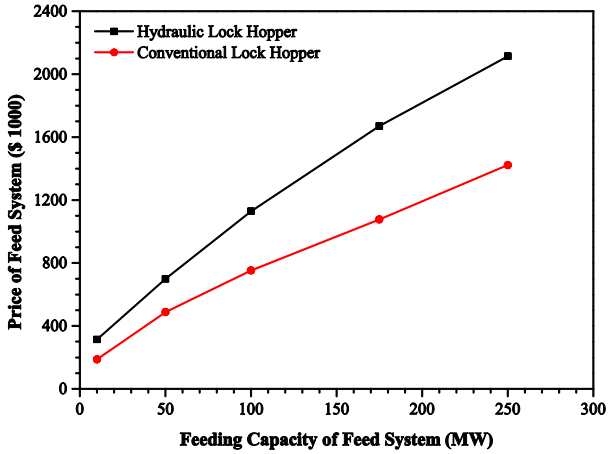

Figure 7-7: Capital cost estimate comparison between a HLH fitted with a pressure leaf filter regenerated twice a day and a conventional lock hopper.

This presents a trade off between regeneration time of the filter area/cost, and to a certain degree, the foot print of the device. Where regeneration times are high, equipment costs and footprint are increased, and where regeneration times are low, equipment is more prone to wear, but cost is reduced. Where the HLH is concerned, a regeneration time of two hours is proposed as a compromise as the filter is not required to be continually active due to the cyclic nature of the HLH. Where capital cost is required to be reduced further, the filter is the key piece of equipment to be re-examined.

7.5.3 Effect of operating pressure on capital cost

The capital cost estimates shown in Section 7.5.1 and 7.5.2 all assume an operating pressure of 25 barg. While such a pressure generates an advantage over atmospheric gasification systems, higher pressures are typically used, not least to allow for pressure drops in the overall system (Higman and Van der Burgt, 2008). Figure 7-8 highlights the effect of increasing the operating pressure on the

capital cost of both the HLH and a conventional lock hopper. The comparison shown is for a system feeding to a gasification plant with a 100 MW output.

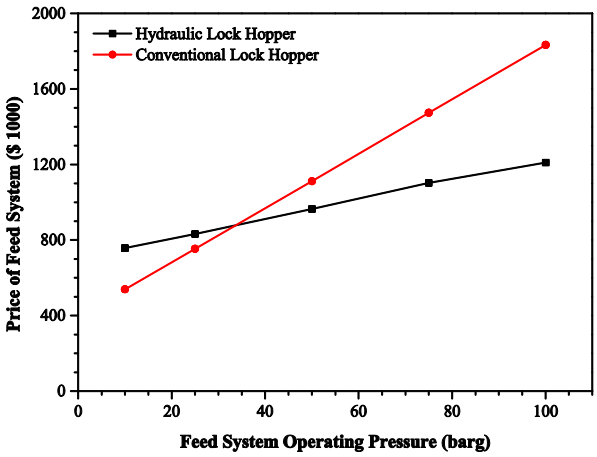

Figure 7-8: Effect of operating pressure on the capital cost of a HLH fitted with a pressure leaf filter regenerated every two hours and a conventional lock hopper. Gasification plant being fed to has a 100 MW output.

Figure 7-8 displays a clear advantage of using the HLH in place of a conventional lock hopper at elevated operating pressures, and shows that where operating pressures in excess of 33.7 barg are present, the HLH becomes more economically favourable (where the plant being fed to has a capacity of 100 MW). Such a pressure corresponds to a price of approximately $878,000. The breakeven pressure is found to decrease where plant capacitates are increased, and therefore it can be said that the HLH is found to be most economically favourable where high plant capacities and high operating pressures prevail.

The key reason for the economic advantage of the HLH is due to the incompressibility of water. Pumping of water at high pressure requires a fraction of the power required by gas compressors and as operating pressures are increased, the capital cost of the compressor required is found to vastly increase. Examining Tables 7-7 to 7-10 it can be seen that the compressor represents the majority of the capital cost for a conventional lock hopper, representing between 34% and 47% for plant capacities of 50 MW to 250 MW. Conversely it can be seen that the high pressure pump required for the pressurisation of the HLH only accounts for between 10% and 17% of the total capital cost. These values are true of systems operating at 25 barg and are found to increase dramatically in both cases for higher operating pressures. This is due to pressure only affecting the means for pressurisation (pump or compressor), the principal valves and pressure vessel thickness. Capital costs for the remaining equipment are found to be unaffected by operating pressure and as such give rise to the cost saving generated by the HLH at higher pressures.

7.6 Summary

This chapter provides details on how the HLH is required to be adapted for use in an industrial setting. It details the changes required to be made to the HLH in its current form and the additional processes necessary to operate it on a continuous basis. It also provides a detailed economic assessment of both the HLH and a conventional single lock hopper sized to feed gasification plants with electrical outputs of 10 MW, 50 MW, 100 MW, 175 MW and 250 MW.

Two key areas were highlighted for optimisation for use in an industrial setting. The valve type used for the principal valves through which solids are passed, and the hopper/vessel geometry. It was suggested that in place of ball valves, either knife gate valves or O-Port valves are to be used if the HLH is to be scaled up. It was surmised that this is due to the size of ball valves with larger diameters (the height of the valve broadly being equal to the diameter) and the complexity of their construction where larger diameters are required. Both knife gate valves and O-Port valves were regarded to present a more resilient valve design for use with solids and a more suitable valve as both require a more modest head space. In addition to valve replacement, it was supposed that the primary pressure vessels (top and bottom hopper) take the form of vessels with straight or flared walls. Such configurations were suggested in order to minimise solids holdup taking place and to allow the consistent flow of material.

Water treatment was also assessed for a commercial unit. A water treatment cycle was proposed involving a pump, a dual filter arrangement and a water storage tank. Due to the solids content of the used water stream being relatively low, conventional plate and frame or pressure leaf filters were assessed to be the most applicable for solids removal. A filter was sized for use with the HLH in its current arrangement and the number of cycles required before filter regeneration was determined. Operation in Mode 1 required a 0.1 m^2 filter to be regenerated after approximately 40 cycles, whereas operation in Mode 2 required regeneration after around 30 cycles.

Daily fuel, electricity, CO_2 and cost savings were calculated for a range of gasification plants where the HLH was implemented in place of a conventional and a dual lock hopper. Operation in Mode 1 without vacuum operation was found to be the most favourable, generating savings compared to a conventional lock hopper of around £7.4 per day per MW output for a typical biomass feed. Fuel, electricity and CO_2 savings were found to increase with decreasing calorific value of the fuel being fed, and savings were found to be greater in all modes of operation when compared to a conventional lock hopper rather than a dual lock hopper.

Lastly, a detailed economic assessment of a HLH and a conventional lock hopper unit required to feed a range of gasification plants was carried out. Capital cost estimates were found to be broadly comparable between both types of feed system for an operating pressure of 25 barg and where a

pressure leaf filter was sized and assumed to be regenerated every two hours in the case of the HLH. Similarly, capital costs were found to be comparable where a plate and frame filter was sized and assumed to be regenerated twice a day and were of the order of $812,500 for a system feeding to a biomass gasification plant with a 100 MW capacity. In both cases the cost of the compressor required to operate a conventional lock hopper was found to be broadly in line with the cost of the high pressure water pump and water treatment cycle required to operate the HLH. Although capital costs were calculated to be broadly similar for an operating pressure of 25 barg, it was found that increasing the operating pressure favoured the HLH. A capital cost estimate for a conventional lock hopper feeding to a 100 MW plant operating at 75 barg was calculated to be around 33.7% greater than for a HLH operating at the same pressure and capacity.

8

CONCLUSIONS AND FUTURE WORK

8.1 Conclusions

The primary objective of this research programme was to develop a novel and more efficient feed system for feeding solid fuels to gasifiers operating at high pressure. The primary objective of this research programme was achieved, and the main conclusions from this study are as follows:

- Feed systems used to feed solid materials to high pressure environments can be split into six key categories: rotary valves, lock hoppers, plug-forming feeders, piston feeders, dynamic feeders and slurry feeders. In the context of gasification, lock hoppers and slurry feeders are the most prevalent and preferred systems for feeding. Although the downstream processes being fed to do differ due to the makeup of the feedstock being fed, a commonality between the two systems is their feeding inefficiency inherent in their operation. Lock hoppers are inefficient due to gas compression cycling, with the bulk of the energy used to pressurise the feedstock being wasted during depressurisation. On the other hand, slurry feeders present a burden on the downstream process in terms of the energy required to vaporise the transport

medium (typically water) which can constitute up to 90 wt% when feeding some biomass species.

- A new feed system for feeding solid fuels to high pressure gasifiers has been developed. The system takes the form of a new type of lock hopper, named the Hydraulic Lock Hopper (HLH), which disposes of conventional gas compression cycling. The HLH utilises water as an incompressible fluid in the compression stage of the feeding operation and requires no gas compressor or pressurised inert gas. The key piece of equipment required for operation is a pump capable of pumping a liquid against the back pressure of the process being fed to, and the volume of water pumped acts to minimise or eliminate the release of gas at high pressure.

- The feeding of commercially available Ø6 mm wood pellets, Ø8 mm torrefied spruce pellets and ~10 mm ground anthracite coal grains has been demonstrated using the HLH in two modes of operation. Fuels have been fed to a range of pressures between 5 barg and a maximum of 25 barg. The HLH has been operated as a conventional single and dual lock hopper utilising a gas compressor to provide a small scale comparison to a conventional feed system. Ø6 mm wood pellets, Ø8 mm torrefied spruce pellets and ~10 mm ground anthracite coal grains have all been fed to pressures as high as 25 barg using the HLH setup in a conventional single and a dual lock hopper configuration.

- Energy savings compared to a conventional lock hopper as high as 82.9% have been recorded when feeding anthracite coal grains at 25 barg. Energy savings were recorded to be greater when operating in Mode 1 compared to Mode 2 while feeding all fuels, due to a larger volume of water being required to be pumped in the compression stage of Mode 2. Energy savings compared to a conventional single lock hopper of the order of 82% and 75% were typical when feeding all fuels in Mode 1 and Mode 2 respectively. Energy savings were found to be lower in all cases when compared to a dual lock hopper, with a dual lock hopper being found to require approximately half the energy required by a conventional lock hopper.

- Energy savings generated by the HLH over both a conventional and a dual lock hopper were found to increase with increasing operating pressure, varying from 48.7% at 5 barg to 81.9% at 25 barg when feeding wood pellets (savings of Mode 1 compared to a conventional lock hopper). Energy savings recorded were found to show the same trend as those determined theoretically and lay between an upper and lower bound calculated assuming an isothermal and an adiabatic compression respectively.

- A direct relationship between the voidage present between the fuel being fed and the volume of water required to be pumped was found when operating in Mode 1. The energy requirement of Mode 1 was found to approach that of Mode 2 as fuel voidage was increased.

- The difference in the energy requirements of Mode 1 and Mode 2 was found to be equal to a lock gas contamination with a medium calorific value syngas (15 MJ/Nm^3) of around 12 vol% for an operating pressure of 25 barg. It was found that where syngas contamination of the gas vented during operation in Mode 1 is equal to or greater than 12 vol% for an operating pressure of 25 barg, Mode 2 becomes the most efficient mode of operation. This phenomenon was found to be true for lower contamination concentrations for operating pressures in excess of 25 barg.

- The mass flow rate through the HLH was found to stay broadly constant with operating pressure. Mass flow rates were found to be greater when operating in Mode 1 than in Mode 2 due to the reduced volume of water required to be pumped and in turn the reduced time it takes for compression and water drainage. The most influential factor affecting the mass flow rate was the mass per batch of fuel fed. The void space present between fuels was also found to affect mass flow rates when operating in Mode 1 but to a lesser extent. Mass flow rates were recorded to be greatest when feeding ground anthracite coal grains in Mode 1, followed by torrefied spruce pellets and lastly by standard wood pellets.

- Stainless steel ball valves were found to be more resilient to feeding solids than chrome-plated brass ball valves. Degradation was found to be greater in the case of the chrome-plated brass valves which gave rise to air leakage rates an order of magnitude greater compared to stainless steel valves. Air leakage rates were recorded to increase with increasing pressure.

- Increases in fuel moisture content were consistently found to be less than 1 wt% when using stainless steel ball valves. Moisture content increases of comparable magnitude were found during initial testing with chrome-plated brass valves; however, valve degradation was found to bring about larger increases in moisture content after successive tests. A direct relationship between air leakage and fuel moisture content increase was also found.

- Explosion risks were minimised by implementing a vacuum precursory stage to the HLH which ensured the evacuation of air contained with the fuel prior to feeding to pressure. Evacuation was brought about using a vacuum pump and a pressure of 0.1 bara was determined to be sufficient to minimise the damage potential from an explosion to nil. The

vacuum precursor was found to increase the energy requirement of operation in Mode 1 and Mode 2 by 17.5% and 12.3% respectively.

- The HLH was found to be cost competitive with a conventional lock hopper irrespective of plant capacity for an operating pressure of 25 barg, and where pressures in excess of 33.7 barg were assumed, the HLH was found to become more economically favourable (assuming a plant with a capacity of 100 MW). Such a breakeven pressure was found to decrease for plants with higher capacities, and therefore it can be said that the HLH is most economically favourable for large capacity plants with high operating pressures.

8.2 Recommendations for future work

The work carried out over the course of this research programme provides proof-of-concept of the HLH. However, work remains if the system is to be scaled up and employed in an industrial setting. Recommendations for further work to be carried out relating to the HLH are as follows:

- Operation with the HLH should be undertaken in conjunction with a hot process, where the temperature of the collection vessel is maintained at a temperature similar to that found in gasification facilities. Work so far has not quantified the effect of temperature on fuel feeding, and the effect it has on the pressurisation/depressurisation stage.

- The HLH should be operated with real downstream gas compositions in order to quantify the level of lock gas contamination with syngas encountered during feeding. Gas measurements should be taken in both the top and bottom hopper in addition to the collection vessel in order to understand the effect feeding has on gas composition and concentration.

- Gas solubility's in water should be explored both while operating the HLH and using a series of standalone systems of varying volume. Such systems will look to quantify the level of absorption of different gases in water used in the compression stage, and how gas composition affects the level of absorption. Operating temperature and pressure should also be varied in order to gauge the effect of both parameters on gas solubility.

- Hopper geometries should be designed in accordance with the results determined in Chapter 4 regarding the hopper half angle and minimum outlet diameter for the range of fuels tested. Implementing the new hoppers will allow the results recorded to be validated, and an assessment to be made of the flexibility of the HLH when feeding a range of materials.

- A water treatment cycle should be designed and incorporated into the HLH in its current form in order to gauge the level of contamination and the magnitude of the cycle required for treatment. In addition to this, a range of vessels should be constructed and subjected to a series of full operational cycles in order to determine the relationship between the vessel volume and the level of contamination. Such tests should be undertaken for a range of materials.

- As water was not found to be consumed in significant quantities during testing, alternative liquids for use in the compression stage should be explored.

- The operational cycle of the HLH should be automated in order to assess the long term reliability of the device. The inclusion of a screw feeder downstream of the process contained in the collection vessel is suggested, which feeds material to a vessel at pressure with a volume far in excess of the hoppers used to construct the HLH. Automating the process will allow a true assessment to be made of parameters such as the mass flow rate and the overall energy requirement for feeding.

- Ultimately steps should be taken to scale up the HLH for use in a pilot setting which incorporates an operational gasifier. The valves used to separate the primary vessels should be substituted for more resilient valves such as knife-gate or O-Port valves, and the degradation of the valves should be monitored over time. Such a version of the HLH should incorporate all aspects of feeding, including a suitably sized water treatment cycle.

8.3 Final remarks

The principal objective of this PhD study has been achieved over the course of the past three years. A new feed system for feeding solid materials to high pressure processes has been designed and developed, and the key conclusions from this work are detailed above.

While the bulk of the work detailed in this thesis has been carried out from an academic standpoint, the Hydraulic Lock Hopper presents a major benefit from the point of view of industry. Where conventional lock hoppers are currently in operation, a relatively simple retrofit enables the full integration of the Hydraulic Lock Hopper and in turn, the benefits that it presents. All that is required is a supply of water, a means to filter the used water stream, high pressure pipe work and fittings, and a high pressure water pump. Conventional gas compressors can be disposed of, and supplies of inert gas are not required. The work presented in this thesis provides a secure foundation on which the

future work detailed previously can be based, and provides the fundamental building blocks for work relating to industrial scale-up and implementation.

REFERENCES

AIR PRODUCTS AND CHEMICALS INC. 1971. Feasibility study of a coal slurry feeding system for high pressure gasifiers. Allentown, Pennsylvania, Office of Coal Research, Department of the Interior.

ALDRED, D. L. & SAUNDERS, T. 2007. Achieve continuous injection of solid fuels into advanced combustion system pressures. North Hollywood CA, Stamet Incorporated.

ALDRED, D. L. 2000. Proof of principal test to feed and meter granular coal into 450 psig gas pressure. Gardena, California.

AMYOTTE, P. R., BAXTER, B. K. & PEGG, M. J. 1990. Influence of initial pressure on spark-ignited dust explosions. Journal of Loss Prevention in the Process Industries, 3, 261-263.

ARNOLD, P. C., MCLEAN, A. G. & ROBERTS, A. W. 1982. Bulk solids: Storage, flow and handling. TUNRA Bulk Solids Handling Research Associates.

ASTM 2012. A240/A240M-12a: Standard specification for chromium and chromium-nickel stainless steel plate, sheet, and strip for pressure vessels and for general applications. American Society for Testing and Materials.

ATKINS, P. & DE PAULA, J. 2006. Atkins' physical chemistry, Oxford University Press.

BAIR, W. G. & TARMAN, P. B. 1977. Slurry pumping techniques for feeding high-pressure coal gasification reactors. Conference on Coal Feeding Systems. California Institute of Technology, Pasadena, California Institute of Gas Technology, Chicago, Illinois.

BAL SEAL. 2001. A guide for selecting the type of chrome Plating for use in contact with BAL seals in rotary and reciprocating service. Amsterdam, BAL Seal.

BARTKNECHT, W. 1978. Explosionen: Ablauf und schutzmassnahmen, Berlin, Springer.

BEDNAR, H. H. 1991. Pressure vessel design handbook, Malabar, Florida, Krieger Publishing Company.

BELL JR, H. S. 1979. Solids feeder apparatus. U.S. patent application 856,365.

BELL, D. A. & TOWLER, B. F. 2010. Coal gasification and its applications, William Andrew Pub.

BERBERAN-SANTOS, M. N., BODUNOV, E. N. & POGLIANI, L. 1997. On the barometric formula. American Journal of Physics, 65, 404.

BERGHEL, J., FRODESON, S., GRANSTRÖM, K., RENSTRÖM, R., STÅHL, M., NORDGREN, D. & TOMANI, P. 2013. The effects of kraft lignin additives on wood fuel pellet quality, energy use and shelf life. Fuel Processing Technology, 112, 64-69.

BERRY, R. 2013. Hopper sizing and geometry. Personal communication. The Wolfson Centre for Bulk Solids Handling Technology, University of Greenwich, September 2013.

BEVERLOO, W. A., LENIGER, H. A. & VAN DE VELDE, J. 1961. The flow of granular solids through orifices. Chemical Engineering Science, 15, 260-269.

BIO-ENERGYSYSTEMS. 1984. Bio-energy systems report: Downdraft gasifier/engine systems [Online]. Available: http://pdf.usaid.gov/pdf_docs/PNAAR954.pdf [Accessed 21st November 2011].

BIRTWISTLE, J. V. 2003. Safety and chemical engineering education workshop: Fundamentals of dust explosions. League City TX, RRS Engineering.

BOLTON, P. 2013. Energy prices, SN/SG/4153. House of Commons, Parliament, UK.

BONIN, J. H., CANTEY, D. E., DANIEL, J., A. D. & MEYER, J. W. 1977. Development of dry coal feeders. Conference on Coal Feeding Systems. California Institute of Technology, Pasadena, California.

BONIN, J. H., MEYER, J. W. & DANIEL JR, A. D. 1983. Coal pump. U.S. patent application 273,606.

BONK, D. L. & HAY, A. 1995. Stamet solids pump feeds coal into 210 psig in a DOE supported project. Power-Gen America 1995. Anaheim, California.

BP. 2013. BP Statistical review of world energy June 2013. London, UK.

BRETZ, G. M. 1980. High pressure coal gasifier feeding apparatus. U.S. patent application 923,322.

BS EN14015. 2005. Specification for the design and manufacture of site built, vertical, cylindrical, flat-bottomed, above ground, welded, steel tanks for the storage of liquids at ambient temperature and above. BSi.

CALDERÓN, C., JOSSART, J. M., GAUTHIER, G. & RAKOS, C. 2013. European bioenergy outlook 2013 - Statistical report. AEBIOM, European Biomass Association.

CASPERSON, J. R. 1983. Liquid seal lock hoppers and method of utilizing same. U.S. patent application 273,558.

CEMA. 2007. Belt conveyors for bulk materials, Florida, USA.

CHAMBERT, L. & SKOG, E. 1992. Device for feeding bulk material into a pressurized space. Swedish patent application PCT/SE1991/000670.

CHANDRASEKHAR, R. & HARDING, J. C. 1978. Development of feed systems for pressurized coal conversion processes. AIChE Symposium Series, 74, 237-242.

CHASE, G. G. 2010. Hopper design [Online]. Available: http://www.inti.gov.ar/cirsoc/pdf/silos/SolidsNotes10HopperDesign.pdf [Accessed 5th December 2011].

CIFERNO, J. P. & MARANO, J. J. 2002. Benchmarking biomass gasification technologies for fuels, chemicals and hydrogen production. US DOE, NETL.

CLAYTON, S. J., STIEGEL, G. J. & WIMER, J. G. 2002. Gasification technologies: Gasification markets and technologies - Present and future: An industry perspective. US DOE, NETL.

CLEVELAND, J. J. R. 1971. Pressure sealed rotary feeder. U.S. patent application 732,775.

COCCHI, M., NIKOLAISEN, L., JUNGINGER, M., SHENG GOH, C., HEINIMÖ, J., BRADLEY, D., HESS, R., JACOBSON, J., OVARD, L. P., THRÄN, D., HENNIG, C., DEUTMEYER, M., SCHOUWENBERG, P. P. & MARCHAL, D. 2011. Global wood pellet industry market and trade study. IEA Bioenergy Task 40 Sustainable Bioenergy Trade.

COKER, A. 2010. Ludwig's applied process design for chemical and petrochemical plants - Volume 2: Distillation, packed towers, petroleum fractionation, gas processing and dehydration, Gulf Professional Publishing.

COMBUSTION ENGINEERING INC. 1994. CE IGCC repowering project: Use of the Lockheed kinetic extruder for coal feeding; Topical report, June 1993. Publication date: 1 Feb 1994. Windsor, Connecticut: U.S. Department of Energy - Office of fossil energy.

CONDE LÁZARO, E. & GARCíA TORRENT, J. 2000. Experimental research on explosibility at high initial pressures of combustible dusts. Journal of Loss Prevention in the Process Industries, 13, 221-228.

COWAN DYNAMICS. 2013. Eliminate the cost and disruptions of sticky, scaling problems once and for all [Online]. Available: http://www.cowandynamics.com/partners_svc [Accessed 7th February 2014].

CROCKER, M. & NEATHERY, J. K. 2010. Thermochemical conversion of biomass to liquid fuels and chemicals (Chapter 4), Royal Society of Chemistry.

CUMMER, K. R. & BROWN, R. C. 2002. Ancillary equipment for biomass gasification. Biomass and Bioenergy, 23, 113-128.

DAHOE, A. E., VAN VELZEN, J., SLUIJS, L. P., NEERVOORT, F. J., LESCHONSKI, S., LEMKOWITZ, S. M., VAN DER WEL, P. G. J. & SCARLETT, B. 1995. Construction and operation of a 20-litre dust explosion sphere at and above atmospheric conditions. Loss Prevention and Safety Promotion in the Process Industries, Proceedings of the 8th Inter-national Symposium, 285-302.

DAVEY, W. L. E., TAYLOR, E. L., NEWTON, M. D., LARSEN, P. S. & WEITZEL, P. S. 1998. Atmospheric pressure, entrained flow, coal gasification re-visited. Gasification Technologies Conference, San Francisco.

DECC. 2012a. Department of energy and climate change: Climate change act 2008 [Online]. Available: http://www.decc.gov.uk/en/content/cms/legislation/cc_act_08/cc_act_08.aspx [Accessed 20th August 2012].

DECC. 2012b. UK greenhouse gas emissions: Performance against emissions reduction targets – 2011 provisional figures. Department of Energy and Climate Change, UK.

DENNISON, G. 1997. An evaluation of high pressure coal dust explosions. Fuel and Energy Abstracts, 38, 100-100.

DEZURIK. 2014. DeZURIK O-port knife gate valves [Online]. Available: http://www.dezurik.com/products/product-line/gate-valves/thruport-gate-valves/oport-knife-gate-valves-kgo/6/43/20/ [Accessed 7th February 2014].

DIPPR. 2012. Design institute for physical properties: Project 801. Design Institute for Physical Property Research, AIChE.

DOE. 1965. Lurgi DOE report: Appendix 3.1 literature search - Annotated bibliography [Online]. Available: http://www.fischer-tropsch.org/DOE/DOE_reports/1207/ocr_r&d20_vol1_int1/ocr_r&d20_vol1_int1-APP-1.pdf [Accessed 10th August 2012].

DUCH, B. P. 1977. Device for introducing a substance, particularly a pulverulent substance, from a chamber having a pressure P1, into a chamber having a pressure P2 higher than P1. U.S. patent application 577,888.

EASTLAND, D. H. 1975. Methanol from coal. American Chemical Society, 170th National Meeting, Division Fuel Chemistry, 20, 191-212.

ECKHOFF, R. K. 2003. Dust explosions in the process industries, Elsevier.

EDWARDS. 2013. Edwards vacuum pump catalogue [Online]. Available: http://www.edwardsvacuum.com/ [Accessed 12th June 2013].

EERC. 2012. EERC and Pratt & Whitney Rocketdyne, Inc. to hold ribbon cutting ceremony to commission revolutionary new energy technology [Online]. Available: http://www.eerc.und.nodak.edu/homearticle.aspx?id=288 [Accessed 30th March 2012].

EN13445. 2009. European standard: Unfired pressure vessels. BSi.

ENERDATA. 2012. Enerdata: Total energy consumption worldwide [Online]. Available: http://yearbook.enerdata.net/#/energy-consumption-data.html [Accessed 24th March 2014].

EXPLOSION HAZARD TESTING LTD. 2013. Explosion indices test (Kst value and Pmax) [Online]. Available: http://www.explosiontesting.co.uk/explosion_ind_10.html [Accessed 14th June 2013].

FERRAZ, M. T. & OLIVEIRA, M. 2008. Steel fasteners failure by hydrogen embrittlement. Ciência & Tecnologia dos Materiais, 20, 128-133.

FERRETTI, E. J. 1974. Feeding coal to pressurized systems. Chemical Engineering, New York, 81, 113-116.

FINCH, M. C. 1985. High pressure piston pumps for feeding boilers. World Pumps, 61-64.

FIRTH, D. 1991. Multiple-choke apparatus for transporting and metering particulate material. U.S. patent application 640,284.

FLACH, B., BENDZ, K., ROSWITHA, K. & LIEBERZ, S. 2013. EU biofuels annual 2013. USDA Foreign Agricultural Service.

FLEMING, J. R., GODRICK, J. A., HARVEY, A. C. & GUZDAR, A. R. 1982. Development and testing of a linear pocket feeder for high-pressure coal feeding. Final report. Foster-Miller Associates, Inc., Waltham MA, USA.

FM GLOBAL. 2013. Prevention and mitigation of combustible dust explosion and fire [Online]. Available: http://www.fmglobal.com/fmglobalregistration/Vshared/FMDS0776.pdf [Accessed 12th June 2013].

FORBO. 2009. Calculation methods - Conveyor belts. Hannover, Germany, Forbo Siegling GmbH.

FUNK, E. & REIMERT, R. 1977. Comparative description of coal feeding systems for fixed bed pressure gasification. Conference on Coal Feeding Systems. California Institute of Technology, Pasadena, California, Kamyr, Inc., Glen Falls, New York and Lurgi Mineraloltechnik GmbH, Frankfurt, West Germany.

FUNK, E. D. & SHERMAN, M. I. 1977. Coal gasification process with improved procedures for continuously feeding lump coal under pressure. U.S. patent application 542,407.

FUNK, E. D. 1983. Continuous feeding of coal to pressurized systems. Chemical Engineering Progress, 79, 37-41.

FUSSELMAN, S. P., SAUNDERS, T. W. & SPROUSE, K. M. 2010. PWR Compact gasification development. 4th International Freiberg Conference on IGCC & XTL Technologies. Freiberg, Germany, Pratt & Whitney Rocketdyne.

GALL, R. L. & JOHNSON, E. K. 1983. An overview of coal-feed systems. Chemical Engineering Progress, 79, 31-36.

GARDNER, J. F., GENCSOY, H. T. & STRIMBECK, D. C. 1977. High pressure rotary piston coal feeder. U.S. Energy Research and Development Administration, 537-549.

GARRETT, D. E. 1989. Chemical engineering economics, Van Nostrand Reinhold New York.

GENCSOY, H. T. 1977. High pressure rotary piston coal feeder for coal gasification applications. U.S. patent application 713,751.

GEORGE, B., MACKE, Y. & TREGO, R. 2013. Oilseeds: World markets and trade, FOP 12-13, December 2013. United States Department of Agriculture.

GOSEWINKEL, M. 2008. Coal and biomass explosivity characteristics. Barcelona, INBUREX Consulting GmbH.

GRACE, T. M., MALCOLM, E. W. & KOCUREK, M. J. 1989. Pulp and paper manufacture, Volume 5: Alkaline pulping.

GRIFFITHS, J. 2012. Winding up our power supply. The Chemical Engineer, Issue 853. Rugby, Warwickshire, Institution of Chemical Engineers.

GUAN, X., GARDNER, B., ANN MARTIN, R. & SPAIN, J. 2008. Demonstration of hot gas filtration in advanced coal gasification system. Powder Technology, 180, 122-128.

GUZDAR, A. R. & HARVEY, A. C. 1982. Feeding coal and biomass into high pressure reactors. Biomass to Methanol: A Specialists' Workshop. Tamarron, Durango, Colorado, US DOE.

GUZDAR, A. R. 1985. Sealing and liquid displacement systems for a linear pocket feeder. U.S. patent application 386,256.

HALLGREN, A. L., BJERLE, I. & CHAMBERT, L. A. 1993. PCFB gasification of biomass. Preprints of Papers American Chemical Society Division Fuel Chemistry, 38, 866-866.

HARDACRE, C., STYRING, P., TAYLOR, R., DOWSON, G. & MERCY, M. 2013. 4CU Separations – Novel Sorbents [Online]. Available: http://4cu.org.uk/sp3-separations-novel-sorbents/ [Accessed 12th March 2014].

HARDIE, D., CHARLES, E. A. & LOPEZ, A. H. 2006. Hydrogen embrittlement of high strength pipeline steels. Corrosion Science, 48, 4378-4385.

HARDING, J. C. 1977. Foster-Miller's development of dry coal feed systems. Conference on Coal Feeding Systems. California Institute of Technology, Pasadena, California, Foster-Miller Associates Inc., Waltham, MA.

HARRISON, B. & FALCONE, G. 2014. Carbon capture and sequestration versus carbon capture utilisation and storage for enhanced oil recovery. Acta Geotechnica, 9, 29-38.

HAUERT, F. 2009. Dust explosions: Requirements for the occurrence, combustion and explosion characteristics measures. Northeastern University, Shenyang, China.

HAWRYCH, J. R. 1981. High pressure coal feeding systems for coal conversion plants. International Gas Research Conference. Worley Engineering Limited.

HELICON. 2010. Slurry pumps - Vhandra helicon pump pvt. ltd. [Online]. Available: http://www.heliconpumps.net/slurry-pumps.htm [Accessed 27th March 2012].

HIGMAN, C. & VAN DER BURGT, M. 2008. Gasification, Gulf Professional Publishing.

HOFFERT, F. D. & STOTLER, H. H. 1973. Method for feeding dry coal to superatmospheric pressure. U.S. patent application 164,381.

HOLDICH, R. G. 2002. Fundamentals of particle technology, Midland Information Technology and Publishing.

HOLT, N. A. H. 2001. Coal gasification research, development and demonstration-needs and opportunities. Gasification Technologies Conference. San Francisco, EPRI.

HUÉSCAR, M. C., PHYLAKTOU, H. N., ANDREWS, G. E. & GIBBS, B. M. 2012. Determination of the minimum explosible and most reactive concentrations for pulverised biomass using a modified Hartmann apparatus. Energy Research Institute, University of Leeds.

HUÉSCAR, M. C., PHYLAKTOU, H. N., SATTAR, H., ANDREWS, G. E. & GIBBS, B. M. 2013. The development of an experimental method for the determination of the minimum explosible concentration of biomass powders. Biomass and Bioenergy.

HYVÖNEN, A., PILTONEN, P. & NIINIMÄKI, J. 2005. Biodegradable substances in wood protection. Sustainable use of renewable natural resources–from principles to practices. University of Helsinki, Department of Forest Ecology Publications, 34.

ISLAM, M. S., HAMDAN, S., RUSOP, M., RAHMAN, M. R., AHMED, A. S. & IDRUS, M. M. 2012. Dimensional stability and water repellent efficiency measurement of chemically modified tropical light hardwood. BioResources, 7, 1221-1231.

JACOB, K. 2000. Bin and hopper design. The Dow Chemical Company.

JENIKE, A. W. & JOHANSON, J. R. 2010. Functional design of silos, bins, and hoppers [Online]. Available: http://www.jenike.com/Services/Engineering/FunctionalDesign/Silo-Hopper-Design.html [Accessed 2nd February 2012].

JENIKE, A. W. 1964. Storage and flow of solids: Bulletin No. 123. Bulletin of the University of Utah, 53.

JENIKE, A. W. 1984. Analysis of solids densification during the pressurization of lock hoppers. Powder Technology, 37, 131-143.

JET PROPULSION LABORATORY 1977. Proceedings of the conference on coal feeding systems. Manvi, R., California Institute of Technology, Pasadena, California, US Energy Research and Development Administration.

JOHANSON, J. R. 1991. Compacting screw feeder. U.S. patent application 509,591.

JONES, S. 2012. Firefighters battle Essex power station blaze [Online]. Available: http://www.guardian.co.uk/uk/2012/feb/27/firefighters-essex-power-station-blaze [Accessed 12th June 2013].

KAMYR. 1973. Equipment specifications for 200 ADT/D continuous cooking system with cold blow for sawdust [Online]. Available: http://www.maynards.com/media/Kamyr%20digester.pdf [Accessed 24th February 2012].

KAMYR. 2006. Pulp mill equipment: Asthma feeder [Online]. Available: http://surpluspaperequipment.com/inventory.php?id=10156 [Accessed 23rd February 2012].

KLIER, K. 1982. Methanol synthesis. Biomass to Methanol: A Specialist's Workshop. Tamarron, Durango, Colorado.

KLINZING, G. E., RIZK, F., MARCUS, R. & LEUNG, L. S. 2010. Pneumatic conveying of solids: A theoretical and practical approach, London, Springer Verlag.

KNOEF, H. A. M. & VIS, M. W. 2001. State of the art of feeding systems for biomass gasifiers. Enschede, BTG Biomass Technology Group BV.

KOCH, T. 2011a. Operation of the TKE feeder . Personal communication. TK Energi, September 2011.

KOCH, T. 2011b. TKE feed system. Gasification Technologies Conference. San Francisco, California.

KOPPEJAN, J. 2011. Safety aspects of solid biomass storage, transportation and feeding. Dublin SP Technical Research Institute of Sweden.

KRAUS, M. N. 1981. Pneumatic conveying of bulk materials. New York, McGraw-Hill.

KUOKKANEN, M. J., VILPPO, T., KUOKKANEN, T., STOOR, T. & NIINIMÄKI, J. 2011. Additives in wood pellet production – A pilot-scale study of binding agent usage. BioResources, 6, 4331-4355.

LABFACILITY. 2012. Thermocouple thermometry: Tolerance classes for thermocouples to IEC 584-2 [Online]. Available: http://www.labfacility.co.uk/pdf/temperature-handbook-9-to-13.pdf [Accessed 23rd 2012 2012].

LACKNER, M., WINTER, F. & AGARWAL, A. K. 2010. Handbook of combustion, Volume 4: Solid Fuels, Weinheim, WILEY-VCH Verlag GmbH & Co.

LAU, F. S., BOWEN, D. A., DIHU, R., DOONG, S., HUGHES, E. E., REMICK, R., SLIMANE, R., TURN, S. Q. & ZABRANSKY, R. 2002. Techno-economic analysis of hydrogen production by gasification of biomass. DOE, NETL. DE-FC36-01GO11089.

LEVELTON, B. H. 1982. Status of biomass feeder technology, Canadian Forestry Service.

LOH, H. P., LYONS, J. & WHITE III, C. W. 2002. Process equipment cost estimation: Final report. NETL, Pittsburgh PA, Morgantown WV.

MAHR, D. 2011. Biomass attributes, handling and processing issues [Online]. Available: https://www.asme.org/engineering-topics/articles/sustainability/biomass-attributes-handling-and-processing [Accessed 30th May 2013].

MANKOC, C., JANDA, A., AREVALO, R., PASTOR, J. M., ZURIGUEL, I., GARCIMARTÍN, A. & MAZA, D. 2007. The flow rate of granular materials through an orifice. Granular Matter, 9, 407-414.

MARCUS, R., LEUNG, L. S., KLINZING, G. E. & RIZK, F. 1990. Pneumatic conveying of solids: A theoretical and practical approach, Chapman and Hall.

MARINELLI, J. & CARSON, J. W. 1992. Solve solids flow problems in bins, hoppers, and feeders. Chemical Engineering Progress, 88, 22-28.

MAURSTAD, O. 2005. An overview of coal based integrated gasification combined cycle (IGCC) technology. Cambridge, Massachusetts Institute of Technology.

MCGLINCHEY, D. 2008. Bulk solids handling: Equipment selection and operation, Blackwell Publishing.

MEDRANO, M., GIL, A., MARTORELL, I., POTAU, X. & CABEZA, L. F. 2010. State of the art on high-temperature thermal energy storage for power generation. Part 2—Case studies. Renewable and Sustainable Energy Reviews, 14, 56-72.

MERRITT, M. 2012. Biomass: energy remedy or safety headache? The Chemical Engineer, November Issue.

METSO. 2009. Metso corporation: Mechanical fiber screw feeder [Online]. Available: http://www.metso.com/MP/Marketing/mpv2store.nsf/BYWID/WID-031120-2256C-3F9E3/$File/MPDU_R_2075_091-02.pdf?openElement [Accessed 23rd March 2012].

METZ, B., DAVIDSON, O., DE CONINCK, H., LOOS, M. & MEYER, L. 2005. IPCC special report on carbon dioxide capture and storage. Intergovernmental Panel on Climate Change, Geneva, Switzerland. Working Group III.

MEYER, J. W., BONIN, J. H. & DANIEL JR, A. D. 1983. Kinetic extruder-a dry pulverized solid material pump. U.S. patent application 188,047.

MEYER, J. W., BONIN, J. H. & DANIEL JR, A. D. 1984. Dry pulverized solid material pump. U.S. patent application 363,539.

MEYER, J. W., DANIEL JR, A. D. & BONIN, J. H. 1982. Means and apparatus for throttling a dry pulverized solid material pump. U.S. patent application 199,861.

MEYER. 2012. Meyer process conveying components, CV Series [Online]. Available: http://www.rotaryvalve.com/index.php?option=com_content&view=article&id=123 [Accessed 30th March 2012].

MIELKE, T. 2013. Oil world monthly: World supply, demand and price forecasts for oilseeds, oils and meals. Oil World, No. 50, Vol. 56, 13, December 2013.

MILLS, D. 2004. Pneumatic conveying design guide, Oxford, Butterworth-Heinemann.

MISTRY, D. K. & CHEN, T. N. 1977. Dry coal feeder development program at Ingersoll-Rand Research Inc. Conference on Coal Feeding Systems. California Institute of Technology, Pasadena, California: Ingersoll-Rand research inc., Princeton, New Jersey.

MISTRY, D. K. & HATHAWAY, T. 1982. Development of high pressure pilot scale piston and screw feeders. Spring National Meeting and Chemical Plant Equipment Exposition. AIChE, New York.

MISTRY, D. K. & WISE, B. A. 1978. Development of coal piston feeder: Phase-I final report. Princeton, New Jersey, Ingersoll-Rand Research, Inc.

MODAK, J. M. 2002. Haber process for ammonia synthesis. Resonance, 7, 69-77.

MOREL, W. C. 1977. Economic comparison of coal feeding systems in coal gasification - Lock hopper vs slurry. American Chemical Society: Division of Fuel Chemistry, 22, 155-164.

MOREY, R. V. & ZHENG, H. 2011. Chapter 2: Integrating super heated steam dryer technology at the plant for energy reduction and water conservation. Saint Paul, University of Minnesota.

MORFEE, J. 2014. Used cooking oil price per litre. Personal communication. Star Oils, January 2014.

MOSS, D. R. 2004. Pressure vessel design manual: illustrated procedures for solving major pressure vessel design problems, Oxford, Gulf Professional Publishing.

MST. 2010. MST Corporation main catalog. Prineville OR.

NATIONALGRID. 2010. How electricity is made and transmitted. Warwick, National Grid.

NEDDERMAN, R. M., TŪZŪN, U. & THORPE, R. B. 1983. The effect of interstitial air pressure gradients on the discharge from bins. Powder Technology, 35, 69-81.

NETL. 2010a. Cost and performance baseline for fossil fuel plants. DOE NETL, DOE/2010/1397.

NETL. 2010b. U.S. Department of energy: Gasification 2010 worldwide database. Pittsburgh, US DOE, NETL.

NETL. 2009. Advanced gasification systems development - PWR High pressure feed pump [Online]. Available: http://www.netl.doe.gov/publications/factsheets/project/Proj328.pdf [Accessed 27th October 2011].

NETL. 2013. Range of syngas compositions across different gasifier type and feedstock produced by the gasification of coal feedstocks [Online]. Available: http://www.netl.doe.gov/technologies/coalpower/gasification/gasifipedia/4-gasifiers/4-3_syngas-table2.html [Accessed 14th June 2013].

NETL. 2014. Types of gasifiers [Online]. Available: http://www.netl.doe.gov/research/coal/energy-systems/gasification/gasifipedia/types-gasifiers [Accessed 25th March 2014].

NEVES, D., THUNMAN, H., MATOS, A., TARELHO, L. & GÓMEZ-BAREA, A. 2011. Characterization and prediction of biomass pyrolysis products. Progress in Energy and Combustion Science, 37, 611-630.

OBERNBERGER, I. & THEK, G. 2010. The pellet handbook: The production and thermal utilisation of biomass pellets, London, Washington DC, Earthscan Ltd.

OFGEM. 2003. Electricity distribution losses - A consultation document. Office of Gas and Electricity Markets.

O'NEILL, P. A. 1993. Industrial compressors: Theory and equipment, Butterworth-Heinemann, Oxford.

PARRETT, W. 2014. Knife gate valve costing. Personal communication. Orbinox UK, June 2014.

PEDERSEN, G. H. & WILKINS, B. A. 1988. Explosibility of coal dusts and coal dust/limestone mixtures at elevated initial pressures. Bergen, Norway, Michelsen Institute.

PERALTA-SOLORIO, D. 2013. Onsite electricity prices for a coal-fired power station. Personal communication, E.ON, July 2013.

PERRY, R. H., GREEN, D. W. & MALONEY, J. O. 1997. Perry's chemical engineers' handbook, McGraw-Hill, New York.

PHILLIPS, J. 2006. Different types of gasifiers and their integration with gas turbines. Electric Power Research Institute, Advanced Coal Generation.

PILÃO, R., RAMALHO, E. & PINHO, C. 2004. Influence of initial pressure on the explosibility of cork dust/air mixtures. Journal of Loss Prevention in the Process Industries, 17, 87-96.

PÖYRY 2011. Pellets - Becoming a global commodity? Global market, players and trade to 2020. Pöyry.

PROUGH, J. R. 1993. High pressure feeder. U.S. patent application 868,345.

PUTZMEISTER. 2009. High density solids pumps KOS: For coarse grain high density solids and high pressure applications - Putzmeister Solid Pumps GmbH [Online]. Available: http://www.pmsolid.com/psp/data/IP_1082_7_GB_KOS.pdf [Accessed 24th February 2012].

PUTZMEISTER. 2010a. EKO 1060 PP high-density solids pump: Specialized Equipment for both Pumping and Pressing - Putzmeister Solid Pumps GmbH [Online]. Available: http://www.pmsolid.com/psp/data/IP_4277_GB_EKO_1060_PP_web.pdf [Accessed 24th February 2012].

PUTZMEISTER. 2010b. KOV piston pumps with ball valves - Putzmeister Solid Pumps GmbH [Online]. Available: http://www.putzmeister-solid-pumps.com/psp/data/IP_1027-5_GB_KOV_web.pdf [Accessed 27th March 2012].

PUTZMEISTER. 2010c. Single piston pump of the EKO series - Putzmeister Solid Pumps GmbH [Online]. Available: http://www.pmsolid.com/psp/data/IP_2253_4_GB_web.pdf [Accessed 24th February 2012].

RAUTALIN, A. & WILÉN, C. 1992. Feeding biomass into pressure and related safety engineering, Technical Research Centre of Finland (VTT).

RENEWABLES INTERNATIONAL. 2011. Following explosion, world's largest pellet plant resumes operation [Online]. Available: http://www.renewablesinternational.net/following-explosion-worlds-largest-pellet-plant-resumes-operation/150/515/31440/ [Accessed 12th June 2013].

REZAIYAN, J. & CHEREMISINOFF, N. P. 2005. Gasification technologies: A primer for engineers and scientists, CRC.

RHODES, M. J. 2008. Introduction to particle technology, Wiley.

RICHARDSON, J. F., COULSON, J. M., HARKER, J. H. & BACKHURST, J. R. 2002. Chemical engineering: Particle technology and separation processes, Butterworth-Heinemann, Oxford.

RICHTER, O. J. & RICHTER, J. C. F. C. 1984. High pressure feeder deflection compensation. U.S. patent application 209,118.

ROLLSROYCE. 2013. Rolls Royce WR-21 marine gas turbine [Online]. Available: http://www.rolls-royce.com/marine/products/diesels_gas_turbines/gas_turbines/wr21.jsp [Accessed 13th March 2014].

ROSILLO-CALLÉ, F., PELKMANS, L. & WALTER, A. 2009. A global overview of vegetable oils, with reference to biodiesel. IEA Bioenergy, Task 40.

ROTHBART, H. A. 1985. Mechanical design and systems handbook, New York, McGraw-Hill.

RYASON, P. R. 1980. Continuous coal processing method. U. S. patent application 727,444.

SATTARI-FAR, I. 2003. Failure study of connecting shafts of a plug screw feeder in a paper production plant. Engineering Failure Analysis, 10, 341-349.

SAUNDERS, T. W. 2012. Dry solids pump development and commercial-scale testing. International Freiberg Conference on IGCC & XTL Technologies. Freiberg, Germany, Pratt & Whitney Rocketdyne.

SCHELL, D. 1988. High pressure solids feeding using a lock hopper system: Design and operating experience. Applied Biochemistry and Biotechnology, 17, 73-87.

SCHLOSSBERG, J. 2013. Biomass Industry Plays With Fire, Gets Burned [Online]. Available: http://www.energyjustice.net/content/biomass-industry-plays-fire-gets-burned-biomass-monitor [Accessed 12th June 2013].

SCHULZE, D. 2008. Powders and bulk solids: Behaviour, characterization, storage and flow, Springer.

SHANNON, K. S. & BUTLER, B. W. 2003. A review of error associated with thermocouple temperature measurement in fire environments. American Meteorological Society.

SHAVIT, A. & GUTFINGER, C. 1995. Thermodynamics: From concepts to applications, Prentice Hall.

SHINODA, K. & BECHER, P. 1978. Principles of solution and solubility, Marcel Dekker, Inc.

SIKKEMA, R., STEINER, M., JUNGINGER, M., HIEGL, W., HANSEN, M. T. & FAAIJ, A. 2011. The European wood pellet markets: Current status and prospects for 2020. Biofuels, Bioproducts and Biorefining, 5, 250-278.

SINNOTT, R. K. 2007. Chemical engineering design: Volume 6, 4th edition, Oxford, Butterworth-Heinemann.

SLIMANE, R., TURN, S. Q. & ZABRANSKY, R. 2002. Techno-economic analysis of hydrogen production by gasification of biomass. Department of Energy and National Renewable Energy Laboratory, DE-FC36-01GO11089.

SMITH, B., EBERLE, C., FRAME, B., BLENCOE, J., ANOVITZ, L. & MAYS, J. 2005. III.A.2 FRP Hydrogen Pipelines. Oak Ridge TN, Oak Ridge National Laboratory.

SMITH, D. A. & POTE, B. M. 1983. Solids pumping apparatus. U.S. patent application 343,688.

SOHNASSOCIATES 2009. Electricity distribution systems losses - Non-technical overiew. Sohn Associates for the Office of Gas and Electricity Markets.

SPATH, P. L. & DAYTON, D. C. 2003. Preliminary screening - Technical and economic assessment of synthesis gas to fuels and chemicals with emphasis on the potential for biomass-derived syngas. National Renewable Energy Laboratory.

SPATH, P., AMOS, W., CHAMBERS, H., MADDEN, D. R., SMITH, D. A. & SHELTON, W. 1999. Technoeconomic analysis of hydrogen production from western coal augmented with CO2 sequestration and coalbed methane recovery. Golden CO, National Renewable Energy Laboratory.

SPROUSE, K. M. & MATTHEWS, D. R. 2006. Linear tractor dry coal extrusion pump.

SPROUSE, K. M. & MATTHEWS, D. R. 2008. Linear extrusion 400 tons/day dry solids pump. Pratt & Whitney Rocketdyne Inc.

STAINLESS VALVE CO. 2014. Stargate O-port valve [Online]. Available: http://www.stainlessvalveco.com/Products/StargateOPort/tabid/64/Default.aspx [Accessed 7th February 2014].

STAUDINGER, G. 1977. Process and apparatus for the supply of a dry, free-flowing coal powder to a high-pressure coal gasification reactor. U.S. patent application 676,725.

STEVENSON, J. S. 1985. Dry feeder for finely divided solids into high pressure atmosphere. U.S. patent application 600,275.

SUGO, H., KISI, E. & CUSKELLY, D. 2013. Miscibility gap alloys with inverse microstructures and high thermal conductivity for high energy density thermal storage applications. Applied Thermal Engineering, 51, 1345-1350.

SWANSON, M. L., MUSICH, M. A., SCHMIDT, D. D. & SCHULTZ, J. K. 2003. Feed system innovation for gasification of locally economical alternative fuels (FIGLEAF). Final technical report for the period 1 Sept. 2000 to 30 Nov. 2002. DOE Agreement No. DE-FC26-00NT40904. US DOE, NETL, Pittsburgh, PA.

SWITHENBANK, J. 2012. The University of Sheffield, Personal communication, February 2012.

SWITHENBANK, J. 2013. Future energy challenges. Helsinki, Finland, Academy of Finland.

SWITHENBANK, J., CHEN, Q., ZHANG, X., SHARIFI, V. & POURKASHANIAN, M. 2011. Wood would burn. Biomass and Bioenergy, 35, 999-1007.

TAKAHASHI, K. 2001. Hydrogen transportation. Energy Carriers and Conversion Systems Vol. II.

TARASOV, D., SHAHI, C. & LEITCH, M. 2013. Effect of additives on wood pellet physical and thermal characteristics: A review. ISRN Forestry, 2013, 6.

THOMAS CONVEYOR CO. 2014. Horizontal screw conveyors [Online]. Available: http://www.thomasconveyor.com/docs/engGuide/Pages005-036SCREWCONVEYORS-Enginering.pdf [Accessed 26th February 2014].

TREWIN, S., MARVIN, J. & O'NEILL, A. 2013. Quarterly energy prices December 2013. National Statistics, Department of Energy and Climate Change, UK.

VAN DER BURGT, M. J. 1978. Apparatus for the supply of fuel powder to a gas-pressurized vessel. U.S. patent application 819,366.

VAN DER BURGT, M. J. 1982. Method and device for the feeding of finely divided solid matter to a gas-containing vessel. U.S. patent application 201,256.

VAN DER DRIFT, A., BOERRIGTER, H., CODA, B., CIEPLIK, M. K., HEMMES, K., VAN REE, R. & VERINGA, H. J. 2004. Entrained flow gasification of biomass. ECN Biomass. Available from: http://www.ecn.nl/docs/library/report/2004/c04039.pdf.

VAN DEVENTER, H. C. & HEIJMANS, R. M. H. 2001. Drying with superheated steam. Drying Technology, 19, 2033-2045.

VAN DEVENTER, H. C. 2004. Industrial superheated steam drying. Apeldoorn NL, TNO Environment, Energy and Process Innovation.

VAN LOO, S. & KOPPEJAN, J. 2008. The handbook of biomass combustion and co-firing, Earthscan.

VATAVUK, W. M. 2002. Updating the CE plant cost index. Chemical engineering, 109, 62-70.

VERHOEST, C. & RYCKMANS, Y. 2012. Industrial wood pellets report. PellCert, Intelligent Energy Europe.

VISCONTY, G. J. 1956. Method of transporting powder into advanced pressure zone. U.S. patent application 269,543.

VON HARBOU, I., HOCH, S., MANGALAPALLY, H. P., NOTZ, R., SIEDER, G., GARCIA, H., SPUHL, O. & HASSE, H. 2014. Removal of carbon dioxide from flue gases with aqueous MEA solution containing ethanol. Chemical Engineering and Processing, Process Intensification, 75, 81-89.

WAKEMAN, R. J. & TARLETON, E. S. 2006. Solid/liquid separation equipment simulation & design — An expert systems approach, Elsevier.

WALTHER, C. D. & SCHACKE, H. 1986. Evaluation of dust explosion characteristics at reduced and elevated initial pressures. Leverkusen, Federal Republic of Germany, Bayer AG.

WARK JR., K. 1989. Thermodynamics, Singapore, McGraw-Hill.

WIEDENHOEFT, A. 2010. Structure and function of wood. Wood handbook: Wood as an engineering material. United States Department of Agriculture Forest Service, Madison, Wisconsin.

WIEDMANN, W. & MACK, W. A. 1977. The use of twin screw extruders for feeding coal against pressures of up to 1500 psi. Conference on Coal Feeding Systems. California Institute of Technology, Pasadena, California, Werner & Pfleiderer, Stuttgart, West Germany and Werner & Pfleiderer Corp., Waldwick, New Jersey.

WIEMANN, W. 1987. Influence of temperature and pressure on the explosion characteristics of dust/air and dust/air/inert gas mixtures. Industrial Dust Explosions, ASTM, 33-44.

WILÉN, C. & RAUTALIN, A. 1993. Handling and feeding of biomass to pressurized reactors: Safety engineering. Bioresource Technology, 46, 77-85.

WILÉN, C. & RAUTALIN, A. 2001. Safe handling of biomass fuels in advanced power production, 1st World Conference on Biomass for Energy and Industry. Sevilla, Spain.

WILÉN, C., RAUTALIN, A., GARCÍA-TORRENT, J. & CONDE-LÁZARO, E. 1998. Inerting biomass dust explosions under hyperbaric working conditions. Fuel, 77, 1089-1092.

WILTSEE, G. 2000. Lessons learned from existing biomass power plants. California, National Renewable Energy Laboratory.

WOODCOCK, C. R. & MASON, J. S. 1996. Bulk solids handling: An introduction to the practice and technology, Chapman & Hall.

YAWS, C. L. 2003. Yaws' handbook of thermodynamic and physical properties of chemical compounds. Knovel.

ZEPPELIN. 2011. Bulk solids components from the system supplier. Houston TX.

ZOANNOU, K.-S., SAPSFORD, D. J. & GRIFFITHS, A. J. 2013. Thermal degradation of monoethanolamine and its effect on CO2 capture capacity. International Journal of Greenhouse Gas Control, 17, 423-430.

APPENDIX A

Journal publications

CRAVEN, J. M., SWITHENBANK, J., SHARIFI, V. N., PERALTA-SOLORIO, D., KELSALL, G. & SAGE, P. 2014. Development of a novel solids feed system for high pressure gasification. Fuel Processing Technology, 119, 32-40.

CRAVEN, J. M., SWITHENBANK, J., SHARIFI, V. N., PERALTA-SOLORIO, D., KELSALL, G. & SAGE, P. 2014. Hydrophobic coatings for moisture stable wood pellets. Biomass and Bioenergy, In Review.

Conference papers

CRAVEN, J. M., SWITHENBANK, J. & SHARIFI, V. N. 2013. High pressure solids feeder. 21st European Biomass Conference and Exhibition, 3-7th June 2013, Copenhagen, Denmark, 753-758.

CRAVEN, J., SWITHENBANK, J. & SHARIFI, V. 2013. High pressure feed system for pressurised biomass gasification. Bioenergy 2013, 4-6th September 2013, Jyväskylä, Finland, 205-212.

Conference presentations

E-Futures Annual Conference, 19-20th September 2012, Sheffield, United Kingdom. Poster presentation.

21st European Biomass Conference and Exhibition, 3-7th June 2013, Copenhagen, Denmark. Poster presentation.

Bioenergy 2013, 4-6th September 2013, Jyväskylä, Finland. Oral presentation.

E-Futures Annual Conference, 16-17th September 2013, Sheffield, United Kingdom. Oral presentation.

SUPERGEN Bioenergy Hub Assembly 2013, 19th November 2013, Leeds, United Kingdom. Poster presentation.

Postgraduate Research Conference, 28th May 2014, Sheffield, United Kingdom. Oral presentation.

Prizes and awards

2013 Energy Institute Foxwell Memorial Prize.

2013 SUPERGEN Bioenergy Hub Assembly Poster Prize.

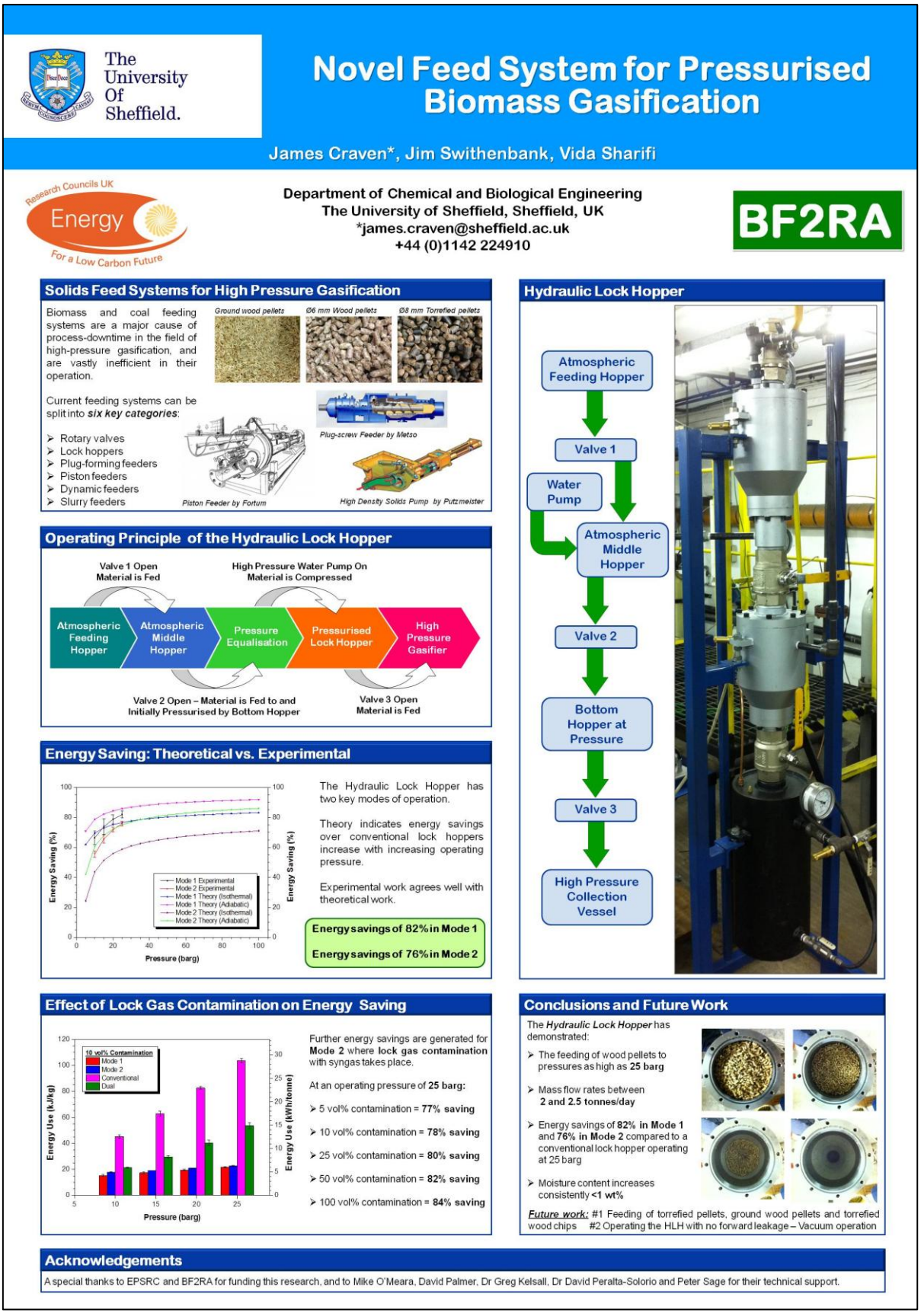

Figure 1: Research poster presented at the 21st European Biomass Conference and Exhibition in Copenhagen, Denmark (June 2013).

APPENDIX B

In addition to the core work carried out over the course of this PhD study is a piece of work relating to the production of moisture stable wood pellets. The following sections provide an overview of the work undertaken in this area, and provide information on a means for enhancing wood pellet moisture stability.

1.1 Introduction

Wood pellet stability is a key factor affecting the economic viability and safe deployment of wood pellet fired systems. Wood pellets are well known for being moisture unstable and present significant problems when being transported, stored and handled. Due to their high hygroscopicity, wood pellets become unstable when wetted and readily disintegrate. This disintegration and loss of mechanical stability is typically accompanied by a large increase in volume, and when pellets are constrained, significant structural damage to process equipment can be brought about. The uptake of moisture also enhances biological activity within the fuel which can cause pellets to rot or self-heat. Where self-heating takes place, a significant fire and/or explosion hazard is brought about due to the release of combustible gases (Obernberger and Thek, 2010). Such phenomena have been noted during the development of the HLH, and the mechanical instability of wood pellets has lead to problems during feeding.

While wood pellets present advantages over many competing biomass fuels in terms of moisture content and energy density, their biggest drawback remains their moisture instability. Additives such as lignosulphonate, starch, dolomite, potato flour, corn flour and kraft lignin have been explored as binding agents to improve the mechanical characteristics of wood pellets; however, such additives have not been found to markedly improve the moisture stability of wood pellets (Kuokkanen et al., 2011, Berghel et al., 2013, Tarasov et al., 2013). This chapter details the work carried out regarding wood pellet encapsulation to produce moisture stable wood pellets. Commercially available 6 mm diameter wood pellets were treated with a range of oils in order to reduce their hygroscopicity. The effect such treatments had on the heating value, grinding behaviour and combustion properties of wood pellets is detailed, in addition to the effect they had on pellet hydrophobicity.

1.2 Wood pellet market overview

The global wood pellet market has grown considerably over the past decade and wood pellets are now one of the largest internationally traded solid biomass fuels (Sikkema et al., 2011). Worldwide

production was recorded to be as high as 22.4 million tonnes in 2012, an increase of more than 55% compared to levels reported in 2010 (Cocchi et al., 2011, Pöyry, 2011, Verhoest and Ryckmans, 2012, Calderón et al., 2013). In 2012, worldwide wood pellet production capacity stood at approximately 29.3 million tonnes per annum, and currently the United States (US) leads the way as the largest wood pellet producing country (Cocchi et al., 2011). Increases in production capacity in the US, Canada and Russia were recorded to be greater than any other competing European country between 2009 and 2010. However, the European Union (EU) as a whole is considered to be the world wood pellet market leader, and produces approximately 50% of the world's wood pellets and consumes around 69% (Cocchi et al., 2011, Pöyry, 2011, Calderón et al., 2013, Flach et al., 2013).

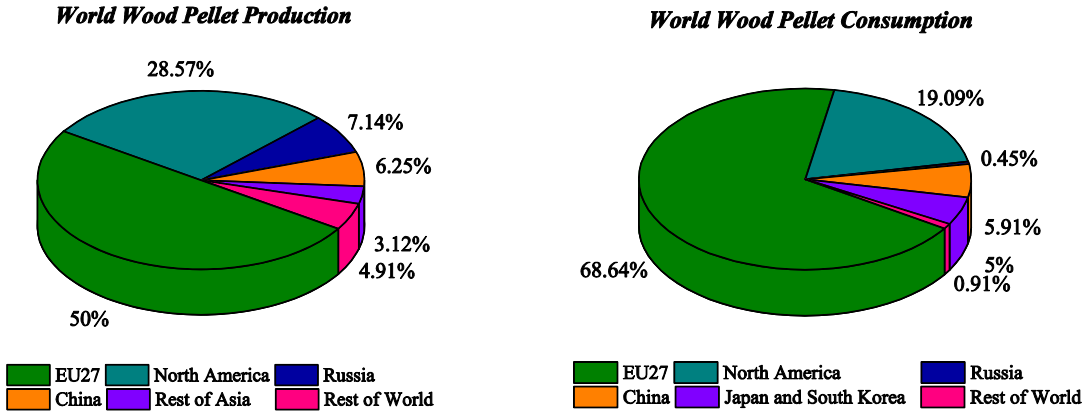

Figure 1: World wood pellet production and consumption share in 2012 (Calderón et al., 2013).

1.3 Materials and methods

1.3.1 Materials

As with the material characterisation tests detailed in Chapter 4, the wood pellets used in this study were 6 mm in diameter and procured from CPL Distribution Ltd. The pellets were made from chemically untreated residues from the wood processing industry and comprise a low ash pellet conforming to the standard EN Plus A1.

Wood pellets were encapsulated using a range of oils, each of which is detailed in Table 1. All of the oils used in this study were procured from Sigma-Aldrich UK Ltd.

Oil	Density (kg/m^3)	Viscosity 25 °C (Pa s)	HHV (MJ/kg)
Paraffin	870 ± 2	0.12 ± 0.01	44.74 ± 0.22
Castor	965 ± 9	0.91 ± 0.01	35.91 ± 0.03
Mineral	868 ± 7	0.04 ± 0.01	44.59 ± 0.01
Linseed	957 ± 5	0.03 ± 0.01	37.72 ± 0.06

Table 1: Overview of the oils used for wood pellet encapsulation.

1.3.2 Methods

1.3.2.1 Wood pellet coating

Two methods were used to apply each of the oils. Where individual pellet strength and mass uptake of oil was being assessed, pellets were submerged in 100 ml of oil using tweezers for up to 10 seconds to ensure surface saturation of oil. Pellets were then air dried on a coarse mesh for 24 hours to allow any excess oil to be removed via gravity. Testing with individual pellets was carried out immediately after the drying stage was complete.

Where the milling behaviour and combustion properties of the oil treated pellets were being assessed, pellets were treated in bulk in 140 g batches. 5 ml of oil was syringed into a volumetric beaker, the batch of pellets was added on top of this and then a further 5 ml of oil was syringed into the beaker. Pellets were then stirred for 5 minutes to ensure the complete uptake of oil and that an even coating was applied. Pellets were then air dried on 5 sheets of Kimberly-Clark industrial 2-ply cleaning towel for 24 hours to ensure the removal of any excess oil present of the surface of the pellets.

1.3.2.2 Three point flexural testing

A Zwick Roell Z050 tensile tester was used to assess the strength of individual wood pellets. Pellets sized between 26 mm and 28 mm were selected, treated with oil as per Section 1.3.2.1 and then seated horizontally on a span measuring 20 mm across. A 5 kN load cell was fitted to the tensile tester and a load was applied at the midpoint of each pellet. An advancing speed of 0.5 mm/minute was used in each case, and a force was exerted until failure was reached.

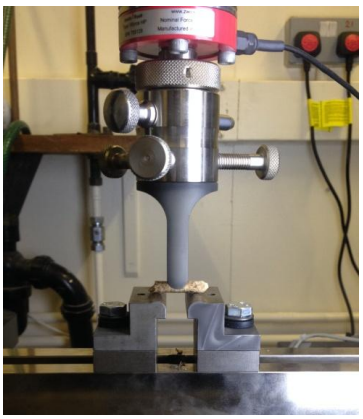

Figure 2: Zwick Roell Z050 tensile tester with a 20 mm span and fitted with a 5 kN load cell.

1.3.2.3 Pellet milling and particle size analysis

A Retsch PM100 planetary ball mill was used to mill pellets both in their treated and untreated state. The ball mill used was fitted with a 500 ml stainless steel bowl containing eight 30 mm diameter

stainless steel balls and a rotational speed of 200 rpm was maintained constant throughout testing. The time taken for milling was varied throughout up to a maximum of 30 minutes.

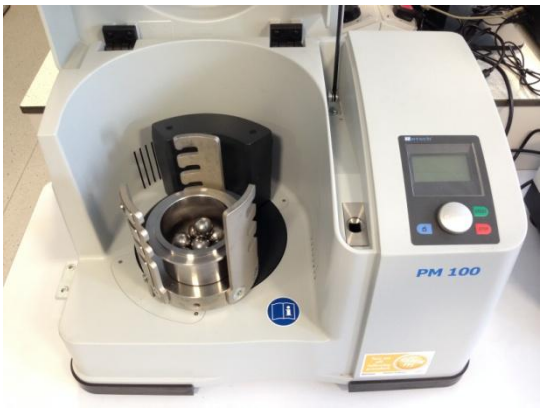

Figure 3: Retsch PM100 planetary ball mill fitted with a 500 ml bowl and eight 30 mm diameter stainless steel balls.

The particle size distribution of each batch of milled pellets was assessed using a Retsch AS200 basic vibratory sieve shaker. Retsch particle sieves conforming to the standard ISO 3310-1 were used in conjunction with this and were sized with apertures of 2 mm, 1 mm, 250 μm, 200 μm and 125 μm.

1.3.2.4 Heating value and thermogravimetric analysis

A Parr 6200 isoperibol oxygen bomb calorimeter fitted with Ni-alloy fuse wire was used to assess the higher heating value (HHV) of each of the wood pellet species. Pure oxygen was used as the oxidant in the calorimeter, and tests were carried out using approximately 1 g of milled material sized at less than 250 μm.

A PerkinElmer TGA 4000 was used to carry out thermogravimetric (TG) analysis to determine the moisture, volatile, fixed carbon and ash content of each of the pellet samples. The cycle imposed was maintained constant throughout testing and is as follows. Samples were initially put under a nitrogen atmosphere, heated to a temperature of 40 °C and held there for 1 minute. Samples were then heated from 40 °C to 110 °C at a rate of 65 °C/minute and held at 110 °C for 3 minutes to ensure the complete removal of moisture. Samples were then heated from 110 °C to 900 °C at a rate of 100 °C/minute and were held at 900 °C for 8 minutes to allow the complete removal of all volatile matter. Samples were then subjected to an oxygen atmosphere and completely combusted to allow the determination of both the fixed carbon and ash content. Following this, samples were then heated from 900 °C to 950 °C at a rate of 50 °C/minute before being returned back to ambient temperature. TG tests were carried out using approximately 15 mg of milled material sized at less than 250 μm.

1.4 Pellet encapsulation results and discussion

1.4.1 Oil absorption

In order to gauge the effect of submersion time on the mass uptake of oil, pellets were submerged in oil samples at time intervals of 1 second, 2 seconds, 3 seconds, 5 seconds and 10 seconds. Table 2 highlights there to be no direct relationship between time submerged and the uptake of oil on a mass basis, and in turn indicates that pellets become saturated with oil after the first second of being submerged.

	Mass Increase (%)			
Time (s)	**Paraffin Oil**	**Castor Oil**	**Mineral Oil**	**Linseed Oil**
1	6.8 ± 0.7	7.8 ± 0.8	6.1 ± 0.5	6.9 ± 0.9
2	6.6 ± 0.4	8.7 ± 1.1	6.2 ± 0.6	7.6 ± 0.5
3	7.3 ± 0.5	8.6 ± 1.2	6.0 ± 0.6	7.5 ± 0.6
5	6.5 ± 0.6	9.0 ± 1.6	6.1 ± 0.6	7.8 ± 0.9
10	7.0 ± 0.5	9.1 ± 1.0	6.2 ± 0.6	7.5 ± 0.4
Bulk	4.4 ± 0.5	6.3 ± 0.3	5.2 ± 0.0	5.2 ± 0.4

Table 2: Effect of submersion time on the mass uptake of oil.

Throughout testing, bubbles were observed to form on the surface of the pellets when submerged. Bubbles form due to internal void spaces present within the pellet structure, and in turn it was envisaged that oil absorption may be related to pellet voidage. However, plotting the volume of voids against the volume of oil absorbed (Figure 4) shows no clear relationship between the two. It is likely that absorption takes place via two mechanisms: by being trapped in internal void spaces contained within the pellet and via active sites within the pellet structure as it does with wood species in their raw form. Wood treatment with oil has been explored in previous work with the aim to stopping biological processes and rotting. It is generally accepted that oil binds to hydroxyl groups contained within the cellulosic and hemi-cellulosic structures via Van der Waals forces (Hyvönen et al., 2005). As the proportion of such structures varies between wood species, oil absorption differs from one wood specie to another. Generally, wood pellets are not made from individual wood species but are produced from residues obtained from saw mills which are comprised of a mixture of different wood species (Obernberger and Thek, 2010). Therefore, it is near impossible to know the exact makeup of an individual wood pellet and the makeup of one wood pellet is likely to be different to another. It is for this reason that such a large error is shown for the values for mass uptake displayed in Table 2, and that no direct relationship is obtained between the physical pellet geometry and oil absorption.

In addition to individual pellet treatment, oil absorption was also undertaken on a bulk basis. Table 2 indicates that oil absorption on a bulk basis is consistently lower than when individual pellets are treated, with individual pellets generating mass increases on average 2.0% higher. Treatment with

mineral oil on a bulk basis was found to be the most similar to individual pellet treatment, and was found to generate mass increases on average 1.0% lower than where pellets were treated individually. Comparably, paraffin oil treatment on a bulk basis was found to be the least similar, and was found to generate mass increases on average 2.6% lower than where pellets were treated individually.

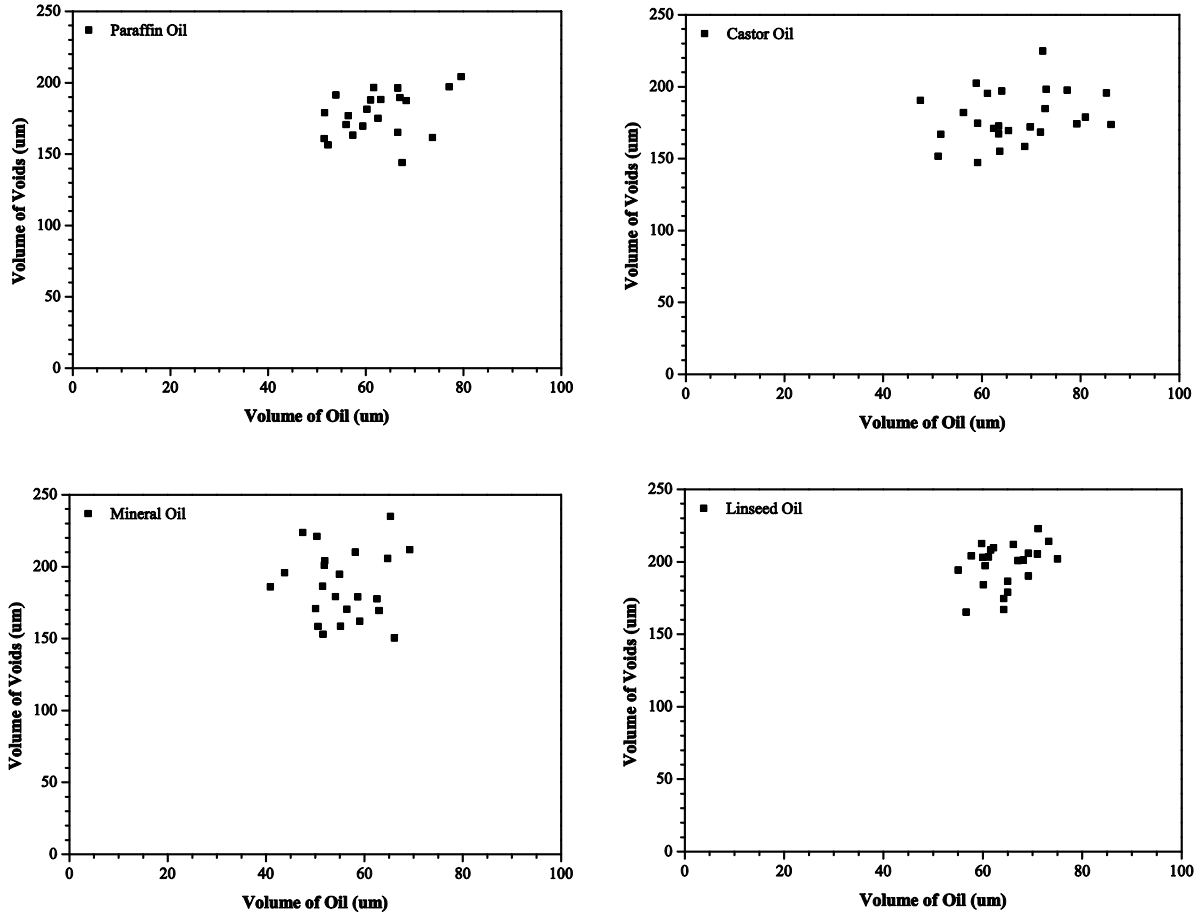

Figure 4: Relationship between the volume of oil absorbed and the volume of pellet voids.

The difference between the two treatments can be accounted for by the drying process used in each case. Where pellets were treated individually, pellets were air dried for 24 hours and excess oil was allowed to be removed via gravity. However, where pellets were dried in bulk, pellets were dried on an absorbent material which allowed both excess and surface oil to be removed. Due to the high viscosity of each of the oils, surface oil was found throughout testing individual pellets and the results relating to mass uptake of oil shown in Table 2 take this into account.

1.4.2 Wood pellet hygroscopicity

Figure 5 shows how wood pellets behave when submerged in water both before and after undergoing treatment with oil. Swelling was found to take place immediately after being submerged in the case of

the untreated pellets, and appreciable degrees of swelling were noted after being submerged for as little as 30 seconds. It is proposed that swelling takes place in pellets in the same way that it does in wood in its raw form. Where wood in its raw form is concerned, water forms hydrogen bonds with hydroxyl groups contained within the hemi-cellulosic and cellulosic structures in the cell wall of the wood. In turn, the volume of the cell wall increases, increasing approximately in proportion to the volume of water that is absorbed (Hyvönen et al., 2005, Wiedenhoeft, 2010, Islam et al., 2012). This process takes place until the fibre saturation point of the wood is reached (Hyvönen et al., 2005). In the case of the untreated wood pellets, the uptake of water and subsequent swelling was found to cause pellets to break up irreversibly. This was primarily noted to be because wood pellets are made from a series of small particles bound together. When pellets were submerged in water, wood particles were initially found to separate from the surface of the pellets, and after time, cracks were found to form laterally along the length of the pellets. As absorption proceeded, the cracks formed in the pellets were found to grow until their structure disintegrated.

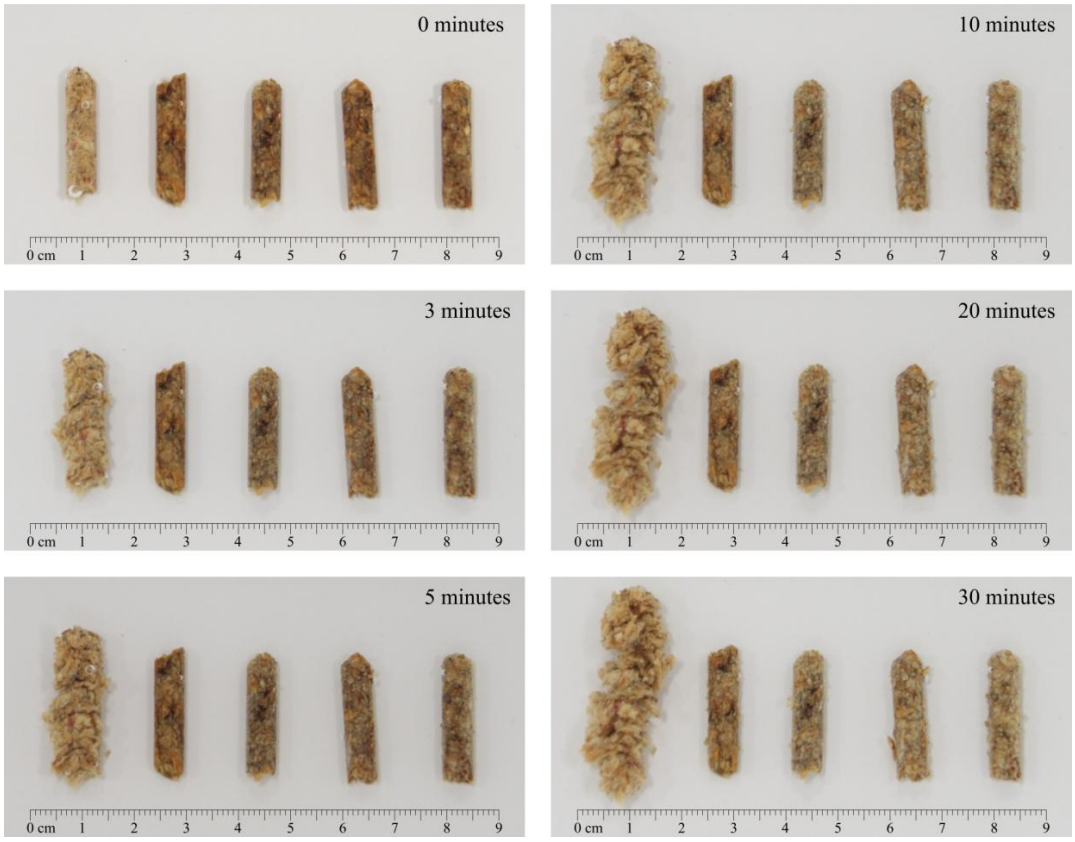

Figure 5: Effect of submersion in water on pellet stability.
Left to right: Untreated, paraffin oil, castor oil, mineral oil, linseed oil.

Comparatively, minimal changes were observed in all cases where wood pellets were treated with oil, with pellets maintaining their structure after being submerged for as long as 30 minutes. Initial signs of wood particles separating from the surface of the pellets were noted after being submerged for 10

minutes in all oil treated cases, and initial signs of wood particle separation were noted after 5 minutes in the case of the linseed and mineral oil treated pellets. However, the structure of the pellets in all cases was found to be maintained over the time period studied (30 minutes). It is proposed that small degrees of particle separation take place due to the relatively weak Van der Waals interactions between the oil treatment and the wood pellet structure. As exposure to water is increased, oil becomes displaced by water which in turn forms stronger hydrogen bonds with the surface of the wood. When left long enough, oil treated pellets were found to disintegrate in the same way as untreated pellets. However, comparable disintegration was only found to occur after pellets were submerged for up to 90 to 120 minutes.

In addition to swelling, air bubbles were found to form on the surface of all pellets after being submerged in water. Air bubbles were found to be largest where untreated pellets were concerned, with smaller air bubbles forming in all cases where pellets had been treated with oil. The formation of bubbles indicates the containment of void spaces within the pellet structures as previously predicted, and in turn indicates that where oil treatment is carried out, treatment acts to reduce the volume of voids within pellet structures.

1.4.3 Wood pellet strength

Pellet strength was determined both before and after being submerged in water through carrying out a series of three point flexural tests. Initial testing exclusively with untreated wood pellets indicated that there is no direct relationship between pellet strength and the length or density of wood pellets. Superficial cracks and signs of wear on the surface of wood pellets were found to act as nucleation points for further degradation and pellet breaking. Therefore, all pellets were inspected for cracks and signs of wear and were selected accordingly prior to carrying out three point flexural tests. Pellets treated with oil were tested after being submerged in 100 ml of distilled water for 3 minutes, 10 minutes, 20 minutes and 30 minutes, and untreated pellets were tested after being submerged for 30 seconds, 1 minute and 3 minutes. The force recorded at specimen failure is shown in Figure 6 for all oil treatments.

Figure 6 highlights that treating wood pellets with oil does not affect a pellet's initial strength, and shows that the strength of untreated pellets is broadly in line with the strength of all oil treated pellets prior to being submerged in water. Figure 6 also shows that the strength of untreated pellets is dramatically reduced after they have been submerged in water, whereas the strength of oil treated pellets is maintained broadly constant in all cases. Pellet strength is maintained after being submerged in water for up to 30 minutes in the case of all of the oil treated pellets, whereas the strength of untreated pellets is found to decrease on average by around 70% of the initial strength after 30

seconds, and 94% after 1 minute. Therefore, it can be said that treating wood pellets with all oil types vastly increases their moisture stability.

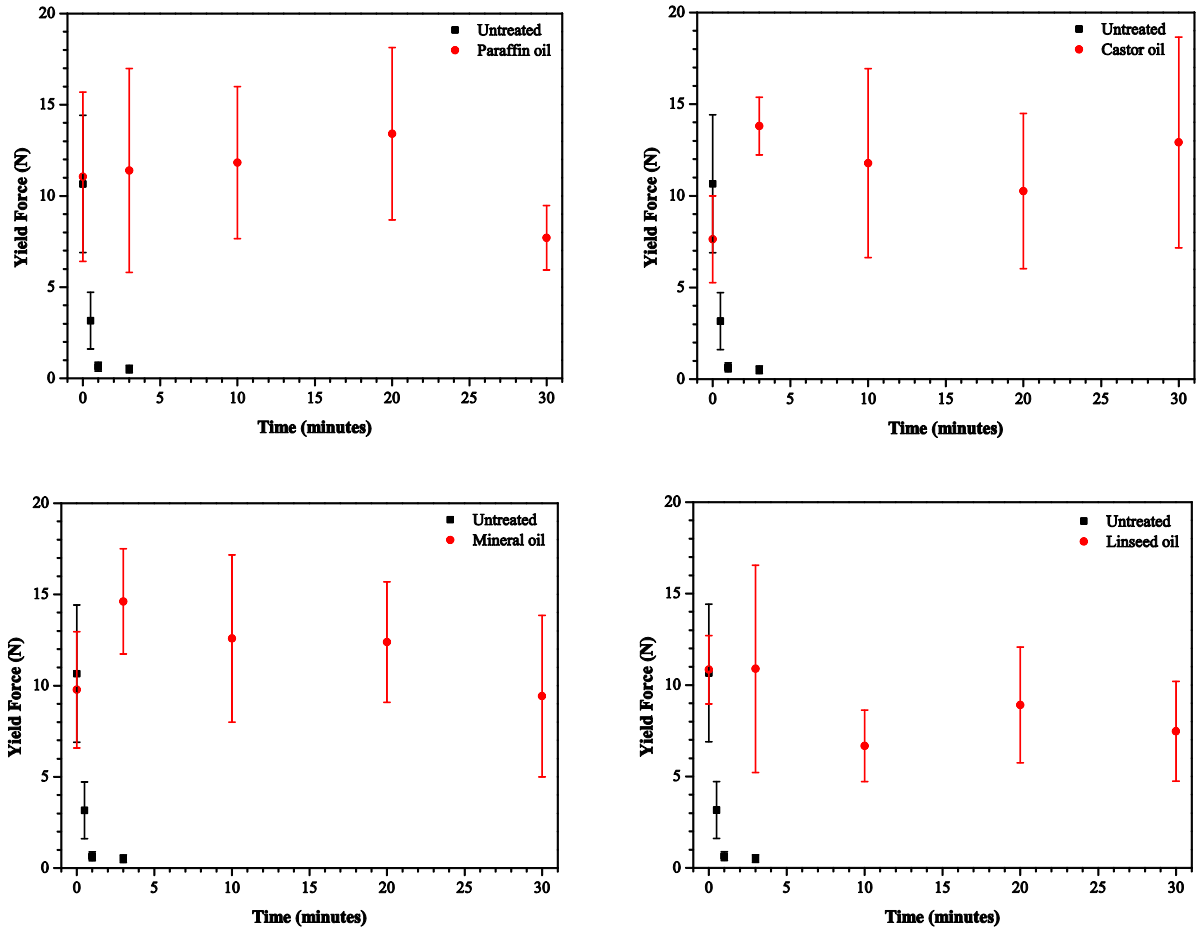

Figure 6: Comparison between the strength of oil treated and untreated wood pellets.

An important point to raise is that the error in the results shown in Figure 6 is relatively large; the error bars shown in Figure 6 representing the standard deviation of the data recorded. Therefore, it should be stated that the results displayed only provide an approximate guide to wood pellet strength and do not pose as absolute values. The values for pellet strength in this case primarily seek to quantify the effect of submersion in water on pellet stability.

1.4.4 Milling behaviour and particle size analysis

Work was undertaken initially with untreated pellets in 50 g batches and with milling times of 1 minute, 3 minutes, 5 minutes, 7 minutes and 10 minutes. Figure 7 shows how the generation of particles less than 2 mm, 1 mm, 250 µm, 200 µm and 125 µm varies with milling time. Generally, as milling time is increased, the proportion of all particle sizes less than the initial pellet size increases.

Pellets are found to be milled to a size of less than 2 mm and less than 1 mm after a relatively short time and longer milling times are required in order to generate particles less than 250 µm, 200 µm and 125 µm. A maximum number of particles sized at less than 2 mm is reached after approximately 5 minutes and less than 1 mm after approximately 10 minutes. Longer milling times are required in order to break down particles further.

The same conditions were then imposed for all oil treated pellets; however, such a mass per batch was found to be insufficient to prompt appropriate milling of the material. The balls contained within the ball mill were found to rotate freely and not interact with the material. Various batch masses were tested and increasing the mass per batch was found to prompt the most favourable results. Consequently, all oil treated pellets were milled in 145-150 g batches at time intervals of 5 minutes, 10 minutes, 15 minutes, 20 minutes and 30 minutes. The mass per batch corresponds to a starting mass of 140 g of untreated pellets plus the additional mass of the oil used for treatment. In addition to varying the mass per batch for the oil treated pellets, a mass per batch of 140 g of untreated pellets was examined. However, as with smaller batches of oil treated pellets, untreated pellets in larger batches were found to mill insufficiently compared to smaller batches.

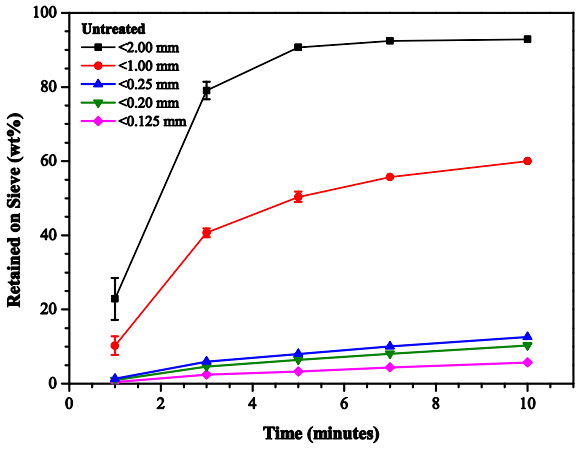

Figure 7: Effect of milling time on particle sizes generated when milling untreated wood pellets.

Figure 8 shows the same general trend for all oil treated pellets as was shown for untreated pellets where particle sizes less than 2 mm and 1 mm are concerned. With the exception of castor oil treated pellets, the proportion of particles sized less than 250 µm were also found to increase as milling time was increased. However, the concentration of such particles was found to be lower in all cases than with untreated pellets, excluding paraffin oil treated pellets which were found to be broadly comparable.

In addition to this, no particle sizes less than 200 µm were formed in any of the cases where wood pellets were treated with oil. This was due to the formation of an impermeable crust which was consistently found to form on the surface of the 200 µm sieve during testing with all oil treated pellets.

Vibrating the 200 µm sieve intermittently enabled the crust to be broken and particles less than 200 µm to pass through the sieve, therefore highlighting that particle sizes less than 200 µm were generated during milling. The formation of the crust on the 200 µm sieve is likely to occur due to the presence of the oil coating the pellets which allows small particle sizes to adhere to each other and larger particle sizes during milling. Therefore, where oil treated pellets are concerned, Figure 8 does not present a ultimate account of particle sizes formed during milling in terms of particle sizes less than 200 µm.

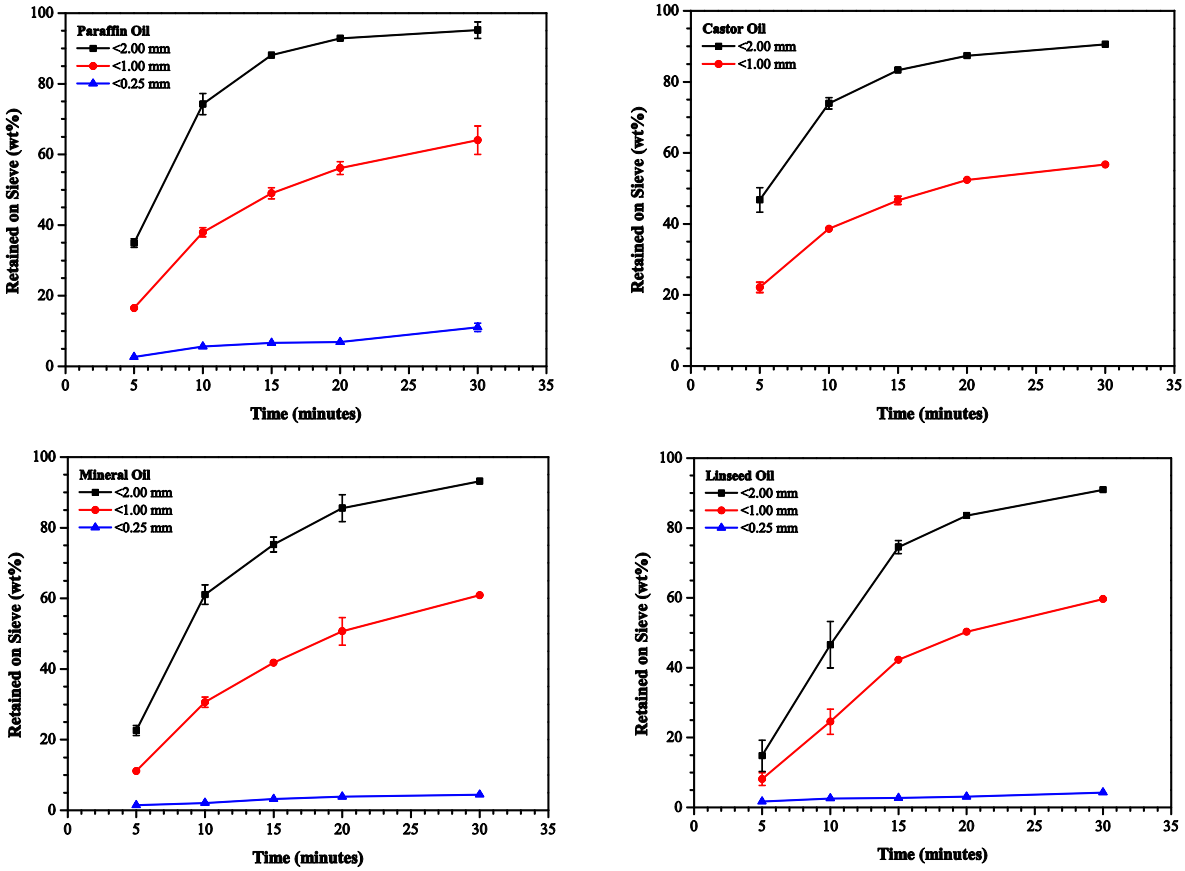

Figure 8: Effect of milling time on particle sizes generated when milling oil treated and untreated pellets.

The formation of an impermeable crust was also found to form consistently on the 250 µm sieve where castor oil pellets were concerned. Examining Table 1, it is found that the viscosity of castor oil is greater than the remaining three oil types and therefore it is proposed that oil viscosity is a key factor affecting crust formation and the adhesion of small particles.

Although particle adhesion and agglomeration is a potential drawback where pellets are required to be milled to particle sizes less than 200 µm, such a phenomenon can be interpreted to be a natural safety mechanism. As smaller particles agglomerate or adhere to larger particles, the volume of airborne particles arising during the milling process is reduced. This in turn reduces the probability of dust

explosions taking place, and hazards associated with hot or electrical equipment through layer accumulation are minimised.

Figure 9: Examples of the impermeable crust formed on the 200 μm sieve.

In addition to particle size analysis, the energy required to mill each batch of pellets was recorded. As the percentage of particles formed that are less 2 mm and 1 mm are broadly equal across all samples and pellet batches/milling time differ by a factor of three, energy requirements can be considered comparable. Expressing the energy requirement for milling per unit mass, an average of 2.10 ± 0.03 MJ/kg was required to mill the untreated pellets, and an average of 2.11 ± 0.06 MJ/kg was required to mill the oil treated pellets. Results in turn indicate that treating pellets with oil does not markedly affect the energy requirement associated with milling where the generation of particles less than 2 mm and 1 mm are concerned.

1.4.5 Wood pellet heating value

The HHV of each of the oil treated pellet samples was assessed via two methods. Via bomb calorimetery using approximately 1 g of milled material sized at less than 250 μm, and via a mass and energy balance. The results from the bomb calorimeter shown in Table 3 indicate that treating wood pellets with mineral oil generates the largest increase in the HHV, increasing the heating value by approximately 3.7 MJ/kg. Paraffin oil treatment follows this, then castor oil and lastly linseed oil which brings about the lowest increase in heating value, increasing it by approximately 2.1 MJ/kg. Increases in heating value were found to be a product of mass uptake and the heating value of the oil used for treatment. Table 1 highlights that the HHV of mineral oil is broadly similar to that of paraffin oil. However, examining the results shown in Table 2, it is found that mineral oil is absorbed preferentially on a bulk basis which constitutes the starting point for the milled sample used in the bomb calorimetery tests.

	Heating Value		
Treatment	**Bomb Calorimeter (MJ/kg)**	**Energy Balance (MJ/kg)**	**Energy Balance (GJ/m^3)**
Untreated	18.4 ± 0.1	18.4 ± 0.1	11.9 ± 0.1
Paraffin oil	21.2 ± 0.2	19.5 ± 2.1	13.2 ± 2.0
Castor oil	20.5 ± 0.1	19.4 ± 1.0	13.4 ± 1.0
Mineral oil	22.1 ± 0.1	19.6 ± 0.2	13.4 ± 0.2
Linseed oil	20.4 ± 0.1	19.3 ± 1.5	13.2 ± 1.5

Table 3: Effect of oil treatment on the heating value of wood pellets.

Table 3 also shows the results generated from carrying out a mass and energy balance using the HHV of the untreated pellets, the individual heating values of each of the oils, and the results relating to mass uptake. As with the results obtained from the bomb calorimeter, Table 3 shows that treating pellets with mineral oil generates the largest increase in heating value. This is followed by paraffin oil, castor oil and lastly linseed oil, as per the results determined via the bomb calorimeter. However, although the trend obtained from carrying out a mass and energy balance matches that determined via bomb calorimetery, heating values differ significantly. An increase in the HHV by approximately 1.3 MJ/kg was recorded where treatment with mineral oil was concerned, and treatment with linseed oil was only found to bring about an increase of approximately 1.0 MJ/kg. Clearly the heating values determined via bomb calorimetery do not match those determined via a mass and energy balance. Therefore, it is proposed that the oil used for treatment is not evenly distributed across all particle sizes after milling has been undertaken. Results show that where mineral oil was used for treatment, particles sized at less than 250 μm contain up to 12.5% more energy than the parent pellet in its bulk form. This has implications for combustion systems that require a feed with a consistent heating value. Where such systems are concerned, it must be ensured that the milled fuel is thoroughly mixed before being introduced into the combustion environment.

In addition to assessing the heating value in terms of energy per unit mass, it is timely to analyse the results generated on a volume basis as this is by and large the limiting factor when biomass fuels are being delivered due to their low energy densities when compared to conventional fuels. It was found that on average, treating wood pellets with oil increases their energy value per unit volume by around 11.6%, and by around 6.0% per unit mass. Such an increase in the energy densities constitutes a real advantage where transportation costs are concerned.

1.4.6 Proximate analysis

The level of moisture, volatiles, fixed carbon and ash were able to be determined by undertaking TG analysis on treated and untreated pellet samples. The proximate analysis of each sample is shown in

Table 4 and results show that treatment with oil brings about an increase in the portion of volatile components in each of the oil treated samples. Undertaking TG analysis on each of the oils used for treatment in their pure form, it can be seen from Figure 11 that all oils breakdown in the volatile region broadly between 200 °C and 500 °C. The least stable oil with fractions arising around 150 °C was found to be mineral oil, which was followed by paraffin oil at 200 °C. Castor and linseed oil were found to interact similarly; however, linseed oil was found to present some larger fractions which were broken down at higher temperatures around 480 °C.

Treatment	Moisture (wt%)	Volatiles (wt%)	Fixed Carbon (wt%)	Ash (wt%)
Untreated	5.4 ± 0.2	76.3 ± 0.2	18.0 ± 0.1	0.3 ± 0.1
Paraffin oil	4.8 ± 0.2	78.2 ± 0.4	16.7 ± 0.2	0.3 ± 0.1
Castor oil	4.4 ± 0.1	78.7 ± 0.2	16.4 ± 0.1	0.5 ± 0.1
Mineral oil	4.8 ± 0.1	78.9 ± 0.1	16.0 ± 0.1	0.3 ± 0.1
Linseed oil	4.7 ± 0.1	78.1 ± 0.1	16.9 ± 0.1	0.3 ± 0.2

Table 4: Proximate analysis of untreated and oil treated wood pellets.

Although the proximate analysis reveals that oil treatment brings about an increase in the overall level of volatile components in pellet samples, Figure 10 highlights the point of inflexion in the derivative thermogravimetric (DTG) curves to be recorded at broadly the same point between 378 °C and 380 °C regardless of treatment. This highlights that the bulk of the matter arising at this point is that contained in the parent pellet. Figure 10 highlights the key difference between samples and shows that treatment with either castor or linseed oil increases the level of volatile components broken down at higher temperatures broadly between 410 °C and 480 °C, and treatment of wood pellets with either mineral or paraffin oil increases the level of volatile components arising at lower temperatures between 150 °C and 300 °C.

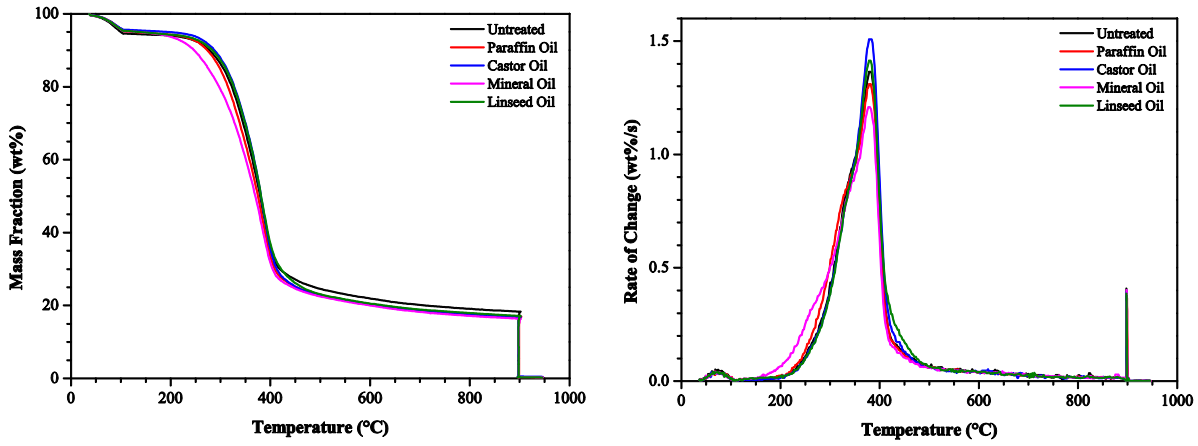

Figure 10: TG analysis of untreated and oil treated wood pellets.

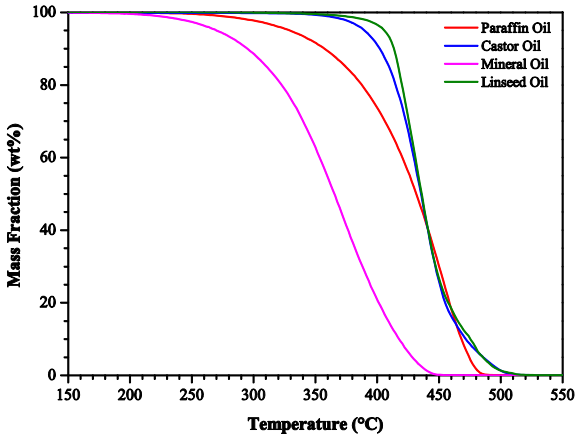

Figure 11: TG analysis of the oils used for wood pellet treatment.

1.5 Economic implications

1.5.1 Wood pellet market prices

Wood pellet prices have varied dramatically from country to country in recent years. Prices as low as 122 €/tonne (166 $/tonne) were recorded in Spain in 2008 and as high as 300 €/tonne (408 $/tonne) in Sweden in 2010 (Cocchi et al., 2011). Prices vary for a number of reasons, but primarily because they are tied to the market dynamics of sawmill residues and in turn, the wood processing industry (Flach et al., 2013, Obernberger and Thek, 2010). In countries where wood pellets are extensively used for domestic heating, wood pellet price is also strongly affected by the price of heating oil; however, it is found that such a factor does not greatly affect the price of pellets used in industrial applications (Cocchi et al., 2011).

Industrial prices for wood pellets are typically found to be much lower than domestic prices; however, as with the domestic market, prices are unstable and can vary considerably (Cocchi et al., 2011, Obernberger and Thek, 2010). To provide context for industrial prices, it is appropriate to examine the US as the US is currently the largest exporter of wood pellets to the EU which is where the majority of pellets are consumed. Although its customer base is far ranging, the US market is predominantly driven by the demand to supply large scale power plants, and currently the US has a wood pellet valuation of approximately 185 $/tonne (Flach et al., 2013).

1.5.2 Heating and plant/seed derived oil market prices

A similar scenario to wood pellets in terms of price volatility is found in the case of heating and plant/seed derived oils. In the case of soybean oil in the US, prices have varied from a low of 486 $/tonne in 2003 to a high of 1173 $/tonne in 2011, and currently stand at 873 $/tonne (Rosillo-Callé et

al., 2009, George et al., 2013). Plant/seed derived oils such as sunflower, palm, peanut and rapeseed oil have showcased similar trends to soybean oil over recent years and are displayed in Figure 12 (Rosillo-Callé et al., 2009, George et al., 2013).

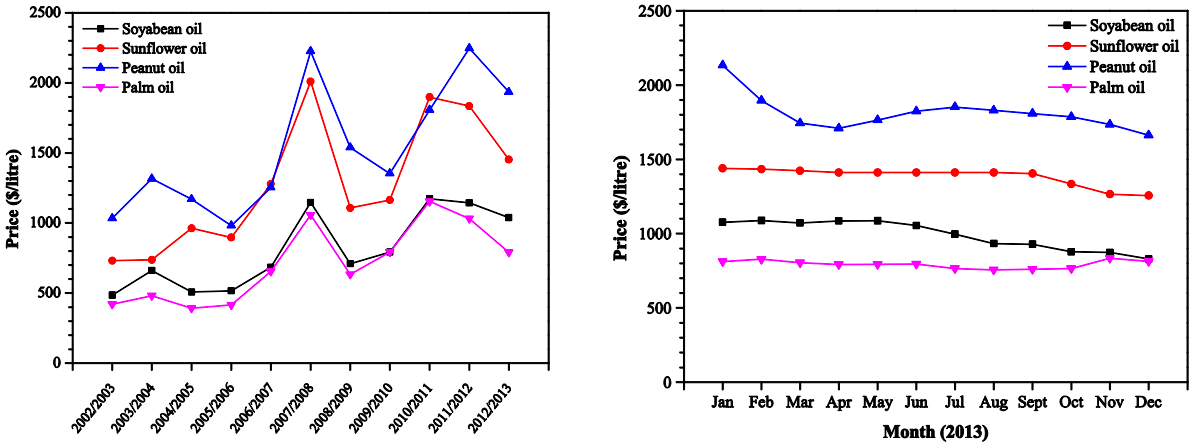

Figure 12: Variation in plant/seed derived oil price over time (George et al., 2013).

Similarly, fluctuations have been recorded in the price for heating oil over the past ten years, with prices mirroring trends found in prices for crude oil. In February 2013, prices were recorded to be more than double those recorded in February 2007; however, prices have decreased since then and as of November 2013, currently stand at approximately 54 pence/litre (0.88 $/litre) in the UK (Bolton, 2013, Trewin et al., 2013).

1.5.3 Economics of wood pellet treatment with oil

The effect that oil treatment has on the price of wood pellets can be assessed by taking the price of oil per litre and combining it with the results shown in Table 2 for the mass uptake of oil on a bulk basis.

Treatment	Oil Price ($/tonne)	Pellet Price ($/tonne)	Price Increase (%/kg)	Price Increase (%/MJ)
Paraffin oil	1017	220	19.1	12.5
Castor oil	1600	269	45.5	37.6
Mineral oil	1020	226	22.1	14.1
Linseed oil	1200	235	27.3	20.9
Used vegetable oil	176	185	0	-5.2

Table 5: Effect of oil treatment on pellet price per unit mass and unit energy.
Oil prices: (Trewin et al., 2013, Mielke, 2013, Morfee, 2014).

Table 5 shows that oil treatment increases the cost per unit mass of pellets by between 19% and 46%. Paraffin oil treatment is shown to be the most cost effective, and castor oil treatment is shown to be the

least. Given that wood pellets are primarily a fuel and in turn used for heating purposes, both industrially and domestically, it is convenient to express the effect of price increase on an energy basis. Taking into account the heating values of each of the oils used for treatment shown in Table 1 it can be seen in Table 5 that price increases are reduced by between 6-8% across the board. Again, paraffin oil treatment is found to be the most cost effective, and increases the price of wood pellets by approximately 12.5% per unit energy. All of the prices shown in Table 5 act as preliminary indicators for the cost of oil treatment and only take into account the cost of the materials used (i.e. wood pellets and oil). Prices do not take into account the cost for treatment and process costs.

Reviewing Table 5 it can be seen that oil treatment presents a relatively large penalty on wood pellet cost, and for treatment to become economically favourable, either the cost of pellets in their raw untreated state would have to increase, or the price of oil would have to decrease. From the data obtained, it is possible to calculate such breakeven points. Where wood pellet price is concerned, if oil prices were to remain constant at current levels, pellet price would need to increase to 818 $/tonne (castor oil), 428 $/tonne (paraffin oil), 420 $/tonne (mineral oil) and 584 $/tonne (linseed oil). Clearly these figures are very high and it is unlikely that pellet prices will increase to these levels due to the competiveness of the solid fuels market. Where oil price is concerned, if wood pellet prices were maintained constant around 185 $/tonne, oil prices would have to decrease to around 0.34-0.38 $/litre. Such figures are not unreasonable. Where palm oil is concerned, prices of this order were fairly common and consistent between 2003 and 2007, although prices have risen since (Rosillo-Callé et al., 2009).

Since the price of oil is likely to be the determining factor as to whether wood pellet treatment with oil will be taken further, an interesting avenue to explore is the waste cooking oil market. Currently waste cooking oil needs to be collected by a licensed waste carrier and disposed of appropriately. However, it is possible to procure such oil from for around 10 pence/litre (0.16 $/litre) in the UK (Morfee, 2014). Although the oil in question is a waste stream and contains unwanted contaminants, such a price is sufficiently low to make wood pellet treatment with oil economically favourable. Table 5 includes figures for treatment with used vegetable oil, assuming a price of 0.16 $/litre.

Table 5 indicates that wood pellet treatment with used vegetable oil does not have a dramatic effect on the price per unit mass of fuel, and breaks even with current pellet prices. However, when expressed on an energy basis, oil treatment is found to be economically advantageous and decreases the price per unit energy. Calculations undertaken incorporate results recorded using fresh vegetable oil. Oil density was determined to be approximately 931 kg/m^3, the heating value of the oil was determined to be around 19.3 MJ/kg and oil treatment on a bulk basis was found to increase pellet mass by around 5.91 wt%. Incorporating such figures was found to reduce pellet price per unit energy by 5.2%.

1.6 Summary

The moisture instability of wood pellets has been highlighted as a key problem where commercial wood pellet fired systems are concerned, and currently considerable lengths have to be taken in order to ensure their stability is maintained. This chapter provides an overview of the work undertaken to increase the moisture stability of commercially available wood pellets.

Initial tests with untreated 6 mm diameter wood pellets revealed swelling to take place immediately after being submerged in water, with swelling taking place laterally and then longitudinally. Pellet diameters were found to increase by around 30-40% after being submerged in water for 3 minutes and break up irreversibly after 5-10 minutes. Wood pellet strength was assessed using a three-point flexural test, and the strength of untreated pellets was found to decease by 95% after being submerged in water for 1 minute.

Wood pellets were treated separately with paraffin oil, castor oil, mineral oil and linseed oil. All oil treatments were found to increase the moisture stability of wood pellets and swelling after initial submersion was found to be negligible compared to untreated pellets. No appreciable reduction in pellet strength was observed after being submerged in water for 30 minutes, and pellet diameters were only found to increase by around 5-10% after the same time period.

All oil treatments were found to increase the heating value of wood pellets. The energy content per unit mass was found to increase on average by 6.0% and the energy content per unit volume was found to increase on average by 11.6%. Mineral oil was found to bring about the greatest increase in the heating value (1.2 MJ/kg), whereas linseed oil was found to bring about the smallest (0.9 MJ/kg). In terms of pellet makeup, oil treatments were found to increase the proportion of volatile components in all cases. Paraffin and mineral oil treated pellets highlighted volatile components being released at lower temperatures between 150 °C and 300 °C, and treatment with castor and linseed oil increased the level of volatile components being realised at higher temperatures between 410 °C and 480 °C.

Where wood pellet price is concerned, oil treatment was found to increase pellet price on a mass basis by between 19% and 46% for paraffin oil and castor oil respectively. Pellet prices were found to be more favourable when expressed on an energy basis, but oil treatment was still found to increase price. Price increases on an energy basis were found to be between 12% and 38% for paraffin oil and castor oil respectively. In addition to economic assessments made with the oils used in this study, an assessment was made taking into account the price of used vegetable oil. Treatment was undertaken with fresh vegetable oil in order to assess the mass uptake of oil. Assuming used vegetable is absorbed in the same quantities as when fresh, treatment was found to have a favourable effect on pellet price reducing the price per unit energy by 5.2%.